



UNIVERSITAT^{DE}
BARCELONA

Peptides: from synthesis to biomedical application in two types of cancer

Omar Fernando Luna González



Aquesta tesi doctoral està subjecta a la llicència **Reconeixement 4.0. Espanya de Creative Commons.**

Esta tesis doctoral está sujeta a la licencia **Reconocimiento 4.0. España de Creative Commons.**

This doctoral thesis is licensed under the **Creative Commons Attribution 4.0. Spain License.**

Programa de Doctorat de Química Orgànica

PEPTIDES: FROM SYNTHESIS TO BIOMEDICAL APPLICATION IN TWO TYPES OF CANCER

Omar Fernando Luna González

Fernando Albericio Palomera

Miriam Royo Expósito



**UNIVERSITAT DE
BARCELONA**

Department de Química Orgànica, Universitat de Barcelona, i Centro de
Investigación Biomédica en Red-Bioingeniería, Biomateriales y Nanomedicina
CIBER-BBN, Barcelona 08028, Espanya.

This work received funding from the European Union's Horizon 2020 research and innovation program under the Marie Skłodowska-Curie PAVE-ITN project (grant agreement number 861190).

Abstract

The aim of this work was to synthesize peptides that would perform two functions in the potential treatment of two types of cancer.

The first group of peptides was used as the antigenic component of a nanovaccine formulation that represents an immunotherapeutic approach to treating pancreatic ductal adenocarcinoma. In some cases, the peptides were modified at the N-terminus through palmitoylation and PEGylation, with the objective of enhancing their immunogenic potential. Additionally, they were synthesized as single epitopes or as multi-epitope constructs derived from tumor-associated antigen proteins. The peptides were formulated in poly(lactic-co-glycolic) acid-based nanoparticles, and the resulting nanoformulation was tested in a mouse model to assess its immunogenic activity. Two multiepitope peptides demonstrated a markedly positive response *in vitro*. These were the Palmitoyl-PLTVAEVQKLLGPHVKKALPLDLLLFLKKSLLFLLFSL-NH₂ peptide and the H-KVYLRVRPLLKKSYPGVLLWEIKKRFVDPGNRI-NH₂ peptide. These findings suggest that long multi-epitope constructs are the most effective alternative for use as nanovaccine components, as single epitope peptides were demonstrated to lack immunogenicity. However, preliminary *in vivo* assays of the two multi-epitope peptides exhibited minimal activity against the tumor in a mouse model. Additional validation is necessary through the repetition of these assays.

The second group of peptides served as targeting units in a quatsome nanovesicle delivery system that is designed to carry a therapeutic nucleic acid for the treatment of neuroblastoma. The peptides were initially synthesized with fluorescein as a probe. In parallel, a small molecule ligand, a thiolated *p*-aminobenzylguanidine derivative, was also synthesized, labeled and evaluated in conjunction with the targeting peptide moieties to determine their internalization capability in a neuroblastoma cell line.

A sequence targeting the GD2 receptor in neuroblastoma cells (H-WHWRLPSGGGC-NH₂) and the thiolated *p*-aminobenzylguanidine derivative, demonstrated the greatest capacity to internalize into these cells and were therefore selected for the development of a conjugation methodology in quatsome nanovesicles using a thiol-maleimide click reaction. The methodology was successfully developed, and the optimal conditions were identified as a pH of 7.5, a reaction time of two hours, the presence of a reducing agent and a clean-up methodology of size exclusion chromatography in Sephadex G50 and aqueous elution followed by mild acidic elution. This allowed for the separation of nanovesicles from unreacted ligands and the indirect estimation of the conjugated targeting moiety in the nanovesicle. The methodology yielded conjugation estimates of 50% to 65% for both the GD2-binding peptide and the thiolated *p*-aminobenzylguanidine derivative. Furthermore, this formulation was demonstrated to have the capacity to deliver a nucleic acid to a neuroblastoma cell line. However, a switch of the PEGyl moiety carrying the maleimide function from PEG₂₀₀₀ to PEG₁₀₀₀ is required to achieve quantitative internalization.

Furthermore, a study was conducted to evaluate the suitability of five different carbodiimides for use in solid-phase peptide synthesis, the methodology employed for the production of all peptide compounds in this research. The objective of this comparative study was to identify an optimal alternative to *N,N'*-diisopropylcarbodiimide (DIC) that can prevent the formation of the toxic compound hydrogen cyanide, which can occur when the reaction is conducted in the presence of oxyma. The study demonstrated that 1-*tert*-butyl-3-ethylcarbodiimide is an effective alternative to DIC. It exhibited comparable synthetic performance in the production of two peptide models and an antigenic peptide, while reducing the occurrence of hydrogen cyanide by threefold compared to DIC.

Resumen

Este trabajo tuvo como objetivo sintetizar péptidos que pudiesen cumplir dos funciones en el tratamiento de dos tipos de cáncer. El primer grupo de péptidos es el componente antigénico en una formulación de nanovacuna terapéutica contra el adenocarcinoma ductal pancreático. Para incrementar su potencial inmunogénico, se incluyeron péptidos modificados en la amina N-terminal y se formularon en nanopartículas de ácido poli(láctico-co-glicólico). Las formulaciones se ensayaron en un modelo de ratón. Dos péptidos multiepitópicos: Palmitoil-PLTVAEVQKLLGPHVKKALPLDLLLFLKKSLLFLLFSL-NH₂ y H-KVYLRVRPLLKKSYPVLLWEIKKRFVDPGNRI-NH₂ mostraron una actividad inmunogénica óptima *in vitro*, lo que sugiere que los péptidos largos multiepitópicos son una excelente opción como componentes de vacunas. Ensayos *in vivo*, sin embargo, demostraron poca actividad antitumoral.

El segundo grupo de péptidos son unidades de direccionamiento en un sistema de entrega tipo quatsoma, que porta un ácido nucleico terapéutico para el tratamiento del neuroblastoma. Estos péptidos se sintetizaron como sondas fluorescentes introduciendo fluoresceína. Conjuntamente, se sintetizó una molécula orgánica, un derivado tiolado de *p*-aminobencilguanidinio. Estos compuestos se ensayaron en su capacidad de acumulación en células de neuroblastoma. El péptido H-WHWRLPSGGGC-NH₂ y el derivado tiolado de *p*-aminobencilguanidinio fueron seleccionados por su excelente actividad y se desarrolló una metodología de conjugación de estas unidades en quatsomas, alcanzando tasas de conjugación de entre el 50 % y el 65 %. Además, se demostró que esta formulación puede entrar en una línea celular de neuroblastoma y entregar un ácido nucleico siempre que la función maleimida se introduzca en un PEG₁₀₀₀.

Todos los péptidos se sintetizaron mediante síntesis en fase sólida. Se realizó un estudio sobre la reacción de acoplamiento de esta metodología, en el que se compararon cinco carbodiimidias, con el fin de evaluar la mejor alternativa a la *N,N'*-diisopropilcarbodiimida (DIC), tanto en cuanto a la calidad de la síntesis como a la minimización de una reacción secundaria de la DIC en presencia de oxima: la formación de cianuro de hidrógeno. Se demostró que la 1-*tert*-butil-3-etil-carbodiimida cumple ambos criterios y puede usarse para este fin.

Table of Contents

Introduction.....	1
I.1 Cancer	3
I.1.1 Pancreatic Ductal Adenocarcinoma (PDAC)	3
I.1.2 Neuroblastoma (NB)	4
I.2 Peptides as bioactive compounds.....	5
I.3 Immunotherapy and peptide-based cancer vaccines.....	7
I.4 Peptide delivery systems.....	12
I.4.1 Delivery systems based on PLGA nanoparticles.....	13
I.4.2 Quatsome nanovesicles for targeted delivery	13
I.5 General aspects of solid phase peptide synthesis	14
I.6 By-production of hydrogen cyanide by a secondary DIC/Oxyma reaction	19
Objectives.....	21
Chapter 1.....	25
1.1 Introduction	27
1.1.1 Pancreatic ductal adenocarcinoma (PDAC): epidemiology and treatment challenges.....	27
1.1.1.1 PDAC characteristics, epidemiology and clinical presentation.	27
1.1.1.2 Multi-agent chemotherapy.....	28
1.1.2 Immunotherapy and peptide-based vaccines.....	30
1.1.3 Selection of antigens for a peptide-based PDAC vaccine.....	31
1.1.4 Types of antigens for peptide vaccine components. Limitations and solutions	31
1.1.4.1 N-terminal modifications to improve immunogenicity	31
1.1.4.2 Mode of presentation to improve immunogenicity	32
1.1.4.3 Advantages and limitations in the production of peptide vaccine components	32
1.1.5 Poly(lactic-co-glycolic) acid nanoparticles (PLGA-NP) as a vaccine delivery system	33
1.2 Results and Discussion	34
1.2.1 Design.....	34
1.2.2 Synthesis of the different peptide vaccine components.....	35
1.2.2.1 Synthesis of Mesothelin (MSLN) peptides	35
1.2.2.2 Synthesis tetanus toxoid (TT) peptides	39
1.2.2.3 Synthesis of peptides derived from the OCV-C01 vaccine.....	39
1.2.2.4 Synthesis of K-Ras peptides: an example of a complicated peptide synthesis	41
1.2.3 <i>In vitro</i> and <i>in vivo</i> assays for MSLN peptide nanovaccines in murine model	49
1.2.3.1 <i>In vitro</i> screening of the MSLN peptide-based nanovaccines.....	50
1.2.3.2 Immunogenic effect studies for the PLGA-NP-P12 nanovaccine	51
1.2.3.3 Efficacy of the PLGA-NP-P12 nanovaccine in PDAC tumors	54

1.2.4 Preliminary screening assays for PLGA-NP-Px OCV peptide nanovaccines in murine model. Comparison with the PLGA-NP-P12 nanovaccine	56
1.2.5 Multivalent antigen peptide constructs	57
1.2.5.1 Synthesis of a fluorescent labelled luciferase-1 multiple antigen peptide as a tumor reporter..	57
1.2.5.2 Synthesis of a mesothelin-based multiepitope multiple antigen peptide	61
Chapter 2.....	67
2.1 Introduction	69
2.1.1 Neuroblastoma.....	69
2.1.2 Ribonucleic acid-based therapeutics for neuroblastoma treatment	69
2.1.3 Quasome-based nanovesicles as delivery systems for miRNA	70
2.1.4 Targeting moieties for neuroblastoma	71
2.2 Results and Discussion	73
2.2.1 Synthesis of the selected targeting moieties and the corresponding 5-fluoresceinated-derivatives. Cellular uptake studies	73
2.2.2 Preparation of quasome nanovesicles and optimization of thiolated-PABG derivative conjugation	76
2.2.3 Optimized Conjugation of P40 peptide and PABG into QSs	82
2.2.4 Complexation of thiolated-PABG-functionalized quasomes with miR-323a-5p RNA and transfection assays	84
Chapter 3.....	89
3.1 Introduction	91
3.2 Results and Discussion	93
3.2.1 Performance of five carbodiimides in the synthesis of model peptides.....	93
3.2.2 Formation of the oxadiazole in carbodiimide/oxyma mixture as indicator of HCN release	96
3.2.3 Synthesis of a MSLN peptide using TBEC.....	99
3.2.4 TBEC urea solubility evaluation	100
Experimental Section	101
4.1 Materials	103
4.1.1 Reagents.....	103
4.1.2 Solvents	104
4.1.3 Instrumentation	104
4.2 General synthetic methods.....	105
4.2.1 Microwave-assisted synthesis	105
4.2.2 Manual synthesis protocol	106
4.2.2.1 Introduction of the first residue in a 2-CTC resin.....	107
4.2.2.2 Introduction of the first residue in a HPMB resin	108
4.2.2.3 Fmoc removal	108

4.2.2.4	Introduction of the first residue in a Rink Amide AM resin	108
4.2.2.5	Introduction of the first residue in a Sieber resin	108
4.2.2.6	Peptide elongation.....	108
4.2.2.7	Single Coupling	109
4.2.2.8	Kaiser test	109
4.2.2.9	Chloranil Test	109
4.2.2.10	Double couplings	109
4.2.3	Final deprotection and N-terminal modification	110
4.2.4	Cleavage	110
4.2.4.1	High TFA cleavage and global deprotection.....	110
4.2.4.2	Low TFA cleavage with no side chain deprotection	111
4.2.5	Characterization by analytical RP-HPLC and HPLC-MS.....	111
4.2.6	Purification of peptides by semi-preparative HPLC.....	111
4.3	Antigenic peptides for nanovaccines	111
4.3.1	Synthesis of the antigenic peptides	111
4.3.2	Characterization of antigenic peptides for nanovaccines	111
4.3.3	PLGA nanoparticle synthesis for nanovaccine production.....	112
4.3.4	Biological assays	112
4.3.4.1	Animals and immunization	112
4.3.4.2	Stimulation of splenocytes and lymph node cells	113
4.3.4.3	ELISA	113
4.3.4.5	Cell viability assay	113
4.3.4.6	Statistical Analysis.....	113
4.4	Targeting moieties for neuroblastoma	113
4.4.1	Synthesis of peptides for neuroblastoma	113
4.4.2	Characterization of neuroblastoma-targeting peptides.....	114
4.4.3	Synthesis of fluoresceinated derivatives of the targeting peptides for neuroblastoma	114
4.4.4	Synthesis of <i>p</i> -aminobenzylguanidine (PABG) derivatives	114
4.4.4.1	Synthesis of DiBoc- <i>p</i> -aminobenzylguanidine (PABG).....	114
4.4.4.2	Synthesis of thiolated-PABG derivative.....	114
4.4.4.3	Synthesis of the fluoresceinyl-PABG derivative	115
4.4.5	Cell localization assays	115
4.4.6	Formulation of QS nanoparticles by DELOS-susp.....	115
4.4.7	Characterization of QS nanovesicles by Dynamic Light Scattering (DLS) and Multi-Angle Dynamic Light Scattering (MADLS).....	116
4.4.8	Isolation of the free PABG in supernatant.....	116
4.4.8.1	Ultracentrifugation	116

4.4.8.2 Filtration by AMICON® filter units	116
4.4.8.3 Size-Exclusion Chromatography in Sephadex G-25.....	116
4.4.9 Optimized method for targeting units conjugation to QS nanovesicles.....	117
4.4.10 Isolation of non-conjugated targeting units by Sephadex G-50 size-exclusion chromatography.....	117
4.4.11 Estimation of the conjugation efficiency by analytical RP-HPLC	117
4.5 Selection of carbodiimides to replace DIC as a coupling reagent.....	117
4.5.1 Manual synthesis of Ile ^{2,3} -Leu-Enkephalin (H-YIIFL-NH ₂) and Leu-Enkephalin (H-YGGFL-NH ₂), model peptides with five different carbodiimides.....	117
4.5.2 Determination of the the oxadiazole formation in carbodiimide/oxyma mixture as indicator of HCN release.....	118
4.5.3 Solubility of urea in DMF.....	118
Conclusions	119
References.....	125
Annex.....	139

Introduction

I.1 Cancer

Cancer is an umbrella term used to describe a number of disorders that are caused by a multifactorial deregulation of the cell cycle which causes uncontrolled multiplication of affected cells. This deregulation of cell proliferation can lead to very well-described deleterious consequences for organisms, potentially culminating in death.¹ Among the numerous types of cancer affecting the general population, two are of particular concern, pancreatic ductal adenocarcinoma (PDAC) and neuroblastoma (NB), due to their aggressiveness, low survival rates, difficulty in early diagnosis and lack of adequate treatment alternatives. Research into alternative treatments to the classical approaches, such as radiotherapy and chemotherapy combined with surgery, has been promising up to the point of clinical trials. Immunotherapy is one of these alternative treatments. However, research into it has not yet shown effective results.²⁻⁴ The development of novel strategies to treat these types of cancer is of paramount interest.

I.1.1 Pancreatic Ductal Adenocarcinoma (PDAC)

PDAC is one of the most aggressive forms of cancer, with a 90% mortality rate within five years after diagnosis.^{5,6} Within EU countries mortality of PDAC has increased in the last decade⁷⁻¹⁴ (**Figure I.1**) and Austria, Czechia, Finland, Germany, and Hungary are in the top ten of the highest mortality rates per 100.000 inhabitants.

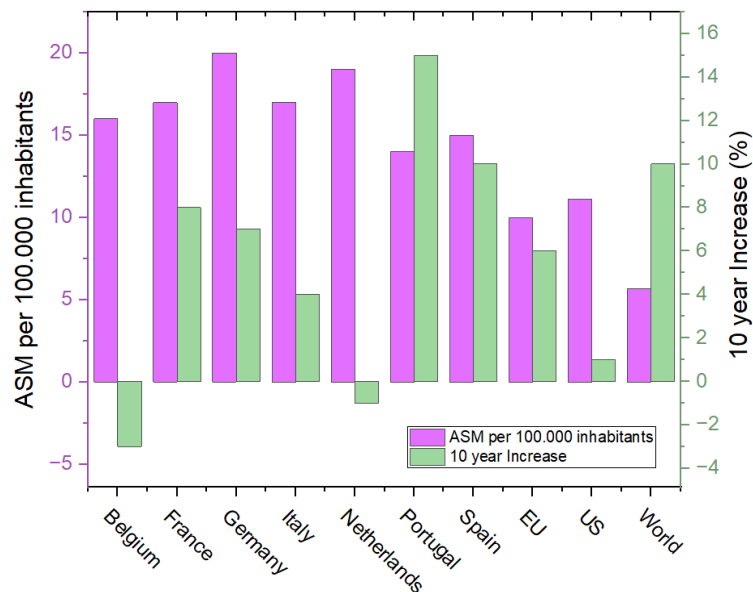


Figure I.1 Pancreatic Cancer Statistics for some western EU and OECD countries, showing current age standardized death rate per 100k inhabitants up to 2023 or nearest year and the % increase of said rate from 2011-2019 or nearest year.

Survival rate of PDAC patients is very low due to the fact that PDAC is extremely silent at early stages, which makes it difficult to diagnose.¹⁵ Consequently, most patients are diagnosed only after the cancer has already metastasized.¹⁶ Currently, the only curative treatment for PDAC is the surgical removal of the tumor, but fewer than 20% of patients have tumors that can be resected at the time of diagnosis.⁶ More than 80% of patients are diagnosed with advanced-stage tumors that should be treated with chemotherapy and median survival is less than one year.^{16,17} Contrasting other tumor types, targeted therapies have been unsuccessful for PDAC until now.¹⁸⁻²⁰ Nonetheless, a broader understanding of PDAC tumor and its interactions with the immune system has opened possibilities for treatment via immunotherapy.²¹ PDAC is a complex and heterogeneous tumor and environmentis consisting of

cancer stem cells and a dense stroma. Within the tumor microenvironment (TME), cancer-associated fibroblasts, pancreatic stromal cells, and recruited immunosuppressive cell populations can be found (**Figure I.2**).²² This last group includes myeloid-derived suppressor cells (MDSCs), tumor-associated macrophages (TAMs), and regulatory T cells (Treg cells) and their activity is key to explain the failure of immune responses to control the tumor and thus the lack of success in immunotherapy research to date.

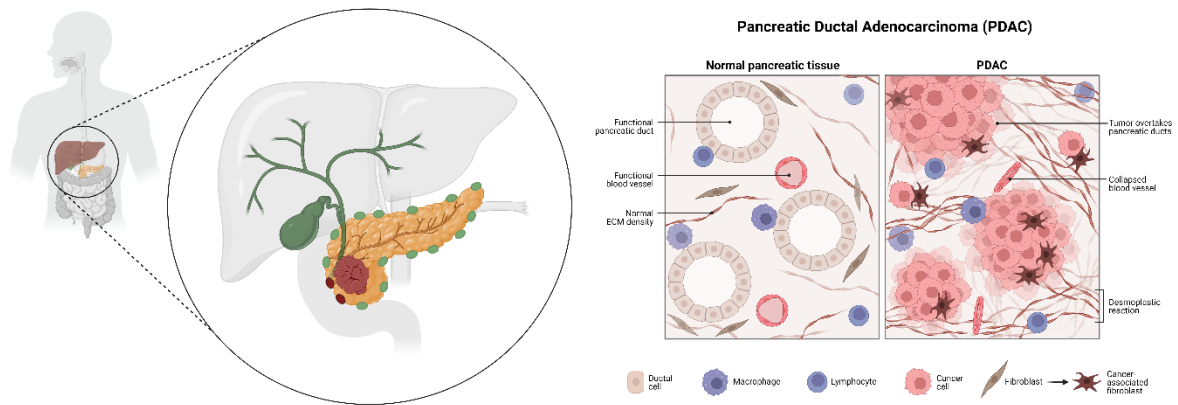


Figure I.2 Tumor structure for Pancreatic Ductal Adenocarcinoma in human (created with BioRender.com).

I.1.2 Neuroblastoma (NB)

NB is a type of cancer that affects neuroblasts, precursor cells to both nerve cells and adrenal medulla cells. The most frequently locations affected by NB are the adrenal glands²³, but it can also appear in the spinal cord, abdomen, head, and thorax (**Figure I.3**). It is the most frequent pediatric solid extracranial solid tumor.^{24,25} Approximately 90% of all cases of NB occur in children under the age of five, and it is the most common form of cancer in the first year of life^{26,27}, sometimes starting before birth. Crucially, by the time it is diagnosed it is often already metastasized.^{28,29} However, survival is inversely related to age, with younger patients more likely to survive and mortality reaching approximately 30-50% in patients 5 years of age or older.²⁴

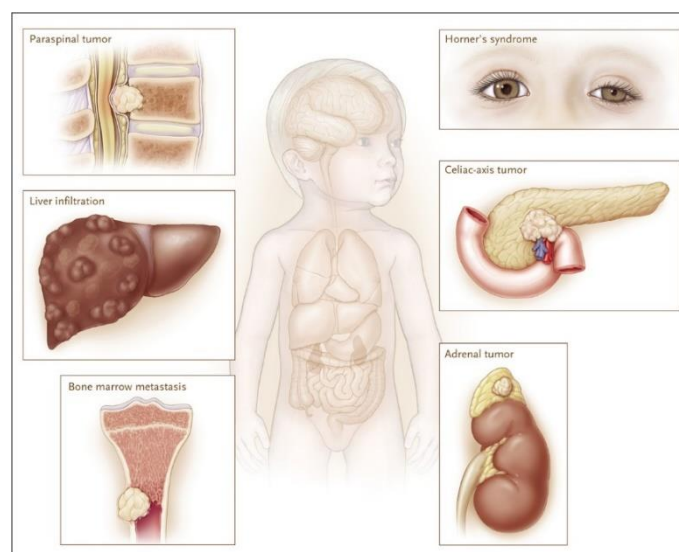


Figure I.3 Clinical presentations of metastatic Neuroblastoma in children (figure extracted from Maris, J.M. "Recent advances in neuroblastoma". *N. Eng. J. Med.* **2010**, 326, 2202-2211).

Neuroblastoma is responsible for approximately 15% of cancer-related deaths in pediatric patients.³⁰ It should be understood that there is great interest in finding effective treatments to eliminate it and better diagnostic tools to detect it in its early stages, so much research has been done to understand its underlying mechanisms. This interest is increased because the target demographic is pediatric and as such this becomes a very sensitive topic.

The difficulty in treating this cancer stems from its complexity due to its high genetic, biological, clinical, and morphological heterogeneity^{31,32}, which makes it a tumor with a diversity of cell types, changing cell phenotypes over time, and multiple instances of mitogenic and antiapoptotic activity caused by the deregulation of different key checkpoints, such as the downregulation of p53. This suppression of apoptosis and increase in mitogenic activity is due to the expression of two major oncogenes: MYCN and ALK.³¹ This cellular diversity and phenotypic plasticity also leads to the development of resistance to chemotherapy and instances of relapse through the expansion of drug-resistant tumor cells.³³ Further complicating the treatment of this cancer, macrophage infiltration upon the development of an immune response results in regrowth of tumor cells.³³ Therefore, novel therapeutic alternatives need to be explored for the treatment of NB.

I.2 Peptides as bioactive compounds

Peptides are widely used in biomedical research and various therapeutic applications (**Figure I.4**) due to their high affinity, selectivity, and specificity for their targets. These properties translate into remarkable safety and efficacy profiles in humans, making them well tolerated as drugs and showing few side-effects.³⁴⁻³⁷ In addition, their synthesis is well optimized³⁸ and allows the preparation of diverse peptides with good yields in a short time frame, becoming good chemical tools for research.

Peptides are an important subset of biological polymers/oligomers, such as proteins, nucleic acids, oligosaccharides, polysaccharides, and others and are defined as short chains of amino acids linked together by amide bonds (also known as peptide bonds). Peptides share the same amide backbone with proteins. In general, chains of 2-50 amino acids are considered peptides, and those with greater numbers of amino acids are considered polypeptides and/or proteins. The amide bond characteristic of the peptide backbone connects the α -amine of one amino acid to the α -carboxylic acid of the next and has a planar conformation and a π -bond-like character due to the resonance resulting from the delocalization of a non-bonding electron pair of the nitrogen atom, being quite stable and unreactive at neutral pH and room temperature.³⁹ Furthermore, the amide bond is one of the most commonly occurring bonds in organic and biological molecules.^{38,40} Peptide functionality is defined by the amide backbone, the side chains of the amino acid sequence, and the secondary and tertiary conformational structure it adopts. Several bioactive peptides have been described, including several hormones, growth factors, various receptor ligands, enzyme inhibitors and antimicrobial effectors, which perform diverse biological functions, such as hormonal, metabolic and cell cycle regulation, cell-to-cell communication, host defense and immune modulation.^{34,41,42} Peptides are also widely used in biomedical research due to their high affinity, selectivity, and specificity for their targets. These properties translate into remarkable safety and efficacy profiles in humans, making them well tolerated as drugs and showing few side-effects.³⁴⁻³⁷ In addition, their synthesis is well optimized³⁸ and allows the preparation of diverse peptides in a short time frame with quite good yields, becoming good chemical tools for research.

Many synthetic peptides are FDA or EMA approved or are in clinical trials for the treatment of diseases^{35,37,43-45} including metabolic⁴⁶, cardiovascular⁴⁷, infectious^{36,48}, diseases of the central nervous system⁴⁹ and cancer.⁵⁰⁻⁵² They can also be used in preventive health such as skincare⁵³, general regenerative medicine and tissue engineering.⁵⁴ Compared to protein-based biopharmaceuticals,

peptide-based therapeutics have greater chemical and physical stability, higher activity per unit mass, and lower immunogenicity.^{35,36} In addition, the complexity and cost of production are lower, generally approaching that of small molecules.^{2,34–36} Indeed, as pharmaceutical compounds, peptides occupy a comfortable niche between complex macromolecules and small organic molecules. An interesting subset within peptide-based therapeutic agents is that of antimicrobial peptides (AMPs), whether antibacterial, antifungal, antiviral or antiparasitic. Their application range from pest control and prophylaxis in the food industry^{55–58} to therapeutic as anti-infective for pathogen control and elimination.^{36,48,59–61} Their mechanism of action may be by direct interaction with the pathogen target or by indirect action as immunomodulators, inducing the action of immune effectors (cytokines, neutrophils) that facilitate clearance of the pathogen.³⁶ This dual mode of action results in a low propensity to generate resistance compared to conventional antibiotic molecules.^{56,60,62}

Peptides are also being used to generate self-assembled nanostructures for drug delivery, vaccination, and therapeutics^{3,63–65} because they can be engineered to exhibit self-assembly and gelation properties. The ability of peptides to form hydrogels has been explored for tissue engineering.^{64,65} Furthermore, peptides serve as models for structure-function analyses⁶⁶ that study, for example, antimicrobial potential⁶⁷, and in the building of libraries for said purposes.⁵⁷

Peptides also function as epitopes in vaccine formulations to generate a monospecific immune response against an antigenic parent protein. This use is widespread, encompassing the production of immunoglobulins for commercialization or research purposes, as well as therapeutic applications such as immunotherapy.^{3,68–71} Notable examples of peptide-based vaccines developed in recent years include candidate vaccines against SARS-CoV-2⁷² and research into *Mycobacterium tuberculosis*-specific antigens with the objective of producing an alternative anti-tuberculosis vaccine to the current BCG (Bacillus Calmette-Guerin) vaccine, which is based on a live attenuated whole pathogen.⁷³

Peptide ligands of specific receptors and proteins expressed on cell membranes are also employed for targeting/homing functions, directing drug delivery systems and compounds to desired tissues, cells, or cell organelles via affinity interactions with these surface membrane cell receptors or guiding drugs towards intracellular targets.^{36,51,60,63,64} Cell Penetrating Peptides (CPPs) are a specific group of this peptide category and are sequences that can cross the cell membrane and deliver loads that target internal cell structures being appropriate to generate targeted drug delivery systems.^{63,64,74} This ability also makes them appropriate vaccine components to ensure their internalization, processing, and presentation by antigen-presenting cells.^{70,71}

Despite all these advantages, peptides have limited physical stability compared to small molecules, variable solubility in aqueous solvents and are highly susceptible to enzymatic digestion. This results in low circulating plasma half-lives, thus reducing their scope and timeframe of action.^{34,36,64} Interestingly, this very fact also implies certain advantages, such as inherent biodegradability, easy clearance from the organism and thus low toxicity. Nevertheless, achieving therapeutic plasma concentrations is a fundamental problem for peptide drugs and because of this, several strategies have been developed to overcome this problem. Another disadvantage derived from the chemical nature of peptides is their low bioavailability and ability to cross physiological barriers such as mucosae and cell membranes due to the presence of a mixture of non-polar, polar, and charged residues in their sequence. This translates into a limited ability to reach tissues and cell targets, compared to organic molecules, with the notable exception of CPPs. Therefore, some systemic delivery routes such as oral administration are complicated, and peptide administration is mostly limited to the parenteral route^{34,64}, with approximately 75% of peptide drugs administered in injectable form.³⁴ For several reasons, including poor patient compliance and the risk of infection, this is not ideal.

Despite these drawbacks, approximately 150 peptide therapeutics are currently in various stages of clinical trials^{34,45}, and more than 100 peptide drugs have been approved by the FDA and the EMA by 2023.^{43,45,75}

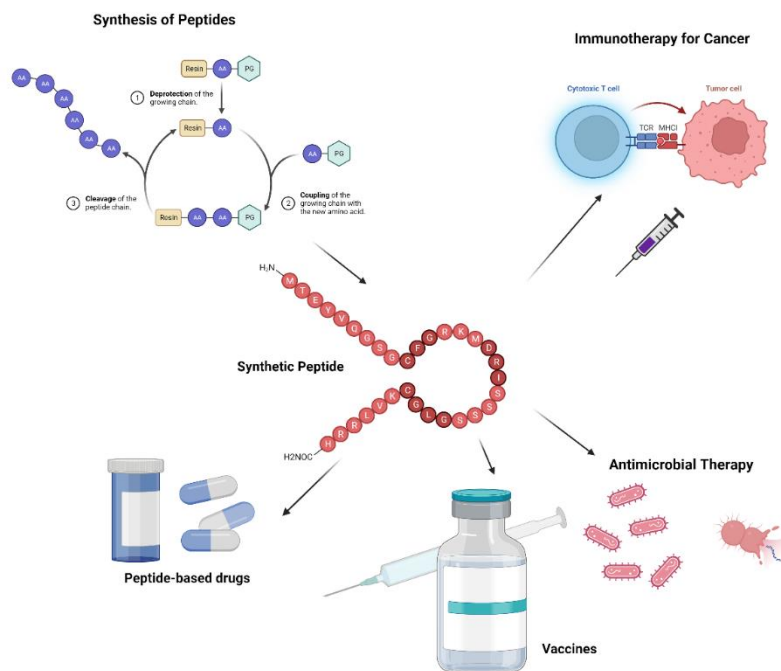


Figure I.4 Summary of some biomedical applications of synthetic peptides (created with BioRender.com).

I.3 Immunotherapy and peptide-based cancer vaccines

Within the universe of the biomedical applications of peptides, cancer treatment is of particular interest to research. Peptides can be used as drugs against tumor cells^{50,51,76}, as targeting molecules for drug delivery⁷⁷ and as vaccines to induce anti-tumor immune responses.^{2,3,68,69,71,78} The latter is a form of immunotherapy and one of the novel alternatives to classical approaches to cancer treatment, which consists of recruiting the patient's immune system to selectively attack and eliminate cancer cells. The immune system has inherent antitumor activity, but it is often insufficient to fight cancer because the proliferation of cancer cells can outpace the rate at which the immune system can eliminate them. In addition, cancer cells can develop mechanisms to evade the immune response.^{79–81} The goal of immune-based therapy is to enhance the antitumor response by enabling the recruitment and activation of immune cells, particularly and critically, tumor-infiltrating CD8+ T cells (TILs) that can reach and kill cancer cells.^{68,70} Recently, the incorporation of immunotherapy in the treatment of various solid tumors has marked a paradigm shift in oncology. Monoclonal antibodies, immune checkpoint inhibitors, T-cell transfer, vaccines, and ribonucleic acids (RNAs) are the main immunotherapeutic strategies for cancer treatment, modulating the antitumor immune response at different points. While monoclonal antibodies bind specific antigens and mark the tumor cell for elimination, immune checkpoint inhibitors (ICIs) block regulatory checkpoint proteins of the immune response, preventing downregulation and thus maintaining the strength of the immune activity. T-cell transfer, or immune cell therapy, consists of using immune cells (i.e., lymphocytes) collected from the patient, conveniently selected and expanded in the laboratory, and then reintroduced into the patient's body to directly eliminate cancer cells. On the other hand, vaccines are produced to train the patient's immune system to fight cancer cells by recognizing specific antigen epitopes in tumor cells. Finally, there is evidence to support that RNAs can serve as regulatory molecules of the immune system as well as suppressing the expression of oncogenes (Figure I.5).^{82–84}

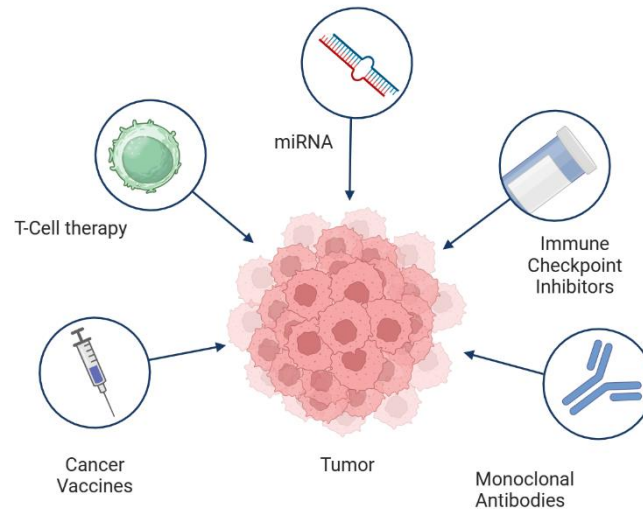


Figure 1.5 Currently applied and researched types of immunotherapies for the treatment of cancer (created with BioRender.com).

Cancer vaccines work on the same principles as vaccines for other diseases, where the active peptide component triggers an immune response that generates long-term immunity against a foreign antigen, with the caveat that their use is therapeutic rather than preventive or prophylactic. In this particular case, the recognition target is a self-antigen produced on the surface of cancer cells, either in a mutated form or overexpressed compared to healthy cells. Cancer vaccines train the immune system to recognize these antigens as foreign, thereby triggering a cellular response based in cytotoxic CD8+ T cells that targets and selectively eliminates cancer cells (**Figure 1.6**).^{85,86}

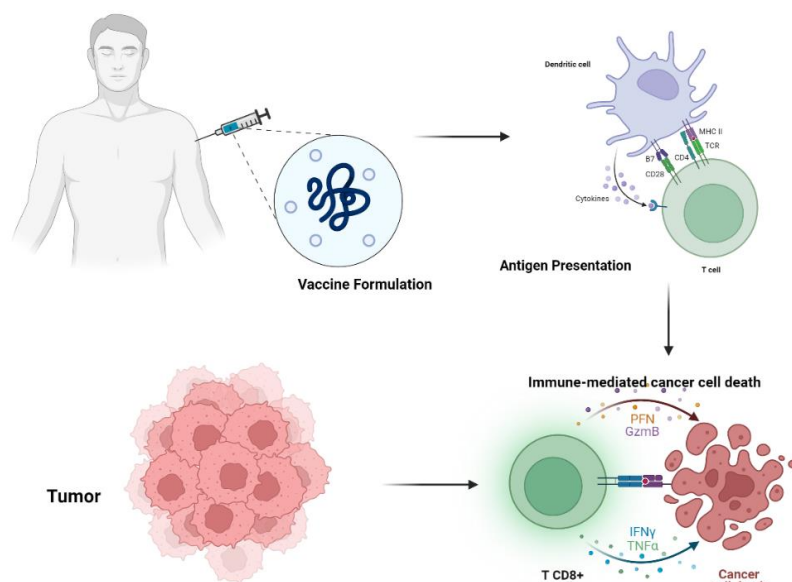


Figure 1.6 The basic strategy behind cancer vaccine immunotherapy. A vaccine formulation is injected, and an immune response is generated against a tumor antigen which is recognized by T CD8+ cells leading to the death of the tumor cell (created with BioRender.com).

Peptide vaccines have advantages compared to standard methods of cancer treatments, such as chemotherapy and radiotherapy. They are specific in their target and have low toxicity. Their specificity

results in few off-target effects and is thus a well-tolerated therapy.^{3,69} Peptide vaccines have several advantages over other types of immunotherapies. Compared to monoclonal antibodies, peptide vaccines are cheaper and faster to produce because the peptide can be synthesized and loaded onto a delivery system to construct a vaccine formulation in generally less time than it takes to extract, culture, select and expand specific clones of T cells, fuse them into hybridomas, and finally have a population of cells that can secrete the antibody. This is a very complex series of steps that can take more than a year. In addition, antibodies must be carefully maintained and preserved to avoid loss of activity because, like most proteins, they are very sensitive to physical challenges such as temperature. Unlike immune checkpoint inhibitors, cancer vaccines do not cause the side effects associated with ICIs, such as diarrhea, rash, and fatigue, or other serious but less common side effects, such as liver inflammation.⁸⁷ With respect to RNA therapies, these nucleic acids are less enzymatically stable than peptides due to their notorious lability to the ubiquitous nucleases and although administration routes are the same for both RNAs and peptides, RNA therapeutics must be administered with greater frequency, bi-weekly for some drugs.⁸⁸ When compared to T-cell transfer, a similar issue arises than for monoclonal antibody production. Isolating and expanding populations of tumor-specific lymphocytes, eliminating unwanted cell populations, maintaining them, and ultimately delivering them to the patient is a costly and lengthy process. Finally, cancer vaccines aim to generate a durable and potent immune response and, unlike all previous alternatives, require a limited number of applications in the form of an initial immunization and one to two boosters to induce antitumor activity, whereas most other alternatives require more frequent applications over longer periods of time.

Peptide vaccines can carry epitopes from two main types of antigens (**Figure I.7, A**). The first are tumor-associated antigens (TAAs), which are proteins expressed in normal cells but overexpressed in cancer cells (**Figure I.7, B**).⁸⁹ Since these are self-antigens, immune tolerance can be expected, and thus they are often poorly immunogenic, eliciting a weak and short-lived immune response. However, they are broadly distributed and common, as they can be found in more than one type of cancer cell.^{3,69,71} The second type of epitope is that of neoantigens, also called tumor-specific antigens (TSAs), which are mutated proteins recognized by the immune system as foreign.⁸⁹ This allows for increased antitumor specificity and generally more responsive CD8+ T cells (**Figure I.7, B**). However, the strength of the immune response depends on the abundance of the neoantigen/TSA, which may be low in contrast to TAAs. In addition, a tumor may change cell types as it develops or modify its phenotype and no longer carry the same neoantigens, thereby escaping the initial immune control.⁶⁹

Additionally, peptide antigens for cancer vaccines should bind to major histocompatibility complex (MHC) class I and II to be presented to T cells and elicit an immune response (**Figure I.7, B**). These protein complexes can be highly polymorphic, i.e. variable from individual to individual. This is a major difficulty in expanding the scope of anticancer vaccines, although it has the advantage of allowing therapies to be personalized to specific individuals by formulating a few key neoantigen peptides to enable precise activation of CD8+ T cells.^{90,91} Therefore, antigen selection is key to meeting all of these requirements. The optimal epitopes should bind MHC complexes, and both class I and class II should be targeted. This ensures that both a CD8+ T cytotoxic (**Figure I.7, B**) and a CD4+ T helper (**Figure I.7, C**) cell response is generated, as an effector cell response (CD8+ Tc) alone is neither sufficient nor sustained over time.⁶⁹

In general, peptides with high affinity for MHC I are short peptides (from 8-mer to 11-mer) and therefore do not require processing to activate CD8+ cytotoxic T cells. A disadvantage in using these peptide epitopes is that in those MHC-I expressing cells that do not contain activating co-molecules, the binding of these peptides does not activate CD8+ T cells, but instead induces immune tolerance.

Antigenic peptides that bind MHC-II are longer (12-mer to 18-mer) and activate a CD4+ T helper cell response. Furthermore, antigenic peptides longer than 20-mer require internalization and processing prior to presentation, which is carried out by professional antigen presenting cells (APCs), such as dendritic cells (DCs). Following this route results in a stronger and more durable immune response.⁶⁹

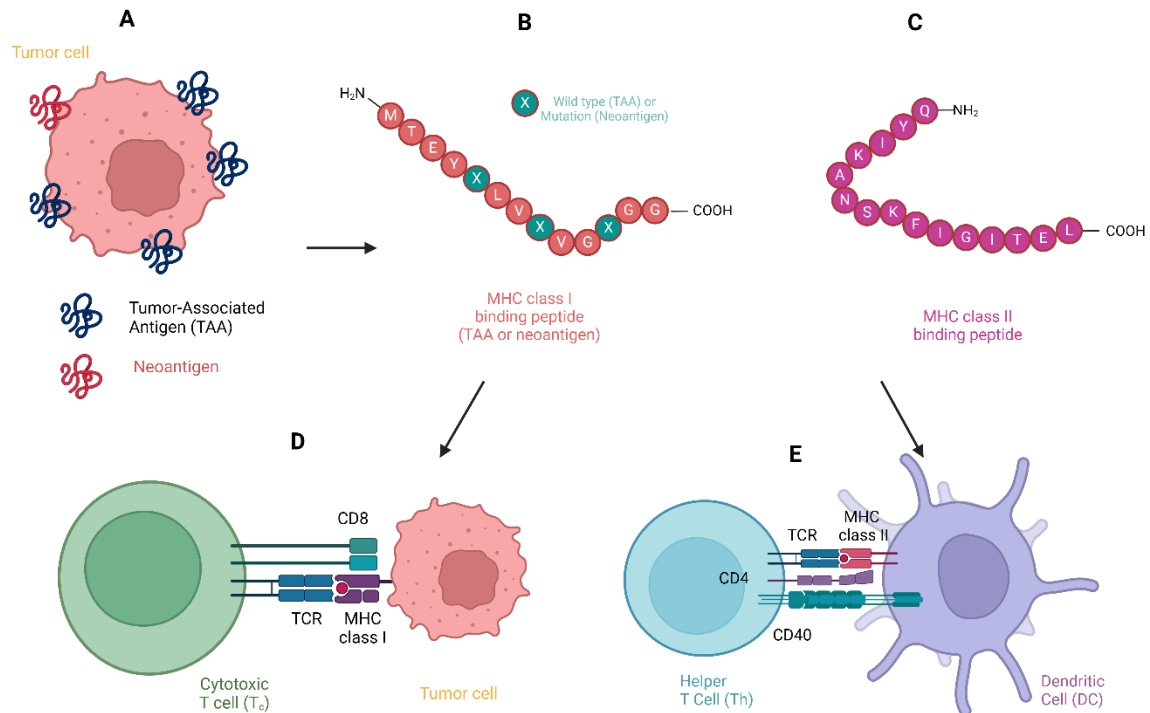


Figure 1.7 A: Antigens derived from tumor cells, including B: MHC I-binding peptides, which are presented by most of the organism cell types to activate T CD8+ cytotoxic lymphocytes and C: MHC II-binding peptides which are presented only by antigen presenting cells to activate T CD4+ helper lymphocytes (adapted with BioRender from templates by Iwasaki & Wu, *Janeway's Immunology Bed*, © Garland Science, 2022).

Another important aspect to consider is the type of construct the antigens are integrating: a single peptide containing multiple epitopes, namely multi-epitope peptide, or a mixture of single epitopes (**Figure 1.8, A and B**). Multi-epitope peptide vaccines are ideal because they elicit a strong immune response, are less susceptible to enzymatic digestion, are better able to withstand other physical and chemical challenges and thus remain at the site of injection for longer periods of time. This gives the epitopes a better chance to reach their APC targets and force their internalization, processing and successful presentation. The use of multi-epitope peptide vaccines allows the formulation of epitopes for many antigenic targets that can be introduced at once, as well as the formulation of both MHC I and MHC II peptides. They are also less expensive to produce than recombinant synthesis of the entire antigen protein. They are also preferred over short peptides (single epitope) as a route of antigen presentation to achieve better immune responses.^{68,92}

A specific class of multi-epitope peptide vaccines are the multiple antigen peptides (MAPs, **Figure 1.8, C**), which incorporate multiple copies of a specific epitope or copies of more than one epitope into a multivalent scaffold, providing for a potent antigenic molecule that improves T cell activation and makes the immune response stronger.⁹³⁻⁹⁵ MAPs are constructed with a central core that carries 2, 4, 8 or more anchoring sites that can be occupied by peptide epitopes. The multivalency of the core is

achieved by building it with appropriate monomers, such as lysine and ethylene diamine. The use of these molecules allows the application of known chemical reactions common to the peptide synthesis process.^{70,96} MAPs are advantageous compared with linear peptides, as they possess greater chemical stability and are able to induce adequate immune responses without the need for a carrier, although it remains difficult to include many types of epitopes into a single structure.^{94,95}

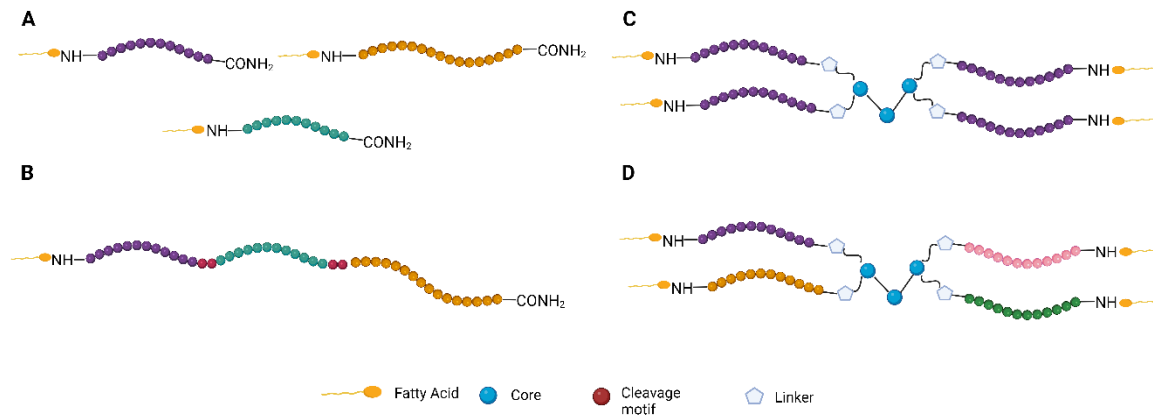


Figure I.8 Three different modes of presentation of peptide epitopes. **A:** Single epitope linear sequences, **B:** multiple-epitope linear sequences and multiple antigenic peptides (MAPs) in both **C:** homotropic and **D:** heterotropic ensembles (created with BioRender.com).

In all of the above cases, it is possible to synthesize self-adjuvanting constructs which positively contribute to better and stronger activation of T cells that provide an efficient, sustained, and potent immune response. This can be achieved by slightly modifying the peptide sequence introducing moieties such as fatty acids that can bind to toll-like receptors (TLRs) and trigger pro-inflammatory signals (**Figure I.9**).⁹⁷

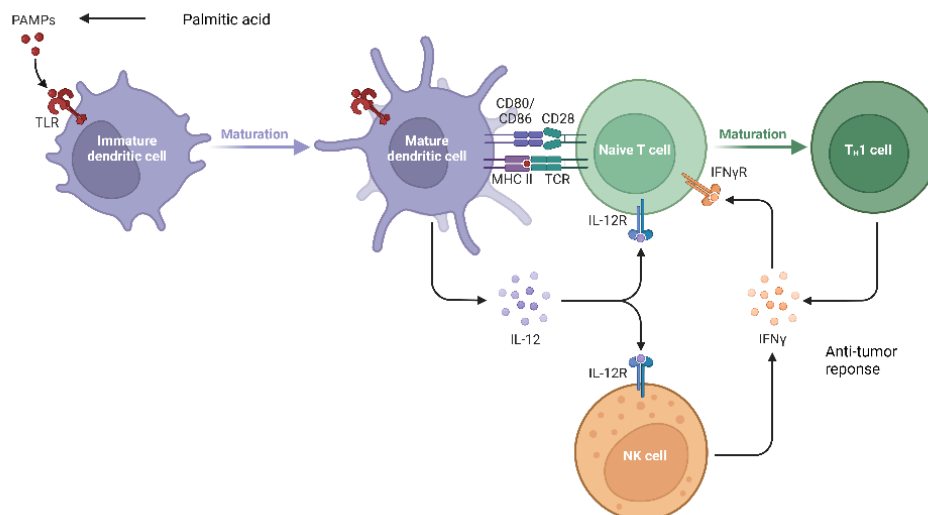


Figure I.9 Activation of antiviral/antitumor immune responses by effector cells and IFN- γ mediated by palmitic acid acting as a ligand for Toll-Like receptors (adapted in BioRender from a template by Mills K. H. TLR-dependent T cell activation in autoimmunity. *Nature reviews. Immunology*. **2011**, *11*, 807–822).

There are many variables that can be tuned in peptide-based vaccines to achieve better efficacy, including formulation into delivery systems, use of appropriate adjuvants, assembly of peptide-based

nanostructures, and others; all of which can result in increased in vivo stability and half-life of the antigenic peptide and efficient delivery to antigen presenting cells (APCs). This in turn helps to produce a vaccine with the potential capacity for improved targeting, enhanced immunogenicity, and efficient induction of cellular and humoral immune responses with very low toxicity and few side effects.⁹⁰

I.4 Peptide delivery systems

As mentioned above, the administration of peptide compounds alone can present some challenges in their application for the treatment of various diseases. Compared to small organic molecules, the physical, chemical, and enzymatic instability of peptides results in low circulating plasma half-life, bioavailability, and tissue penetration capacity, thus limiting their efficacy.^{34,36,64} For cancer vaccines, this results in poor immune responses and thus ineffective treatment. One way to overcome these complications is to formulate the peptides into appropriate delivery systems consisting of ensemble particles of inorganic or organic components, including metals, polymers, or lipids, usually in the form of nanoparticles (NPs).^{70,74} Interestingly, peptides themselves can serve as delivery systems through the self-assembly of a specific subset of sequences that can interact, either naturally or by design, to form ordered nanostructures. In addition, some peptides are prone to gelation, and these hydrogels can also serve as delivery systems.^{65,74}

The delivery system either encapsulates or incorporates the bioactive peptide on its surface, ensuring its stability and localized distribution at the desired target sites. It also increases the half-life of the peptide component by protecting it from enzymatic degradation, chemical degradation, and rapid renal clearance due to its greater size. Delivery systems can also help overcome problems of solubility and bioavailability of therapeutic compounds, allow their distribution in the organism and localization to target tissues, reduce their concentrations at off-target sites, and control their release. In addition, they can serve as platforms to carry not only the active peptide but also other components.^{71,98} Drug delivery platforms such as liposomes, dendrimers, emulsions, polymer nanoparticles and others have all been used as nanocarriers for the delivery of various therapeutic agents. **(Figure I.10).**⁹⁹

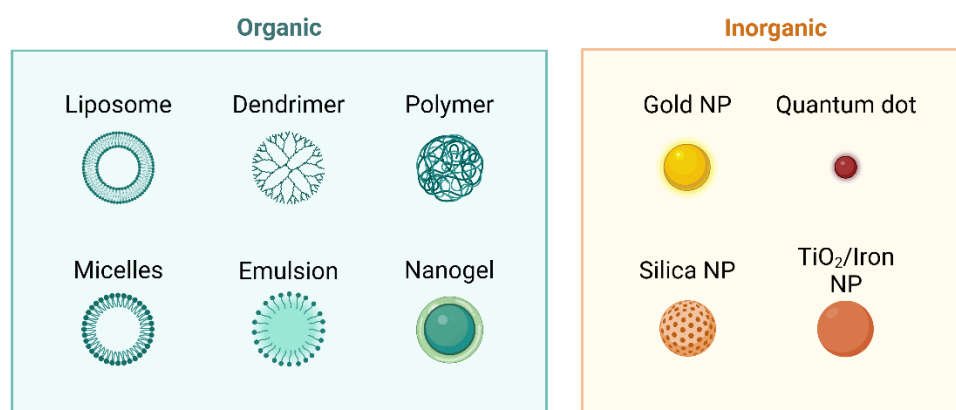


Figure I.10 Organic and Inorganic types of nanostructures that are used as delivery systems for therapeutics that include peptides (adapted in BioRender from template by Zhu et al. Recent advance in tailoring the structure and functions of self-assembled peptide nanomaterials for biomedical applications. *Coord. Chem. Rev.* **2023**, 494 2153-2174).

Nanovaccines, the subset of vaccines formulated in nanoparticles or nanomaterials in general that contain antigenic peptides, have been developed in recent years to overcome the challenges of antigen delivery and elicit a specific immune response. NPs smaller than 100 nm are able to intrinsically

improve antigen presentation by enhancing antigen uptake and internalization by APCs and facilitating maturation of dendritic cells (DCs), resulting in potent anti-tumor specific response.⁷¹

While there are many alternatives of delivery systems for peptide drugs and vaccines, in this work we will focus on two particular systems and their application: polymeric nanoparticles based on poly (lactic co-glycolic acid) (PLGA) (**Figure I.11, A**) and the lipid-based quatsomes (Qs), nanovesicles based in sterol lipids, stabilized by cationic surfactants. (**Figure I.11, B**).

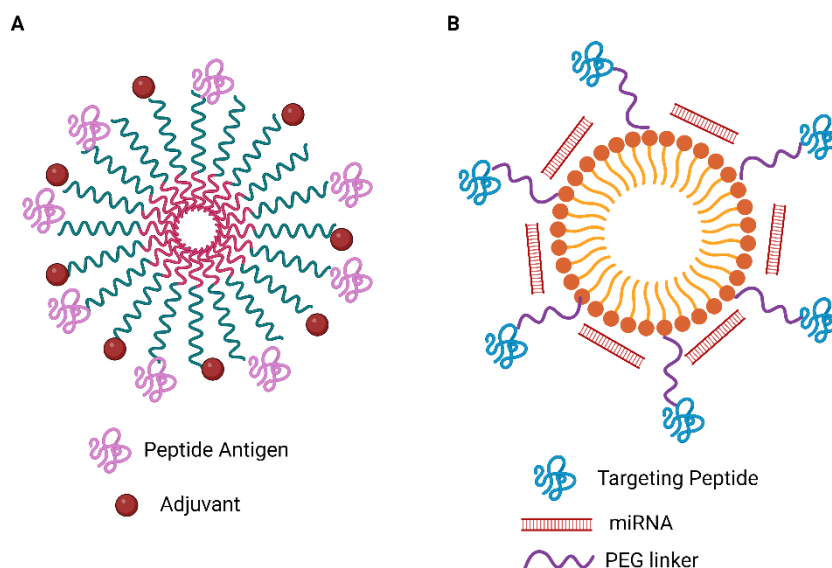


Figure I.11 Schematic representation of two delivery systems. **A:** PLGA-based formulation for nanovaccines. **B:** quatsome nanovesicle for targeting and delivery of a load.

I.4.1 Delivery systems based on PLGA nanoparticles

PLGA is a polymer with attractive properties to be used as a delivery platform, such as biocompatibility, low potential toxicity, biodegradability and hydrophilicity. It can enter cells through pinocytosis and clathrin-mediated endocytosis, allowing for well-tuned and controlled drug release.¹⁰⁰ In general, PLGA is used to produce systems for parenteral administration. Upon degradation, the constituent monomers enter normal metabolic pathways, culminating in their elimination as water and carbon dioxide, which explains their minimal systemic toxicity.¹⁰⁰ In cancer treatment research, coating PLGA with chitosan can improve targeting and delivery of NPs towards the tumor site. Chitosan is a known CD44 ligand, and thus targets cancer stem cells, which can facilitate penetration of the tumor microenvironment and like PLGA is biocompatible and biodegradable.¹⁰¹

PLGA NPs are excellent candidates for anticancer drug delivery due to their increased permeability and retention, as well as their ability to carry targeting molecules on their surface, which promotes drug release in the tumor and minimizes the deleterious off-target side effects that these drugs typically have.⁷⁴ The same is true for a PLGA-based nanovaccine (**Figure I.11, A**), as it will consist of a formulation that can carry the immunogenic peptides and adjuvants and deliver them to APCs at the site of injection. Crucially, it is an FDA-approved compound, and this fact makes it a preferred platform for nanovaccine formulations.¹⁰⁰

I.4.2 Quatsome nanovesicles for targeted delivery

Liposomes are one of the most widely used drug delivery platforms for the treatment of cancer and other diseases. Liposomes are nanovesicles formed by a phospholipid bilayer similar to a cell membrane, allowing for an aqueous pocket in which hydrophilic compounds can be encapsulated and

protected from external conditions. Additionally, hydrophobic compounds can be carried in the bilayer and delivered to biological targets. These lipid nanovesicles can fuse with cell membranes, which makes them very advantageous for the delivery of drugs and various therapeutic agents across impermeable barriers. Within this group of vesicles, we find quatsomes (QS), which are sterol-based lipid nanovesicles that self-assemble into a bimolecular lipid bilayer in aqueous media in the presence of quaternary ammonium surfactants. They have attractive properties for pharmaceutical applications, including high thermodynamic stability, remarkably homogeneous size distribution, unilamellarity, ability to encapsulate and adsorb a wide range of small molecules and macromolecules, and very good stability under in vivo conditions.^{99,102,103}

These nanovesicles have a positively charged surface, which is due to the chemical nature of the surfactant component, either myristalkonium chloride (MKC) or hexadecyltrimethylammonium bromide (CTAB). Furthermore, cholesterol, which is the sterol most commonly used to build Qs, can be switched with the 3 β -[N-(N',N'-dimethylamino-ethane)carbamoyl]-cholesterol (DC-chol), adding to the positive surface charge. This positive charge gives Qs the ability to bind negatively charged molecules to its surface via electrostatic interactions. In particular, it allows pH-dependent loading of nucleic acids, especially small and micro RNAs (miRNA), which can interfere with the proliferation of cancer cells. The pH-dependent nature of the interactions allows for controlled release into the neutral environment of the cytosol upon incorporation into the cells. This approach is ideal for the treatment of complex and aggressive cancers such as neuroblastoma and colorectal cancer.⁹⁹ The targeting of Qs to cancer cells can be achieved by introducing peptides, ligands or other molecules on their surface that can specifically bind to cell surface receptors. The idea behind this type of formulation is to parenterally inject the QS with the drug, such as miRNA, complexed on its surface and targeted to a specific tissue or cell type by the presence on its surface of peptides that are known ligands of receptors found in these tissues or cell types. This formulation will deliver the treatment upon internalization or fusion of the quatsome into the cell and release the drug into the cytosol in a pH-dependent manner. This multi-step process ensures localized and specific delivery in the target cell, which is particularly useful in cancer treatment, as conventional chemotherapeutic agents are known for their lack of specificity, leading to toxicity and various off-target side effects.

1.5 General aspects of solid phase peptide synthesis

The various therapeutic systems studied in this thesis, either cancer nanovaccines or targeted RNA delivery systems based on quatsomes, contain peptide components that were synthesized in this thesis. Their synthetic process should be optimal to produce final compounds with high yields and purities. In general, the solid phase peptide synthesis (SPPS) methodologies are used for this purpose because it is very well standardized, increasingly reliable, robust and allows the rapid modification of the sequence with natural and non-natural amino acids as well as other molecules, making it easily adaptable to the needs of the field of application.

In SPPS, the peptide chain is constructed by sequentially incorporating amino acids through an amide bond, usually from the C-terminus to the N-terminus, into a solid polymeric support, called a resin, of varying chemical nature. The most commonly used resins have polystyrene (PS) or polyethylene glycol (PEG) cores and sometimes a copolymer blend of the two, such as the TentaGel resin¹⁰⁴ (**Figure 1.12**). In general, the solid support anchors the peptide chain through a linker that can release the final peptide with a carboxylic acid or amide at the C-terminus by acidolysis treatment. The incorporation of each amino acid of the peptide sequence is maximized by the use of excess reagents, which can be eliminated along with the soluble by-products by filtration and multiple peptidyl-solid support washes with different solvents, avoiding purification steps until the peptide is complete.

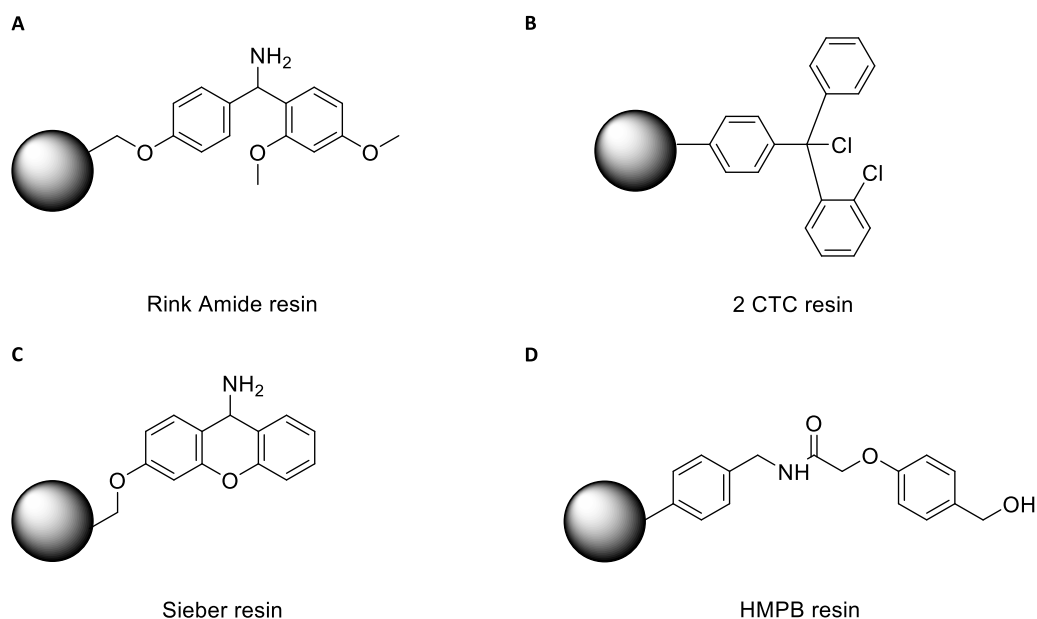
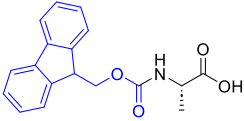
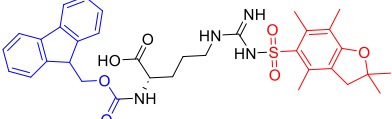
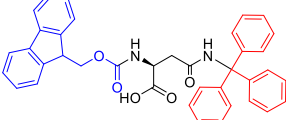
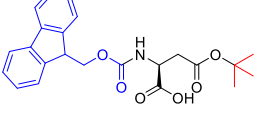
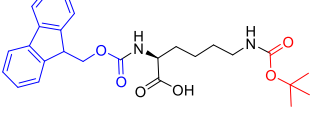


Figure I.12 Four different solid supports used in this work with **A** and **B**: PS core. **C**: Tentagel (PS/PEG) core and **D**: PEG core, providing for both **A** and **C**: amide and **B** and **D**: carboxylic acid terminus as well as **A**: high and **B**, **C** and **D**: low acid sensitivity for cleavage.

The incorporation of each amino acid during the peptide elongation lies in the coupling reaction, which consists in the acylation of the α -amine of the amino acid already incorporated to the solid support with the carboxylic acid of the next amino acid, which has been activated to a more electrophilic form, whether as an active ester, a symmetrical anhydride, an azide or an acid halide, the active ester being the most commonly used. To ensure that this acylation is selective, protected amino acid building blocks are used that contain a protecting group for the α -amine and in those amino acids with functional groups on their side chain with an adequate protecting group that is stable to the elimination conditions of the α -amine protecting group. The use of this orthogonal protection synthesis scheme is necessary to avoid secondary reactions. In the early developmental stages of peptide chemistry, the preferred scheme was the Boc/Bzl protection¹⁰⁵, in which the acid-labile *tert*-butoxycarbonyl (Boc) group served as α -amino protection and was mainly used with the much less acid-labile benzyl (Bzl) group, among others, for side chain protection. The Boc group is deprotected with a solution containing a percentage of trifluoroacetic acid (TFA), while side chain and global cleavage of the peptide from the resin is achieved with much stronger acids such as hydrogen fluoride (HF). This last key aspect of the Boc/Bzl strategy meant that while it became a very robust technique for producing high quality peptides, there were very serious safety hazards involved.¹⁰⁶ The Fmoc/*t*Bu strategy emerged as an alternative protection strategy¹⁰⁷ in which a base-labile group, the 9-fluorenylmethoxycarbonyl (Fmoc), is used as the α -amino protecting group, while the side chains carry, among other groups, the acid-labile *tert*-butyl (*t*Bu) group (**Table I.1**). The Fmoc group is eliminated by treatment with bases, usually cyclic secondary amines, of which piperidine is the reagent of choice^{108,109}, although some alternatives have been proposed over time.¹¹⁰ In contrast, global cleavage of the peptide from the resin and deprotection of side chain functions is achieved by acidolysis treatment with TFA.^{111,112} This involves less harsh conditions compared to HF treatment and fewer safety risks. Thus, the Fmoc/*t*Bu scheme is currently the preferred strategy for the preparation of synthetic peptides. The elongation of the peptide chain involves continuous cycles of removal of the Fmoc group and coupling of the incoming amino acid, ending with the acidolytic cleavage of the peptide from the resin and the global elimination of the side chain protecting groups (**Figure I.13**).

Table I.1 The 20 standard Fmoc-protected amino acids

Amino acid	Side chain protection	Example
Ala, Gly, Ile, Leu, Met, Phe, Pro, Val	Not needed	 Fmoc-L-Ala-OH
Arg	2,2,4,6,7-pentamethyl-2H-benzofuran-5-sulfonyl	 Fmoc-L-Arg(Pbf)-OH
Asn, Cys Gln, His	trityl	 Fmoc-L-Asn(Trt)-OH
Asp, Glu, Ser, Thr, Tyr	<i>tert</i> -butyl	 Fmoc-L-Asp(tBu)-OH
Lys, Trp	<i>tert</i> -butoxycarbonyl	 Fmoc-L-Lys(Boc)-OH

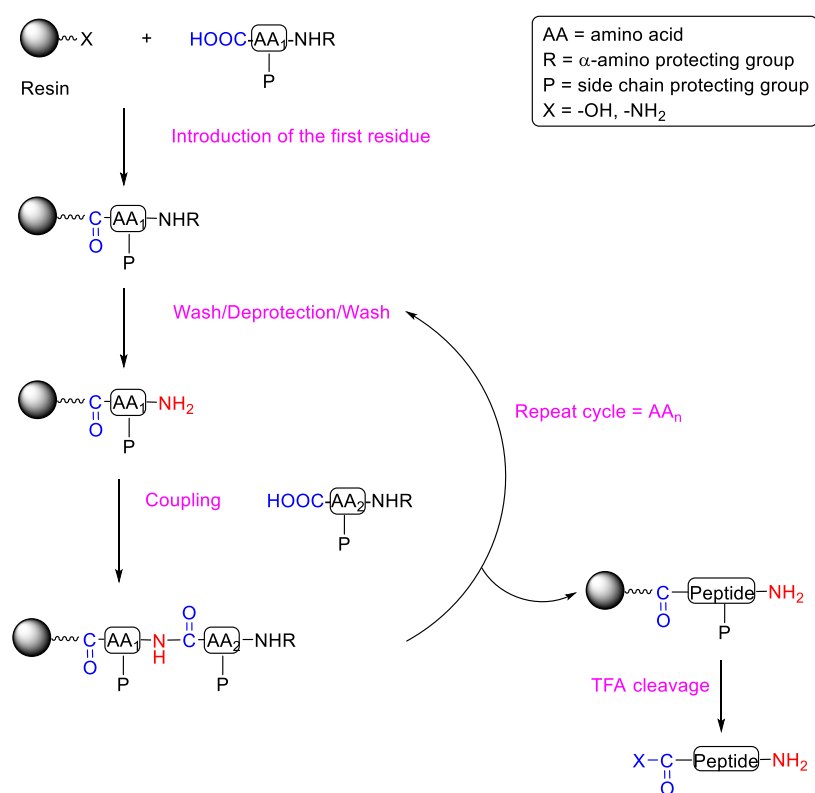


Figure I.13 General protocol for the cycles of the solid-phase peptide synthesis (adapted from, J.M. Solid-phase peptide synthesis: An overview focused on the preparation of biologically relevant peptides. *RSC Adv.*, **2014**, *4*, 32658-32672).

The elimination of Fmoc occurs via deprotonation of the 9-position in the fluorene ring by piperidine (**Figure I.14, 1**) and a β -elimination process (**Figure I.14, 2**) that releases CO_2 and the dibenzofulvene group, which is promptly captured by forming an adduct with a second piperidine molecule (**Figure I.14, 3**). Finally, the piperidine gives back an H^+ to form a free amine. (**Figure I.14, 4**).

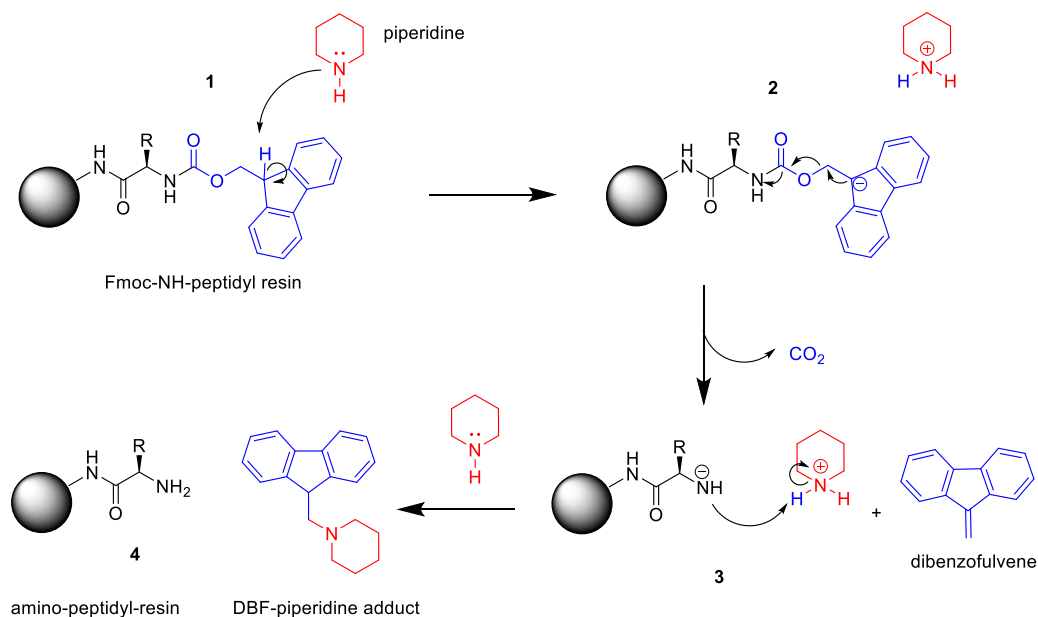


Figure I.14 Fmoc elimination mechanism.

Once Fmoc elimination is complete and the α -amine is free, the next amino acid is incorporated through a coupling reaction to produce an amide. An impressive number of coupling reagents have been developed over the decades for this purpose.¹¹³ These convert the carboxylic acid of the protected amino acid into a carbonyl with increased electrophilicity, attached to a good leaving group that can be easily attacked by the α -amine. Among the many options for coupling reagents, the most commonly used combination is that of *N,N*-diisopropylcarbodiimide (DIC)¹¹⁴ and HOBt¹¹⁵ or ethyl 2-cyano-2-(hydroxyimino)acetate (Oxyma)¹¹⁶ as summarized in **Figure I.15**. In this case, the coupling reaction begins with an attack of the hydroxyl oxygen on the electrophilic carbon of the carbodiimide (**Figure I.15, 1**), with concomitant proton removal. This produces a highly reactive *O*-acylurea, which is then attacked by the oxygen to produce a second active ester and release *N,N*-diisopropylurea (**Figure I.15, 2**). Finally, the α -amine from the amino acid previously anchored to the resin in the extended chain attacks the active ester (**Figure I.15, 3**) and acylation continues with the release of oxyma (**Figure I.15, 4**). HOBt was widely used in SPPS, however it was reported that it has potential explosive properties, which makes it hazardous to transport and store.¹¹⁷ Oxyma was developed as an alternative that presented comparable activity, without this dangerous property.¹¹⁶

When peptide elongation is complete, the final Fmoc group is removed and the finished product is cleaved from the resin with trifluoroacetic acid (TFA), which is also capable of removing the side chain protecting groups. This process generates highly reactive carbocations from these protecting groups, which must be captured to prevent their irreversible reincorporation onto functional groups of the peptide side chains. Nucleophilic molecules called scavengers are added to the cleavage mixture to react and suppress these carbocations. These have historically included many different reagents used throughout the development of SPPS^{106,111,118}, but the most commonly used for the standard protecting groups are H_2O and triisopropylsilane (TIS).

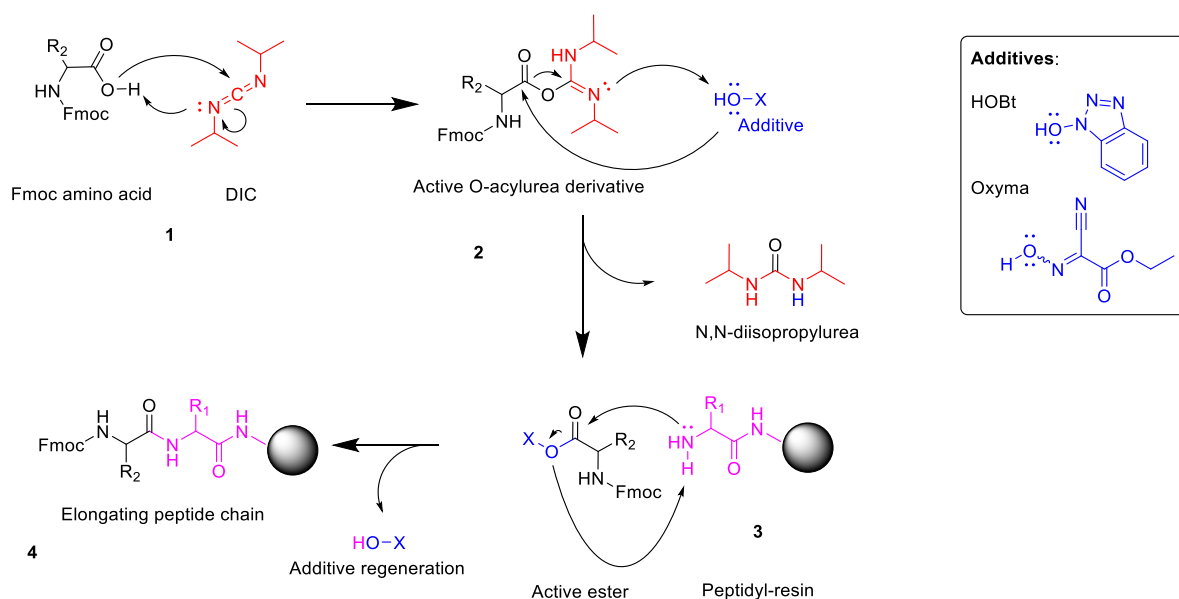


Figure I.15 Mechanism of the coupling reaction between two amino acids using DIC and oxyma or HOBt as additives.

When cysteine and methionine are present in the sequence, additional stronger nucleophiles must be added because their thiol and methylthio functions are easily alkylated under acidic conditions. A suitable reagent for this purpose is 1,2-ethanedithiol (EDT), which also acts as a strong reducing agent to prevent reactions of the free thiol moieties of cysteine or the oxidation of methionine. TFA plays three important roles in the process: it provides protons for acid cleavage, it acts as an excellent solvent for peptides, scavengers, and by-products, and it also acts as a scavenger itself.

Both cleavage and removal of sidechain protecting groups by TFA occur by similar mechanisms: the carbonyl oxygen is protonated by TFA, withdrawing an electron pair from a carbon in either the resin linker (**Figure I.16, 1 and 2**) or the protecting group (**Figure I.16, 3**). The linker (**Figure I.16, 2**) and protecting groups are released as carbocations that are rapidly captured by nucleophilic scavengers (Nu) (**Figure I.16, 4**), leaving the cleaved, unprotected peptide as the final product (**Figure I.16, 5**). Note that the resin linker can also be cleaved at a few additional sites (**Figure I.16, 2**). Once the crude peptide has been analyzed and purified, it can be used for several applications.

SPPS has become a staple in the production of bioactive peptides because its processes allow for relatively quick and quantitative production of peptides with high purity and very well characterized identity. Introducing modification to the sequences is easy, whether it is the use of D-enantiomeric, non-standard and/or non-natural amino acids, N-terminal modifications such as acylation or C-Terminal modifications such as switching from carboxyl to amide or thioester.¹¹⁹ The known advantages and flexibility of the synthetic protocol for peptides compounds is at the base of its choosing in this project for the production of both antigenic components of nanovaccines aimed at the immunotherapeutic treatment of PDAC as well as the production of targeting peptides and strategies to conjugate it into quatsome nanovesicles for the treatment of neuroblastoma.

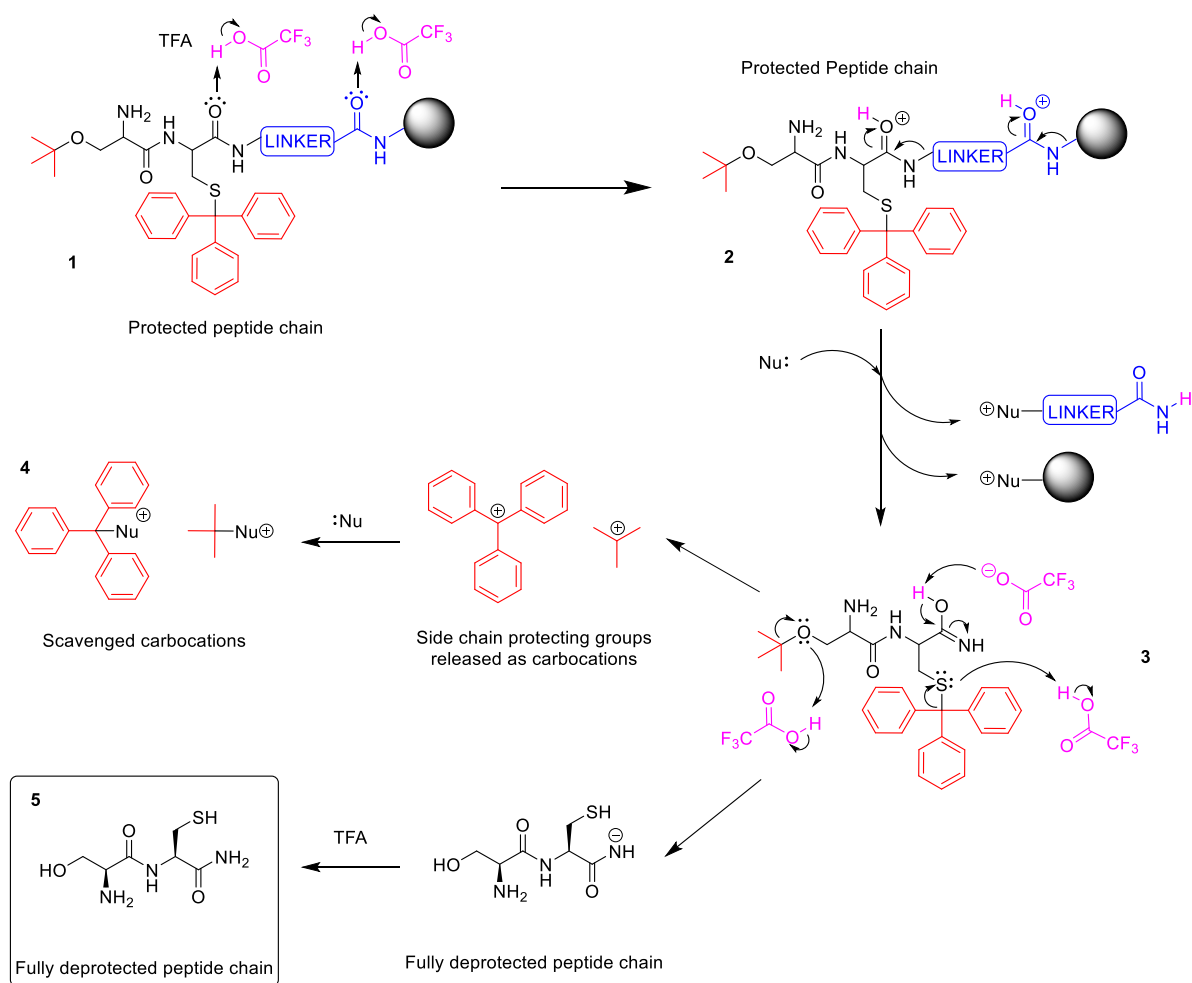


Figure I.16 Mechanism for the cleavage and global deprotection of a dipeptide from a Rink Amide resin using TFA and scavengers.

I.6 By-production of hydrogen cyanide by a secondary DIC/Oxyma reaction

Oxyma provided a solution to the safety concerns raised by the use of HOBT, serving as a suitable replacement for this compound due to its performance, solubility, and comparable cost. It was therefore widely used in SPPS, and for more than a decade SPPS has relied on the DIC/oxyma coupling mixture due to its remarkable performance.¹¹⁶ It should be noted, however, that HOBT remains the reagent of choice for solution chemistry and is now commercialized as a monohydrate to minimize its explosive properties.

Despite the many benefits that oxyma has brought to peptide synthesis, it was reported in 2019 that an unwanted byproduct, hydrogen cyanide HCN, can be formed.^{120,121} Hydrogen cyanide is a toxic compound that is gaseous, rapidly penetrates mucosal membranes, and interferes with respiratory metabolism by disrupting the normal function of electron chain transport.¹²²

When working at the research scale, the amount of HCN generated is likely to be negligible and easily removed under a fume hood. However, the safety situation changes when industrial facilities are used. The larger scales involved may present a safety hazard that must be considered. For this purpose, commercially available alternative carbodiimides can be tested against oxyma to see if a candidate can be found that does not show this side reaction while showing synthetic performance comparable to that of DIC.

Objectives

The aim of this work is to produce synthetic peptides for use as immunogenic components in a nanovaccine formulation and as targeting moieties in a nanovesicle formulation for the treatment of two types of cancer, pancreatic ductal adenocarcinoma and neuroblastoma. In parallel, an alternative coupling reagent to N,N-diisopropylcarbodiimide for standard peptide synthesis protocols is explored to avoid the release of HCN generated in the coupling step.

The specific objectives of the present thesis are:

- 1.- Synthesize different chemical presentations of selected immunogenic tumor-associated peptide antigens or neoantigens and epitopes expressed in human PDAC to bind both MHC I and MHC II. PGLA-based multi-component nanovaccines will be formulated with the best antigen peptide presentations and evaluated in vitro and in vivo in a mouse model.
- 2.- Synthesize targeting/homing units that bind various overexpressed proteins in neuroblastoma cells and evaluate their internalization ability. The targeting/homing units with the best internalization properties will be conjugated to a quatsome nanovesicle system to produce a targeted miRNA delivery system.
- 3.- Development of a synthesis methodology to reduce HCN formation in carbodiimide/oxyma-based peptide synthesis protocols by evaluating different carbodiimides.

Chapter 1

Synthesis of antigenic peptide components of a pancreatic cancer nanovaccine

1.1 Introduction

1.1.1 Pancreatic ductal adenocarcinoma (PDAC): epidemiology and treatment challenges.

1.1.1.1 PDAC characteristics, epidemiology and clinical presentation.

Pancreatic ductal adenocarcinoma (PDAC) is a very aggressive form of cancer that accounts for 90% of all cases of pancreatic cancer.⁵ PDAC is an ailment with very low five-year survival rate, which has reached a 10% in 2020.^{4,5,123} It is currently the seventh leading cause of cancer-related deaths, and it is estimated that it will become the second leading cause by 2030.⁵ Specifically, in Western European countries, the incidence of PDAC has generally increased over the last decade, reaching a 14% in countries such as Germany.⁷⁻¹⁴

The high mortality rates can be explained by a variety of compounding factors. Biologically, PDAC presents a complex tumor microenvironment (TME) with a dense, reactive tumor stroma composed of activated stellate cells, cancer-associated fibroblasts, and leukocytes (**Figure 1.1**).⁸³ The TME promotes peritumoral fibrosis and poor vascularization, resulting in a mechanical barrier that impedes the reach and access of both chemotherapeutic agents and tumor-infiltrating lymphocytes (TILs).^{81,124} Clinically, PDAC presents with non-specific symptoms and is difficult to diagnose in its early stages. When the tumor expands sufficiently, contact with local blood vessels and some major blood vessels further complicates surgical removal.¹⁵

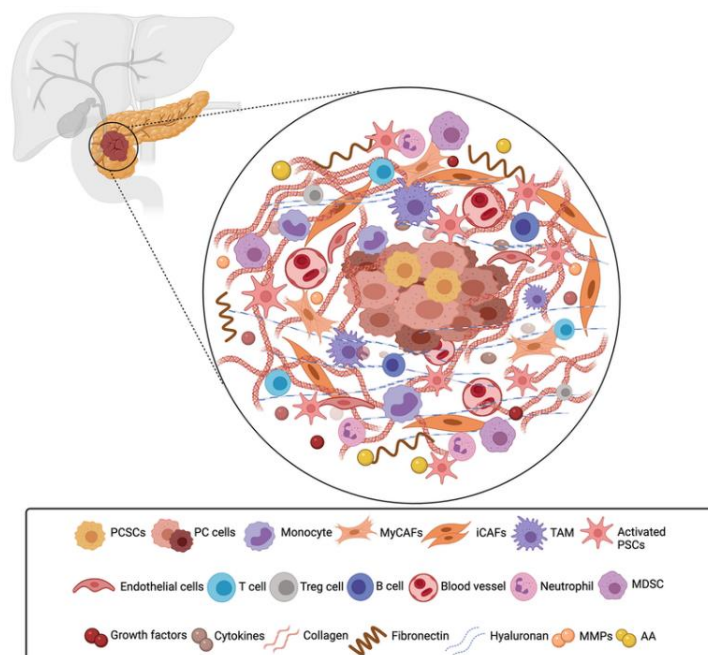


Figure 1.1.- Structure and cell composition of the PDAC tumor (figure extracted from K. Patil et al., The plasticity of pancreatic cancer stem cells: implications in therapeutic resistance. *Cancer and Metastasis Reviews*. **2021**, *40*, 691-720).

As a result of these various interacting characteristics of the PDAC tumor is that 50% of patients have metastatic disease at diagnosis, 30% have locally advanced disease and only 20% have surgically resectable tumors.^{6,16} Surgical removal of the tumor increases the 5-year survival rate to 25%.⁶ The majority of PDAC patients are treated with chemotherapy throughout their treatment. In addition, the standard and well-known treatments available, such as chemotherapy, become much less effective at this late stage. In addition, multidrug resistance to classic anticancer drugs has been reported in PDAC

5-fluorouracil is also a thymidylase synthase inhibitor and shows similar effects to gemcitabine, but it can also be incorporated as a metabolite in during RNA synthesis instead of uracil, which has direct cytotoxic effects on the tumor cell. The mechanisms by which tumor cells resist this drug are not yet known.¹²⁶

Irinotecan is a prodrug of SN38, a topoisomerase I inhibitor, which inhibits DNA synthesis during the S phase of the mitotic cycle leading to cell cycle arrest and apoptosis. The mechanisms of resistance are not clear, although it has been proposed that the SN38 is exported by an efflux pump and that topoisomerase I is mutated in tumor cells.¹²⁶

Finally, **oxaliplatin** is a platinum-based anticancer drug that is proposed to be a DNA crosslinker. Modification of the DNA strands lead to cell cycle arrest and apoptosis. Resistance to these drugs has largely been associated with a variety of transporter proteins. It is noteworthy that this compound is not effective on its own and is always used in combination.¹²⁶

The Treatment of PDAC (**Figure 1.3**) is now largely relegated to chemotherapy, which is used as multi-agent therapy to avoid the many resistant tumor phenotypes that PDAC patients present to the individual drugs. Primarily, 5-FU, irinotecan and oxaliplatin are combined along with folinic acid (which enhances the activity of 5-FU) in a combination chemotherapy regimen called **FOLFIRINOX**. Depending on the case, this combination strategy may also include the other two drugs mentioned above.¹²⁶

While chemotherapy in a combination regimen represents an improvement in survival for PDAC patients, this improvement remains modest. The normal prognosis for PDAC is a median survival of only 12 to 18 months. The 5-year survival rate is improved to 25% with combination chemotherapy t after surgical resection and to 21.8% with combination chemotherapy alone.¹²⁶

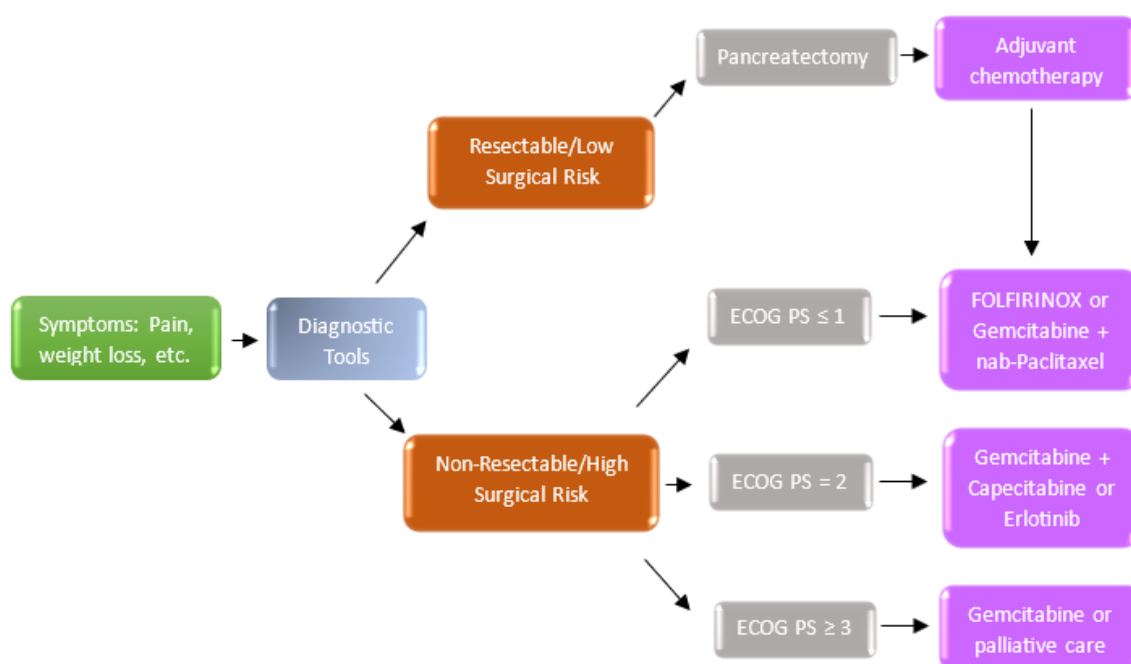


Figure 1.3 General treatment guidelines for PDAC patients. Treatment applied depends on Eastern Cooperative Oncology Group Performance Status (ECOG PS) where ECOG PS = 0 is a fully active patient, while ECOG PS = 4 is a severely disabled patient incapable of self-care (figure adapted from D. Principe et al., The current treatment paradigm for pancreatic ductal adenocarcinoma and barriers to therapeutic efficacy. *Front. Oncol.* **2021**, *11*, 688377).

Given that only 20% of patients are candidates for surgery, chemotherapy remains the best available treatment for the majority of patients. However, chemotherapy is associated with severe toxic side effects. To cite just one such side effect, multi-agent chemotherapy has been reported to increase grade 3 neutropenia (a decrease in circulating white blood cells) from 27% to 38%.¹²⁶

The best available treatment of PDAC with aggressive cytotoxic agents has not been shown to provide clinically relevant improvements for PDAC patients. Therefore, it is important to explore new treatment alternatives.

1.1.2 Immunotherapy and peptide-based vaccines

Immunotherapy is a type of treatment that aims to modulate the immune system to control a disease. In the case of PDAC, immunotherapy uses various means to target and eliminate tumor cells. Immunotherapy has many advantages over radiation and chemotherapy because it has fewer harmful side effects.^{3,69} In addition, it is selective towards tumor cells.³⁴⁻³⁷ This results in good patient tolerability. As mentioned in the introduction, there are several types of immunotherapies:

Monoclonal antibodies (mAbs)¹²⁵ bind specific tumor antigens and mark the tumor cell for elimination.

Immune checkpoint inhibitors (ICIs)^{82,87} block regulatory checkpoint proteins of the immune response, preventing downregulation and thus maintaining the strength of the immune response.

T-cell transfer (CART)^{82,127}, or immune cell therapy, relies on treating the patient with his or her own T- cells, which are collected and expanded in the laboratory before being reintroduced into the patient's body to directly eliminate cancer cells.

RNA therapy¹²⁸ can promote the expression of pro-inflammatory cytokines or directly suppress the expression of oncogenes.

Cancer vaccines^{82,86} aim to train the patient's immune system to recognize and attack cancer cells by targeting specific antigen epitopes on tumor cells. The goal is to generate TILs that can reach and penetrate the tumor to exert this cytotoxic effect. They can be based on peptides or protein antigens.

Of these alternatives, mAbs and T-cell therapy are slow and expensive to produce. ICIs have not shown good results in pancreatic cancer in a sufficient number of patients. An mRNA vaccine has shown promising results, but only in a very limited trial.⁸⁸ In several conducted studies, peptide/protein-based vaccination strategies have been established to yield antigen-specific immune responses in patients with PDAC.¹⁸⁻²⁰ Thus, peptide-based cancer vaccines remain a good avenue of PDAC treatment research.

However, despite their good initial results and positive immune responses in early phase trials, many vaccines that have advanced to Phase III trials including TeloVac (anti-telomerase), PrimoVax (anti-telomerase), PANVAC-V (anti-CEA and anti-MUC1) and algenpantucel-L (against two allogeneic PDAC cell lines) failed to show significant clinical results.^{21,86}

Therefore, it is necessary to perform adequate selection, design and synthesis of its antigenic components so that initial good immune responses can be maintained all the way throughout clinical trials.

1.1.3 Selection of antigens for a peptide-based PDAC vaccine

To overcome the problem of poor immune recognition of PDACs, researchers have explored various vaccine therapies to enhance antigen presentation and tumor-specific T-cell activation^{68,70} as a way to induce a new response or boost existing immune responses. Strategies targeting PDAC-associated antigens, such as telomerase^{82,129}, K-Ras,^{129–132} MUC1^{82,129}, and mesothelin^{133–137} have included peptide-based vaccines, virus-based vaccines, DNA-based vaccines (neoantigens), and cell-based vaccines.⁸⁶

The lack of success of candidates that reach Phase III trials can be explained by the nature of the tumor and its microenvironment. PDAC is a complex and heterogeneous tumor, which makes its antigenic profile very diverse. First, the tumor supports a mechanical barrier.⁸³ But more importantly, it recruits immune cells with down-regulating functions during development.⁸¹ This results in a highly immunosuppressive environment in which the tumor can thrive without interference from the immune system. It is therefore critical to enhance the response by appropriately selecting, modifying and presenting antigens in the most optimized manner to generate a potent and durable immune response that overcomes the low immunogenicity of the tumor and the immunosuppressive TME.

Choosing the appropriate targets for immunization is crucial. There are some markers in PDAC tumor cells that are more commonly reported in the literature. One such surface antigen is mesothelin (MLSN), a 40 kDa protein with proposed functions related to proliferation, growth, and adhesion signaling.¹³⁵ Mesothelin is a tumor differentiation antigen, which is highly expressed in several solid neoplasms, including pancreatic, ovarian, and lung cancer and non-solid ones like hematologic cancers.^{134,135} Due to its selective expression on malignant cells and on only a limited number of healthy tissues it has become an interesting candidate for a therapeutic target. A second such candidate is K-Ras, a GTPase that transduces signals from cell surface receptors to cytoplasmic signaling effector proteins, such as mitogen-activated protein kinase (MAPK) and phosphoinositide 3-kinase (PI3K), and is thus also associated with to mitogenic stimuli.¹³¹ In addition to overexpression of the wild-type K-Ras protein, PDAC often has a neoantigenic form (G12D mutation) and thus can act as both a broad antigen target and as a specific tumor marker by synthesizing the target sequence with a simple amino acid switch.^{130,132} Other targets include six short sequences that comprise a formulated vaccine named OCV-C01.¹³⁸ This formulation includes some TAAs and, more interestingly, also targets the VEGFR-1 and -2 proteins, which are related to angiogenesis, and consequently vascularization of the tumor. So, the goal is to also target the tumor microenvironment and not just the tumor cells.

1.1.4 Types of antigens for peptide vaccine components. Limitations and solutions

A cancer vaccine must be formulated to target either self-antigens overexpressed in the tumor cell called tumor-associated antigen (TAA)⁸⁹ or mutated surface proteins specific to the tumor called tumor-specific antigen or neoantigen (TSA).^{89,90} The limitation with TAAs is the low immunogenicity of self-antigens. While with TSAs for the PDAC tumor the mutation frequency is low, compared to other types of cancer, such as lung cancer. Such low levels of mutated proteins on the surface of cells means that the immune response that is generated against them is essentially ineffective.⁶⁹ Furthermore, in both cases, the antigenic profile of tumor cells can change over time until an initially successful vaccine becomes obsolete and tumor growth resumes.⁶⁹ Several strategies have been explored to overcome these problems and ensure the vaccine efficacy.

1.1.4.1 N-terminal modifications to improve immunogenicity

First-line solutions include formulation improvements. For example, the use of appropriate human compatible potent adjuvants, for instance, is a must.¹³⁹ However, the modification of the peptide

component is one of the most explored strategies to modulate its antigenicity, and usually this modification is placed at the N-terminus of the peptide.

One such example is acylation of the N-terminus with a fatty acid. It has been reported that palmitoylation (C16) increases the immunogenicity of peptides^{140,141} although the mechanisms by which this occurs are not very clear, with some proposing a TLR-4 dependent pathway¹⁴¹ and others and suggesting improved presentation via an endocytic-independent pathway.¹⁴⁰ Other fatty acids have been used for similar purposes with varying results, some positive, some negative, depending on the length and position of the modification.¹⁴⁰

PEGylation is another commonly used N-terminus modification for therapeutic peptides and proteins.¹⁴² This modification is straightforward and aims to increase the half-life of the peptide by increasing its hydrodynamic radius, thereby protecting it from degradation and reducing its renal clearance. PEG moieties are also non-immunogenic in most cases.¹⁴²

1.1.4.2 Mode of presentation to improve immunogenicity

In addition to direct modifications, another option is to construct chimeric peptides carrying 2 or more epitopes, from the same or different antigens, and capable of binding either MHC I or MHC II, so that antigen presentation can activate both a Th CD4+ and a Tc CD8+ response. On paper, this allows for a more durable sequence with respect to enzymatic degradation due to its length, capable of presenting a combined multi-targeting scheme that activates multiple key immunological response pathways.

Another option is to generate a multiple antigenic peptide (MAP), which is used as a vaccine component to induce immunoglobulin production^{94,95,143}, instead of a linear antigenic peptide. MAPs are advantageous over linear peptide antigens because of their high molar ratio, which in some cases approaches the size and potency of proteins.⁹⁴ This overcomes the low immunogenicity of some single epitope peptides and eliminates the need to conjugate these peptides to carrier proteins. In addition, MAPs present multiple copies of the antigenic peptides because they consist of a branched scaffold based on a lysine core that can be used to anchor multiple identical or different peptide sequences (≤ 8). MAPs can be produced in their entirety by linear solid-phase peptide synthesis (SPPS), or the core and peptides can be produced separately by SPPS and then condensed by chemical ligation.⁹³ The latter strategy is preferred because it allows rapid assembly of MAPs, avoids amino acid deletions due to increased steric hindrance, and the possibility of aggregation in the branched structure. Crucially, chemical ligation can allow the integration of different peptide sequences and/or chromophores or other molecules of interest for targeting and delivery.

The design of peptide vaccine components proposed in this study includes both single epitope peptides, linear multiple epitope peptides, and multiple antigen peptides (MAPs). This design includes peptides containing more than one epitope, such as a chimeric construct with a cathepsin-like cleavage Lys-Lys motif¹⁴⁴ for lysosomal processing and subsequent presentation by antigen presenting cells (APCs). The design and selection of peptide epitopes and their modifications then follow a logic of multi-pathway enhanced activation of the immune response, both Th CD4+ and Tc CD8+ lymphocytes that can target and eliminate the tumor cells. In this work, MHC I epitopes were combined with the MHC II epitope of tetanus toxoid. Tetanus toxoid is a peptide sequence that has been used and reported to induce immune responses by priming the Th-dependent pathway.^{145,146}

1.1.4.3 Advantages and limitations in the production of peptide vaccine components

Peptide components are a class of compounds that represent a compromise between the specificity and biocompatibility of macromolecules, such as proteins and nucleic acids, and the relative ease and

lower cost of design and production associated with small organic molecules, making them a robust alternative for many bio-applications, including vaccines^{129,147,148}. Solid phase peptide synthesis (SPPS) has become the go-to strategy for the production of peptide components since its introduction, because it is a technique that combines some very solid, well-studied chemistry on amide bond formation strategies with a surprising degree of adaptability that has allowed for continuous improvement over the decades. This is evidenced by an ever-expanding array of solid supports, reagents, and solvents that address minimization of side reactions, speed of reaction, purity of intermediate and final products, ability to produce long and short sequences, and, more recently, more environmentally friendly methods.¹⁴⁹ In addition, the peptide itself is a highly modular molecule, and residues can be substituted as needed, not only within the 20 standard amino acids, but also with other non-conventional or even non-natural amino acids. In addition, non-amino acidic modifications can be easily introduced. Thus, the variety of modified products that can be obtained is a very attractive feature of the peptide synthesis process.

However, long peptide sequences in general can be challenging, especially if they contain numerous hydrophobic residues.^{150,151} When finding these types of sequences, it is critical to optimize the entire synthetic process to obtain the product with the highest possible purity and yield. From the resin selection to the identification of difficult couplings, the synthetic process requires constant monitoring and modulation, which is fortunately where SPPS excels.

1.1.5 Poly(lactic-co-glycolic) acid nanoparticles (PLGA-NP) as a vaccine delivery system

The success of a vaccine depends on the appropriate delivery of the active peptide component. A well-known delivery system, poly(lactic-co-glycolic) acid nanoparticles (PLGA-NP), was chosen for this purpose. PLGA is a polymer with attractive properties for use as a delivery platform, such as biocompatibility, hydrophilicity, low potential toxicity, and it is readily biodegradable. PLGA-NP can enter cells through pinocytosis and clathrin-mediated endocytosis, allowing for well-tuned and controlled drug release.¹⁰⁰

PLGA-NP can be prepared by various formulation techniques such as emulsification, nanoprecipitation, dialysis, or spray drying. Emulsification (**Figure 1.4, A**) is the most commonly used method for nanoparticle production, in which the drug and polymer are dissolved in an organic solvent and then mixed with an aqueous solution containing a surfactant. The mixture is homogenized, and the solvent is evaporated to collect the final nanoformulation.

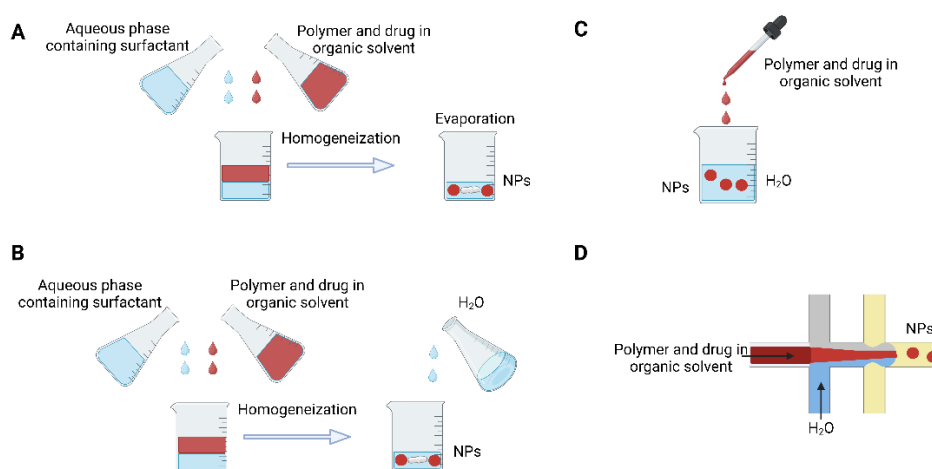


Figure 1.4 Methods of production of PLGA nanoparticles: **A:** emulsification, **B:** salting out, **C:** dialysis and **D:** spray drying (adapted from S. Rezvantlab et al., PLGA-based nanoparticles in cancer treatment. *Front. Pharm.* **2018**, *9*, 1260).

Upon degradation of PLGA, the monomers enter normal metabolic pathways, culminating in their elimination as water and carbon dioxide, which explains their minimal systemic toxicity.^{100,152} In cancer treatment research, coating PLGA with chitosan may improve the targeting and delivery of NPs to the tumor site. Chitosan is a known CD44 ligand and thus targets cancer stem cells, which can facilitate penetration of the tumor microenvironment, and like PLGA, is biocompatible and biodegradable.¹⁰¹

PLGA-NPs are excellent candidates for anticancer drug delivery due to their increased permeability and retention, as well as their ability to carry targeting molecules on their surface, which promotes drug release in the tumor and minimizes the deleterious off-target side effects that these drugs typically have.⁸⁶ The same is true for a PGLA-based nano-vaccine, as it will consist of a formulation that can carry the immunogenic peptides and adjuvants and deliver them to APCs at the site of injection. Crucially, it is an FDA-approved compound, and this fact makes it a preferred platform for nanovaccine formulations.⁸⁵ In addition to the formulation of adjuvants, the incorporation of nanoparticles aims to achieve the best possible result in delivering the active agent to the site of action, protecting its cargo from degradation and generating a strong and tumor-selective or even tumor-specific immune response.

1.2 Results and Discussion

1.2.1 Design

For the present work, epitope sequences were selected from the proteins mesothelin (MSLN), Kirsten rat sarcoma virus (K-Ras), tetanus toxoid (TT), and peptides formulated in the OCV-C01 anticancer vaccine. The selected epitopes were predicted to induce an immune response using publicly available epitope prediction servers^{153,154} namely SYFPEITHI¹⁵⁵ and BIMAS¹⁵⁶, as well as consideration of existing literature (Table 1.1).

Table 1.1 peptide constructs synthesized for a PDAC nanovaccine candidate.

Epitope	Sequence	Construction
MSLN1	PLTVAEVQKLLGPHV	
MSLN2	ALPLDLLLFL	Tumor-associated antigen
MSLN3	SLLFLLFSL	
MSLN4	PLTVAEVQKLLGPHVKKALPLDLLLFLKKSLLFLLFSL	Chimera combining MSLN1, 2 and 3 epitopes through a cathepsin-like KK cleavage motif
TT1	QYIKANSKFIGITEL	T-Cell epitope
K-Ras1	MTEYKLVVVGAGGVGKSALTIQLIQ	Tumor-associated antigen
K-Ras2	MTEYKLVVVGADGVGKSALTIQLIQ	Neoantigen
K-Ras3	MTEYKLVVVGAGGVGKSALTIQLIQKKQYIKANSKFIGITEL	Chimera combining K-Ras 1 and TT epitope through a cathepsin-like KK cleavage motif
K-Ras4	MTEYKLVVVGADGVGKSALTIQLIQKKQYIKANSKFIGITEL	
OCV1	KVYLRVRPLL	
OCV2	SYGVLLWEI	Tumor-associated antigen
OCV3	RFVDPGNRI	
OCV4	KVYLRVRPLLKKSQYGVLLWEIKKRFVDPGNRI	Chimera combining epitopes OCV1, 2 and 3 through a cathepsin-like KK cleavage motif

The mesothelin epitopes were synthesized in different formats: Single epitopes (MSLN1, MSLN2, and MSLN3), a linear multiepitope (MSLN4) combining the three single epitopes, and an attempt at a multimodal multivalent (MAP). These peptides were also synthesized with an unmodified, palmitoylated or PEGylated N-terminus. Similarly, OCV epitopes were synthesized in two formats, as single epitopes (OCV1, OCV2, and OCV3) and as a linear multiepitope (OCV4) combining the three single epitopes. Finally, the K-Ras epitopes were also synthesized in two formats, the single epitopes (K-Ras1 and K-Ras2) and hybrid linear multiepitope peptides combining a K-Ras epitope with the tetanus toxoid epitope (K-Ras3 and K-Ras4). All these forms of presentation are aimed at increasing the immunogenicity of the potential nanovaccine formulation.

1.2.2 Synthesis of the different peptide vaccine components

To produce the peptide sequences selected and designed sequences a Solid Phase Peptide Synthesis (SPPS) protocol was followed⁹¹ following a standard Fmoc/tBu protection scheme⁹² and microwave-assisted/automated approaches were applied for the synthesis of some peptides.

The use of Tentagel (PEG-PS) or PEG-based resins of low loading and high-swelling capacity for the synthesis of these peptides was deemed the preferable choice. The reasoning behind this choice is multi-factorial: 1) The generally hydrophobic nature of the sequences, with repetitive hydrophobic motifs, which makes them prone to in-resin aggregation and thus to deletions.^{150,151,157} 2) It is noted that the presence in most of these of β -branched amino acids (Ile, Thr and Val), sometimes in repetitive segments, makes sequential couplings difficult due to a sterically hindered substituent near the carboxyl group.⁹⁰ 3) The intrinsic propensity of some of the sequences to aggregation, which complicates both synthesis and purification. 4) The length of some antigenic peptides as the chimeric constructs (38 to 42 residues). This is not difficult to understand, as if each coupling reaction is carried out to 99.0% or 99.9% completion, the remaining 0.1% or 1% accumulates over time, increasing with each consecutive coupling. The more couplings are needed to finish a synthetic peptide, the lower the yield and the greater the chance of deletions and truncated sequences. This issue is further complicated by all the previously mentioned problems.

Microwave-assisted automated synthesis in Liberty Blue™ equipment (CEM Corp., USA) is faster and allows easier scale-up, and while it is always necessary to fine-tune methods, it is the best overall strategy for the synthesis of practically all the antigenic peptides designed.

1.2.2.1 Synthesis of Mesothelin (MSLN) peptides

Mesothelin epitopes frequently reported as immunogens in PDAC phenotypes were selected and synthesized in a 0.1 mmol scale. Three small epitopes, MSLN1, 2 and 3 were synthesized individually with free N-terminus amine or PEGylated and palmitoylated at this position. A multiepitope linear peptide, MSLN4, was also synthesized combining MSLN1, 2 and 3 in a single sequence. These epitopes were joined by a cathepsin-like KK cleavage motif. MSLN4 was also synthesized with its N-terminus position as free amine, PEGylated or palmitoylated, to compare their capacity for activating an immune response in a murine model and prove the validity of these modifications.

All peptides were synthesized automatically using a Fmoc Rink Amide ProTide LL resin (0.18 mmol/g loading, 100-200 mesh). PEGylation and palmitoylation steps were performed manually using monodisperse Fmoc-PEG₂₃-propionic acid and palmitic acid, respectively. Once the peptides were cleaved from the resin, their crudes were characterized HPLC and LC-MS and purified by semi preparative HPLC. The crude yield and recovery of the synthesized peptides are summarized in **Table 1.2**.

The results of the analysis of the crude peptides show an erratic synthetic performance. For example, all palmitoylated peptides showed lower yields and recoveries compared to amine free and PEGylated peptide versions.

Table 1.2 Summary of yield, purity, and solubility of synthesized MSLN peptides

Epitope	ID	N-terminal	MW (Da)	% Crude Purity	% Crude Yield ^a	% Final Purity	% Recovery ^b
MSLN1	P1	NH ₂ -	1599.9	84	67	100	37
	P2	PEG23-NH-	2728.3	81	68	100	24
	P3	Palmitoyl-NH-	1838.4	83	38	95	22
MSLN2	P4	NH ₂ -	1126.5	82	78	99	61
	P5	PEG23-NH-	2254.8	86	63	96	70
	P6	Palmitoyl-NH-	1364.9	76	55	99	23
MSLN3	P7	NH ₂ -	1051.3	56	33	95	11
	P8	PEG23-NH-	2179.7	55	40	95	33
	P9	Palmitoyl-NH-	1289.8	75	27	98	47
MSLN4	P10	NH ₂ -	4256.4	71	41	73 ^c	19
	P11	PEG23-NH-	5384.7	81	56	100	36
	P12	Palmitoyl-NH-	4494.8	57	28	97	53

^a% yield = (crude mmol x crude purity) / (theoretical mmol)

^b% recovery = (purified mmol x purified purity) / (crude mmol x crude purity) x 100

^cCannot be purified to more than 90% due to a des-Leu impurity. Gelates in water/acetonitrile at high concentrations

Since the automated peptide synthesis process for the same base sequence is the same up to the final modification of the N-terminus, the variation in yield of the peptide can be explained in relation to the N-terminal modification and its effect in the efficiency of the cleavage from the solid support and/or the following work-up. It is not too plausible to think that cleavage from the resin is particularly different among the variants as the acydolysis treatment used in the peptide cleavage is an optimized process. Therefore, these results may be attributed to the work-up after cleavage and more specifically, to the precipitation in cold diethyl ether. Palmitoylated peptides show a markedly increased hydrophobicity which can cause incomplete precipitation in diethyl ether unless TFA is removed by evaporation first. This requirement is not common for most cleaved synthetic peptides, which normally precipitate readily in cold diethyl ether. Therefore, the lower yields observed are most likely explained by losses of the peptide in the diethyl ether precipitation and also in the subsequent washes. Moreover, it is worth noting that the sequences themselves exhibit high hydrophobicity, as indicated by their negative hydrophilicity scores (**Table 1.3**). Specifically, the base sequences of MSLN 2, MSLN 3, and MSLN 4 are predominantly composed of 66-90% of hydrophobic amino acid residues (**Table 1.3**). This makes precipitation challenging even in the absence of fatty acids, as we observed in situ. This problem is a hallmark of hydrophobic peptides whereas most peptides carry enough polar and charged residues to not be semi-solvated by diethyl ether and thus can precipitate. It is clear that the palmitoyl moiety increased the hydrophobicity of the sequence and made it more difficult for these peptides to fully precipitate in diethyl ether when TFA is present, because it is an excellent solvent for peptides. If the TFA is evaporated prior to the precipitation step, this process is improved, but the subsequent washes with diethyl ether are still a likely source of product loss.

Table 1.3 Hydrophobicity of mesothelin epitopes.

Epitope	Sequence	Length	% Hydrophobic residues ^a	Hydrophilicity Score ^b
MSLN1	PLTVAEVQKLLGPHV	15	60	-0.34
MSLN2	ALPLDLLLFL	10	90	-1.08
MSLN3	SLLFLLFSL	9	78	-1.49
MSLN4	PLTVAEVQKLLGPHVKKALPLDLLLFLKKSLLFLLFSL	38	66	-0.46

^aPeptide relative hydrophobicity (% hydrophobic residues) was calculated using: peptide2.com hydrophobicity calculator

^bHydrophilicity scores calculated via the BACHEM peptide calculator tool (<https://www.bachem.com/knowledge-center/peptide-calculator/>).

Another issue that we found during cleavage, when characterizing the crude product is the propensity of the MSLN3 and MSLN4 peptides to undergo trifluoroacetylation when the amine is not capped. This is noted as a +96 Da impurity that can be prominent. A direct modification of this amine can be thought of, although it is very unlikely that this will happen in the very acidic environment provided by TFA. Other possible residues that can be trifluoroacetylated are the Ser and Thr residues⁹⁴ as these are present in the MSLN3 and MSLN4 peptides that underwent this modification, although it is unclear to us why this happens when the N-terminal amine is not capped. Optimizing the cleavage and reducing exposure times to TFA to the minimum required for all protecting groups to be removed while minimizing the amount of trifluoroacetylation is a step that must be taken should any of the MSLN3 or MSLN4 peptide prove biologically relevant.

A final performance behavior to note is that recovery of palmitoylated peptides is higher for MSLN3 and MSLN4, despite the initial low yields of the crude products, compared to the non-palmitoylated peptides. In the case of MSLN3, this is mainly due to the higher purity of the **P9** crude, perhaps due to the absence of the +96 Da impurity, while for MSLN 4 the impurities of **P12** are spread widely across the gradient and are thus more easily resolved (**Figure 1.5, E**). While the overall purity is lower for **P12** than for **P10** and **P11**, this distribution facilitates the purification. This is not the case for **P10** and **P11**, in which we observe most of the impurities overlapping with the main peak. This leads to sacrificing more of the desired product as perfect resolution of impurities close to the product peak is not possible.

These results can be explained by various causes: first, PEGylated peptides generate sharper chromatographic peaks, whereas both the palmitoylated and unmodified versions have more triangular and wider, dragging peaks. This affects resolution, especially in semi-preparative scales, which means that collecting less of the peak is necessary to maintain adequate purities, which in turn results in the loss of more product in exchange for higher purity. For MSLN 4, the increased retention in the column of the unmodified sequence **P10** shown as these “dragging” peaks is less affected by PEG₂₃, yet PEGylation proves adequate for obtaining a pure product **P11**. In fact, for the unmodified MSLN4 **P11** peptide a des-Leu impurity (amongst others), present in the long MSLN 4 sequence, could not even be resolved and we were unable to obtain a purified peptide **P10**. This is the only instance for the MSLN peptides that a product could not be purified in a single step. At best, we improved the purity from 71 to 73%.

The second variable is hydrophobicity. The PEG moiety has a greater effect on the solubility, for example, of the MSLN2 peptide **P4** than for the more hydrophilic sequence MSLN1 **P1**, in which the effect is even reversed as **P2** has a marginally longer retention time in a C₁₈ stationary phase.

Hydrophobic sequences are retained in the column due to stronger interactions with the hydrocarbon chain of the stationary phase, which was clearly seen in all cases of palmitoylated peptides, which require more aggressive organic solvent gradients to elute. As an example, peptide **P6** elutes in an 80-100% acetonitrile gradient while **P9** elutes in a 90-100% acetonitrile gradient, both in a C_8 stationary phase. This is a clear indication of how much the palmitoyl moiety has increased the overall hydrophobicity of the sequences. In contrast the hydrophilic PEG moiety favors improved solvation in the mobile phase. The third variable is size. The shorter MSLN 2 peptide **P4** is more affected by PEGylation as seen for peptide **P5** and by palmitoylation as seen in **P6**. The recovery of **P4** is greatly increased compared to a longer sequence like MSLN 4 **P10** and **P12**, in which the effect is lessened.

Overall, all peptides were obtained in the minimum required amounts by the LUMC group of at least 20 mg of product with purity $\geq 95\%$, except for **P3**, **P6**, **P7** and **P9**, of which less amount was obtained while **P10** could not be purified to 95% in a single step. Additionally, the multipeptide presentation of **P12** in a MAP construct was attempted without success.

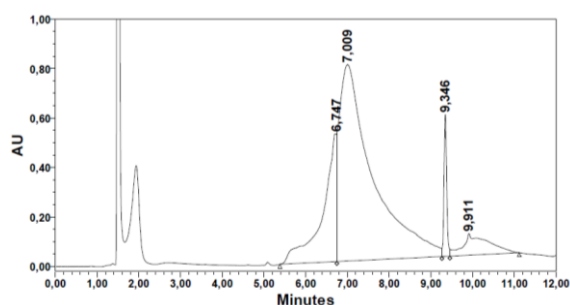
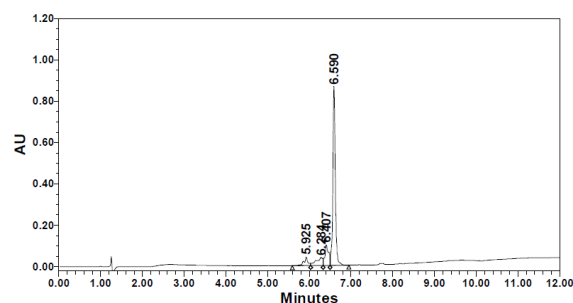
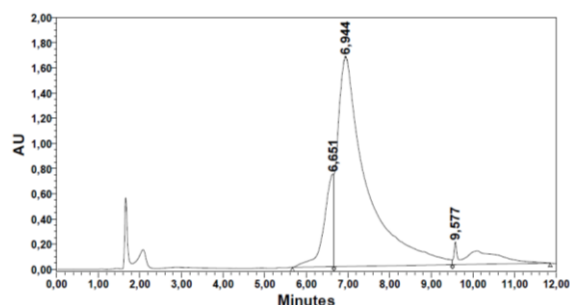
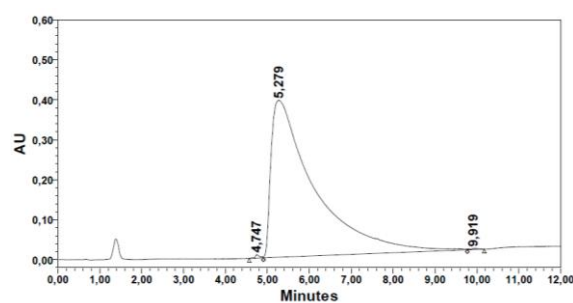
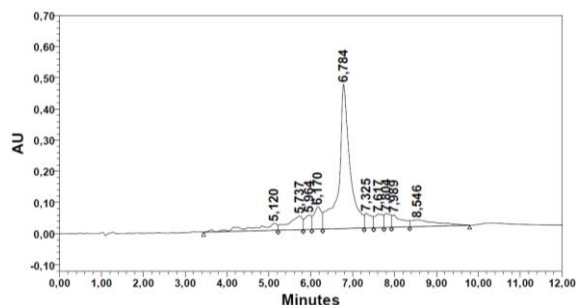
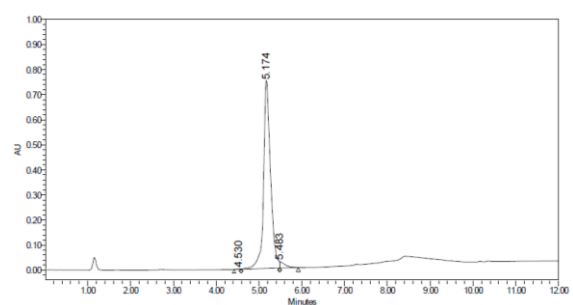
A P10 unmodified MSLN4 crude**B P10 unmodified MSLN4 pure****C P11 PEG-MSLN4 crude****D P11 PEG-MSLN4 pure****E P12 Palm-MSLN4 crude****F P12 Palm-MSLN4 pure**

Figure 1.5 RP-HPLC of crude and pure MSLN4 multipeptide peptides **A** and **B**: free-N-terminal amine, **C** and **D**: PEGylated, and **E** and **F**: palmitoylated using gradients of 5-100% B at r.t. in a C_{18} column (**A-D**) or 50-100% B at 60°C in a C_8 column (**E** and **F**) (A: H_2O + TFA 0.045%, B: CH_3CN + TFA 0.036%).

1.2.2.2 Synthesis tetanus toxoid (TT) peptides

The tetanus toxoid sequence was selected as an MHC class II-binding epitope with reported activity and use spanning decades. It is intended to be used in a mix with some MHC class I-binding epitopes produced in this work, as well as in a multiepitope peptide for K-Ras constructs (see section 3.2.2.4) with the goal of activating CD4+ helper T cell pathways in addition to the CD8+ cytotoxic T cell effectors to produce a strong and durable immune response. This peptide was synthesized in a 0.1 mmol scale as a free peptide and as a PEGylated peptide. No palmitoylation was introduced because unlike MHC class I-binding peptides, this is a known strong immunogen.

TT peptides, due to their hydrophilicity and relatively small size showed good synthetic performance with crude purities above 85% and relatively easy purification towards values above 95% (Table 1.4 and Figure 1.6). We did, however note that the PEGylated peptide has markedly improved recovery (89%) compared to the free peptide (19%), and this is likely due to increased affinity of the PEG moiety with the aqueous solvents of the mobile phase and decreased interaction with the C₁₈ stationary phase during semi-preparative purification.

Table 1.4 Summary of yield and purity of tetanus toxoid peptides.

Epitope	ID	N-terminal	MW (Da)	% Crude Purity	% Crude Yield ^a	% Final Purity	% Recovery ^b
TT	P13	NH ₂ -	1724	87	59	97	19
	P14	H-PEG ₂₃ -NH-	2852.4	85	66	100	89

^a% yield = (crude mmol x crude purity) / (theoretical mmol)

^b% recovery = (purified mmol x purified purity) / (crude mmol x crude purity) x 100

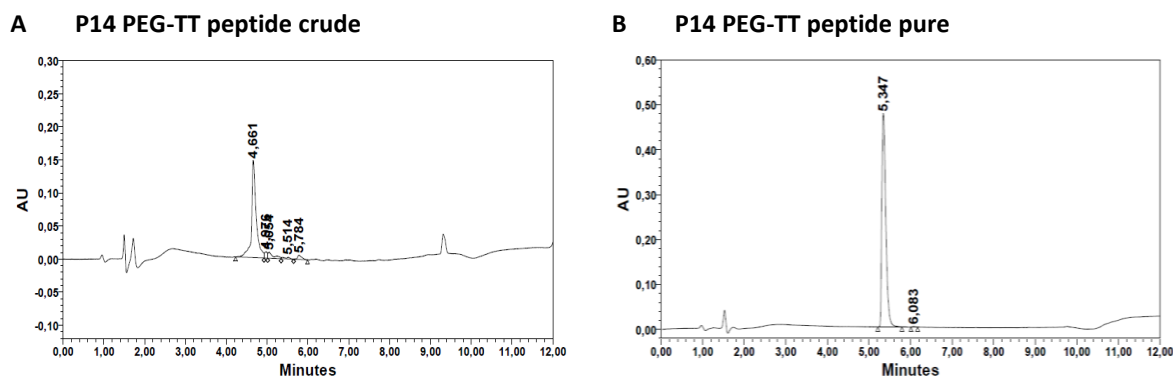


Figure 1.6 RP-HPLC of crude and pure PEGylated TT peptide using a gradient of 10-70% B at r.t. in a C₁₈ column (A: H₂O + TFA 0.045%, B: CH₃CN + TFA 0.036%).

1.2.2.3 Synthesis of peptides derived from the OCV-C01 vaccine

The OCV peptides 1 to 4 are immunogenic components of the OCV-C01 cancer vaccine¹³⁸, which is administered to PDAC patients following surgical resection of the tumor in combination with gemcitabine and has been shown to increase disease-free survival over 18 months. This vaccine targets the antigens Kinesin-like protein (KIF20A), Vascular Endothelial Growth Factor Receptor 1 (VEGFR1) and 2 (VEGFR2) which are associated with angiogenesis and thus tumor vascularization. Therefore, this vaccine directly targets the tumor microenvironment.

OCV peptides were synthesized as three single epitopes, OCV1, OCV2 and OCV3, one for each of these proteins KIF20A, VEGFR1 and VEGFR2 and as a multiepitope peptide chimera, OCV4, with the three epitopes linked by a KK cathepsin-like cleavage site. All peptides have an unmodified N-terminus.

Table 1.5 Summary of yield and purity of OCV-C01 vaccine peptides.

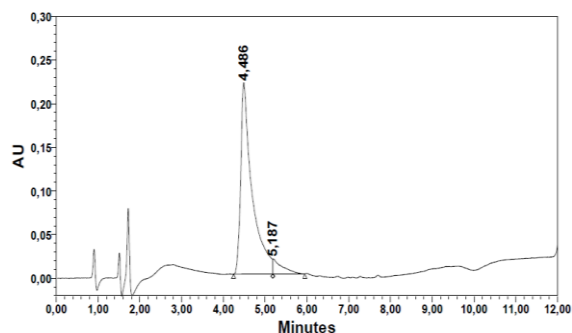
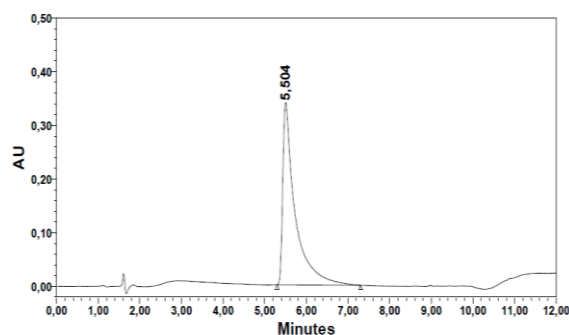
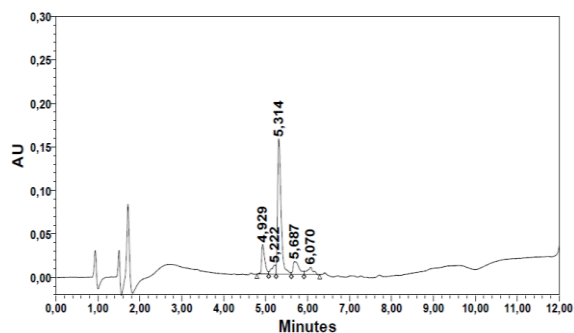
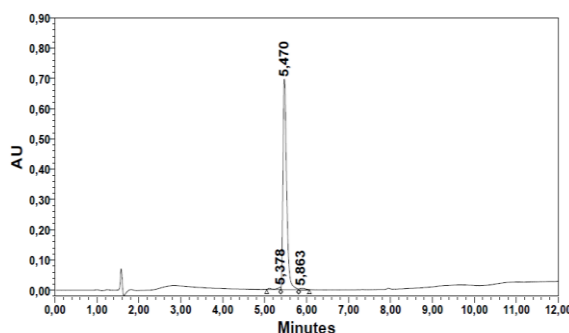
Epitope	ID	N-terminal	MW (Da)	% Crude Purity	% Crude Yield ^a	% Final Purity	% Recovery ^b
OCV1	P15	NH ₂ -	1255.6	94	68	100	48
OCV2	P16	NH ₂ -	1078.3	65	45	100	58
OCV3	P17	NH ₂ -	1072.2	82	51	98	36
OCV4	P18	NH ₂ -	3884.8	82	34	100	11

^a% yield = (crude mmol x crude purity) / (theoretical mmol)

^b% recovery = (purified mmol x purified purity) / (crude mmol x crude purity) x 100

OCV peptides did not show major synthetic difficulty. They are short and manageable, and they were produced by microwave-assisted automated synthesis. A single point of observation is the presence of a DG motif in **P17** and **P18**, in which the glycine residue must be introduced as a protected Fmoc-(Dmb)Gly-OH building block to minimize the aspartimide secondary reaction. The Dmb (dymethyloxybenzyl) is an acid labile protecting group introduced on the α -amine of the glycine to minimize the reaction of this nitrogen with the side chain of the aspartic acid.

In this regard, crude purities were generally good, ranging from 82 to 94% except for **P16** (OCV2), which showed a purity of 65% (**Table 1.5**). Recoveries after purification approach 40-50% in all cases except for the multiepitope **P18** peptide (OCV4). The recovery for this peptide was 11% which means a great amount is lost during purification. **Figure 1.7** shows the chromatographic characterization of these peptides.

A P15 OCV1 crude peptide**B P15 OCV1 pure peptide****C P16 OCV2 crude peptide****D P16 OCV2 pure peptide**

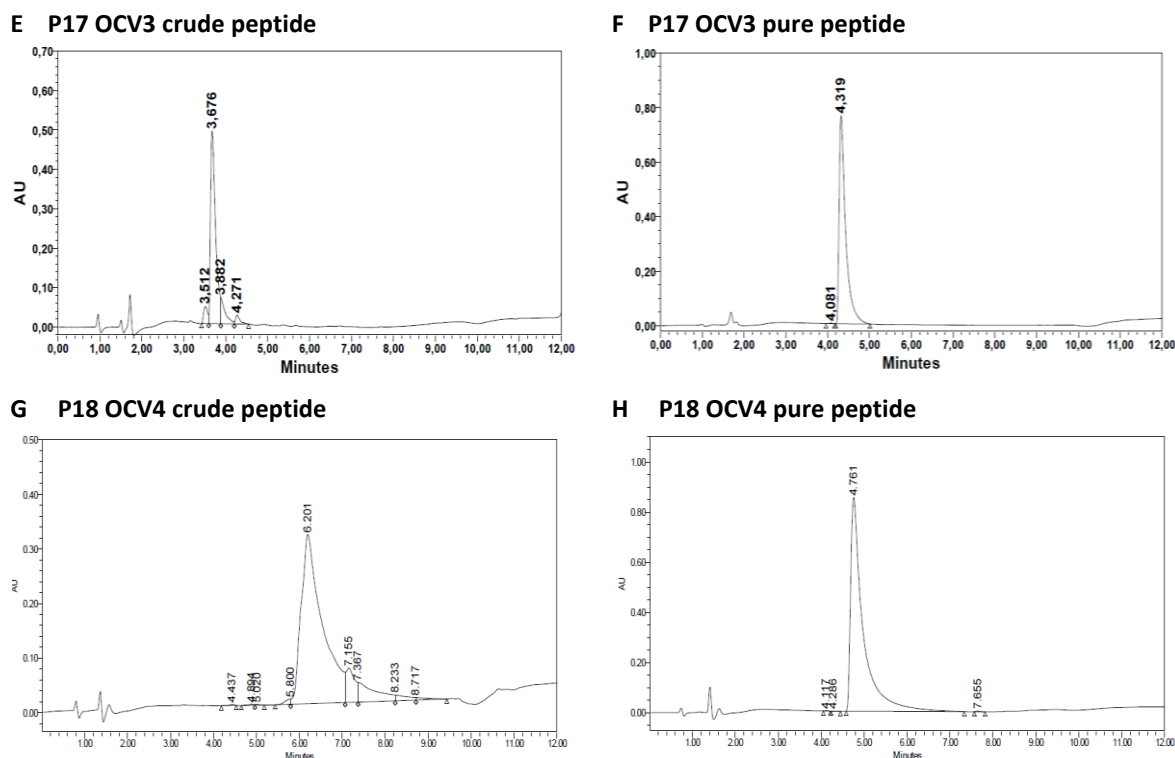


Figure 1.7 RP-HPLC of crude and pure OCV-CO1 single epitope peptides **A** and **B**: OCV1 **C** and **D**: OCV2, **E** and **F**: OCV3 and the multi-epitope peptide **G** and **H**: OCV4 using gradients of 5-100% B at r.t. (**A**, **C**, **E**, **G** and **H**) or 5-70% B at r.t. (**B**, **D**, and **F**) in a C₁₈ column (A: H₂O + TFA 0.045%, B: CH₃CN + TFA 0.036%).

1.2.2.4 Synthesis of K-Ras peptides: an example of a complicated peptide synthesis

A reported 25-mer epitope from the K-Ras protein was selected and synthesized both in its wild-type form and its neoantigenic form which carries a single point G12D mutation. These epitopes were palmitoylated to increase their immunogenicity. Two chimera constructs were also synthesized combining each epitope with the tetanus toxoid MHC II-binding epitope, linked by a cathepsin-like KK cleavage motif and palmitoylated at the N-terminus.

These peptides were synthesized using a microwave-assisted automated strategy following standard protocols. In the case of K-Ras2 and K-Ras4, both of which contain the G12D mutation producing a DG motif, glycine was introduced as Fmoc-(Dmb)Gly-OH. This protected amino acid minimizes the formation of the aspartimide secondary reaction characteristic of the DG motif.

The first approach for the synthesis of these peptides yielded crudes with low purity, especially for the longer peptides (**Table 1.6**, 1st S).

Table 1.6 Summary of yield and purity of crude K-Ras peptides in the first (1st S) and second synthesis (2nd S)

Epitope	ID	N-terminal	MW (Da)	%Purity 1 st S	%Yield 1 st S ^a	%Purity 2 nd S	%Yield 2 nd S ^a
K-Ras1	P19	Palm-NH-	2813.6	73	32	84	37
K-Ras2	P20	Palm-NH-	2871.6	71	26	77	28
K-Ras3	P21	Palm-NH-	4776.9	39	25	24	16
K-Ras4	P22	Palm-NH-	4834.9	51	40	56	44

$$^a\% \text{ yield} = (\text{crude mmol} \times \text{crude purity}) / (\text{theoretical mmol})$$

Furthermore, in K-Ras3 and K-Ras4 peptides a noticeable Glu3 deletion was observed and subsequent Met1 and Thr2 deletions at the N-terminus. Finally, Gly, Val and Lys deletions were also observed and due to their frequency in the sequence we could not determine where these occur. Overall, these sequences were shown to be synthetically challenging. Therefore, a second synthetic approach was designed where during the elongation process the synthesis was stopped every 10 residues and its quality was checked by analysis of a small aliquot of peptide-resin cleaved. The idea was to determine the conflictive residue couplings on each peptide fragment. As an example, it was detected that the incorporation of Val14 (fragment 3) and Glu3 (fragment 4) were not complete using the standard coupling protocol (**Figure 1.8**).

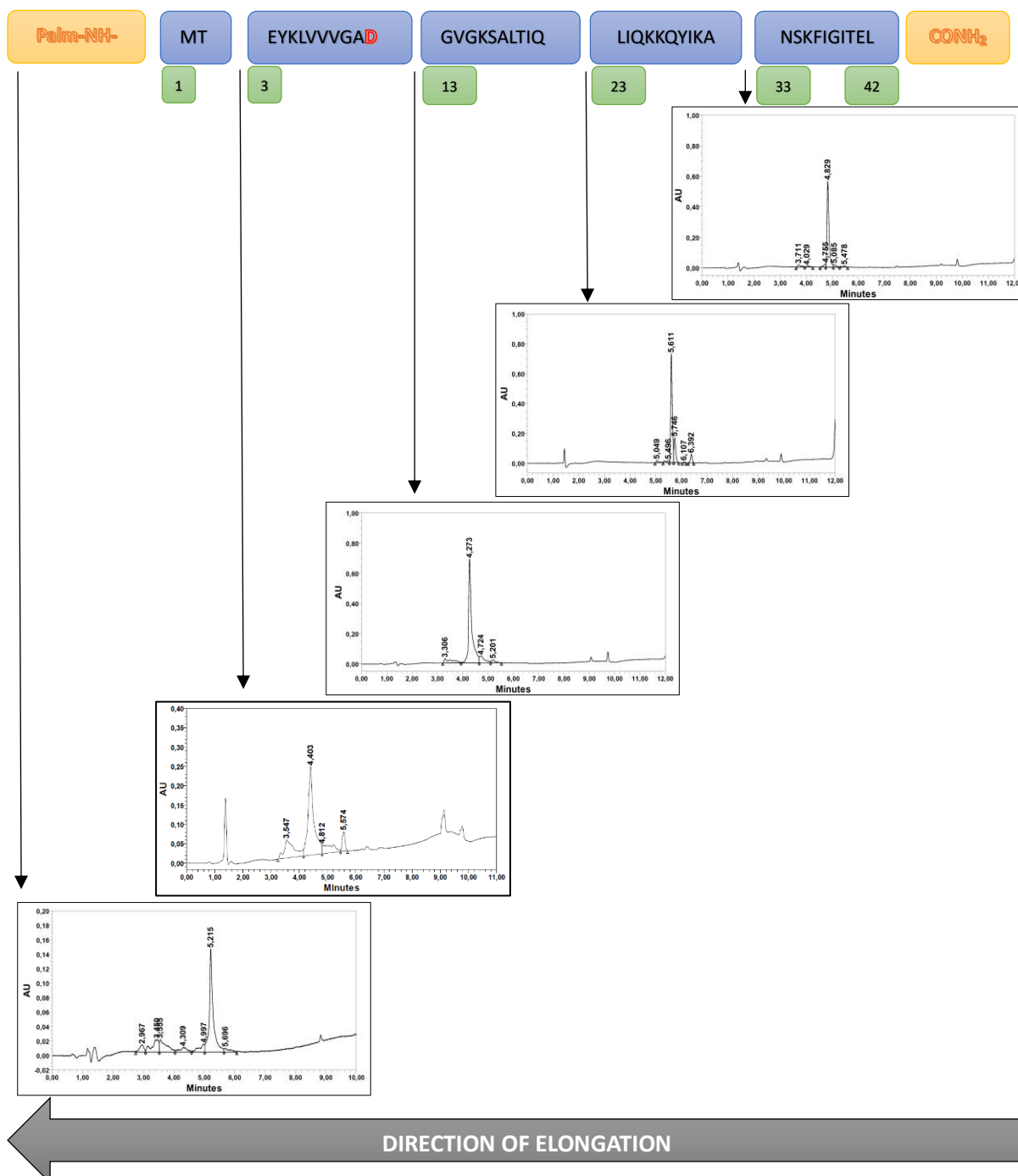


Figure 1.8 The checkpoint methodology for the screening of the synthetic peptide K-Ras 4.

This problem was solved by introducing double couplings in all observed problematic couplings, a longer coupling was introduced in the last five residues and a triple coupling for the Glu3 position. The results of the optimized synthesis are shown in **Table 1.6** in the columns indicated as second synthesis (**2nd S**).

Figure 1.8 shows the HPLC traces of the peptide fragments associated to the quality check points of the final synthesis of KRas4 (G12D neoantigen chimera). Despite this synthesis being already optimized at several residues along the sequence, the HPLC analysis of the different peptide quality check points allowed to still identify the most problematic peptide sections.

In addition to this checkpoint approach, we also decided on a split batch strategy for the synthesis of these peptides. This decision was based on the fact that both the single epitope peptides (K-Ras1 and K-Ras2) and the multiepitope peptides (K-Ras3 and K-Ras4) differ from one another only in the 12th position (G12D mutation) and consequently each pair can be synthesized as one peptide up to the point of divergence, located at the DG motif (12th and 13th positions) from which then the synthesis of each peptide is completed separately. Therefore, K-Ras1 and 2 were synthesized as one peptide from Gln25 up to Val14, after which the batch was split, and the synthesis was continued separately. K-Ras 1 continued coupling Gly13 and Gly12 normally, while K-Ras 2 continued coupling Gly13 as a Fmoc-(Dmb)Gly-OH and then coupling Asp12. The exact same process was repeated for the K-Ras 3 and K-Ras 4 pair. This strategy is visualized in **Figure 1.9**. Each parent pro-peptide and the resulting peptides were synthesized using the checkpoint methodology.

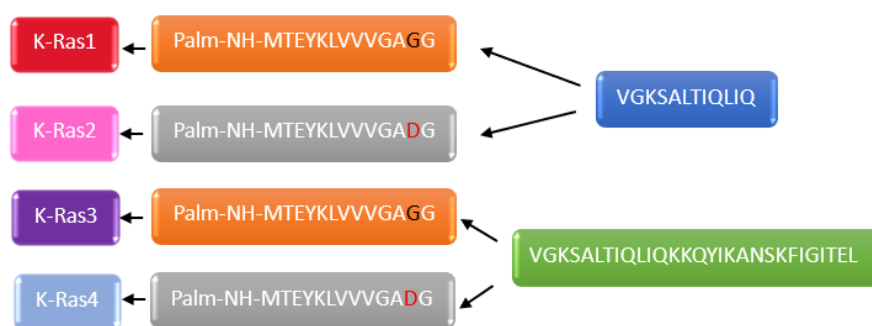


Figure 1.9 The split batch methodology for the second synthesis of K-Ras peptides.

We observed that as the synthesis progressed, the purity of the peptide remained in the 70-80% range once Gly13 was introduced (**Table 1.7**), and then decreased to 24-60% at the end of the sequences. This fragment/section of these peptides requires careful and thorough synthesis, and the checkpoint method is a useful and sensible approach to optimize the synthesis of long peptide sequences with an automated synthesizer, significantly reducing production times. **Table 1.7** summarizes the purities obtained at each checkpoint.

Table 1.7 Summary purities for the second synthesis of K-Ras peptides at each checkpoint.

Checkpoint	N-terminal	%Purity K-Ras1	%Purity K-Ras2	%Purity K-Ras3	%Purity K-Ras4
Asn33	Fmoc-NH-	-	-	72	-
Leu23	Fmoc-NH-	-	-	85	-
Gly13	Fmoc-NH-	80	-	81	-
Glu3	Fmoc-NH-	75	91	42	60
Final Product	Palm-NH	84	77	24	56

The K-Ras 3 and K-Ras 4 peptides are indeed the most difficult sequences to produce. Both showed synthetic problems as well as problems with purification and isolation by semi-preparative HPLC. They also showed low solubility in aqueous solvents and DMSO at the high concentrations required for bulk purification, and solubilization was therefore limited to TFA. Furthermore, the recovery of fractions after attempted purifications was not greater than 5%, and in the best cases the purity achieved for only one peptide was in the 90% range (**Figure 1.10**). These problems can be explained by the concentration of hydrophobic residues in the N-terminal part of these peptides and the presence of a palmitoyl moiety at the N-terminal position, which probably leads to an aggregation of these molecules. This leads to increased retention even on a C8 column, which affects the recovery and interferes with the separation process, as the product and impurities are entrained and not properly separated to achieve >90% purity.

However, it is noteworthy that one peptide of the family (KRas4) could be obtained in high purity, although in small quantity. The synthesis protocol applied to this peptide yielded crudes with a purity of about 56%, but its chromatographic profile was improved compared to previous attempts. The application of this synthetic approach to peptides K-Ras1 and 2 yielded crudes with slightly improved purity from 73% to 84% and from 71% to 77%, respectively. Despite the efforts to improve the synthesis, the results were not sufficiently good, and the purification process remains the bottleneck, and no fraction with a purity higher than 85% was obtained due to the complete loss of chromatographic resolution in the semi-preparative equipment, probably related to the low solubility of the peptides. Finally, K-Ras3 does not show any synthetic improvement. Due to the high hydrophobicity of these peptides, several attempts were made to purify these crudes on a C8 and a C4 semi-prep column. However, none of these stationary phases helped to improve the purification.

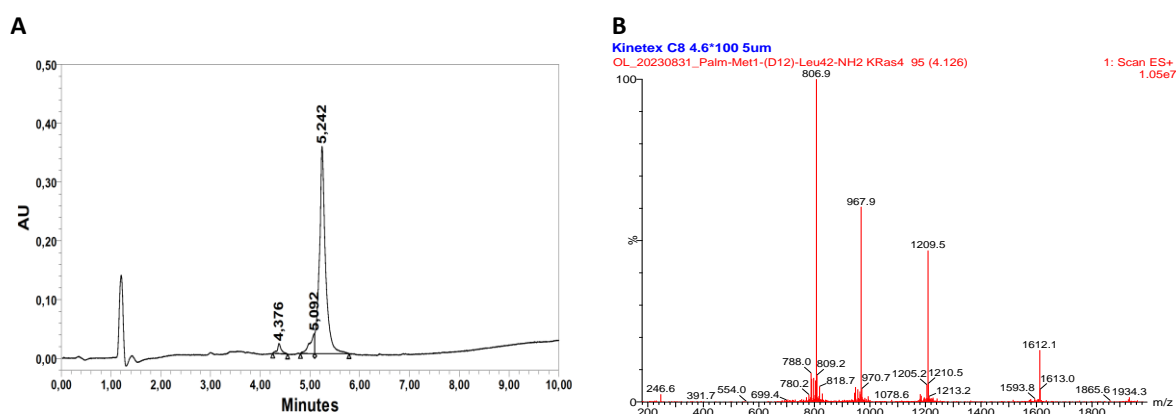


Figure 1.10 Characterization of the purified K-Ras4 (D¹² chimera) **P22** peptide. **A**: RP-HPLC using a 15-100%B gradient in a C₈ column (A: H₂O + TFA 0.045%, B: CH₃CN + TFA 0.036%). **B**: HPLC-MS of K-Ras4 (D¹² chimera) using a 15-100%B gradient in a C₈ column (A: H₂O + FA 0.1%, B: CH₃CN + FA 0.07%).

The difference in the quality of the crude products obtained from the G12 chimera (K-Ras3) vs. the D12 chimera (K-Ras4) (**Figure 1.11**) may also be clearly related to an aggregation problem. The use of the protected glycine (Fmoc-(Dmb)Gly-OH) in the synthesis of the K-Ras4 peptide to avoid the formation of aspartimide, which is common in DG motifs^{158,159}, seems to improve the quality of this peptide compared to K-Ras3. The Dmb group provides backbone protection and likely alters the conformation of the linear peptide, disrupting cross-chain interactions that lead to in-resin aggregation.^{158,160} This effect improves the final crude product from 23% purity in the G12 chimera (K-Ras3) to only 55% purity (K-Ras4).

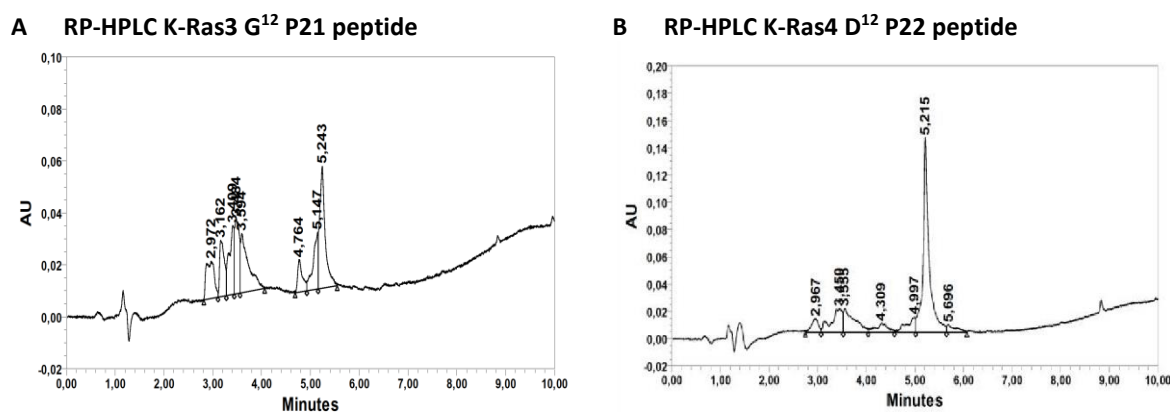


Figure 1.11 RP-HPLC for **A:** K-Ras 3 (G¹² chimera) and **B:** K-Ras 4 (D¹² chimera) using a gradient used of 15-100% B in a C₈ column (A: H₂O + TFA 0.045%, B: CH₃CN + TFA 0.036%).

1.2.2.4.1 Synthesis of K-Ras peptides with N-terminal palmitoyl moiety introduced by thiol-maleimide reaction.

Other strategies were explored to overcome the problems related to the high hydrophobicity of these peptides. First, to facilitate the purification of the peptides, we decided to purify them before introducing the palmitoyl moiety, which would then be introduced through a conjugation reaction. To apply this strategy, the K-Ras peptides were modified with a 6-maleimidohexanoyl moiety at the N-terminus and the palmitic acid was derivatized with a cysteine to generate the palmitoyl-L-Cys-OH moiety. Once the peptide is purified, the palmitoyl thiolated moiety is introduced through a thiol-maleimide reaction to produce the final compound shown in **Figure 1.12**.

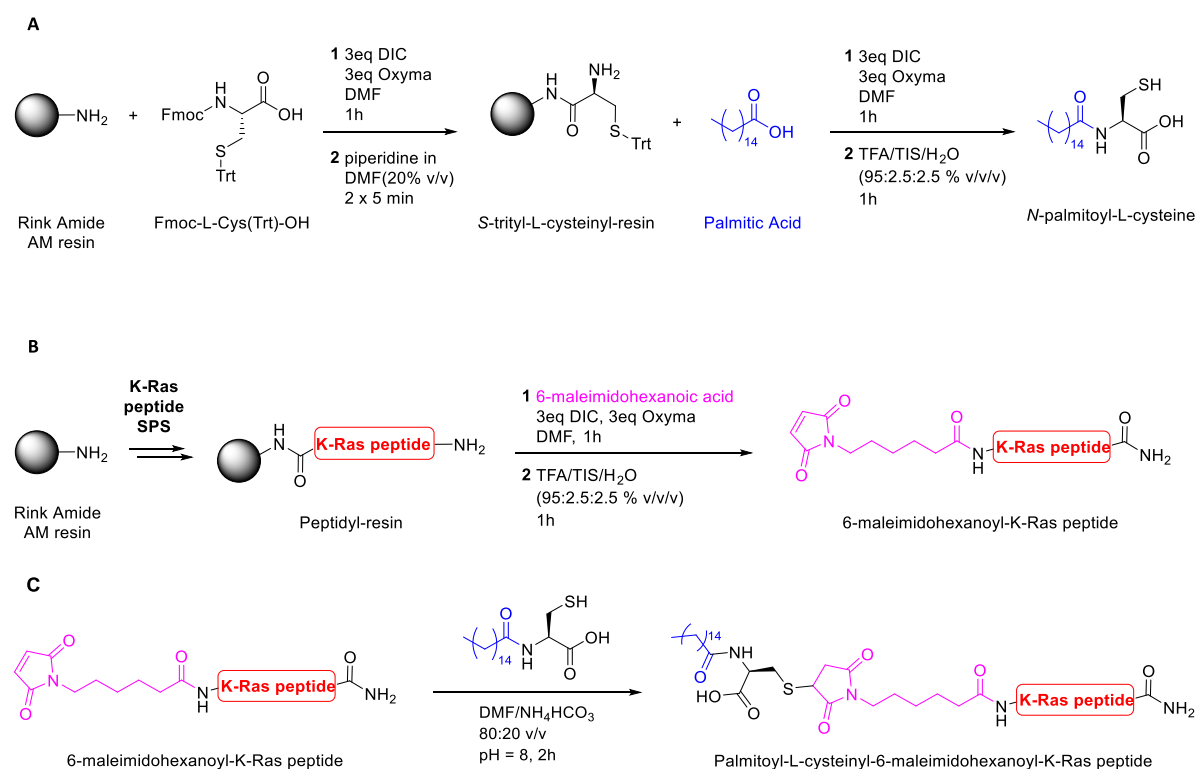


Figure 1.12 Three-step synthetic strategy for a modified K-Ras peptide. **A:** Synthesis of a Palmitoyl-L-cysteine, **B:** Synthesis of a 6-maleimidohexanoyl-K-Ras peptide and **C:** Conjugation of both moieties to form the final palmitoylated K-Ras peptide

Our rationale was that the lack of a palmitoyl moiety would allow for easier purification with much better yields. The addition of the palmitoyl moiety via a well-described Michael reaction between the cysteine thiol and the maleimide groups would then provide the desired fatty acid modification. This reaction should be fast, clean, and efficient enough to provide a final product that meets the requirements for incorporation into nanoparticles without fundamentally altering the epitope.

These modified versions of the K-Ras family peptides with a 6-maleimidohexanoyl moiety at the N-terminus were synthesized and purified by semi-preparative HPLC in a C₁₈ or C₈. **Table 1.8** summarizes the synthetic performance for these peptide crudes.

Table 1.8 Summary of yield and purity of crude K-Ras maleimide-hex peptides

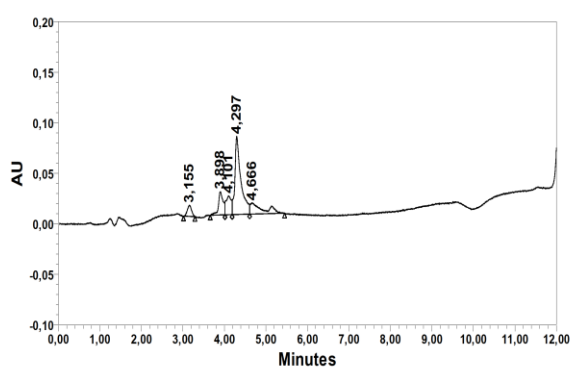
Epitope	ID	N-terminal	MW (Da)	%Purity	%Yield ^a
K-Ras1	P23	6-malhex-NH-	2754.32	54	26
K-Ras2	P24	6-malhex-NH-	2812.32	71	30
K-Ras3	P25	6-malhex-NH-	4717.62	54	34
K-Ras4	P26	6-malhex-NH-	4775.72	40	27

^a% yield = (crude mmol x crude purity) / (theoretical mmol)

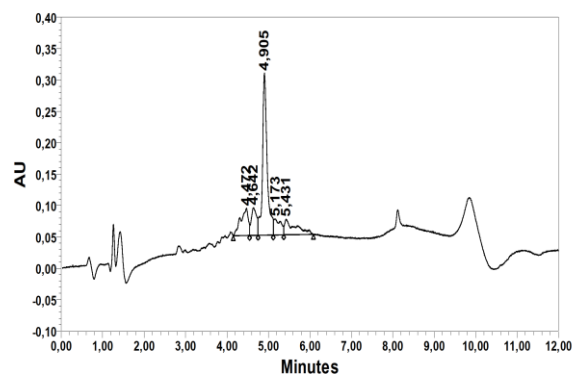
In general, the purities of the products obtained are lower than those of the directly palmitoylated K-Ras peptides. The exception is the K-Ras3 peptide, which has a better purity than its counterpart (54% vs. 26%). However, when we tried to purify these peptides by semi-preparative RP-HPLC, we found the same problems as for the palmitoylated K-Ras peptides: a complete loss of resolution and an impossibility to obtain a fraction more than 80% pure. Furthermore, we had to rely on TFA as a solvent for these peptides to be injected into the semi-preparative RP-HPLC, either H₂O:CH₃CN (1:1) or DMSO-induced peptide gelation. This problem was also observed with the unmodified K-Ras peptides. **Figure 1.13** shows the chromatographic traces for the modified K-Ras crude products.

Gelification seems to be an intrinsic problem of the KRas sequence, which is curiously avoided by palmitoylation, although it further increases their hydrophobicity and decreases their solubility. Indeed, an analysis using the AGGRESCAN tool (<http://bioinf.uab.es/aggrescan/>)¹⁶¹ shows hotspots of aggregation for all sequences over most of their length (**Figure 1.14, A-D**), confirming our suspicion.

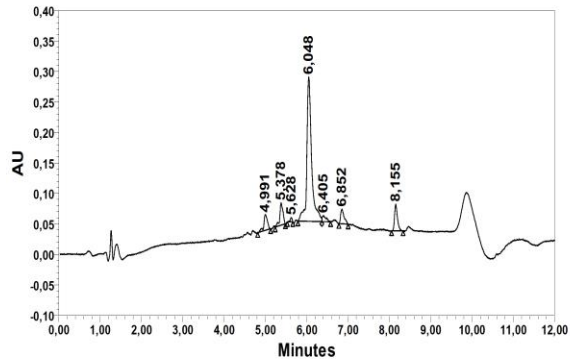
A P23 6-malhex K-Ras1



B P24 6-malhex K-Ras2



C P25 6-malhex K-Ras3



D P26 6-malhex K-Ras4

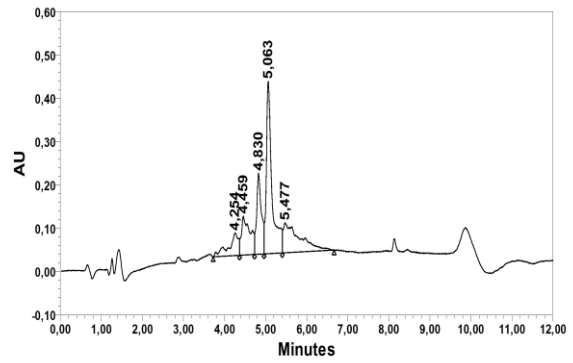
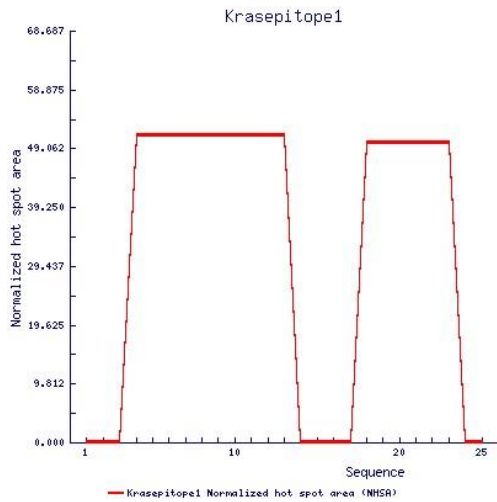
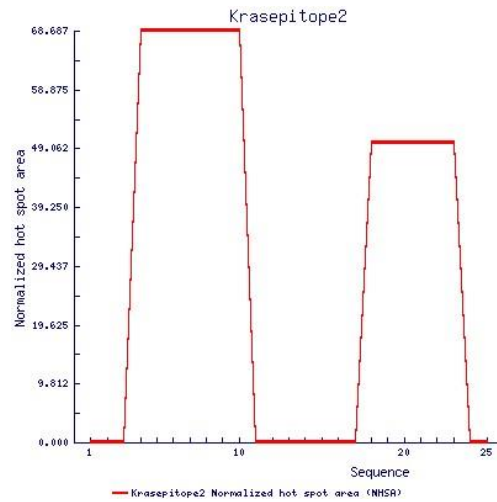


Figure 1.13 RP-HPLC for **A:** K-Ras 1, **B:** K-Ras 2, **C:** K-Ras 3 and **D:** K-Ras 4 modified with 6-maleimidohexanoic acid in the N-terminal. Gradient used was 5-100% B in a C₁₈ column (A: H₂O + TFA 0.045%, B: CH₃CN + TFA 0.036%).

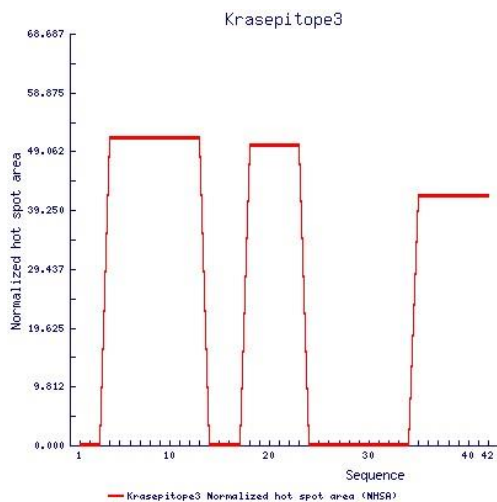
A K-Ras1 G¹² single epitope P19 peptide



B K-Ras2 D¹² single epitope P20 peptide



C K-Ras3 G¹² multiepitope P21 peptide



D K-Ras4 D¹² multiepitope P22 peptide

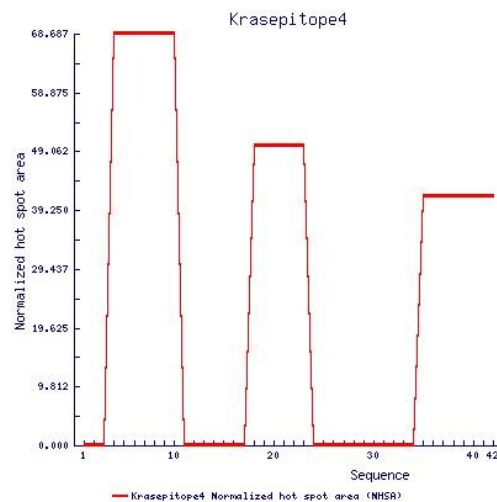


Figure 1.14 Prediction of aggregation hot-spots for **A:** Gly¹² Kras epitope (**K-Ras1**), **B:** Asp¹² Kras epitope (**K-Ras2**), **C:** Gly¹² K-Ras-Tetanus toxoid chimera (**K-Ras3**) and **D:** Asp¹² K-Ras-Tetanus toxoid chimera (**K-Ras4**).

1.2.2.4.1 Synthesis of the K-Ras peptides by a convergent strategy

A convergent synthetic approach was also explored to minimize the problems associated with the hydrophobicity of the K-Ras peptide sequences. This involves the separate synthesis of two or three peptide sequence fragments, that are coupled together to generate the final K-Ras epitope. This strategy may be particularly useful for the longer 42-mer sequences (**K-Ras3** and **K-Ras4**). Considering that **K-Ras1** and **K-Ras2** are homologous sequences with a single point mutation at (G12D), these peptide sequences were split into two fragments, Palm-[Met¹-Val¹⁴]-COOH and NH₂-[Gly¹⁵-Gln²⁵]-CONH₂, the latter being common to both epitopes. **K-Ras3** and **K-Ras4** are also homologous sequences with of a single point mutation at the 12th residue (G12D), but both contain the tetanus toxoid epitope. In this case the peptide sequence was split into three fragments Palm-[Met¹-Val¹⁴]-COOH, Fmoc-NH-[Gly¹⁵-Gln²⁵]-COOH and NH₂-[Lys²⁶-Leu⁴²]-CONH₂, being the last two being common to **K-Ras3** and **K-Ras4** (see **Figure 1.15** and **Table 1.9**).

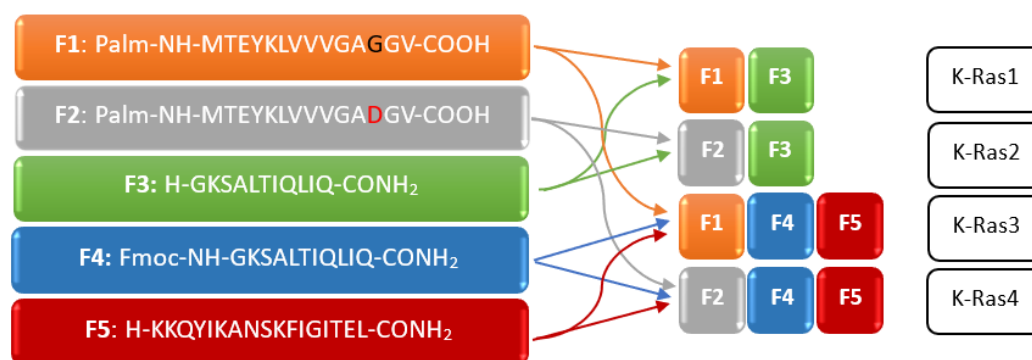


Figure 1.15 Convergent synthetic strategy of K-Ras peptides using fragments.

Table 1.9 Fragment design for the synthesis of K-Ras peptide for a convergent strategy.

Fragment	ID	Sequence	Resin
Palm-[Met ¹ -Val ¹⁴]-COOH	P27	Palm-NH-MT(tBu)E(tBu)Y(tBu)K(Boc)LVVVGAGGV-COOH	HMPB
Palm-[Met ¹ -Val ¹⁴]-COOH	P28	Palm-NH-MT(tBu)E(tBu)Y(tBu)K(Boc)LVVVGAD(tBu)GV	HMPB
NH ₂ -[Gly ¹⁵ -Gln ²⁵]-CONH ₂	P29	NH ₂ -GK(Boc)S(tBu)ALT(tBu)IQ(Trt)LIQ(Trt)-CONH ₂	Sieber
Fmoc-NH-[Gly ¹⁵ -Gln ²⁵]-COOH	P30	Fmoc-NH-GK(Boc)S(tBu)ALT(tBu)IQ(Trt)LIQ(Trt)-COOH	2-CTC
NH ₂ -[Lys ²⁶ -Leu ⁴²]-CONH ₂	P31	NH ₂ -K(Boc)K(Boc)Q(Boc)Y(tBu)IK(Boc)AN(Trt)S(tBu)K(Boc)FIGIT(tBu)E(tBu)L-CONH ₂	Sieber

The synthesis of each fragment requires different solid supports that are hypersensitive to acids (capable of releasing peptides with 1% or 3% TFA in DCM), depending on the functionalization of the C-terminus, which can yield fully protected fragments. Palm-[Met¹-Val¹⁴]-COOH peptide fragments were synthesized using the 4-(4-Hydroxymethyl-3-methoxyphenoxy)butyric acid (HMPB) Chemmatrix resin (**Figure 1.16, A**), because this fragment contains the most problematic synthetic part of the peptide due to its high hydrophobicity, presenting difficult couplings and prone to aggregation. This selected solid support is tailored for these types of difficult sequences as it is a high swelling, low loading resin with excellent reported performance.

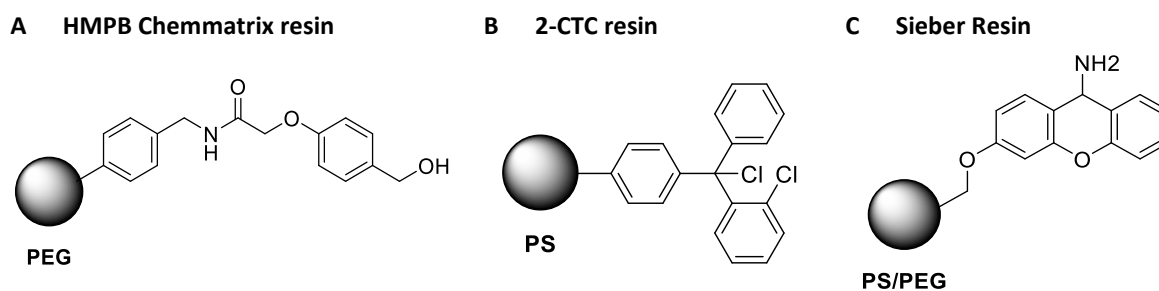


Figure 1.16 The three acid-hypersensitive solid supports used to synthesize fragments for the convergent synthesis of the K-Ras peptides.

The peptide fragment, Fmoc-NH-[Gly¹⁵-Gln²⁵]-COOH was synthesized using the 2-chlorotrityl chloride resin (2CTC) (**Figure 1.16, B**), because this sequence is less difficult. Finally, the C-terminal peptide fragments, NH₂-[Gly¹⁵-Gln²⁵]-CONH₂ (for K-Ras1 and K-Ras2) and NH₂-[Lys²⁶-Leu⁴²]-CONH₂ (for K-Ras3 and K-Ras4), were synthesized using the Sieber resin (**Figure 1.16, C**), which, when is treated with low concentrations of acid produces fully protected peptides with an amide at the C-terminus. The synthesis of the different fragments was done manually because, besides the 2-CTC resin, we were not sure about the thermolability of the different solid supports used in the microwave-assisted peptide synthesizer.

While the purity of the N-terminal fragments synthesized with the HMPB Chemmatrix resin was very good, the fragments synthesized with the Sieber resin yielded highly impure peptides. All protected fragments showed very low solubility in different solvents such as DCM, DMF and DMSO, and consequently their purification was not possible even though different conditions and columns were tested. An exploratory attempt to couple the fragments to generate K-Ras 4 was made using PyOAP and HOAt as coupling reagents with unsuccessful results due to the low solubility of the fragments.

With all these results in hand, it seems that a redesign of the convergent approach to synthesize the K-Ras peptides is necessary, which is beyond our current work. The problems to be solved here are to obtain purer peptide fragments and to find a suitable solvent to carry out the reactions to complete them. Ideally, a 90%> pure protected fragment must be produced that does not need to be purified. This is not an impossible task, but it is expensive and time-consuming.

It is clear that the synthesis of the K-Ras peptide is challenging. Unmodified K-Ras 25-mer epitope was commercially available and is offered at 85% purity for immunological assays. This is an indication that this sequence is notoriously difficult to synthesize and purify and adds value to our attempts to obtain these modified peptides, including a much larger sequence that we were able to obtain at 90% purity, albeit in small quantities.

1.2.3 *In vitro* and *in vivo* assays for MSLN peptide nanovaccines in murine model

Biological assays were conducted using nanovaccine formulations (PLGA-NP-Px), that were developed by Sana Sayedipour of the Translational Nanobiomaterials and Imaging group at the Leiden University Medical Center (LUMC). These *in vitro* and *in vivo* assays were conducted by Daniele Ferrari from the Translational Molecular Imaging Group at the Max Planck Institute. The PLGA-NP-Px nanovaccines comprise the MSLN peptides **P1-P9**, **P11**, and **P12** (see **Tables 1.1** and **1.2**), which have been conjugated in PLGA-NPs. The unmodified MSLN4 peptide **P10** was not used in these assays because it was not obtained in adequate purity. To enhance the immune response, R848, a Toll-like receptor (TLR) 7/8 agonist, and poly(I:C), a TLR3 agonist, were included in the formulation, as adjuvants.

The NetMHCpan algorithm (<https://services.healthtech.dtu.dk/service.php?NetMHC-4.0>), which is capable of predicting the binding between a peptide and the MHC class I for any allele of known sequence in both human and mouse, was employed to confirm the mouse MHC restriction of all peptide sequences. The overexpression of the MSLN protein in patient samples and in the syngeneic murine model tumor cells (KPC), which were utilized in some of these bioassays, was previously confirmed by Daniele Ferrari through immunohistochemistry with an α -MSLN antibody.

1.2.3.1 *In vitro* screening of the MSLN peptide-based nanovaccines

In vitro assays were conducted by immunizing C57BL6 male mice with the PLGA-NP-Px nanovaccine, with three doses administered at seven-day intervals. On day 16, the mice were euthanized, and the splenocytes were collected from the spleen (**Figure 1.17, A**). The splenocytes were then cultured and re-stimulated *in vitro* with 10 μ g of the peptides (Px) present in the PLGA-NP-Px nanovaccine that was administered. The re-stimulation was carried out for 48 hours.

The cell viability in the presence of the stimulating peptides was determined by performing the XTT (2,3-bis-(2-methoxy-4-nitro-5-sulphenyl)-(2H)-tetrazolium-5-carboxanilide) cell proliferation assay after 48h of exposure to the peptides. No significant differences were found in the proliferation of the cells when stimulated with the peptides (**Figure 1.17, B**), except for peptide **P12** where the cells were more proliferative. This suggests that palmitoylation of MSLN4 is not toxic and induces cell growth. Overall, the peptides are not toxic to cells, making them safe to use as vaccine components.

The activation of CD8⁺ T cells in the presence of stimulating peptides was also investigated by enzyme-linked immunosorbent assay (ELISA), with the objective of measuring the secretion of IFN- γ in the culture supernatant. IFN- γ is a well-established as a marker for T-cell activation, specifically Th1 cells which are involved in downstream T-CD8⁺ cell response and is used, as such, as an indicator of antitumoral immunity. The results demonstrate no statistically significant difference in the levels of IFN- γ secreted in the supernatant of stimulated cells, with the exception of the MSLN4 peptides **P11** and **P12** (**Figure 1.17, C**). Moreover, the observed IFN- γ levels were predominantly below 10 pg/mL, indicating an absence of immune response activation. A level of 15 pg/mL or above is typically indicative of activation. This indicates that the MSLN4 multiepitope peptides are the only candidates of the peptides studied, capable of activating a cytotoxic antitumor immune response. This finding is consistent with the established knowledge that short peptides are less effective in eliciting robust immune responses compared to longer peptides and proteins. This finding is further supported by the fact that the MSLN4 multiepitope peptide (**P12**) encompasses the three individual MSLN epitopes. These peptides were tested individually and were unable to reach the levels of activity shown by the multiepitope peptide (**Figure 1.17, C**). All these results indicate that the antigenicity of these peptides was accurately predicted; however, they only demonstrate adequate immunogenicity when they are part of a larger construct. The elevated IFN- γ levels observed for both the palmitoylated **P12** and the PEGylated long peptide **P11** provide further support for this rationale and make the palmitoylated multiepitope MSLN4 **P12** the most significantly active peptide. It is also noteworthy that the **P5** peptide (PEGylated MSLN2 single epitope) exhibited minimal production of IFN- γ . This result may be attributed to the possibility that the long PEG chain may have impeded the interaction of the peptide with the immunoglobulin receptor.

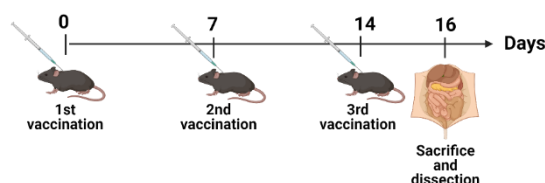
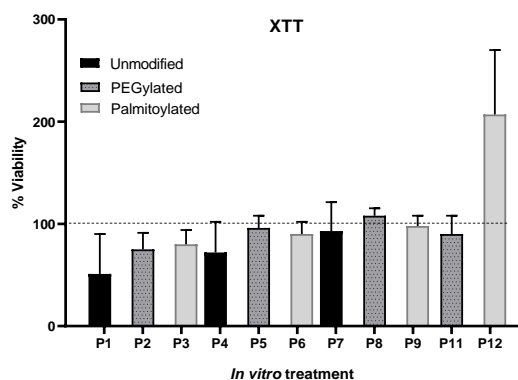
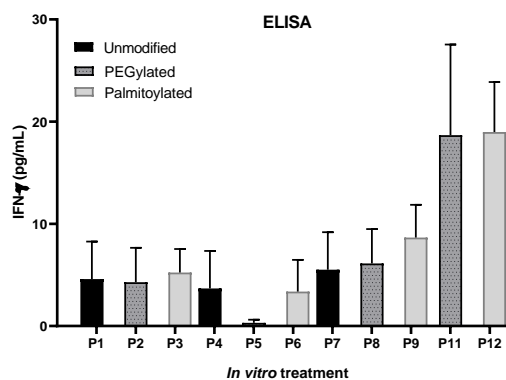
A Immunization schedule

B Stimulated splenocyte viability

C IFN- γ production in splenocytes


Figure 1.17 Preliminary screening of MSLN peptides immunogenicity. **A:** Scheme for the immunization of C57BL/6 mice with the PLGA-NP-Px nanovaccines. **B:** Splenocyte viability measured by the XTT cell proliferation assay and **C:** Splenocyte activation measured by anti-IFN γ ELISA after immunizing C57BL/6 mice with PLGA-NP-Px nanovaccine formulations for peptides **P1-P9**, **P11** and **P12**.

1.2.3.2 Immunogenic effect studies for the PLGA-NP-P12 nanovaccine

After the screening of peptide activity and the selection of the **P12**-based nanovaccine due to its initial promising results, more thorough assays were carried out for this nanovaccine.

C57BL6 mice were vaccinated once per week, for 3 weeks, with four different conditions. **C1:** phosphate-buffered saline (PBS) negative control, **C2:** PLGA-NPs negative control, **C3:** **P12** peptide and **C4:** the PLGA-NP-P12 nanovaccine (n=3-5 per group). Mice were euthanized on day 16, and then inguinal lymph nodes, spleen, and blood were taken for *in vitro* analyses (see **Figure 1.17, A**).

Cells derived from inguinal lymph nodes were collected from mice immunized with conditions C1, C2 and C4 and were stimulated with PBS or 10 μ g of either P12 peptide or PLGA-NP-P12 nanovaccine during 48h. Then, the levels of IFN- γ were measured by ELISA. Cells from mice vaccinated with the PLGA-NP-P12 nanovaccine showed the highest response in all cases of stimulation, and especially those stimulated with PLGA-NP-P12 achieved the highest response compared with those stimulated with either PBS ($p < 0.05$) or the P12 peptide ($p < 0.05$) for this same vaccination group. Mice immunized with PBS showed no response, while vaccination with the P12 peptide achieved very low responses of which the highest was observed when the stimulation was performed with the PLGA-NP-P12 nanovaccine (**Figure 1.18, B**). This indicates that the immunization with the nanovaccine works very well to elicit a strong immune response, and it is more effective as an immunogen than the peptide alone.

To corroborate whether the reported IFN- γ measurements correlate with CD8⁺ cytotoxic T cell activation, splenocytes were collected from mice immunized with conditions C2, C3, and C4. The cells were then cultured and restimulated with 2, 10, or 20 micrograms of the P12 peptide. Subsequently, the splenocytes were stained with labeled anti-IFN- γ and anti-CD8 antibodies and flow cytometry was performed. The results demonstrate the presence of a cell population that expresses the CD8 surface

marker and also secretes the IFN- γ cytokine. This finding suggests that this splenocyte population corresponds to activated cytotoxic T cells. The percentage of CD8⁺ cells increased up to 4% in mice immunized with the PLGA-NP-P12 nanovaccine (C4) compared to immunization with either the PLGA-NPs (C2) or the P12 peptide (C3) (**Figure 1.18, C**). These results provide substantial support for the immunogenicity of the P12 peptide-based nanovaccine in the preliminary screening. Furthermore, it was observed that the highest level of stimulation was achieved when 10 μ g of the PLGA-NP-P12 nanovaccine was utilized.

Similarly, splenocytes from mice vaccinated with the PLGA-NP-P12 nanovaccine (C4) were collected, cultured, and re-stimulated *in vitro* with PBS, or with 2, 10, and 20 micrograms of the P12 peptide or the PLGA-NP-P12 nanovaccine. The results demonstrate that the supernatant of cells stimulated with the P12 peptide and the PLGA-NP-P12 nano vaccine exhibited elevated levels of IFN- γ in comparison to non-stimulated cells (PBS group) (**Figure 1.18, D**). These results are consistent with those observed in lymph node cell cultures and align with the preliminary screening performed on splenocytes. Furthermore, this assay validates that 10 μ g represents the optimal quantity of peptide or nanovaccine to stimulate splenocytes from immunized mice, thus enabling the assessment of the generated immune response.

Additionally, an assay was conducted to evaluate the effectiveness of the stimulated splenocytes in a tumor cell killing assay. Splenocytes from mice immunized with conditions C2 or C4 were re-stimulated *in vitro* with PBS or with 20 micrograms of the P12 peptide for 48 hours, and then added to KPC tumor cells in an effector-to-target ratio of 20:1. Following a 48-hour period of co-culture, the XTT assay was conducted to measure the proliferation of KPC cells. The data demonstrate that splenocytes stimulated with the P12 peptide were capable of inducing cytotoxicity in KPC cells, as evidenced by a statistically significant difference when compared to non-stimulated splenocytes (**Figure 1.18, E**). The immunization with the PLGA-NP-P12 nanovaccine did not result in a notable difference in the cytotoxic response compared to that observed in mice immunized with the PLGA-NP alone and both these responses are elevated. This outcome can be attributed to the nanoformulation's robust activating capabilities, even in the absence of immunogenic peptides, due to its incorporation of potent adjuvants that elicit non-specific cellular responses via TLR-related pathways. This non-specific response elicited by the PLGA-NPs cannot be differentiated from the specific response generated by the PLGA-NP-P12 nanovaccine by this assay alone. Therefore, an analysis of the supernatant from the co-culture was conducted. The results revealed that the P12 peptide-stimulated splenocytes from PLGA-NP-P12 vaccinated mice exhibited higher levels of IFN- γ compared to the P12 peptide-stimulated PLGA-NP-vaccinated mice ($p < 0.05$) or the non-stimulated splenocytes ($p < 0.05$) (**Figure 1.18, F**). This suggests that the nanovaccine is capable of stimulating a cytotoxic CD8⁺ T cell response whereas the PLGA-NP nanoformulation is not and that the latter's antitumoral activity is due to non-specific cellular responses. This is further demonstrated by measuring the anti-MSLN immunoglobulin G (IgG) antibodies in the sera of mice vaccinated with conditions C2 and C4. The sera of mice vaccinated with the PLGA-NP-P12 nanovaccine (C4) exhibited higher levels of specific IgGs when compared to mice that received PLGA-NPs (C2), which demonstrated low or no presence of specific IgGs (**Figure 1.18, A**). These findings reinforce the assertion that the PLGA-NP-P12 nanovaccine is a promising vaccine candidate capable of eliciting a robust immune response and, furthermore, that this response is specifically directed towards MSLN, indicating a tumor-specific immune response.

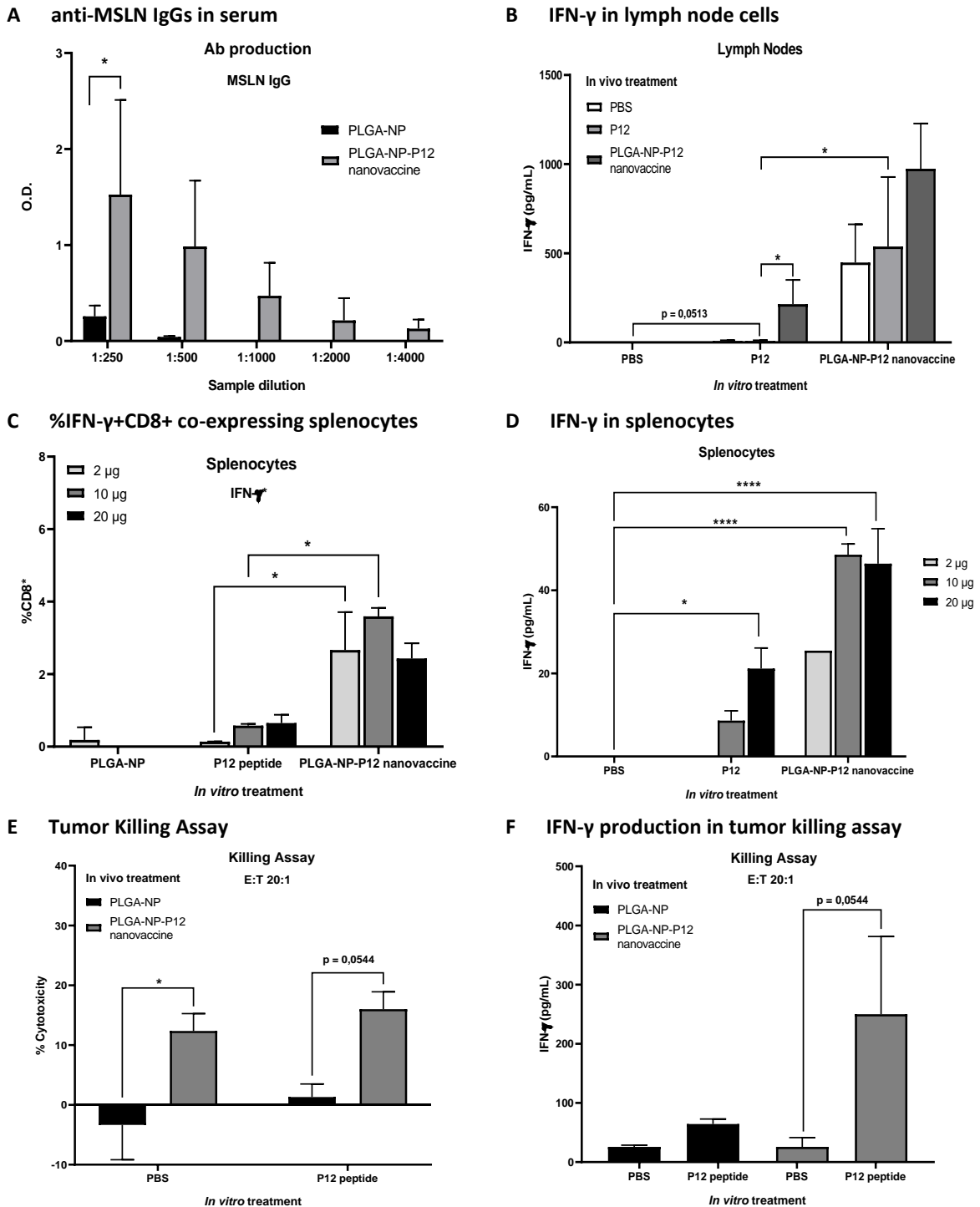


Figure 1.18 Immunogenic effect of MSLN nano vaccine *in vitro*. **A:** anti-MSLN IgG antibody production in the serum of mice after vaccination with the PLGA-NP control or the PLGA-NP-P12 nanovaccine **B:** IFN- γ measured in cells extracted from lymph nodes of PLGA-NP, P12 peptide or PLGA-NP-P12 nanovaccine immunized mice and stimulated with PBS, P12 peptide or PLGA-NP-P12 nano vaccine. **C:** Flow cytometry of CD8 and IFN- γ co-expressing splenocyte populations collected from PLGA-NP, MSLN4 or PLGA-NP-P12 vaccinated mice stimulated with different doses of P12 peptide. **D:** IFN- γ measured in splenocytes collected from mice vaccinated with the PLGA-NP-P12 nanovaccine and stimulated with PBS and different doses of the P12 peptide and the PLGA-NP-P12 nanovaccin. **E:** Cytotoxic effect of P12 peptide-stimulated splenocytes from PLGA-NP and PLGA-NP-P12 vaccinated mice on KPC cells. **F:** IFN- γ levels in the supernatant of the co-culture of KPC cells and stimulated splenocytes.

1.2.3.3 Efficacy of the PLGA-NP-P12 nanovaccine in PDAC tumors

An *in vivo* assay to measure both the prophylactic and therapeutic capacity of the PLGA-NP-P12 nanovaccine was performed in the C57BL6 murine model. For the prophylactic activity assay, mice received two doses of a mix of the R848 and poly(I:C) adjuvants (C1), PLGA-NPs (C2) or the PLGA-NP-P12 nanovaccine (C3). Mice were then challenged with KPC cells after which they received two more boosters of the nanovaccine. Mice were euthanized 8 days after the last dose (**Figure 1.19, A**). Tumor size was measured by ultrasound after 10, 17 and 24 days of inoculation and no significant differences were found between the treatment groups (**Figure 1.19, B**). After euthanasia, no differences were found between the treatment groups (C1, C2 or C3) neither in the primary tumor size (**Figure 1.19, C**), the scar tumor size which grows at the incision site (**Figure 1.19, D**), nor in the number of metastases presented in the mice (**Figure 1.19, E**). Due to the low number of animals in each group, however, this experiment will be repeated.

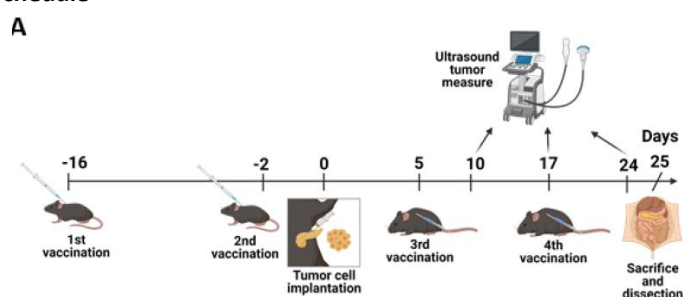
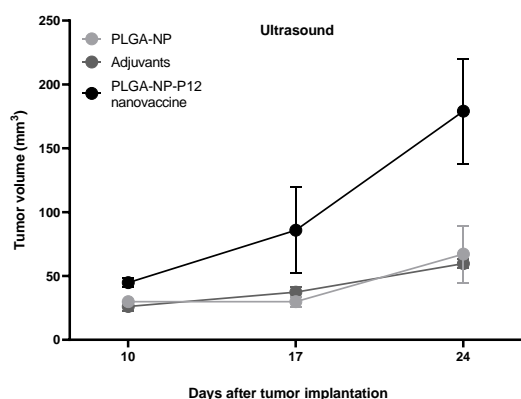
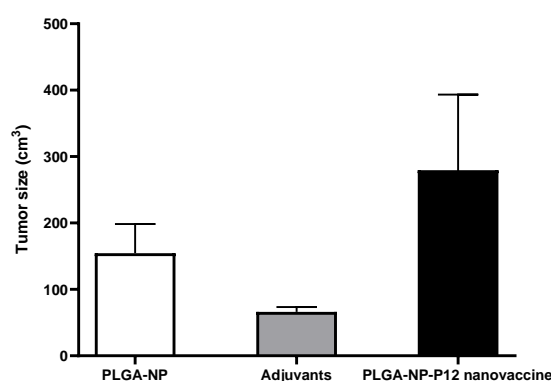
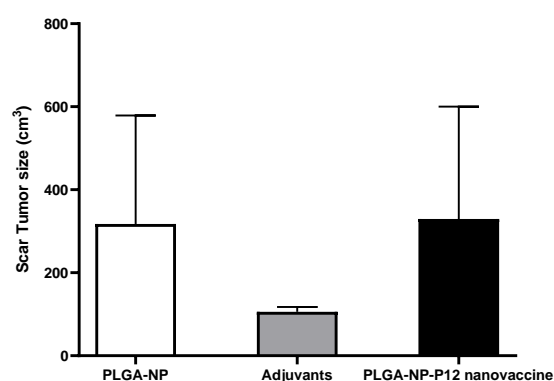
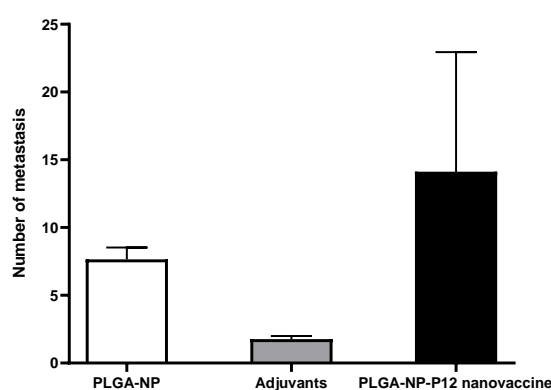
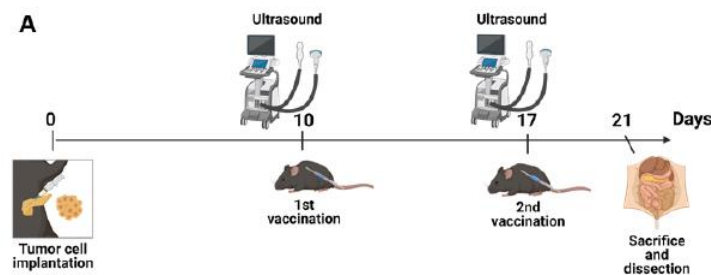
A Immunization Schedule**B Tumor size measured by ultrasound****C Tumor size measured after euthanasia****D Tumor scar size measured after euthanasia****E Metastases measured after euthanasia**

Figure 1.19 Prophylactic effect of mesothelin nano vaccine in a mouse model of PDAC. **A:** Vaccination scheme of C57BL/6 mice prior and after challenge with KPC tumor **B:** Evaluation of tumor volume by ultrasound over the

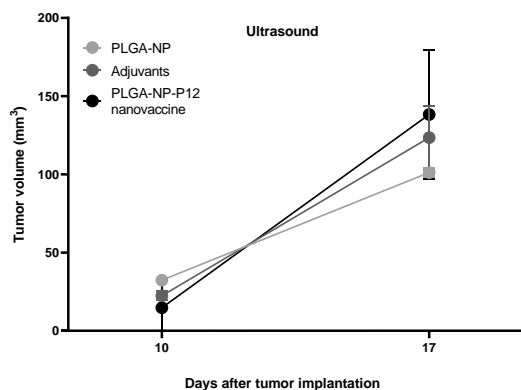
course of the vaccination scheme. **C:** Primary tumor size, **D:** scar tumor size and **E:** number of metastases on the day of sacrifice (n=1-3 per group).

To study the therapeutic capacity of the PLGA-NP-P12 nanovaccine tumor-bearing mice were orthotopically implanted with a tumor. After 10 days after implantation, mice were vaccinated with two doses of a mix of the R848 and poly(I:C) adjuvants (C1), PLGA-NPs (C2) or the PLGA-NP-P12 nanovaccine (C3). Mice were euthanized four days after the last inoculation (**Figure 1.20, A**). The tumor volume was evaluated by ultrasound during the vaccination scheme. There was an increase in the tumor volume over time in all groups and this increase was similar between the treatment groups (**Figure 1.20, B**). All groups showed similar size of the primary tumors (**Figure 1.20, C**), the scar tumor (**Figure 1.20, D**), and in the number of metastases (**Figure 1.20, E**).

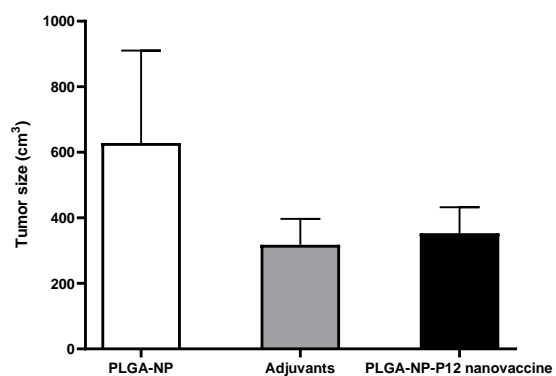
A Immunization Schedule



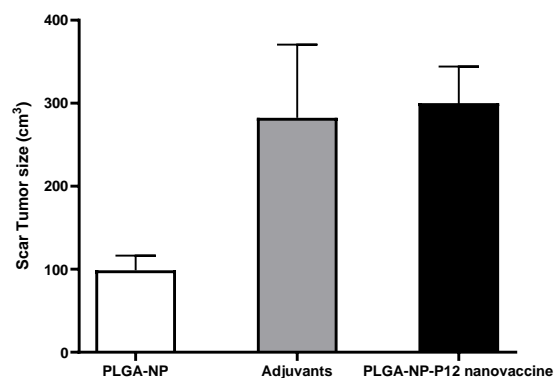
B Tumor size measured by ultrasound



C Tumor size measured after euthanasia



D Tumor scar size measured after euthanasia



E Metastases measured after euthanasia

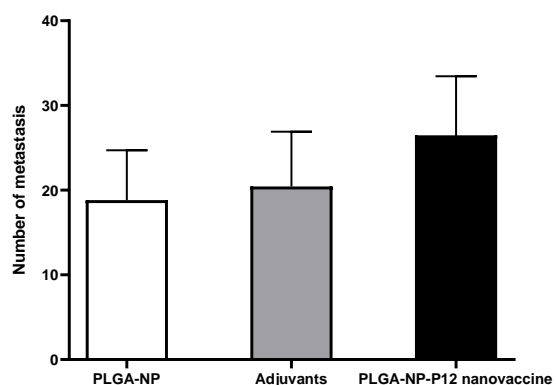


Figure 1.20 Therapeutic effect of the PLGA-NP-P12 nanovaccine in a mouse model of PDAC. **A:** Vaccination scheme of C57BL/6 mice after challenge with KPC tumor. **B:** Evaluation of tumor volume by ultrasound during vaccination. **C:** Primary tumor size, **D:** scar tumor size and **E:** number of metastases at the day of sacrifice (n=3-4 per group).

The palmitoylated chimeric construct **P12** containing three epitopes of the mesothelin antigen seems to be the best candidate for immune response at the *in vitro* level, where it shows remarkable capability of inducing a tumor-specific CD8+ cytotoxic T cell response that is able to eliminate model KPC tumor cells in a co-culture. However, *in vivo* assays show poor immune effectiveness on the KPC tumor, both in a prophylactic and in a therapeutic vaccination scheme. However, the assay must be repeated to corroborate these results with a greater number of mice and over longer periods of time. The likely cause for this discrepancy could be related to the accessibility of these effector T cells to the tumor cells in the tumor structure due to the complexity of its microenvironment, even though results show that the nanovaccine is very capable of generating a response against individual tumor cells in a culture.

1.2.4 Preliminary screening assays for PLGA-NP-Px OCV peptide nanovaccines in murine model. Comparison with the PLGA-NP-P12 nanovaccine

The PLGA-NP-Px nanovaccines containing the OCV peptides **P15** to **P18** (see **Tables 1.1** and **1.5** were formulated with PLGA-NPs by Sana Sayedipour of the Translational Nanobiomaterials and Imaging group at the Leiden University Medical Center (LUMC). Biological assays were conducted by Daniele Ferrari from the Translational Molecular Imaging Group at the Max Planck Institute. Following the rationale of these peptides as components of a previously reported anticancer vaccine⁶⁰ and noting the poor immunogenicity of short individual epitopes results in the MSLN screening, the single epitope OCV peptides (**P15-P17**) were tested as a mix of the three peptides in a nanovaccine (**PLGA-NP-OCVmix**). This formulation was then compared with the activity of the PLGA-NP-P18 nanovaccine which is based in the multiepitope OCV P18 peptide, which is a linear multi epitope composed by the three OCV epitopes (OCV1-3).

Nanovaccine formulations were injected into C57BL6 mice twice. Immunizations were performed seven days apart from one another (**Figure 1.21, A**). Mice were sacrificed two days after the last inoculation and splenocytes were collected, cultured and challenged with OCVmix (**P15-P17**) or the **P18** multiepitope OCV peptide for 48h, after which IFN- γ in the culture supernatant was measured by ELISA. Furthermore, to compare this assay to our PLGA-NP-P12 nanovaccine candidate, this scheme was also tested to the MSLN peptides, in which the single epitopes **P3**, **P6** and **P9** (palmitoylated MSLN1, 2 and 3 single epitopes) were combined as a mix in a nanovaccine formulation (PLGA-NP-MSLNmix) and compared to the PLGA-NP-P12 nanovaccine, which carries the palmitoylated multiepitope P12 peptide.

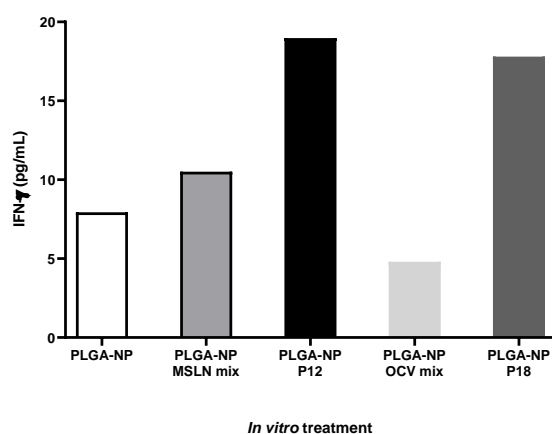


Figure 1.21 Preliminary screening of the activity of OCV and MSLN4 peptides as single epitope mixes and long multiepitope peptides

Preliminary screening results indicate that the PLGA-NP-P18 nanovaccine is able to induce activation of cytotoxic CD8⁺ T cells as measured by an elevated secretion of the IFN- γ marker (**Figure 1.21, B**), and that IFN- γ levels in this vaccination group are higher than in splenocytes from mice vaccinated with the PLGA-NP-OCVmix nanovaccine ($p < 0.05$). A similar result is obtained with the MSLN formulations (**Figure 1.21, B**). Stimulated splenocytes from mice vaccinated with the PLGA-NP-P12 nanovaccine secrete significantly higher levels of IFN- γ than the group vaccinated with the PLGA-NPs-MSLNmix. Furthermore, the preliminary screening shows that the PLGA-NP-P18 nanovaccine (OCV multipeptide peptide) achieves IFN- γ levels similar to the PLGA-NP-P12 nanovaccine, which makes it another potential candidate, although an extensive battery of *in vitro* and *in vivo* assays must be performed for this nanovaccine as it was done for the PLGA-NP-P12 nanovaccine. Considering that the OCV nanovaccine aims to target tumor proteins associated with the tumor microenvironment, these results are a promising starting point. These results further support the idea that in order to obtain a good vaccine candidate, a linear multipeptide format is a good strategy to generate novel peptide-based vaccines.

1.2.5 Multivalent antigen peptide constructs

Considering the good results obtained with the MSLN4 P12 peptide-based nanovaccine, a new presentation of this multipeptide was planned by placing the three single epitopes (MSLN1, MSLN2 and MSLN3) and the palmitic acid at different positions of a lysine-based MAP core (**Figure 1.22**). Due to the high hydrophobicity of these epitopes, before attempting this multipeptide MAP construction, we decided to test the feasibility of synthesis with two model constructs: a MAP with 4 copies of a carboxyfluoresceinated luciferase-1 peptide and a MAP with three different short peptides.

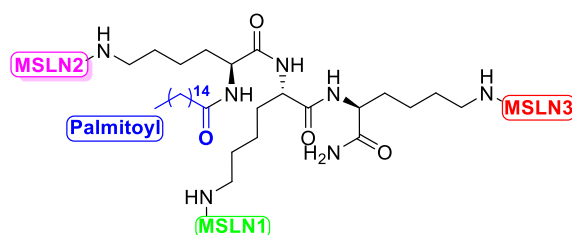


Figure 1.22 Multiple antigen peptide construct based on the assembly of the three mesothelin epitopes (MSLN1 to 3) and a palmitoyl group in a tri-lysine core.

1.2.5.1 Synthesis of a fluorescent labelled luciferase-1 multiple antigen peptide as a tumor reporter

At the suggestion of the Translational Molecular Imaging Group of the Max Planck Institute, we prepared a luciferase-1 peptide-based reporter for the antitumor activity of CD8⁺ T cells in the mouse model used for the biological assays. We decided that a multiple epitope MAP presentation might be the most appropriate to have a higher affinity to CD8⁺ T cells due to their ability to cross-present epitopes to more than one MHC I-TCR complex at any given time. In addition, the introduction of a fluorescent probe on each peptide copy can increase the intensity of the fluorescence signal and improve detection. A murine luciferase-1 epitope (LUC1) LMYRFEEEL, which specifically binds to the T cell receptor of murine CD8⁺ T cells, was selected and synthesized as a carboxyfluoresceinyl-labeled peptide and assembled onto a tri-lysine core (compound **1**, **Figure 1.23**), rendering a four-copy multiple antigen peptide construct which will be used for visualization of CD8⁺ T cell activity at the tumor site. The LUC1 peptide was synthesized as previously described, with a 5(6)-carboxyfluorescein coupled in the N-terminal amine and a C-terminal cysteine added (CF-LUC1-Cys) to incorporate the peptide into the MAP core via maleimide-thiol chemistry. A sequential coupling and protecting group removal scheme was performed to synthesize the MAP core (compound **1**, **Figure 1.23**) using Fmoc-Lys(Fmoc)-OH as the building block, yielding a core with four free amines upon final Fmoc elimination,

which are then coupled to 6-maleimidohexanoic acid, providing four maleimide functional groups (mal₄-MAP core) to conjugate the CF-LUC-1-Cys peptide in a click reaction.

Prior to conjugation of the CF-LUC-1-Cys peptide with the mal₄-MAP core, both products were purified. The mal₄-MAP core crude product showed a remarkable purity of 81% (**Figure 1.24, A**) and allowed for purification up to >99.9% with no procedural issues (**Figure 1.24, B**). Recovery for this product is high at 75% owing to its high crude yield and initial purity (**Table 1.11**) as well as the uncomplicated one-step purification. The CF-LUC1-Cys **P32** peptide crude, however, was very impure. Furthermore, this peptide showed two peaks at ~5.8 min and ~6.0 min with 21% and 29% of purity, respectively (**Figure 1.24, C**) with the mass of the expected peptide product when were analyzed by LC-MS. These two products are obtained because the starting material 5(6)-carboxyfluorescein is a mix of two isomers carrying a carboxyl group in two different positions. Focus was put on the second peak and purification of this product was carried out up to 99% (**Figure 1.24, D**). Recovery of this peptide was low at 7% due to low crude purity (**Table 1.11**). However, there was sufficient pure **P32** peptide to continue with the synthesis of the (CF-LUC1)₄ MAP (compound **2**, **Figure 1.23**).

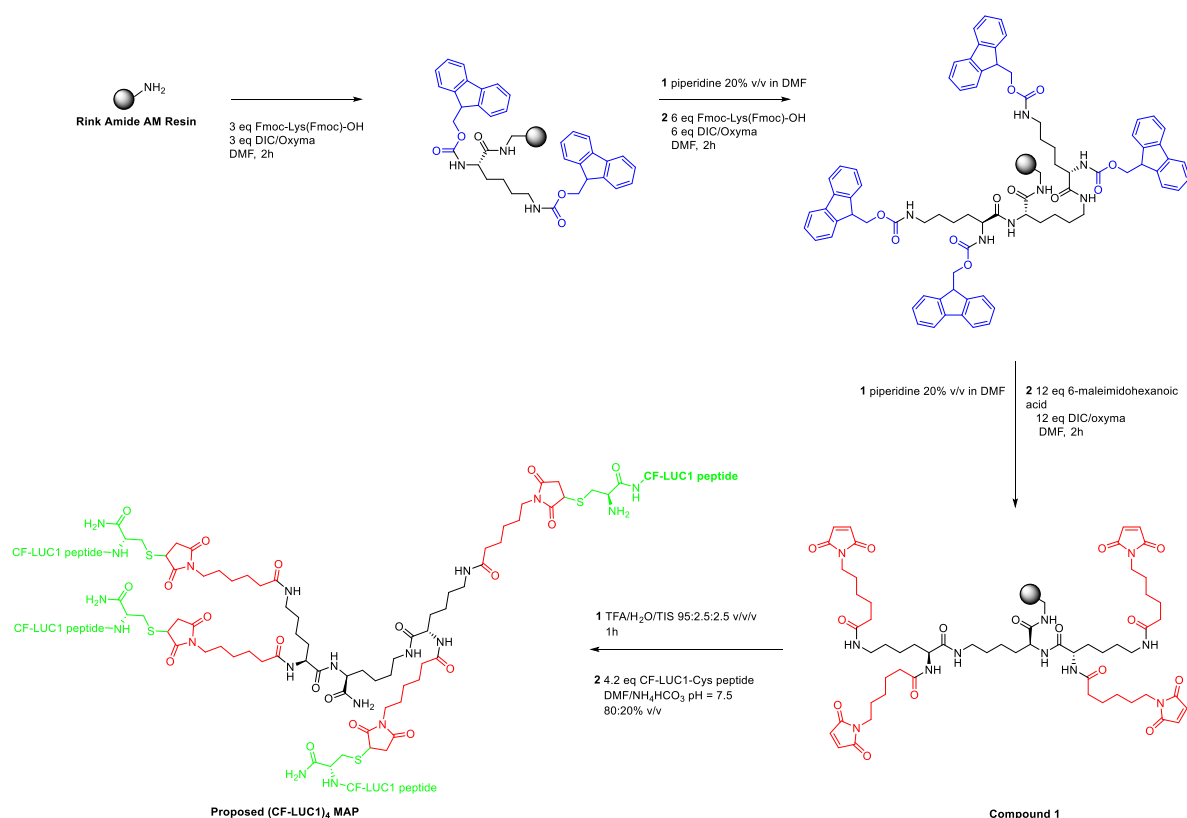


Figure 1.23 Synthetic route of the tetrameric CF-LUC-1 MAP construct production.

Table 1.11 Summary of yield and purity of CF-LUC-1-Cys peptide and mal₄-MAP core.

Product	ID	N-terminal	MW (Da)	% Crude Purity	% Crude Yield ^a	% Final Purity	% Recovery ^b
CF-LUC1-Cys	P32	CF-NH-	1689.98	29 ^c	26	99	7%
mal ₄ -MAP core	Compound 1	(mal) ₄	1174.36	81	87	100	75%

^a% yield = (crude mmol x crude purity) / (theoretical mmol)

^b% recovery = (purified mmol x purified purity) / (crude mmol x crude purity) x 100

^c% crude purity considers one of two possible P32 products.

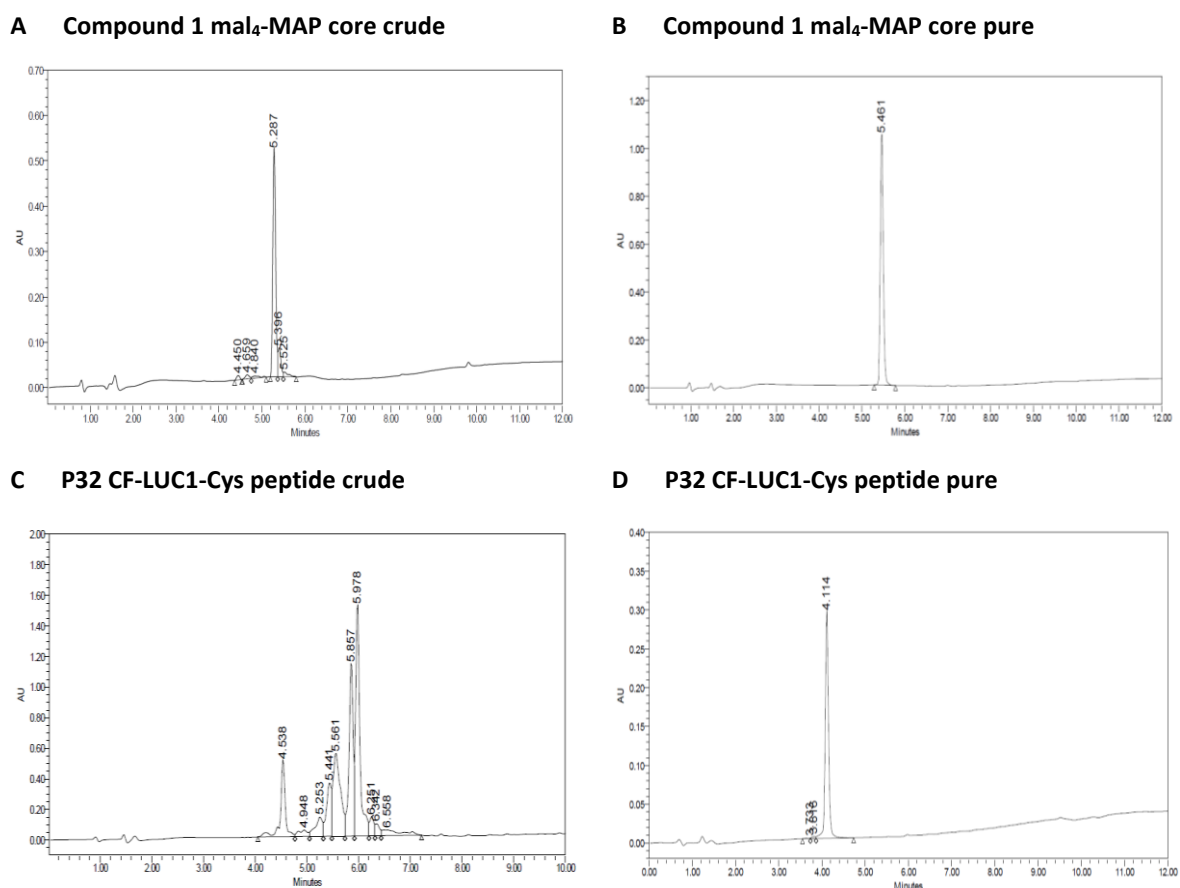


Figure 3.14 RP-HPLC for **A:** CF-LUC1-Cys **P32** peptide crude, **B:** CF-LUC1-Cys **P32** peptide pure, **C:** mal₄-MAP core crude and **D:** mal₄-MAP core pure. Gradient used was 5-100%B (CF-LUC1-Cys crude) or 30-100% B in a C₁₈ column (A: H₂O + TFA 0.045%, B: CH₃CN + TFA 0.036%).

The conjugation reaction was performed by dissolving the CF-LUC1-Cys peptide (0.044 mmol, 1.1 eq.) and the mal₄-MAP core (0.01 mmol, 1 eq.) in DMF and an equal volume of 10 mM NH₄HCO₃ buffer (pH 8.0) with 1% p/v TCEP and allowed to react. After 2 hours, analysis by RP-HPLC revealed no end product and no starting material. Diverse HPLC gradients and columns (C₁₈ and C₈) were explored to analyze the crude reaction, but none of them allowed us to detect the final product (CF-LUC1)₄ MAP. It is likely that the end product was formed but was too large and hydrophobic to be seen on C₁₈ or C₈ columns. It was also not possible to assess whether the reaction is complete or whether there was a mixture of two, three and four peptide copies incorporated onto the MAP. Although a slight excess of peptide has been added to avoid such a scenario, it still needs to be confirmed by mass spectrometry.

Considering this problem, a new approach was explored with a new core (compound **3**, **Figure 1.25**) consisting of a Lys-Cys backbone with the amines modified with a shorter 3-maleimidopropionic acid linker to anchor two peptide epitopes by thiol maleimide conjugation. The main objective was to facilitate the analysis of the final peptide conjugation product. After peptide incorporation onto the mal₂-MAP, the resulting (CF-LUC1)₂ Lys-Cys construct (compound **4**, **Figure 1.25**) can be dimerized to obtain the tetrameric MAP (compound **5**, **Figure 1.25**) through the formation of an intermolecular disulfide bridge. Following this synthetic scheme, we were able to synthesize and characterize the mal₂Lys-Cys core.

Chapter 1 Synthesis of antigenic peptide components of a pancreatic cancer nanovaccine

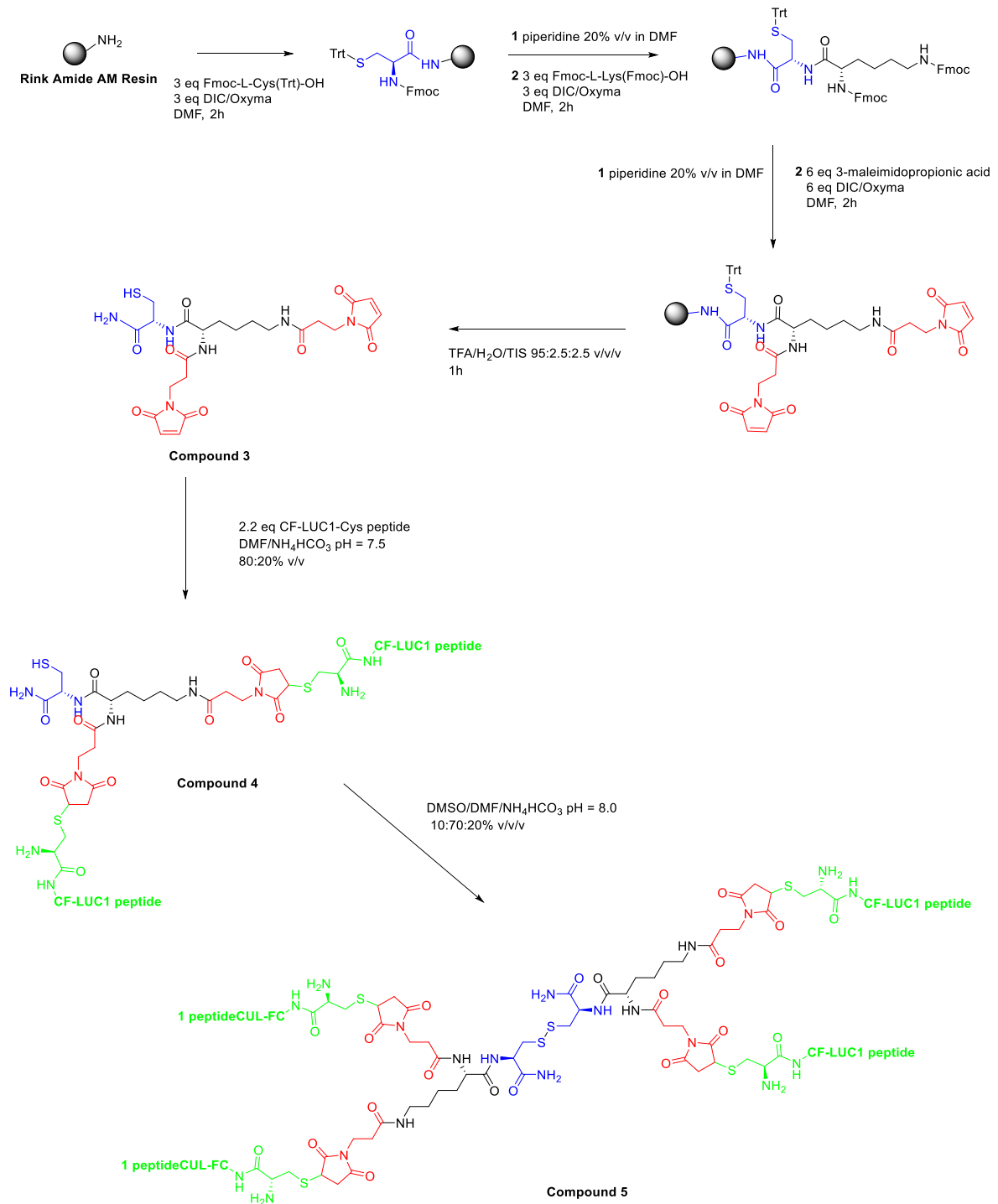


Figure 1.25 Strategy for the synthesis of the (CF-LUC1)₄ Lys-Cys MAP

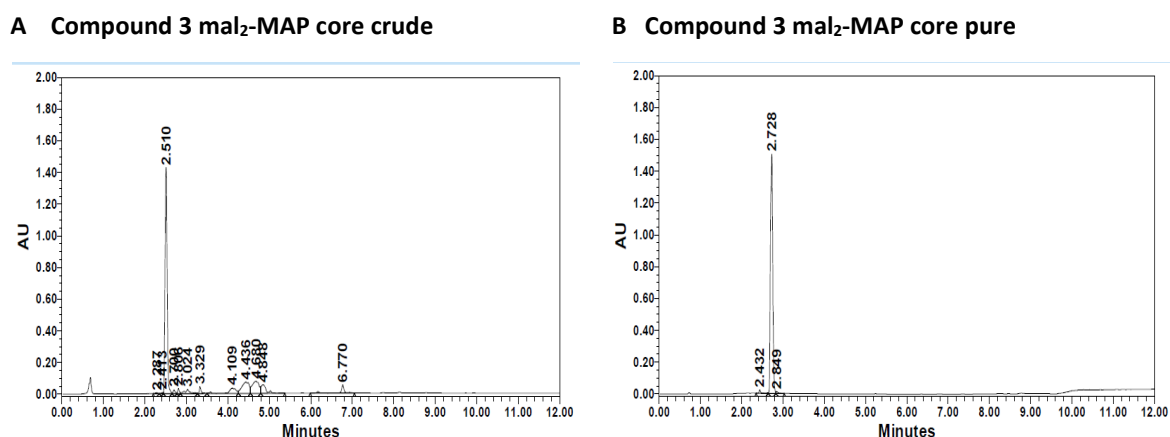


Figure 1.26 RP-HPLC for **A**: mal₂-MAP core crude, **B**: mal₂-MAP core pure. Gradient used was 5-70%B in a C₁₈ column (A: H₂O + TFA 0.045%, B: CH₃CN + TFA 0.036%).

This core showed a crude purity of 59% (**Figure 1.26, A**) and was purified to reach up to 98% purity in a single step (**Figure 1.26, B**). Although the analysis by RP-HPLC of the pure mal₂Lys-Cys core confirmed a high degree of purity, its ¹H-NMR showed a duplicity of the CH_α of Cys, indicating that this residue was racemized in the synthesis process. In terms of the final tetravalent MAP synthesis, racemization makes no difference in the introduction of peptides at the mal₂Lys-Cys and its dimerization, but it may complicate the characterization of the final bivalent and tetravalent MAPs. Furthermore, we did not consider it advisable to introduce a variable for subsequent bioassays, as we do not know if the loss of chiral integrity of the cysteine residues will affect the intended effects when tested in cells of animal models. At this point, we decided to abandon the synthesis of the fluorescence-labeled luciferase-1 multiple antigen peptide.

1.2.5.2 Synthesis of a mesothelin-based multiepitope multiple antigen peptide

Since the linear multi-epitope peptide construct (MSLN4) was the only one to show immunogenic activity in the initial bioassays (OCV multiepitope peptide requires further confirmatory assays), it was considered to also attempt to create a novel multi-epitope presentation construct by incorporating the individual epitopes into a MAP core. In contrast to MAPs carrying the same type of epitope, the construction of a multimodal MAP carrying different epitopes cannot be prepared by thiol-maleimide conjugation, as this reaction does not discriminate between the different epitopes. Due to the large number of protecting groups described for amines, the sequential introduction of the peptide epitopes onto the MAP core can be accomplished through an amide bond. A lysine-based branched scaffold with an orthogonal protection scheme for the different amines was chosen, since lysine is commercially available with several different combinations of protecting groups on its α- and ε- amines. In this work, we synthesized an orthogonally protected lysine scaffold bearing four different amino protecting groups: 2-nitrobenzenesulfonyl or nosyl (Ns), 9-fluorenylmethoxycarbonyl (Fmoc), 4-methoxytrityl (Mmt), and allyloxycarbonyl (Alloc). These groups can be removed independently to introduce the different peptides sequentially on the MAP core. The Ns group is eliminated by treatment with thiols such as thioglycolic acid or 2-mercaptoethanol, the Fmoc group is usually removed with piperidine or 4-methylpiperidine, the Alloc group is removed by hydrogenolysis carried out with catalytic amounts of tetrakis(triphenylphosphine)palladium(0) (Pd(PPh₃)₄) in the presence of phenylsilane, and the Mmt group is removed by acidolysis at low percentages of acid, such as 1% TFA or CH₃COOH in DCM.

To produce this multimodal core, we used commercially available protected amino acids Fmoc-L-Lys(Alloc)-OH, Fmoc-L-Lys(Mmt)-OH and H-L-Lys(Fmoc)-OH. The latter was used to synthesize the Ns-

L-Lys(Fmoc)-OH building block following the scheme shown in **Figure 1.27**. Briefly, the carboxyl of this amino acid (5 mmol, 1 eq) was protected with methoxyl to generate H-L-Lys(Fmoc)-OMe after which the Ns group was incorporated to produce Ns-L-Lys(Fmoc)-OMe. Finally, the methoxy protecting group was removed with lithium iodide to obtain the Ns-L-Lys(Fmoc)-OH as the final product with 96% purity (80% yield)

The multimodal core (compound **6**) was then synthesized by SPPS as shown in **Figure 1.28**. As a proof of concept, three model peptides were selected to be incorporated onto the compound **6**: adrenomorphin (**P33**), leu-enkephalin (**P34**), and endomorphin (**P35**). These were synthesized via SPPS as protected acetylated peptide models using a 2-chlorotrityl chloride resin, obtained by a very mild acydolysis treatment with 1% TFA, and then purified by semi-preparative HPLC. Synthesis performance for **P33**, **P34**, **P35** and compound **6** are summarized in **Table 1.12**.

Table 1.12 Summary of yield and purity of CF-LUC-1-Cys peptide and mal₄-MAP core.

Product	ID	N-terminal	MW (Da)	% Crude Purity	% Crude Yield ^a	% Final Purity	% Recovery ^b
Adrenomorphin	P33	Ac-NH-	1587.20	41	56	72	43
Leu-Enkephalin	P34	Ac-NH	653.65	66	77	93	71
Endomorphin	P35	Ac-NH-	809.27	85	90	95	83
multimodal-MAP core	Compound 6	Alloc-NH, Fmoc-NH, Ns-NH-, NH ₂ -	896.03	92	80	97	77

^a% yield = (crude mmol x crude purity) / (theoretical mmol)

^b% recovery = (purified mmol x purified purity) / (crude mmol x crude purity) x 100

The strategy followed for the introduction of the different model peptides to compound **6** is summarized in **Figure 1.28**. The couplings were performed in liquid phase using 1-ethyl-3-(3-dimethylaminopropyl)carbodiimide (EDC) and 1-hydroxybenzotriazole (HOBt) as coupling reagents. A liquid phase coupling strategy is preferred to incorporate the peptides into the core, as it allows working with equimolar ratios of the different components with a relatively fast assembly, avoiding deletions due to increased steric hindrance and potential aggregation in the branched structure.

The MAP core scaffold was synthesized using Fmoc-L-Lys(Alloc)-OH, Fmoc-L-Lys(Mmt)-OH and Ns-L-Lys(Fmoc)-OH as starting materials. The core was cleaved from the resin with TFA and TIS treatment which yielded compound **7** (**Figure 1.28**). Separately, the peptides were synthesized as described and cleaved from the solid support with 1% TFA in DCM and purified. These peptides did not show great difficulties in their synthesis and purification. However, adrenomorphin showed more impurities than the other two peptides (**Figure 1.29, A**). The MAP core is a relatively uncomplicated molecule to synthesize as evidenced by its RP-HPLC characterization (**Figure 1.29, D**).

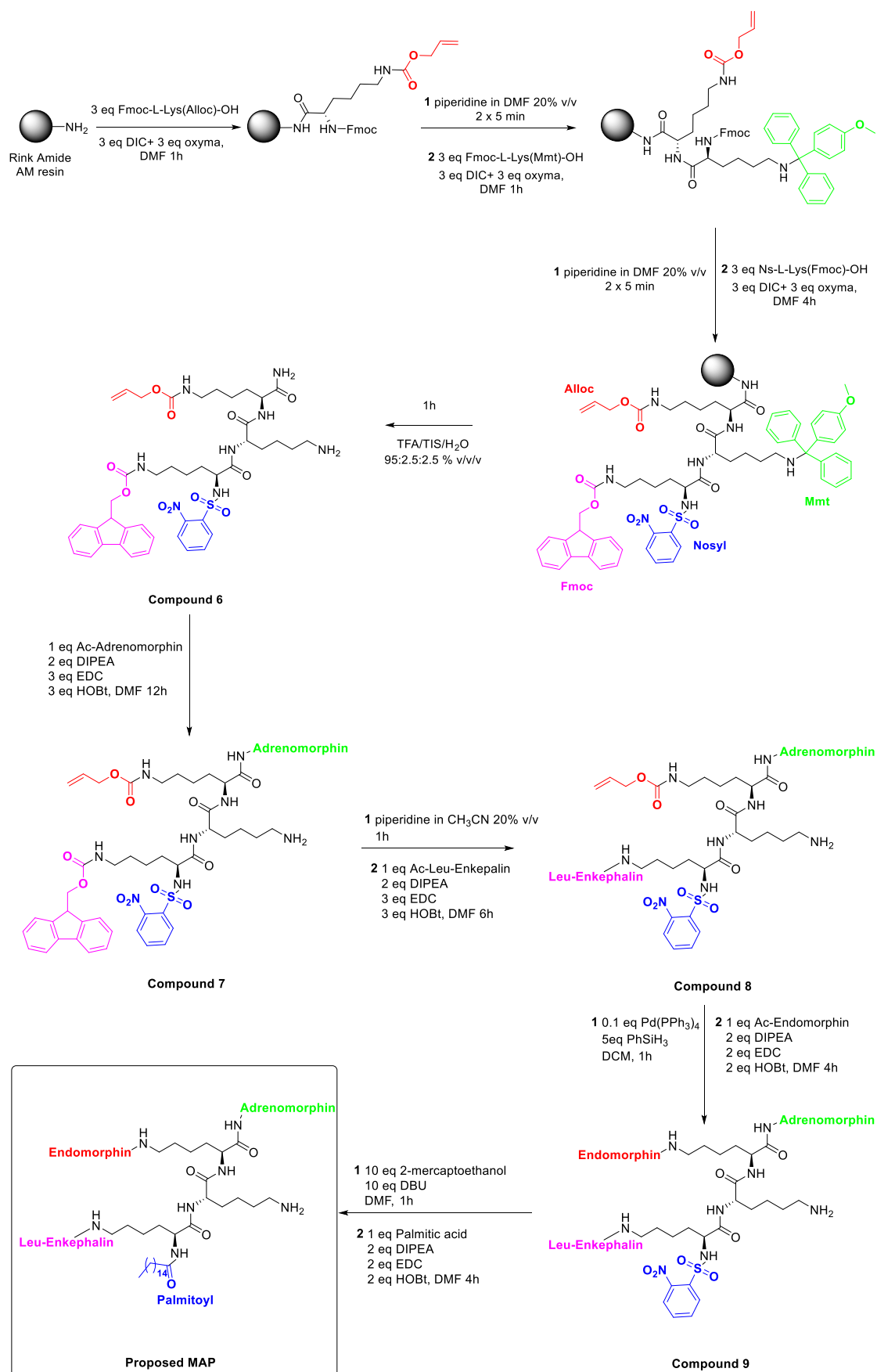


Figure 1.28 Strategy for the synthesis of the multivalent multimodal MAP carrying three peptides.

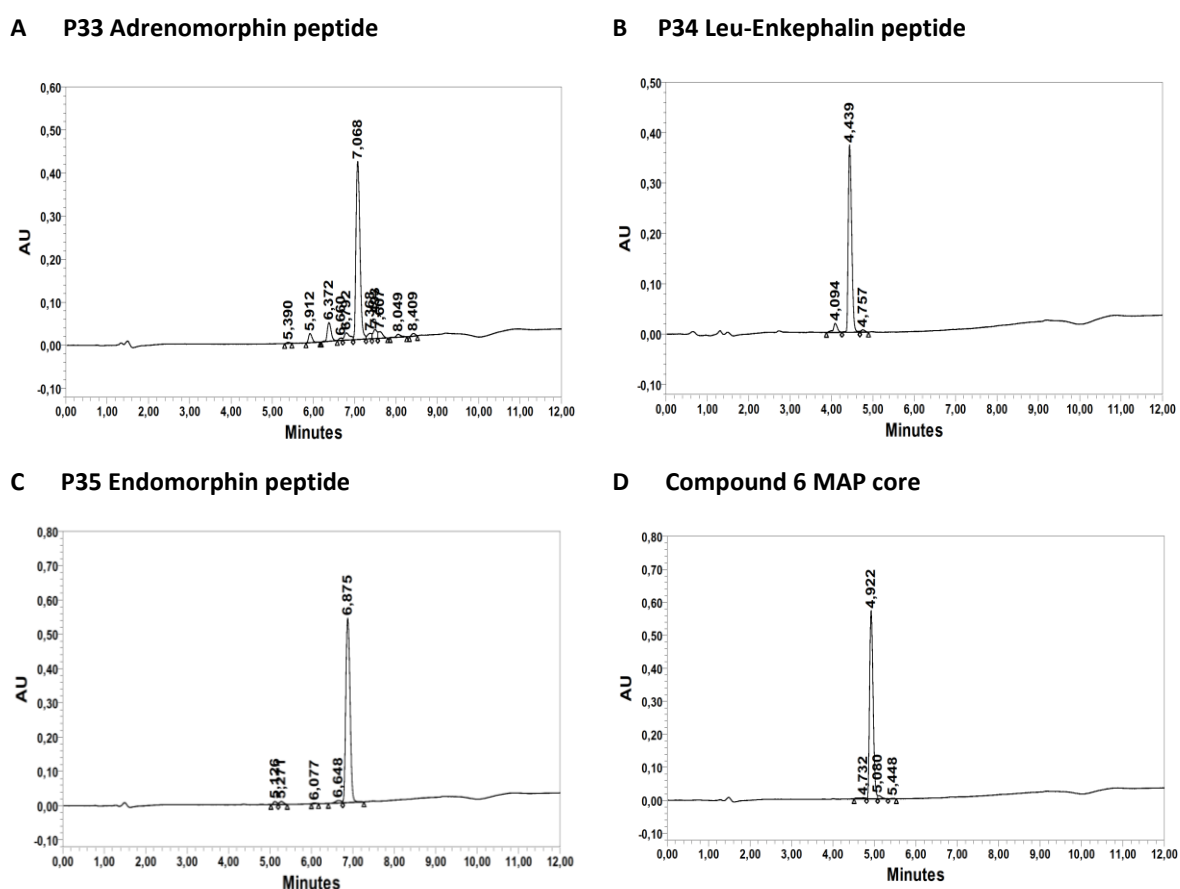


Figure 1.19 RP-HPLC for **A: P33** adrenomorphin peptide purified up to 72%, **B: P34** Leu-enkephalin peptide pure, **C: P35** endomorphin peptide pure, **D: Compound 6** multimodal MAP core pure. Gradient used was 30-100%B in a C₁₈ column (A: H₂O + TFA 0.045%, B: CH₃CN + TFA 0.036%).

We decided to perform the synthesis of the MAP by introducing the largest peptide first, adrenomorphin, with the rationale that it would be more difficult to couple it to the core if it already carried other peptides due to steric hindrance. This peptide was introduced by amide bond formation with a conversion of 80%, and the purity of the resulting α -N-Fmoc-lysyl(ϵ -N-Ns)-lysyl(ϵ -N-P33)-lysine(ϵ -N-Alloc)-CONH₂ intermediate (compound **7**, **Figure 1.28**) is of 53%, which can be expected (**Figure 1.30, A**) given the purity of the **P33** adrenomorphin peptide (**Figure 1.29, A**). The Fmoc group of compound **7** was removed with piperidine and the **P34** Leu-enkephalin peptide was introduced to form the α -N-P34-lysyl(ϵ -N-Ns)-lysyl(ϵ -N-P33)-lysine(ϵ -N-Alloc)-CONH₂ intermediate (compound **8**, **Figure 1.28**) with a 64% conversion and purity remained at 53% (**Figure 1.30, B**). The Alloc group of compound **8** was then removed and the **P35** endomorphin peptide was introduced to form the α -N-P34-lysyl(ϵ -N-Ns)-lysyl(ϵ -N-P33)-lysine(ϵ -N-P35)-CONH₂ intermediate (compound **9**, **Figure 1.28**) with a conversion of the 60% and very low purity of 25% (**Figure 1.30, C and D**). However, when we tried to remove the nosyl group of compound **9**, this was unsuccessful. This may be due to steric hindrance and poor exposition of the Ns group to the reagents, because this protecting group is generally readily removed in an hour upon treatment with thiols. Optimization of nosyl removal and purification of the starting material are necessary requirements to achieve the final compound.

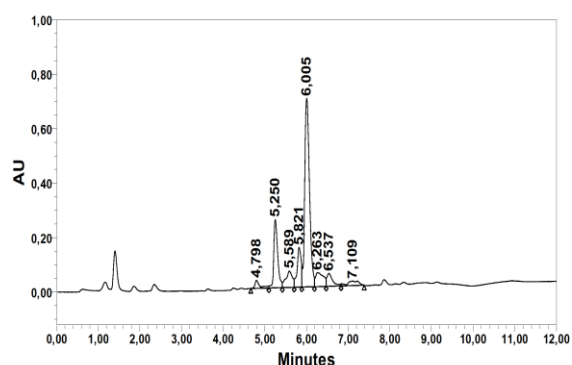
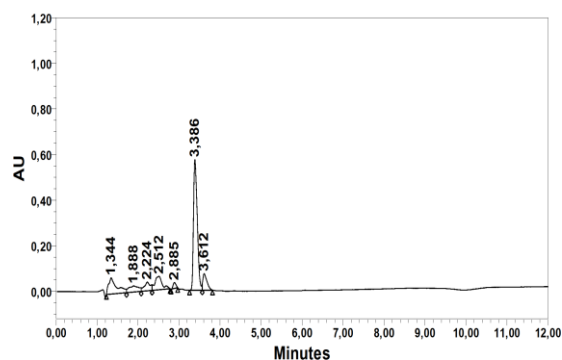
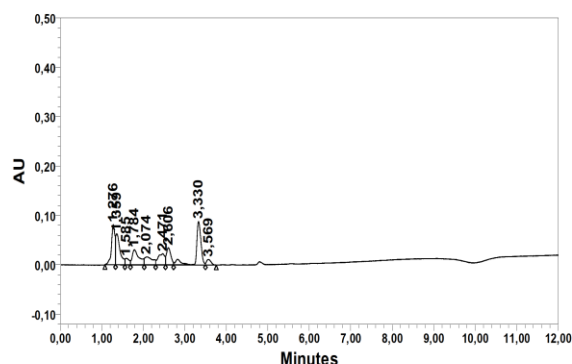
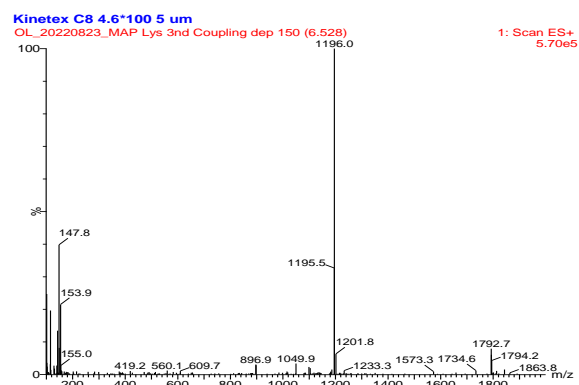
A Compound 7 α -N-Fmoc-lysyl(ϵ -N-Ns)-lysyl(ϵ -N-P33)-lysine(ϵ -N-Alloc)-CONH₂

B Compound 8 α -N-P34-lysyl(ϵ -N-Ns)-lysyl(ϵ -N-P33)-lysine(ϵ -N-Alloc)-CONH₂

C Compound 8 α -N-P34-lysyl(ϵ -N-Ns)-lysyl(ϵ -N-P33)-lysine(ϵ -N-P35)-CONH₂

D Compound 8 α -N-P34-lysyl(ϵ -N-Ns)-lysyl(ϵ -N-P33)-lysine(ϵ -N-P35)-CONH₂


Figure 1.30 RP-HPLC monitoring for the coupling of **A**: P33 adrenomorphin peptide to the MAP core, **B**: P34 Leu-enkephalin to the P33-MAP, **C**: P35 endomorphin peptide to the P33-P34-MAP and LC-MS monitoring of the coupling of **D**: P35 endomorphin peptide to the P33-P34-MAP. Gradient used was 40-100%B for **A** and 50-100%B for **B** and **C** in a C₁₈ column (A: H₂O + TFA 0.045%, B: CH₃CN + TFA 0.036%).

Our results indicate that a multimodal MAP can be produced carrying up to three different epitopes and possibly, in future work, a fourth peptide sequence or other types of moieties (lipids, fluorophores, etc.) in a single molecule, which has interesting potential applications as vaccine components. However, the starting materials need to be thoroughly purified and different deprotection schemes need to be explored considering the difficulties encountered in removing the nosyl group.

Chapter 2

**Synthesis of neuroblastoma-targeting peptides for a
quatsome delivery system**

2.1 Introduction

2.1.1 Neuroblastoma

Neuroblastoma (NB) is a form of pediatric cancer that is highly aggressive. The survival rates are inversely related to age, reaching 50% in children aged five years and older.²⁴ It is also difficult to detect in its early stages^{28,29}, and the classical treatment options are ineffective because the tumor is heterogenous, phenotypically plastic and the immune response generated against it is counterproductive as it can aid tumor growth.^{31–33} As such there is marked interest in finding adequate alternative treatments for this disease. One alternative that has emerged from research as a potential treatment for complex cancers, including neuroblastoma, is the use of ribonucleic acids (RNAs) as therapeutic agents.¹²⁸ This is due to the specificity with which they act. Specificity allows for targeted activity and fewer off-target effects, resulting in low toxicity. This is in stark contrast to traditional cancer treatments such as chemotherapy and radiation.

2.1.2 Ribonucleic acid-based therapeutics for neuroblastoma treatment

Ribonucleic acids (RNAs) are macromolecules composed of multiple copies of four base nucleotides: adenine, cytosine, guanine and uracil. These nucleotides are linked by a 5′-3′ phosphodiester bond between the ribose moiety of one nucleotide and the phosphate group of the following nucleotide.^{162–164} RNAs have biological functions primarily in gene expression and regulation.^{162–165} Therapeutic RNAs, including small interfering RNAs (siRNAs) and microRNAs (miRNAs) have emerged as an attractive alternative in cancer research.^{88,166–168} These RNAs can selectively target the genes of cancer cells, thereby avoiding the toxic side effects on healthy cells seen with both chemotherapy and radiation therapy.¹²⁸

RNAs can target cancer cells in two main ways: 1) as interfering agents that block genes associated with cancer, and 2) as messenger RNAs that can induce gene expression of specific proteins. This can include expression of antigens to generate an immune response or expression of immunomodulators, such as cytokines, to increase the potency of the anti-tumor immune response (**Figure 2.1**).^{88,128,163–165,168}

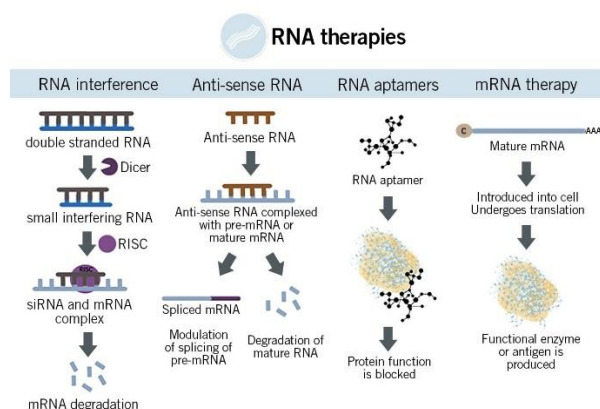


Figure 2.1 Alternatives for RNA-based therapies and their mechanism of action. **Dicer**: endoribonuclease, **RISC**: RNA-induced silencing complex.

Despite these advantages, the implementation of RNAs as a treatment for cancer remains challenging due to several factors. First, RNAs are highly susceptible to enzymatic degradation by RNAases which can degrade RNA in the bloodstream within thirty minutes. Second, the accumulation of these macromolecules in the desired target cells is a significant challenge. Systemically, they accumulate in the liver and are rapidly metabolized and cleared.^{128,166} They can also induce Toll-like receptor (TLR)-

mediated immune responses and consequently they can be degraded. Locally, RNAs have poor internalization capabilities because they are unable to cross the cell membranes due to their high molecular weight, hydrophilic nature, and negative charge. While they are highly specific for the genes they target, this selectivity is useless outside of the cell.^{128,166}

These limitations result in poor bioavailability and biodistribution, making their use in *in vivo* models and thus clinical application very challenging. This underscores the need for a delivery system that can encapsulate the RNA, protect it from enzymatic degradation, allow it to be internalized into the cell and nucleus, and enable it to reach its specific gene target while minimizing off-target effects such as activation of TLR pathways. Lipid-based nanovesicles represent an optimal delivery system that can maintain the integrity of the RNA cargo, be internalized into the cell via endocytosis, and thus allow delivery of the RNA cargo to its intracellular target. Within these lipid-based nanovesicles, liposomes are the most widely used type of lipid nanocarrier for nucleic acid loads. These spherical, bilayer phospholipid-based vesicles have been used in FDA-approved formulations. Recently, another type of non-liposomal nanocarrier based on sterols, called quatsome, has been developed with some interesting properties.^{102,103}

2.1.3 Quatsome-based nanovesicles as delivery systems for miRNA

Quatsomes (Qs) are non-liposomal lipid nanovesicles composed of sterols, primarily cholesterol or cholesterol derivatives, and stabilized by cationic surfactants, of which cetyltrimethylammonium bromide (CTAB) and myristalkonium chloride (MKC) are the most commonly used (**Figure 2.2**). These nanovesicles are capable of carrying drug loads, whether encapsulated or on their surface. Qs are thermodynamically stable, homogeneous in size, unilamellar, and have the ability to encapsulate and adsorb a wide range of small molecules and macromolecules. These physical properties are sometimes not present in liposomes. In addition, they exhibit remarkable stability under *in vivo* conditions.^{102,103}

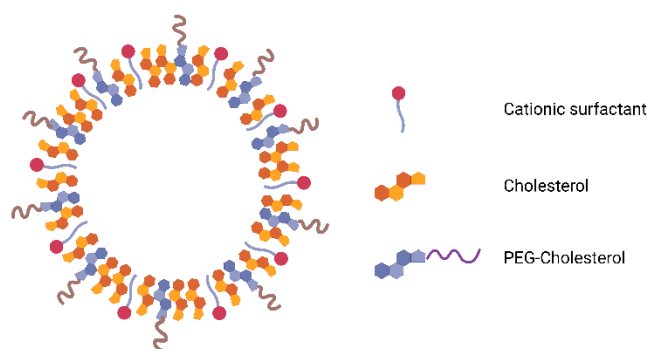


Figure 2.2 Basic structural composition of a quatsome nanovesicle (created with BioRender.com).

Qs can be prepared by sonicating a solution of the components, resulting in self-assembly of the nanovesicle, or they can be prepared in a more modulated manner using a compressed fluid-based method. In both cases, lipid vesicles require an external energy input for self-assembly. The second method, DELOS-susp (Depressurization of an Expanded Liquid Organic Solution into Aqueous Solution), involves dissolving the components in ethanol as a solvent, which is then expanded with CO₂ in a pressurized chamber. Depressurization with N₂ to water containing the surfactant yields the vesicle. The process is shown in **Figure 2.3** and results in a set of nanovesicles that are homogeneous and stable. The vesicles can be characterized and functionalized as desired.¹⁰²

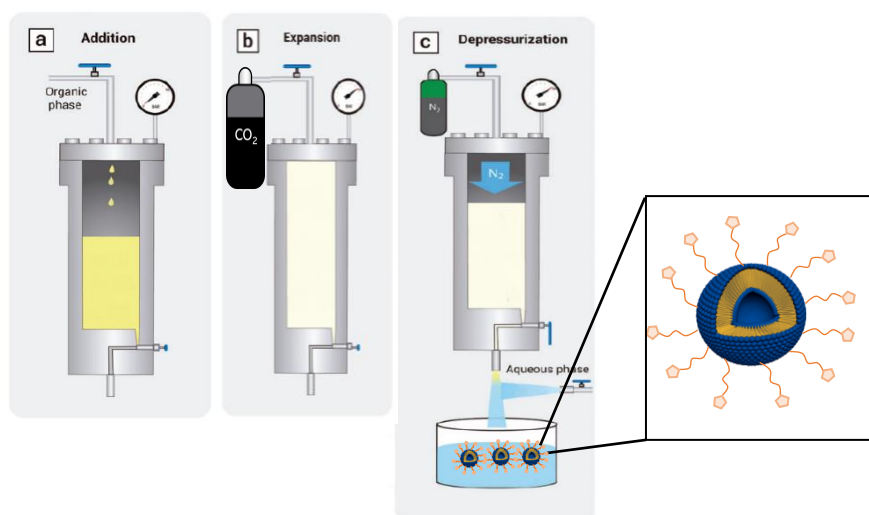


Figure 2.3 Schematic representation of the stages of the DELOS-susp methodology for the preparation of quatsomes. Components dissolved in organic solvent are added to the chamber (a), which is then expanded by gas (b) and then depressurized into water with surfactant (c) to yield the nanovesicle.

Lipid-based nanocarriers such as quatsomes and liposomes serve as potent systems that fulfill many of the requirements to protect and deliver therapeutic RNA. However, neither the RNA nor the lipid-based nanovesicle can accumulate in a specific tissue or cell type. The lack of target tissue specificity is an important issue that needs to be addressed in order to fully exploit the advantages of RNA therapeutics and lipid-based delivery systems in the treatment of cancer. While in some cases this problem can be circumvented if the tumor is accessible and the formulation can be injected directly at the tumor site, this is not the case for other cancers such as neuroblastoma. In addition, lipid-based nanocarriers readily accumulate in the kidney and, once inside the cells, in the reticuloendothelial system, ultimately leading to rapid renal clearance. Therefore, systemic distribution via the bloodstream is necessary. However, relying on passive targeting of the tumor is not suitable, so the introduction of specific targeting moieties is crucial to direct the formulation to the target tumor and facilitate rapid internalization and accumulation of the nanovesicles in the specific tumor cells. At the same time, this increased specificity will result in fewer off-target effects and thus reduced toxicity.

2.1.4 Targeting moieties for neuroblastoma

A targeting moiety is a molecule that specifically interacts with a receptor present on the targeted cell type or tissue and is typically introduced with, directly linked to, or within the formulation of the bioactive compound. For tumor cells, these receptors are typically overexpressed in the cell membrane. Targeting moieties can include macromolecules such as immunoglobulins, or ligands such as peptides and smaller molecules. The addition of these moieties to a drug formulation allows active targeting of the tumor cells, thus solving many of the problems that can be expected with passive targeting schemes. The active targeting scheme is shown in **Figure 2.4**.

The use of targeting peptide ligands represents an optimal option for incorporation onto the surface of the QS delivery system to facilitate the accumulation of therapeutic RNA in neuroblastoma cells. To select good targeting ligands for neuroblastoma, a bibliographic search was performed to localize receptors/proteins overexpressed on the surface of neuroblastoma tumor cells that have known specific ligands. Several peptide ligands were identified that specifically bind three receptors/proteins overexpressed on neuroblastoma tumor cells, the diasilanglioside receptor (GD2), the tropomyosin receptor kinase B (TrkB), and the norepinephrine transporter (hNET). A total of five peptide ligands were selected because of their relatively short lengths and the absence of post-synthesis modifications

such as disulfide bridges, which can complicate final incorporation into the QSs. These sequences are shown in **Table 2.1**. Furthermore, a known ligand molecule for hNET, p-aminobenzylguanidine (PABG), was selected as an additional targeting moiety.¹⁶⁹ PABG is an analogue of the *meta*-iodobenzylguanidine (MIBG) a synthetic norepinephrine ligand, that selectively binds to hNET. MIBG labelled with radioactive iodine (^{123/131}I-MIBG) is widely used for the diagnosis of NB.¹⁶⁹

Table 2.1 Neuroblastoma-targeting labelled peptide sequences.

Peptide	Sequence	Target
NB1	YSHSHSYWLRSGGGC	GD2 ¹⁷⁰
NB2	SHSYWLRSGGGC	GD2 ¹⁷⁰
NB3	WHWRLPSGGGC	GD2 ¹⁷¹
NB4	CSMAHPYFAR	TrkB ^{172,173}
NB5	GASNGINAYLC	hNET ¹⁷⁴

In the present work, the peptide ligands were synthesized by SPPS with an additional cysteine at the C-terminal of their sequence, except for peptide NB4, whose sequence naturally presented a cysteine at the N-terminal position. A thiol derivative of PABG was also synthesized. All selected targeting ligands were conjugated to a fluorescent probe to study their internalization ability on neuroblastoma cells in order to select the most suitable targeting ligand candidate to be incorporated on the surface of a QS-based delivery system. It is expected that the peptide and molecule incorporated into the QS delivery system will facilitate accumulation in neuroblastoma tumor cells.

The work of this thesis chapter was done in collaboration with the Neural Tumors Laboratory of the Translational Research Group on Cancer in Childhood and Adolescence at the Vall d'Hebron Institut de Recerca (VHIR) and the Nanomol group at the Institut de Ciències dels Materials de Barcelona (ICMAB-CSIC). My work focused on the synthesis of the targeting ligands and their derivatization with a fluorescent probe. Together with Júlia Piqué from the Nanomol group, I carried out the work related to the conjugation of two targeting ligands to the QSs, work that was carried out during a short stay at the ICMAB-CSIC. Finally, the biological evaluation was carried out by the Neuronal Tumors Laboratory of the Translational Research Group on Childhood and Adolescent Cancer at the VHIR.

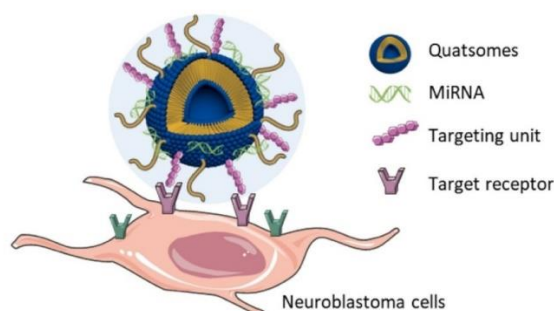


Figure 2.4 Active targeting scheme in a quatsome delivery system for a therapeutic RNA aimed at neuroblastoma tumor cells.

2.2 Results and Discussion

2.2.1 Synthesis of the selected targeting moieties and the corresponding 5-fluoresceinated-derivatives. Cellular uptake studies

Neuroblastoma targeting peptides (**Table 2.2**) were synthesized using manual standard SPPS protocols. These peptides were selected for their optimal length for rapid synthesis and their ability to target both the neuroblastoma microenvironment and the tumor. Peptides without a cysteine in their sequence were synthesized with a C-terminal cysteine separated from the rest of the sequence by three glycine residues. The peptides were purified by semi-preparative HPLC, and all final products were characterized by RP-HPLC and LC-MS.

The synthetic addition of cysteine provides a thiol function that allows conjugation to the nanovesicle via a cholesterol-PEG-maleimide moiety, which was also used to introduce a fluorescent probe onto the purified peptides by reaction of the thiol with fluorescein-5-maleimide. Both conjugation reactions are based on the Click-Michael addition reaction between thiol and maleimide functions (**Figure 2.5**), which is fast, clean and selective.^{175,176} As an example, **Figure 2.6** shows the analytical HPLC of the final pure conjugated peptide ligands.

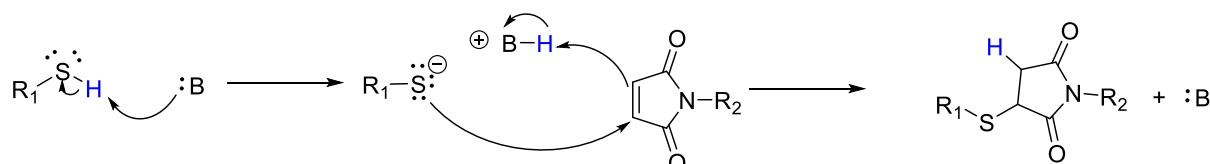


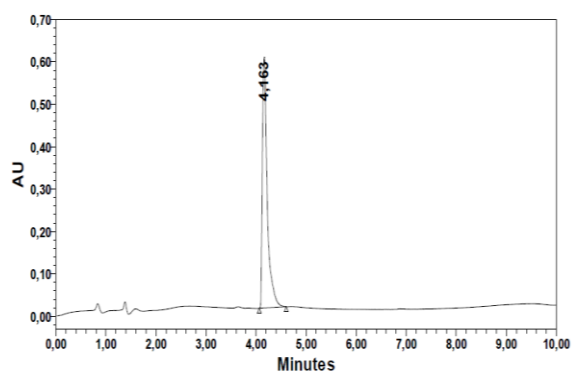
Figure 2.5 The thiol-maleimide Michael addition reaction mechanism.

Ten to twenty milligrams of each peptide was labeled with fluorescein-5-maleimide and then purified by HPLC to yield the corresponding 5-fluoresceinyl peptide. This process yielded five to ten milligrams of 5-fluoresceinyl peptides with purities ranging from 93% to >99.9%, which was sufficient for cell localization assays.

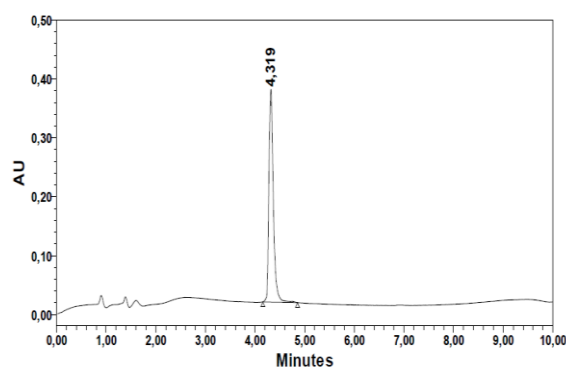
Table 2.2 Synthetic performance of neuroblastoma-targeting peptides

Peptide	ID	Cysteine Thiol	MW	% Crude Purity	%Yield	% Final	%Recovery
NB targeting peptide 1	P36	-SH	1695.8	64	46	>99.9	46
	P37	-S-mal-Fl	2036.1	90	93	>99.9	92
NB targeting peptide 2	P38	-SH	1308.4	60	59	>99.9	59
	P39	-S-mal-Fl	1648.7	89	94	>99.9	97
NB targeting peptide 3	P40	-SH	1254.4	94	92	>99.9	92
	P41	-S-mal-Fl	1681.8	92	95	>99.9	95
NB targeting peptide 4	P42	-SH	1181.4	85	79	94	75
	P43	-S-mal-Fl	1608.8	96	85	94	89
NB targeting peptide 5	P44	-SH	1081.2	74	67	93	63
	P45	-S-mal-Fl	1508.6	89	90	94	85

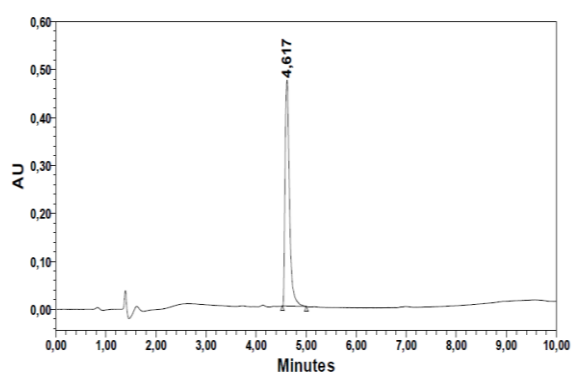
A P37 S-mal-FI peptide



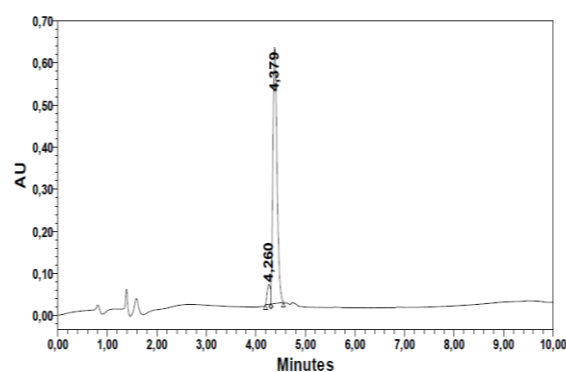
B P39 S-mal-FI peptide



C P41 S-mal-FI peptide



D P43 S-mal-FI peptide



E P45 S-mal-FI peptide

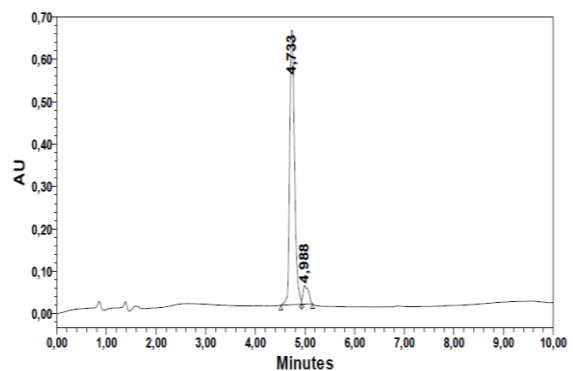


Figure 2.6 RP-HPLC of pure fluorescein-conjugated neuroblastoma-targeting peptides using a gradient of 5-100% B at r.t. in a C_{18} column (A: H_2O + TFA 0.045%, B: CH_3CN + TFA 0.036%).

The thiolated-PABG derivative was synthesized (**Figure 2.7**) from 4-aminobenzylamine by first guanidylating the benzylamine with N,N' -DiBoc-1H-pyrazole-1-carboxamide to give the intermediate N,N' -DiBoc-PABG (**1**) (96% yield). The thiol function was then introduced by the addition of 3-(tritylthio)propanoic acid (3TTPA) to the aromatic amine of intermediate **1** through an amide linkage using the symmetrical anhydride method (**2**) to give intermediate **3** (85% yield). Boc and trityl protecting groups were chosen as acid labile groups to avoid unwanted secondary reactions. TFA treatment of the intermediate **3** quantitatively afforded the thiolated-PABG derivative (**4**), which was derivatized with fluorescein-5-maleimide by a maleimide-thiol reaction under basic conditions (pH 8) to afford the 5-fluoresceinyl-PABG (**5**) (49% yield).

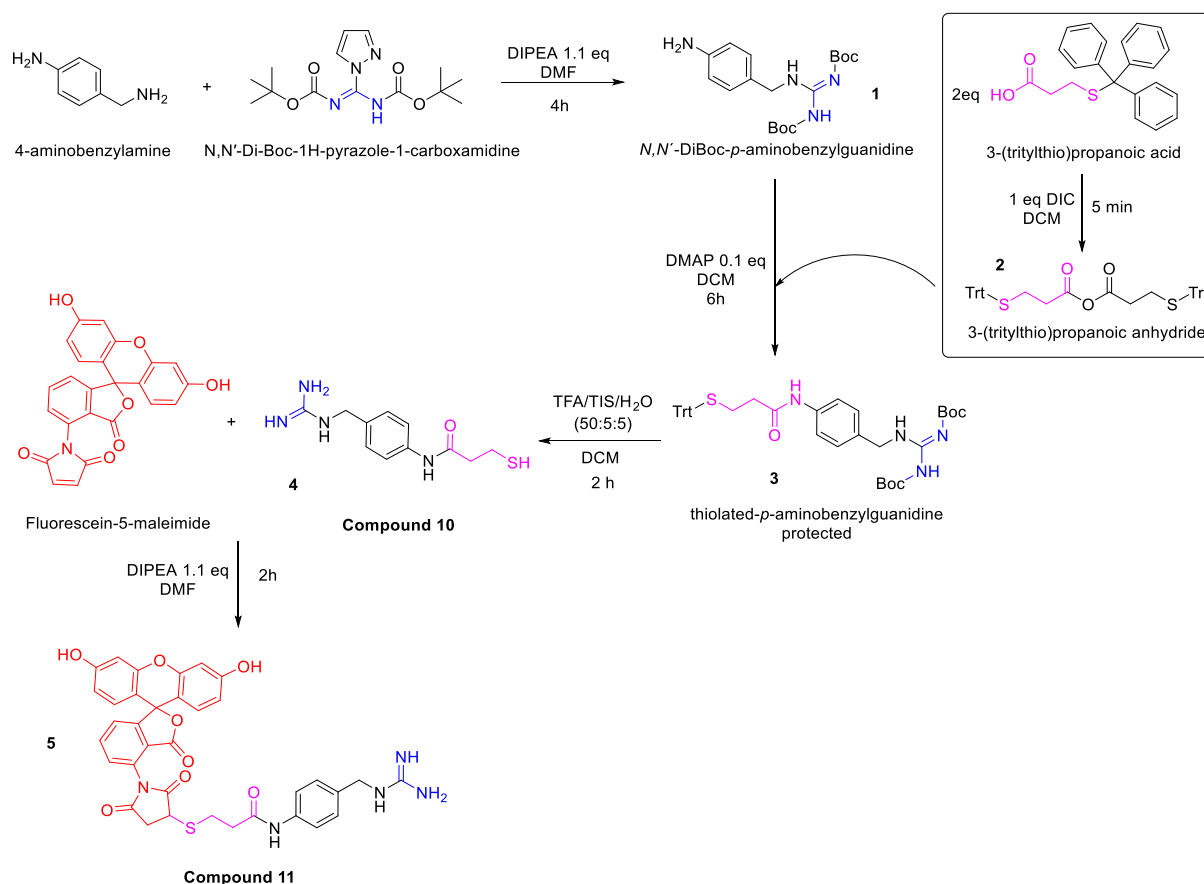


Figure 2.7 Synthetic scheme of thiolated-PABG derivative and the corresponding fluoresceinyl conjugate.

The fluorescently labeled peptides and the fluoresceinyl thiolated-PABG derivative were generated to facilitate cell uptake studies by confocal microscopy of these targeting moieties in neuroblastoma cell lines. This cell uptake assay was performed by Dr. Ariadna Boloix from the research group of Dr. Miguel Segura at the Vall d'Hebron Institut de Recerca. The results showed that the **P41** peptide H-WHWRLPSGGGC(s-mal-FI)-NH₂ has the strongest binding affinity for the CHLA-90 cell line after 1 h of incubation (**Figure 2.8, A**). The **P39** peptide H-SHSYWLRSGGGC(s-mal-FI)-NH₂ ranks second, while the **P37** peptide is not a promising homing candidate. In addition, the **P43** and **P45** peptides showed non-specific binding to a non-neuroblastoma cell line, thus eliminating their potential use as targeting peptides. As expected, the fluoresceinyl thiolated-PABG derivative ligand also exhibits robust homing capability for CHLA-90 (**Figure 2.8, B**). Therefore, the **P40** peptide and the thiolated-PABG (**Figure 2.9**) were the selected candidates for conjugation, while the **P38** peptide was retained as a potential candidate if needed for further investigation.

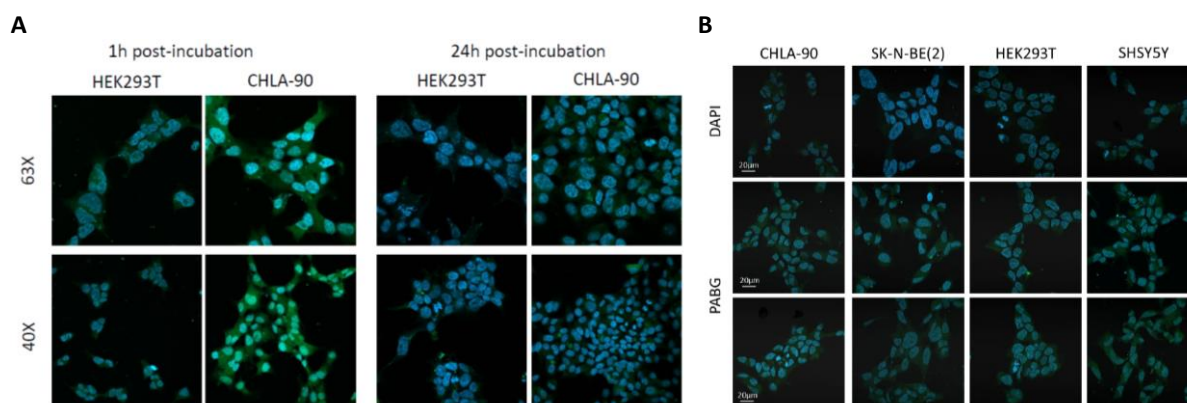


Figure 2.8 Binding assay for Peptide 3 in CHLA-90 cell line at 1 and 24 h (A) and PABG in different neuroblastoma cell lines (B). DAPI was used as a DNA intercalant reagent to dye cell nuclei.

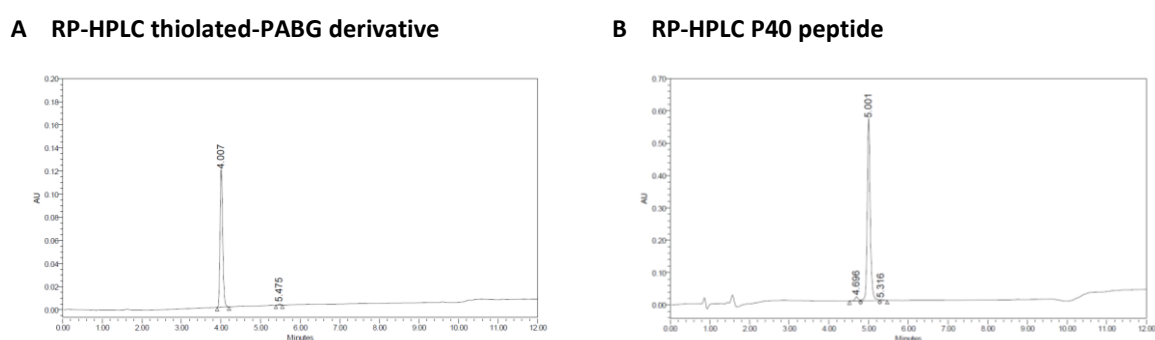


Figure 2.9 RP-HPLC of A: thiolated-PABG and B: P40 peptide after purification in a C_{18} column using a 5-70%B gradient. Thiolated-PABG is detected at 254 nm while the P40 peptide is detected at 220 nm.

2.2.2 Preparation of quatsome nanovesicles and optimization of thiolated-PABG derivative conjugation

All the work on the formulation of QSs and the conjugation of synthetic ligands was carried out during a short secondment at the Institut de Ciències dels Materials de Barcelona (ICMAB-CSIC) in collaboration with Júlia Piqué, under the supervision of Dr. Mariana Köber and Professor Nora Ventosa.

The components (Figure 2.10) for the formulation of QS nanovesicles include 3β -[N-(N',N'-dimethylaminoethyl)-carbonyl]cholesterol (DC-Chol), myristalkonium chloride (MKC) as a surfactant, and cholesterol-PEG₂₀₀₀-maleimide (Chol-PEG₂₀₀₀-mal). The positive charges of DC-Chol are critical for the incorporation of the therapeutic miRNA, while the PEG moiety of the Chol-PEG₂₀₀₀-mal carries the maleimide group onto which the thiol of the targeting ligands (thiolated-PABG derivative and P40 peptide) is incorporated. QSs containing 2 μ mol of cholesterol-PEG₂₀₀₀ maleimide (QS 001) were formulated by DELOS-susp method and characterized for particle size distribution and Z-potential determination in a Zetasizer ZEN 3600 (Malvern Panalytical Ltd., United Kingdom). The formulation was first diafiltrated to remove any excess reagents. The pH was then adjusted to 7.5 with 2-[Bis(2-hydroxyethyl)amino]-2-(hydroxymethyl)propane-1,3-diol (Bis-Tris) buffer. This was done to ensure the formation of the nucleophilic thiolate. Among the available buffers, phosphate buffered saline (PBS) was excluded because it would have resulted in the addition of unnecessary sodium and potassium chloride salts. Tris(hydroxymethyl)aminomethane (Tris) was also excluded from consideration because it is a primary amine and there was uncertainty as to whether its nucleophilicity would result in competition with the thiolate for maleimide groups, as occurs with lysine ϵ -amino groups.^{175,177}

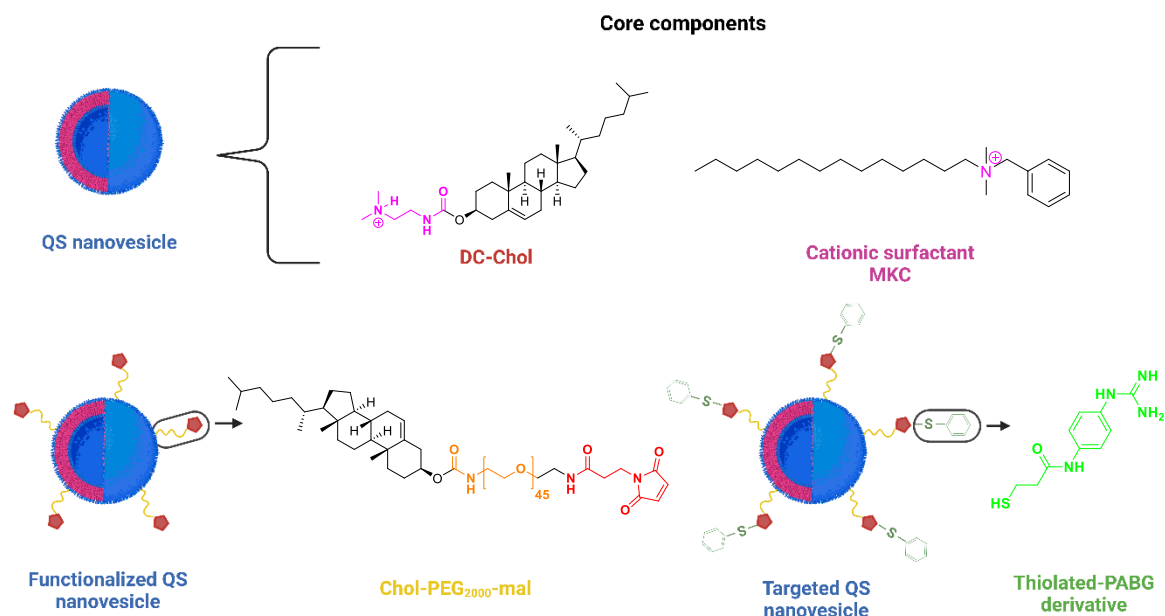


Figure 2.10 Strategy for the formulation of quatsomes composed of DC-cholesterol and Chol-PEG₂₀₀₀-maleimide for miRNA loading and conjugation of targeting PABG. This strategy is also valid for the incorporation of cysteinyl-peptide.

As a first conjugation assay (**QS 001**) 1.2 equivalents of thiolated-PABG derivative (compound **10**, 2.4 μmol) were added to a QS suspension and stirred for three hours. This equivalent value was determined considering the quantity of Chol-PEG-Mal formulated. Subsequently, sample aliquotes were taken at 1, 1.5, 2, and 2.5 hours, and ultracentrifugation was performed on each of them to eliminate the reagents that have not reacted from the QS. The estimation by HPLC of the non-reacted targeting ligand in the supernatant fraction permitted us to determine indirectly the targeting ligand incorporated to the QSs.

The ultracentrifugation conditions tested were mild, with a force of 3,000 x G for 10 minutes. This method was not sufficient to completely remove the nanovesicles from the solution. The supernatant still contained 5.5×10^{11} particles per milliliter, as shown in **Table 2.3**. The supernatant was analyzed by RP-HPLC and compared to a PABG control. It was observed that the consumption of the available PABG stopped after one hour (**Figure 2.11**). By comparing the areas under the integrated peak of the PABG derivative in the HPLC traces, it can be observed that approximately 80% of the available PABG remains in solution. Consequently, the results indicate that initially there is a conjugation of 20% of the theoretical maleimide units present in QS. (**Table 2.3**). This inefficiency of the conjugation process can be explained by several reasons. First, it was observed that the thiolated-PABG derivative sample exhibited 24% bi-product due to dimerization by disulfide formation between two PABG derivative units, even when it was stored at -20°C . This reduced the amount of PABG derivative available for conjugation, indicating the need to treat this compound with a reducing agent, TCEP, prior to conjugation to QSs. Second, we considered the possibility that the availability of functional maleimides for conjugation in QS was limited. The underlying cause can be attributed to the high probability that the Chol-PEG₂₀₀₀-mal is incorporated into the nanovesicle on both sides of the bilayer of QS, the inner and outer layers, resulting in an immediate reduction in the functionality for QS surface conjugation. This problem cannot be controlled, but an attempt was made to circumvent this limitation by doubling the amount of Chol-PEG₂₀₀₀-mal, thereby increasing the surface density of maleimide functions. This should result in an increased conjugation rate. Another possible cause of the low conjugation

supernatant carries 10^9 particles/mL, a 2-log reduction in the amount of suspended nanovesicles and representing 0.1% of the total nanovesicle content. No other setting could achieve this efficiency.

Table 2.3 Ultracentrifugation of QS suspension, analysis of particle concentration by MADLS and estimation of conjugation by RP-HPLC after 2h of conjugation

#	Sample	Conditions	% Conjugation	particles/mL
1	QS001 UCF	1000 x G, 10 min	20	5.5×10^{11}
2	QS004 UCF	10000 x G, 30 min	43	8.0×10^{11}
3	QS004 UCF	100000 x G, 30 min	38	4.0×10^{11}
4	QS005 UCF	600000 x G, 6 h	47	1.0×10^9

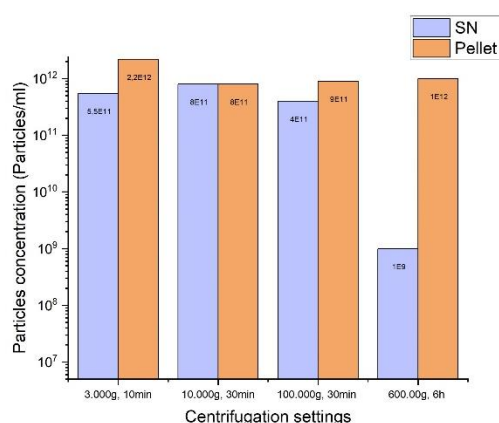


Figure 2.12 Quantification by MADLS of the particles in all ultracentrifugation conditions that were tested after 2 h of conjugation (SN: supernatant, pellet: QS).

AMICON filtration units work by molecular weight exclusion, using a dialysis membrane as a filter to separate all molecules above a certain molecular weight cutoff from all molecules below that cutoff during solution centrifugation. In this case, the thiolated-PABG derivative is filtered through the membrane and separated from the much larger nanovesicles, which are retained. The separation efficiency obtained with AMICON filters was then compared with the best ultrafiltration conditions (**QS005 UCF**). The results show that these give similar results to ultracentrifugation (**Table 2.4**), but one of the samples (**QS 006 Amicon**) contained 1 log more particles. This shows that ultracentrifugation is slightly better and more reproducible than separation with AMICON. However, the conjugation efficiency on each batch (**QS 005** or **QS 006**) is slightly different depending on the separation method used, being higher when the AMICON filtration method is used. This suggests that the ultracentrifugation process may affect the integrity of the QS due to the harsh mechanical forces applied.

Table 2.4 Comparison of ultracentrifugation (UCF) and AMICON filtration (Amicon) separation methodologies.

Sample	% Conjugation	particles/mL
QS005 UCF	47	1×10^9
QS005 Amicon	53	1×10^9
QS006 UCF	7	1×10^9
QS006 Amicon	19	1×10^{10}

A third separation method is based on size-exclusion chromatography (SEC) methodology. SEC is the simplest, fastest, and mildest (in terms of vesicle integrity) method for separating nanovesicles from solutes. A pre-packed Sephadex G-25 column, with an exclusion limit of approximately Mr 5000, was used to perform the separation of the thiolated-PABG derivative, which did not react with the QSs. The cutoff of this column allows the separation of QSs from molecules with molecular weights below 1000, as thiolated-PABG derivative (MW = 252 Da). This column is eluted by gravity, and as first choice we used miliQ H₂O as eluent. In this case we did not detect any thiolated-PABG derivative in the elution fractions.

Since the thiolated-PABG derivative is a positively charged compound due to the presence of a guanidinyll group, it can easily interact with the polysaccharide matrix of the Sephadex resin via hydrogen bonding, resulting in retention of the compound by the matrix and preventing its elution. Eluents other than miliQ H₂O were investigated to minimize this problem. Different solutions with different percentages of CH₃COOH in H₂O were considered as eluents to overcome this problem. First, a solution of 10% CH₃COOH in H₂O (pH ~ 1) was selected as an eluent to perform the separation by Sephadex G-25 chromatography of a sample from **QS 006** batch (despite the low conjugation efficiency results with this batch, it was selected as a more expendable sample). The sample was eluted with 3 mL H₂O (1 mL/fraction) and then with 10% CH₃COOH in H₂O in 10 fractions of 1 mL each. (**Figure 2.13**, **Table 2.5**). Indeed, the analysis of the fractions by RP-HPLC showed that the thiolated-PABG derivative elutes in the acidic fractions and is not present in any of the H₂O fractions. In addition, the first acidic fraction contains 10⁸ particles/mL (**Table 2.5**), which is 0.1% of the total particle population. The 2nd and 3rd aqueous fractions, immediately before, carry 10¹⁰ and 10¹¹ particles/mL, so there is not complete separation between QSs and the thiolated-PABG derivative. This situation is not ideal.

Table 2.5 Percentage of free thiolated-PABG derivative estimated by HPLC-PDA and number of particles/mL determined by MADLS in the acidic elution fractions of the separation of the QS 006 by G-25 Sephadex chromatography.

Sample	% Free PABG	particles/mL
QS 006 Fraction 4	36.2	1 x 10 ⁸
QS 006 Fraction 5	28.5	1 x 10 ⁰
QS 006 Fraction 6	15.9	1 x 10 ⁰
QS 006 Fraction 7	0.5	1 x 10 ⁰

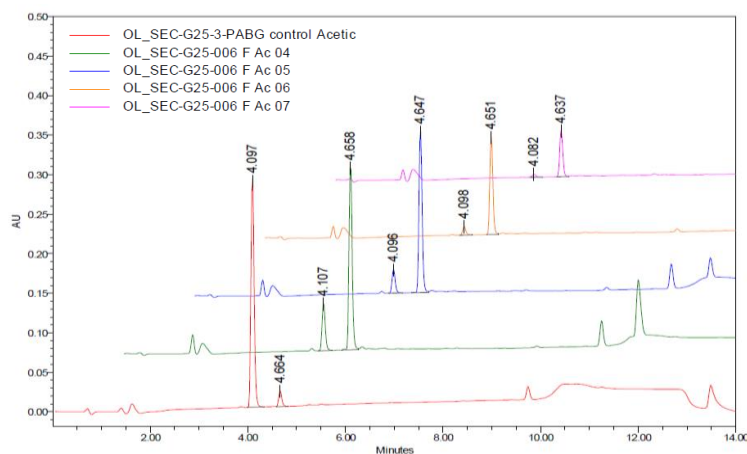


Figure 2.13 RP-HPLC analysis of the thiolated-PABG derivative in the acidic elution fractions of the separation of the QS 006 by G-25 Sephadex chromatography.

A new formulation, **QS 007**, was then prepared with 4 μmol Chol-PEG₂₀₀₀-mal content, its pH was adjusted to 7.5, and then it was used to perform the conjugation reaction with 0.6 (0.72 mg, 2.4 μmol) and 1.2 equivalents (1.43 mg, 4.8 μmol) of thiolated-PABG derivative and TCEP (0.6 and 1.2 μmol respectively) for 2 h with gentle stirring at room temperature. The two conditions studied, which differ in the amount of the thiolated-PABG derivative added for conjugation, were chosen after noting in all of our previous assays the amount of free thiolated-PABG derivative that dimerizes after only 1-2 hours of reaction and for this reason an equivalent amount of TCEP with respect to the thiolated moiety was added to improve the conjugation. Due to the high pKa of the guanidiny group (12.5 at 25°C), purification was performed by size exclusion chromatography on Sephadex G25 using miliQ water and a decreasing pH gradient of 4.5, 3.0, and 2.0. (**Figure 2.14**).

Conjugation rates in these assays ranged from 40 to 60% when the reaction was performed with 1.2 and 0.6 eq. of thiolated-PABG derivative, respectively (**Table 2.6**). PABG-derivative was eluted in the pH 4.5 fractions. However, it is noteworthy that the MADLS analysis shows some overlap between the acid fractions and a residual amount of up to 10^{11} particles/mL, representing up to 90% of the particles loaded on the column. This suggests that it is essential to increase the length of the column and also to use a higher resolution Sephadex G-50.

Table 2.6 Thiolated-PABG derivative percentage content and number of particles per mL of the fractions obtained by G-25 Sephadex size exclusion chromatography of QS007 conjugation crudes with 2.4 or 4.8 μmol of thiolated-PABG derivative. Estimated rate of conjugation of PABG based ligand to **QS 007**.

Sample	% Free PABG 2.4 μmol	particles/mL	% Free PABG 4.8 μmol	particles/mL
QS 007 pH 4.5 Fraction 1	3.5	1×10^{11}	13.1	1×10^8
QS 007 pH 4.5 Fraction 2	34.2	1×10^9	44.4	1×10^8
QS 007 pH 3.0 Fraction 1	1.0	1×10^8	1.6	1×10^7
QS 007 pH 3.0 Fraction 2	0.4	1×10^7	0.0	1×10^8
% Conjugated	61.1	-	40.9	-

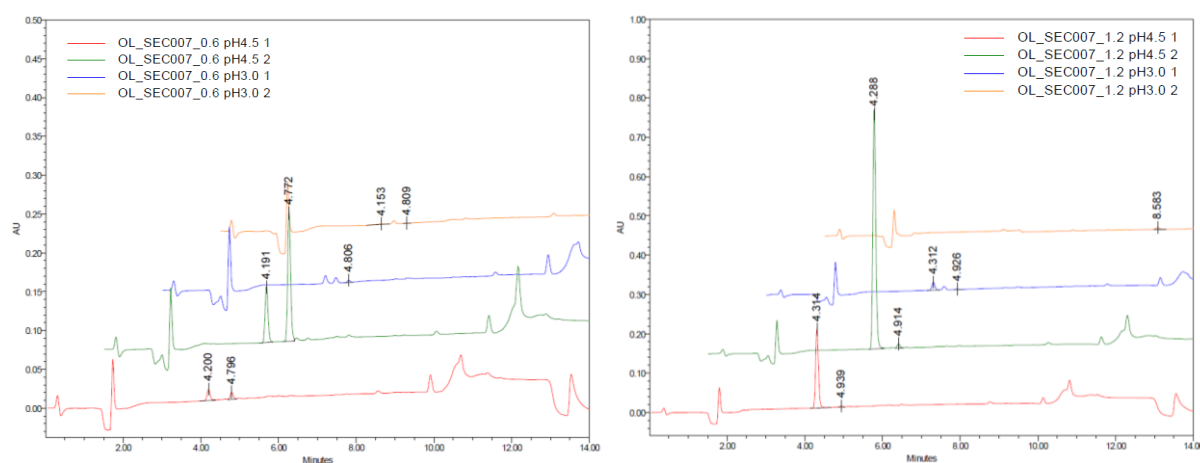


Figure 2.14 RP-HPLC analysis of the thiolated-PABG derivative contained in the acidic elution fractions generated by Sephadex G-25 size-exclusion chromatography separation of the conjugation crude of **QS 007** with the thiolated-PABG derivative. **A**: Elution fractions corresponding to the conjugation reaction using 2.4 mmol of thiolated-PABG derivative. **B**: Elution fractions corresponding to the conjugation reaction using 4.8 mmol of thiolated-PABG derivative.

2.2.3 Optimized Conjugation of P40 peptide and PABG into Qs

A similar, optimized protocol was now used to conjugate the **P40** peptide (H-WHWRLPSGGGC-NH₂) and the thiolated-PABG derivative, using formulation conditions (batch **QS 008**) 4.8 μmol of Chol-PEG₂₀₀₀-mal was used and after adjusting the pH of the final QS suspension to 7, conjugation was performed using 1.2 eq of both **P40** peptide (4.8 μmol) and thiolated-PABG derivative (4.8 μmol). After completion of the conjugation reaction, free ligands were separated from the QS suspension on a longer column with Sephadex G-50, to improve the resolution observed with G-25. In addition, controls of free **P40** peptide and PABG (4.8 μmol each) were loaded and eluted on the G-50 Sephadex column to determine their recovery on this column. Elution was performed with H₂O followed by CH₃COOH aqueous solutions at pH 5.5 and 4.5. This optimized protocol incorporates all that we have learned from previous assays such as the use of 4 μmol Chol-PEG₂₀₀₀-mal content, the conjugation once the Qs were stabilized, i.e. one day after their formulation, and the use of size exclusion chromatography as an effective separation technique that preserves the integrity of the nanovesicles. However, we introduce a new stationary phase in G-50 instead of G-25 and in a longer column to increase the resolution and to better separate the nanovesicles, which elute earlier with water, from the ligands, which elute later with weak acid solutions. The results of the control size exclusion chromatography give recoveries of 84% for the **P40** peptide (**Figure 2.15, A** and **Table 2.7**) and 86% for the thiolated-PABG derivative (**Figure 2.15, B** and **Table 2.7**). Although the recovery data are high, this technique does not allow a complete recovery of the ligands loaded on the stationary phase. This is taken into account when calculating the conjugation rates for both.

Table 2.7 Estimation of recovered P40 peptide and thiolated-PABG derivative from size-exclusion chromatography in Sephadex G-50

Sample	P40 peptide		PABG	
	Area	% Recovery	Area	% Recovery
Control	3029644	100	561071	100
H ₂ O F01	18750	0.62	0	0
H ₂ O F02	3483	0.12	0	0
H ₂ O F03	2236	0.07	0	0
pH 5.5 F01	1589	0.05	0	0
pH 5.5 F02	1740541	57.45	425253	75.79
pH 4.5 F01	678519	22.39	58465	10.42
pH 4.5 F02	35360	1.16	0	0
Acetic 10%	60907	2.01	0	0
Total	2541385	83.88	483718	86.21

Table 2.8 Ligand percentage content and number of particles per mL of the fractions obtained by G-50 Sephadex size exclusion chromatography of QS008 conjugation crudes with **P40** peptide or thiolated-PABG derivative. Estimated rate of conjugation of the two ligands to QS 008.

Fraction	% Free P40 peptide	Particles/mL	% Free PABG	Particles/mL
5.5 F01	0	10^7	1.1	10^0
5.5 F02	21.8	10^6	21.6	10^7
4.5 F01	8	10^5	2.3	10^7
4.5 F02	0.1	10^0	0	10^0
Total	29.9	2×10^7	25.1	1.1×10^7
Conjugated	58.8		62.8	

2.2.4 Complexation of thiolated-PABG-functionalized quastomes with miR-323a-5p RNA and transfection assays

Once the conjugation process was established, complexation of mi-RNA 5 with the modified QSs was performed. These experiments were carried out by Julia Piqué from the Nanomol group (ICMAB-CSIC). Therapeutic RNA miR-323a-5p was complexed to three QS versions, the free QS (non-functionalized), QS functionalized with Chol-PEG₂₀₀₀-mal (QS-mal) and QS functionalized with PABG (QS-PABG). The three QS versions were prepared according to the previously described procedures (section 2.2.3). Complexation with miRNA was performed at RNA:QS ratios ranging from 1:6 to 1:0.4. Non complexed RNA was determined by electrophoresis in a 2% agarose gel (Figure 2.15).

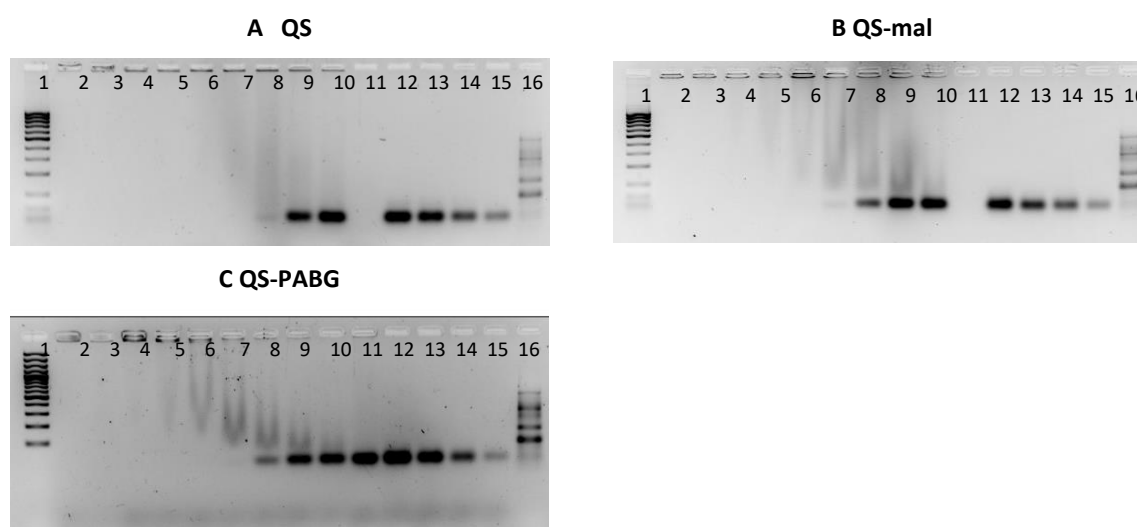


Figure 2.15 Agarose electrophoresis of non-complexed RNA in QS (A) QS-mal (B) and QS-PABG (C) at different RNA:QS ratios.

The results show that the minimum RNA:QS ratio at which all the added RNA is successfully complexed is 1:1.5 (Figure 2.15, A to C, lane 7). At this ratio and higher, complexation of RNA to the nanovesicle is complete. Below this level, free RNA is detected. The loading capacity of the nanovesicle is then about 50% of its molar amount. There is no significant difference between the formulations. Thus, the addition of a maleimide function via a Chol-PEG₂₀₀₀-mal and its conjugation with a thiolated-PABG does not affect the complexation of RNA by the nanovesicle. A cell uptake assay was then performed in the SK-N-BE(2) neuroblastoma cell line, using a fluorescent miRNA that was complexed in each of the three formulations: QS (Figure 2.16, A), QS-mal (Figure 2.16, B) and QS-PABG (Figure 2.16, C). The

fluorescent probe was visualized by confocal microscope (experiments carried out by Dr. Ariadna Boloix from VHIR).

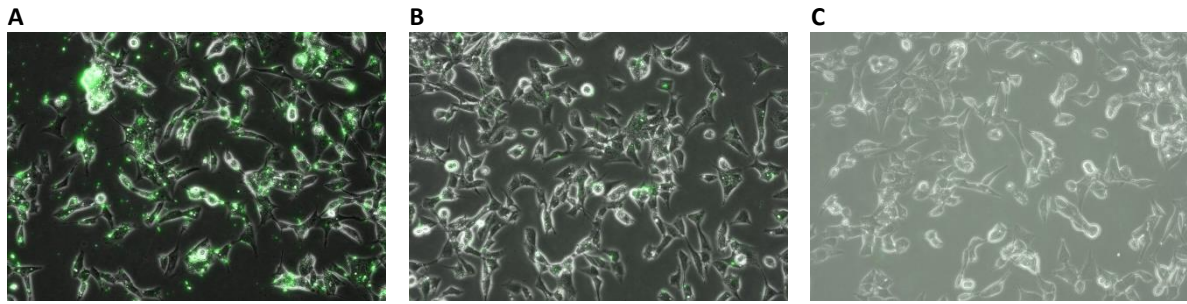
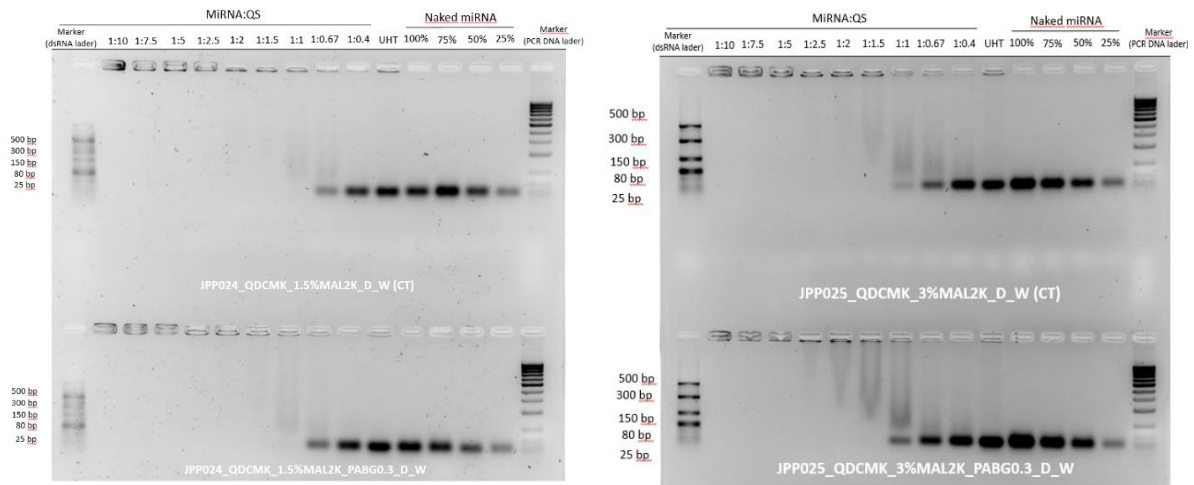


Figure 2.16 Cell uptake assay in the SK-N-BE(2) neuroblastoma cell line with **A:** QS, **B:** QS-mal and **C:** QS-mal-PABG carrying a miRNA fluorescent reporter.

The results clearly show that both QS formulations containing Chol-PEG₂₀₀₀-mal and Chol-PEG₂₀₀₀-PABG are inefficiently taken up by the neuroblastoma cell (**Figure 2.16, B and C**), indicating that the PEG moiety may interfere with the uptake of the nanovesicle. This may be due to the high molecular weight of the PEG and the hydrophilicity it confers on the surface of the nanovesicle, both of which are incompatible with an endocytic uptake process. Therefore, lower amounts of Chol-PEG₂₀₀₀-mal (1 and 2 μ mol) were considered and a shorter PEG (Chol-PEG₁₀₀₀-mal) was investigated.

A QS formulated with 1 μ mol of Chol PEG2000-mal non conjugated and conjugated with thiolated-PABG **B QS formulated with 2 μ mol of Chol PEG2000-mal non conjugated and conjugated with thiolated-PABG**



C QS Chol PEG₁₀₀₀-mal 1 μ mol non conjugated and conjugated with thiolated-PABG **D QS Chol PEG₁₀₀₀-mal 1 μ mol non conjugated and conjugated with thiolated-PABG**

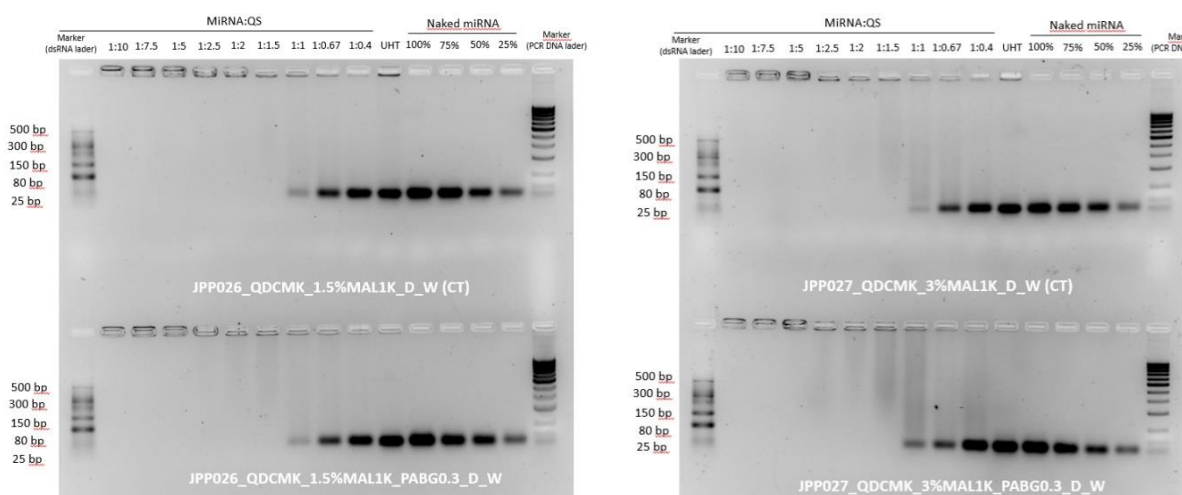


Figure 2.17 Agarose electrophoresis of non-complexed RNA in QS-PEG₂₀₀₀-mal 1 μ mol (A) QS-PEG₂₀₀₀-mal 2 μ mol (B) and QS-PEG₁₀₀₀-mal 1 μ mol (C) QS-PEG₁₀₀₀-mal 2 μ mol (D) from complexation experiments with decreasing RNA:QS ratios from 1:6.2 to 1:0.4 and showing free RNA controls. All cases are studied with (bottom gels) and without (upper gels) conjugation to thiolated PABG derivative.

In all cases, both with 1000 and 2000 PEG and using 1 and 2 μ mol, the results of RNA complexation remain the same as the previous experiment, with 1:1.5 of RNA:QS ratio as the minimal relation between the two for a successful complexation (Figure 2.17 A to D). Neither the modification of the PEG length nor its molar amount within the formulation affect the capacity of the nanovesicle to complex the RNA, as can be expected.

For the uptake assay, IMR-90 cell line was chosen as a control as it does not express the target receptors, while IMR-32 does express the hNET and Trkb receptors and was chosen as the target tumor cell type for this assay

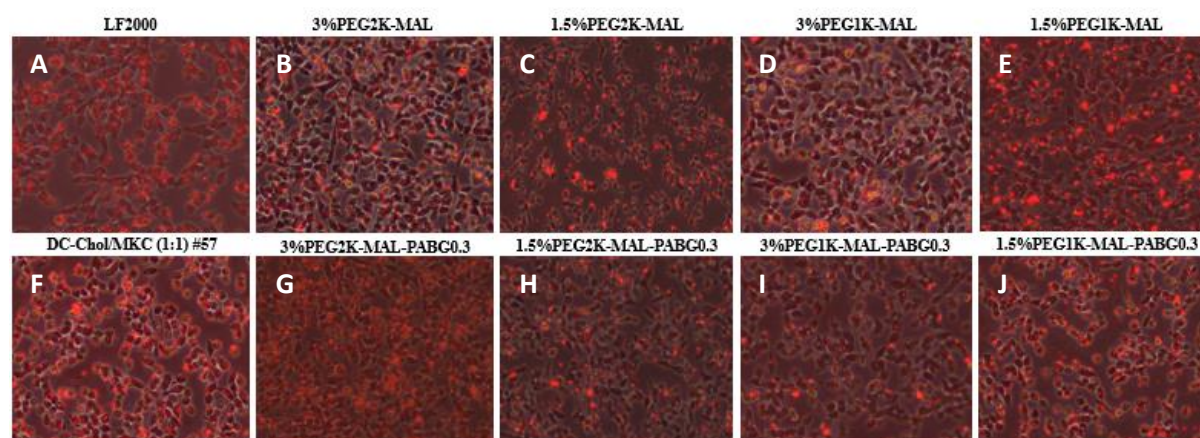


Figure 2.18 Formulation uptake assay in the IMR-32 neuroblastoma cell line for QS formulation with or without conjugation with thiolated-PABG and with 1 or 2 μ mol.

The results of this assay show improved uptake activity for QSs formulated with Chol-PEG₁₀₀₀-mal (Figure 2.18, D and E) and conjugated with thiolated-PABG (Figure 2.18, I and J), compared with the same sample formulated with Chol-PEG₂₀₀₀-mal (Figure 2.18, B and C) and their conjugated with thiolated-PABG (Figure 2.18, G and H). Lipofectamine and a QS nanoformulation of DC-Chol/MKC (1:1) were used as non-specific RNA transfection controls (Figure 2.18, A and F).

These results indicate that the uptake of QS by the cell is affected by the length and amount of the PEGyl moiety and that the use of lower amounts and smaller sizes of PEG has increased this uptake activity when assessed in the IMR-32 cell line.

Chapter 3

Selection of a carbodiimide alternative to DIC to minimize the generation of HCN

3.1 Introduction

N,N'-diisopropylcarbodiimide (DIC) is a reagent that has been used for decades to form amide bonds¹¹⁴ and has replaced the classic *N,N'*-dicyclohexylcarbodiimide (DCC)¹⁸¹ in solid-phase peptide synthesis (SPPS) mainly because the by-product of the coupling reaction, *N,N'*-diisopropylurea, is more soluble than *N,N'*-dicyclohexylurea in the common organic solvents used in this process.¹⁸² Consequently, DIC allows for much easier cleanup between steps and purification of the final product at the end. For this reason, DIC has been widely employed in combination with coupling additives for manual and automated solid-phase peptide synthesis.¹⁸³ Coupling additives minimize the racemization in the α -carbon of the amino acid upon activation.¹¹³ This undesirable secondary reaction is related to the acidity of the α -hydrogen of the amino acid and the high reactivity of the *O*-acylisourea intermediate (Figure 3.1).⁴⁰

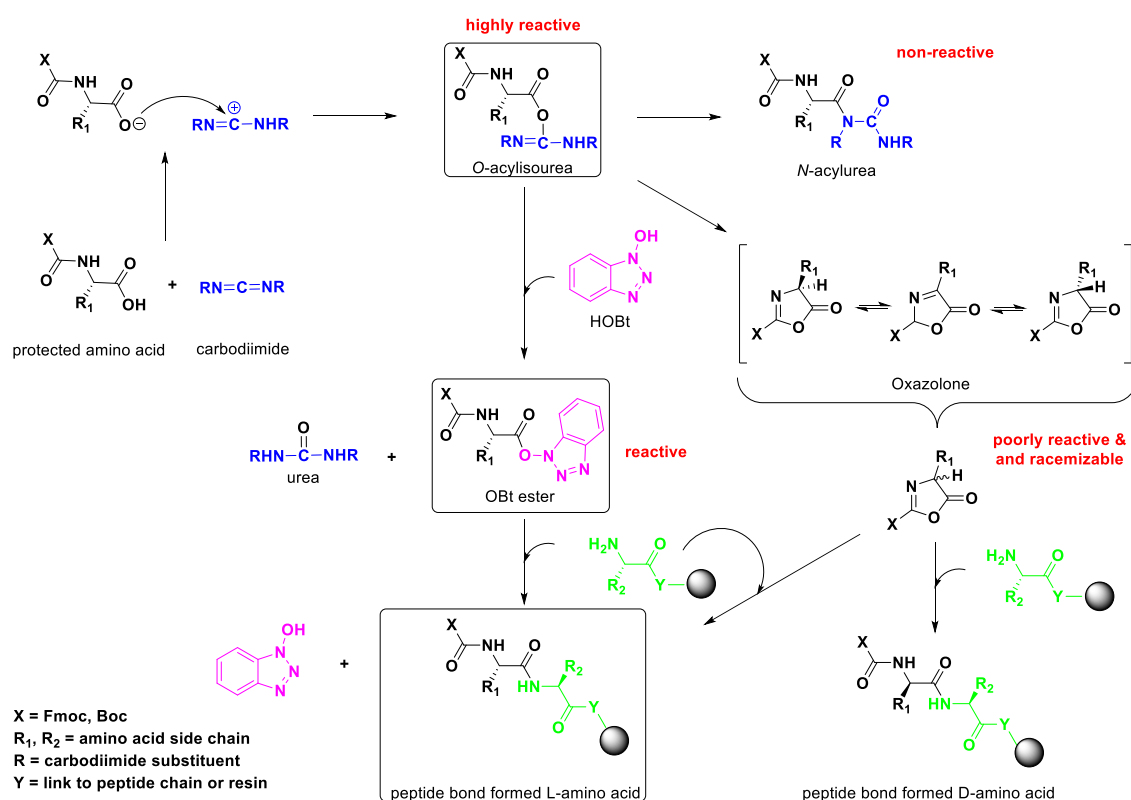


Figure 3.1 Mechanism and side reactions of N_{α} -protected amino acid activation and coupling by a carbodiimide and HOBT.

Oxyma is one such additive that has recently become established as one of the key reagents in SPPS¹⁵⁸, replacing the classically used HOBT¹¹⁵ due to safety concerns regarding its potential explosive properties.¹¹⁷ Oxyma, and previously other additives, avoid the secondary reactions associated with the *O*-acylisourea intermediate that result in the loss of chiral integrity by reacting with it to produce a less reactive but still active ester that serves as a powerful acylating reagent without the problems associated with *O*-acylisourea (Figure 3.2).⁴⁰

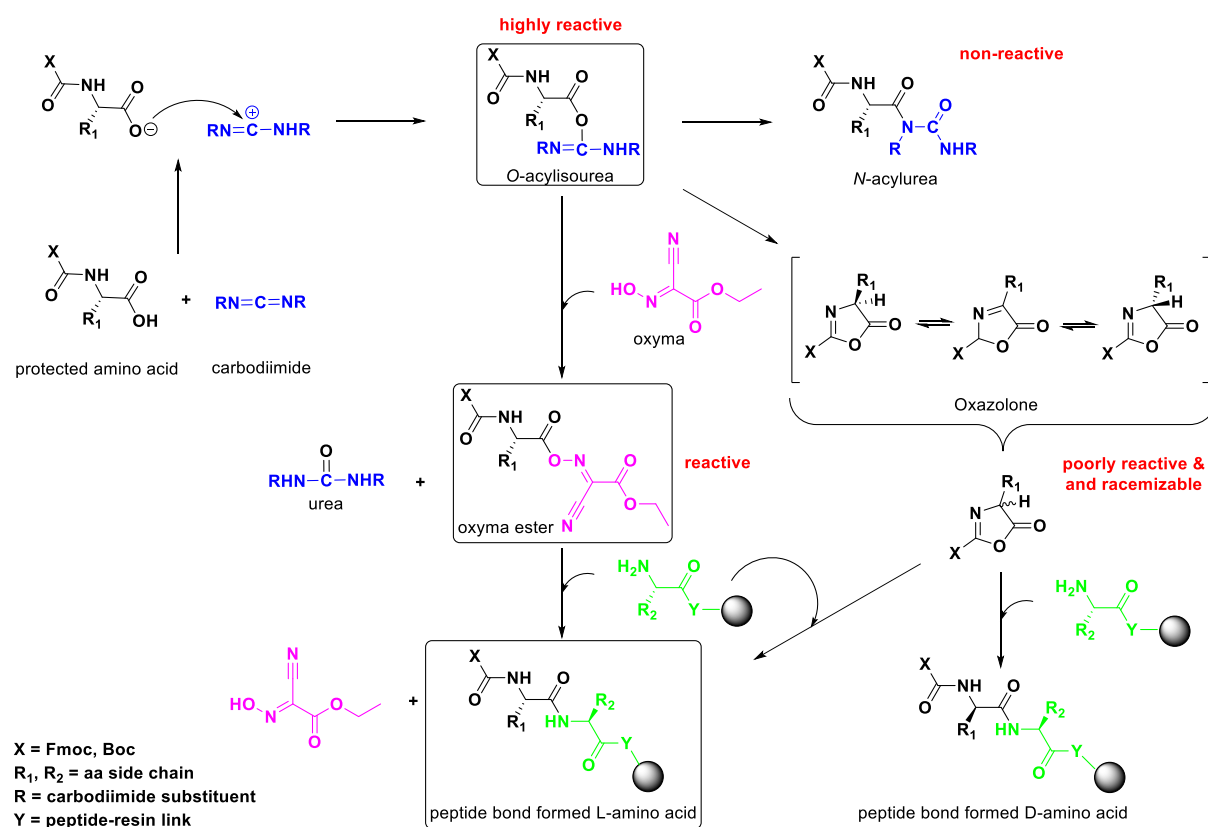


Figure 3.2 Mechanism and side reactions of N_{α} -protected amino acid activation by carbodiimide and oxyma.

The combination of DIC and oxyma as a coupling reagent mixture has been successfully used in SPPS for over a decade, both in manual and automated peptide synthesis, with particular relevance in the latter, where it is the main coupling reagent mixture suggested by the manufacturers (CEM Corp., Biotage, CSBio, Gyros Protein Technologies). This combination allows synthesis in much shorter times under high temperature conditions (75 to 90°C) with minimal side reactions. The DIC/oxyma mixture can be used under these conditions even if the sequence contains the racemization-prone cysteine (Cys) and histidine (His) residues in their standard trityl side-chain protected variants.^{184–186}

However, this particular combination has recently been reported to have a drawback: the unwanted formation of hydrogen cyanide (HCN).^{120,121} HCN is a toxic gaseous compound that acts rapidly by binding ferric heme groups, including those present in the proteins hemoglobin and cytochrome c oxidase, resulting in disruption of electron transport chain activity, severe hypoxia, and ultimately death.^{122,187} The proposed mechanism for the formation of this dangerous by-product is illustrated in **Figure 3.3**. It begins with an acid-base exchange between oxygen and the carbodiimide (**1** and **2**), followed by the formation of an adduct (**3**), which then undergoes cyclization (**4**) to form an oxadiazole (**5**) with the concomitant release of HCN.

It is therefore important to investigate alternatives to DIC that can minimize the generation of HCN while maintaining the excellent performance of DIC in obtaining high quality peptides. This is critical considering that peptides that show promise for bioactivity and pharmaceutical application require production scale-up.

Given the effectiveness of oxyma as an additive, the objective of this chapter is to evaluate the performance of four additional carbodiimides when used in conjunction with oxyma in peptide synthesis in comparison to DIC. The chemical structure of these carbodiimides is believed to strongly influence the formation of the cyclic oxadiazole intermediate, thereby preventing the release of HCN.

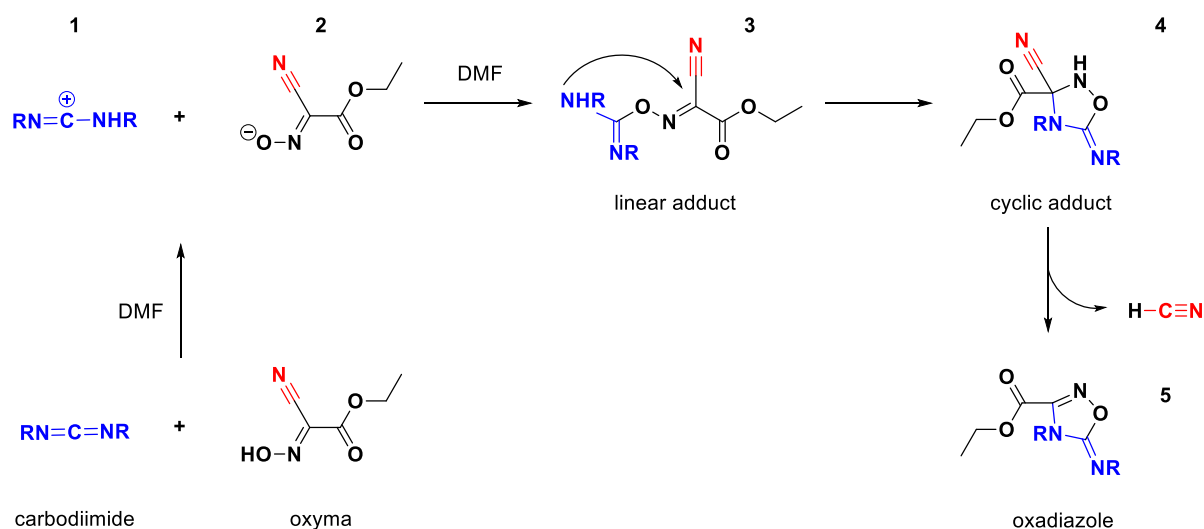


Figure 3.3 Proposed mechanism of reaction for the release of HCN. Carbodiimide and oxyma undergo an acid-base exchange (1 and 2) and form an adduct (3) which transitions into a cyclic compound (4). This product can then form an oxadiazole (5) releasing HCN.

3.2 Results and Discussion

3.2.1 Performance of five carbodiimides in the synthesis of model peptides

The carbodiimides selected for this study were *N*-ethyl-*N'*-(3-dimethylaminopropyl)carbodiimide hydrochloride (**EDC*HCl**), *N,N'*-di-*sec*-butylcarbodiimide (**DSBC**), *N,N'*-di-*tert*-butylcarbodiimide (**DTBC**), and *N-tert*-butyl-*N'*-ethylcarbodiimide (**TBEC**). (**Figure 3.4**), which were compared to *N,N'*-diisopropylcarbodiimide (**DIC**) in the synthesis of two model peptides, to evaluate their to investigate peptide synthesis efficiency and propensity to generate oxadiazole intermediates and release HCN.

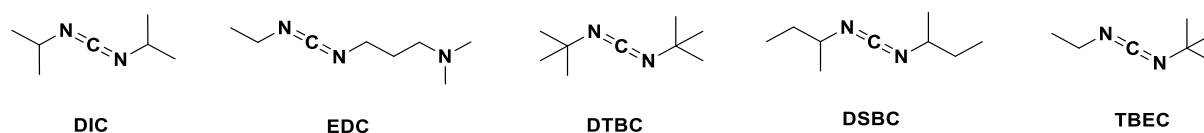


Figure 3.4 Structure of the five carbodiimides studied

The selected carbodiimides represent some contrasting properties: **1**) symmetric vs. asymmetric (DIC, DSBC and DTBC vs. TBCE and EDC), **2**) bulky/hindered substituents vs. unhindered/small substituents (DTBC, DSBC vs. DIC, EDC and TBEC), and **3**) substituents with primary, secondary and tertiary carbons directly attached to the nitrogen ($C_{\text{primary-N}}$: DSBC and EDC; $C_{\text{secondary-N}}$: DIC; $C_{\text{tertiary-N}}$: DTBC and hybrid $C_{\text{primary-N}}$ with $C_{\text{tertiary-N}}$: TBEC).

The performance of the five commercially available carbodiimides in SPPS was evaluated using two model peptides: Ile^{2,3}-Leu-enkephalin (H-YIIFL-NH₂) and Leu-enkephalin (H-YGGFL-NH₂), shown in **Figure 3.5**. Ile^{2,3}-Leu-Enkephalin contains two β -branched residues in a row (Ile-Ile) as an example of challenging couplings. The peptides were manually synthesized by solid phase, following the Fmoc/tBu strategy using Rink Amide AM resin as solid support. The final crude peptides were released from their respective peptidyl-resins using standard acydotytic cleavage conditions (TFA:TIS:H₂O, 95:2.5:2.5 ,

v/v/v). The peptide crudes were analyzed by high-performance liquid chromatography (HPLC) and liquid chromatography-mass spectrometry (LC-MS).

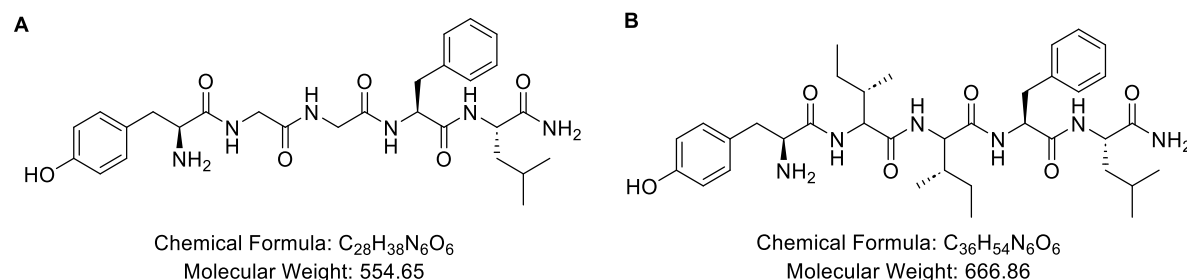


Figure 3.5 Structure of the two model peptides synthesized, Leu-Enkephalin (A) and Ile^{2,3}-Leu-Enkephalin (B)

Figure 3.6 shows the different HPLC traces corresponding to the peptides synthesized using the different carbodiimides in the coupling mixture are shown. The results show that the different substituents attached to the nitrogen of the carbodiimide affect the quality of the final product. These results are summarized in **Table 3.1**.

Table 3.1 Purity determined by HPLC-PDA of the peptides synthesized using different carbodiimides with oxyama.

#	Carbodiimide	Leu-Enkephalin		Ile ^{2,3} -Leu-Enkephalin	
		%	Impurities	%	Impurities
1	DIC	> 99	-	97	-Y, -I
2	EDC-HCl	90	-	80	-Y, -YI
3	DTBC	73	-G, -F, -GF	40	-Y, -I, -F, -II, -YI
4	DSBC	91	-Y, -G	83	-Y, -I
5	TBEC	98	-G	97	-Y

Both DIC and TBEC yielded excellent results, with final compound purities of approximately 99% for Leu-enkephalin and 97% for Ile^{2,3}-Leu-enkephalin, which is a more synthetically challenging peptide (**Figure 3.6 A, B, I and J; Table 3.1, #1 and #5**). On the other hand, peptides synthesized with DSBC and EDC-HCl, yielded crude products of slightly lower quality, showing with 90-91% purity for Leu-enkephalin and 80-82% purity for Ile^{2,3}-Leu-enkephalin (**Figure 3.6, C, D, G and H; Table 3.1, #2 and #4**).

The use of a sterically hindered DTBC gave the worst result, which is unacceptable in SPPS. The purity of the crude peptides was approximately 40% for Ile^{2,3}-Leu-enkephalin and 72% for Leu-enkephalin (**Figure 3.6 E and F; Table 3.1, #3**). This is a suboptimal quality product, considering the length of this peptide. The number of impurities present in these products is higher with this carbodiimide, as was evidenced by LC-MS characterization (**Figure 3.8, C**). It was observed that the use of DTBC leads to the highest number of truncated peptides resulting from different amino acid deletions due to incomplete couplings (**Table 3.1, #3**).

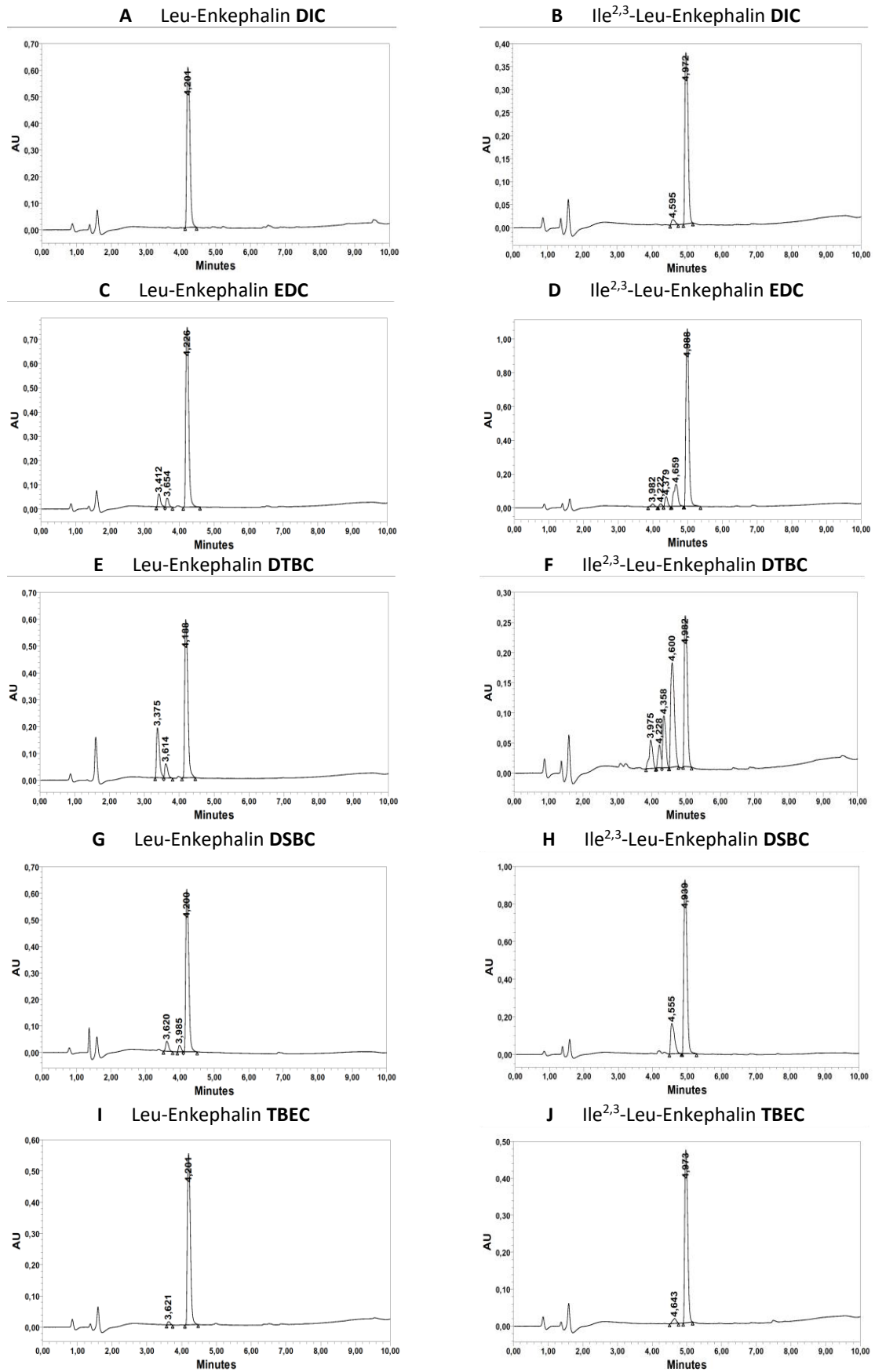


Figure 3.6 Chromatograms of crude peptides Leu-Enkephalin (A, C, E, G and I) and Ile^{2,3}-Leu-Enkephalin (B, D, F, H, and J) synthesized with DIC (A, B), EDC (C, D), DTBC (E, F), DSBC (G, H) and TBEC (I, J) in a 5-100% B gradient (A: H₂O + TFA 0.045%, B: CH₃CN + TFA 0.036%).

These results indicate that TBEC has the closest performance to DIC, with the least quantitative deletions in the sequence (**Figure 3.6, I and J; Table 3.1**). In general, it was observed that the alkyl groups of carbodiimides negatively affect the synthesis when they are more sterically hindered. Bulkier groups make it more difficult to form the reactive *O*-acylurea, resulting in slower couplings and incomplete reactions after 30 minutes of reaction. This is clearly seen with DTBC (**Figure 3.4; Figure 3.6, E and F; Table 3.1, #3**), which has *tert*-butyl substituents. This tertiary carbon directly attached to the nitrogen atom affects its reactivity by steric hindrance. The *sec*-butyl substituents of DSBC, which represent a secondary carbon attached to the nitrogen atom, work adequately (**Figure 3.4; Figure 3.6, G and H; Table 3.1, #4**). DSBC is structurally similar to DIC, but is slightly more hindered, which may explain its slightly lower performance in SPPS. Carbodiimides with primary carbon substituents such as the ethyl present in both EDC and TBEC also show high purity end products (**Figure 3.4; Figure 3.6, C, D, I and J; Table 3.1, #2 and 5**). It can be assumed that TBEC is rapidly converted to an active *O*-acylurea by the nitrogen bound to the ethyl substituent, as it is less hindered than the *tert*-butyl moiety. This rapid reaction combined with the unreactive *tert*-butyl substituent results in a product comparable to that obtained with DIC. Similarly rapid conversion to the corresponding active *O*-acylurea is expected for EDC, which has shown similar synthetic performance to DSBC. In addition to the adequate performance of EDC, this reagent is also the most commonly used carbodiimide in solution synthesis because of the water solubility of the urea by-product at the end of the reaction, which allows for easy extraction with aqueous solutions. However, it is not as inexpensive as DIC, and some care must be taken to prevent its hydrolysis to its urea by-product by ambient moisture.¹⁸⁸ It also undergoes self-cycling to two tautomeric forms, one of which is non-reactive.¹⁸⁹ This may be the reason for its synthesis performance being similar to that of DSBC but lower than that of DIC and TBEC. Therefore, from the perspective of synthesis performance, DSBC and TBEC could initially be considered as suitable candidates to replace DIC in SPPS.

3.2.2 Formation of the oxadiazole in carbodiimide/oxyma mixture as indicator of HCN release

For this study, we have considered oxadiazole formation as a marker of HCN release (see **Figure 3.3**). To determine which of the selected carbodiimides has the least capacity to generate the unwanted HCN by-product, we analyzed the formation of the carbodiimide-oxyma adduct and the corresponding oxadiazole when the five reagent mixtures were incubated in DMF at 25 °C and 60 °C for 24 hours and analyzed by LC-HRMS. In the absence of the protected amino acid in the solution, the oxadiazole side reaction was forced to occur.

The results are summarized in **Table 3.2** and in **Figure 3.7**. The results obtained with DIC are consistent with those reported by Eli Lilly and Polypeptide groups (**Table 3.2, #1, 6, 11**).^{120,121} When the reaction was performed with DSBC, which is structurally similar to DIC, no linear adduct is identified following the trend of DIC (**Figure 3.7, D**), and the cyclic oxadiazole formation occurs to a lesser extent. These results can be explained by the fact that DSBC is slightly more hindered than DIC due to its *sec*-butyl substituents, and therefore the reaction with oxyma is slightly less favorable. At 60 °C the linear adduct is again not identified, but the amount of oxadiazole has increased slightly. The importance of the steric hindrance was confirmed by studying the reaction with DTBC, where the carbodiimide moiety is flanked by two *tert*-butyl groups. In this case, the carbodiimide remained unchanged even after 4 days at 25 °C (**Figure 3.7, C; Table 3.2, #8**) or 18 hours at 60 °C (**Figure 3.7, C; Table 3.2, #13**).

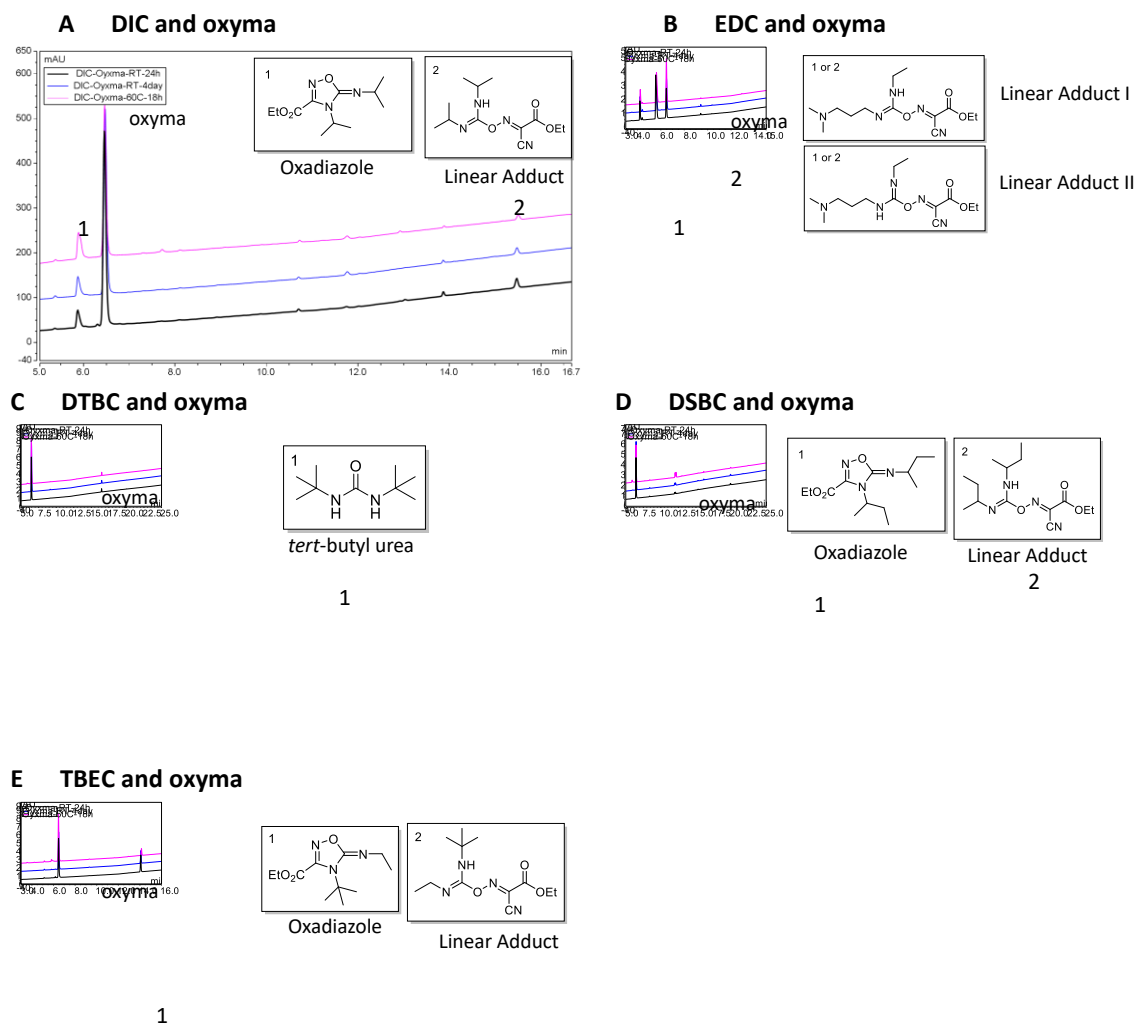


Figure 3.7 LC-MS traces of the crude reaction between oxyma with DIC (**A**), EDC (**B**), DTBC (**C**), DSBC (**D**) and TBEC (**E**) after 1d at 25°C (**black line**), 4d at 25°C (**blue line**) or 18 hrs at 60°C (**pink line**).

When the reaction was studied with the much less hindered EDC·HCl (asymmetric carbodiimide with ethyl and 3-dimethylaminopropyl groups flanking the carbodiimide moiety), no formation of the oxadiazole was detected, but the presence of the linear adduct was the most important in all the series (**Table 3.2, #2, 7, 12**). Due to the asymmetry of EDC·HCl, two peaks for the linear adduct appeared in the chromatogram (**Figure 3.7, B**).

Table 3.2 LC-HRMS analysis results of the crude reaction of oxyma with the different carbodiimides

Time	Temperature	#	Carbodiimide	Oxyma [%]	Linear adduct [%]	Oxadiazole [%]
24 h	25 °C	1	DIC	88.9	3.5	7.6
		2	EDC·HCl ^a	26.3	15.0	-
			EDC·HCl ^b	-	58.7	-
		3	DTBC	100	-	-
		4	DSBC	94.7	-	2.6
		5	TBEC	71.8	28.2	-
4 d	25 °C	6	DIC	87.7	2.6	9.7
		7	EDC·HCl ^a	38.9	15.8	-
			EDC·HCl ^b	-	45.3	-
		8	DTBC	100	-	-
		9	DSBC	93.2	-	3.4
		10	TBEC	75.8	23.7	0.6
18 h	60 °C	11	DIC	78.6	2.4	18.9
		12	EDC·HCl ^a	47.2	13.3	-
			EDC·HCl ^b	-	39.5	-
		13	DTBC	100	-	-
		14	DSBC	78.5	-	10.5
		15	TBEC	83.5	10.4	6.1

a, b The EDC reaction with oxyma shows two products for the linear adduct because it can react via either of the nitrogen atoms. The asymmetry of the carbodiimide gives two adducts that are distinguishable by RP-HPLC.

Finally, TBEC is a carbodiimide that combines the properties of DTBC and EDC, due to its substituents, the *tert*-butyl, which due to its steric hindrance induces low reactivity of the associated nitrogen and the less bulky ethyl group, which gives only the linear adduct, without progressing to the cyclic oxadiazole structure. As such, it behaved as expected from the DTBC and EDC·HCl results, with some linear adduct formation but, crucially, negligible oxadiazole formation and thus little release of HCN (**Figure 3.7, E; Table 3.2, #5, 10 and 15**). Under the most energetic conditions (18 h at 60 °C) some oxadiazole formation was detected. However, the amount was three times lower than for DIC under the same conditions (**Table 3.2, #11 and #15**).

All carbodiimides tested are less likely to release HCN than DIC at 25 °C after one and four days. EDC, DTBC and TBEC show no oxadiazole by-product at all. At 60 °C, all carbodiimides also have a lower tendency to release HCN than DIC, and EDC and DTBC do not release HCN under these conditions. In terms of peptide synthesis performance, only TBEC is fully comparable to DIC in the synthesis of the model peptides in SPPS. Therefore, we can confidently say that TBEC is the best alternative to DIC. Its use at 25 °C produces no by-production of HCN and at 60 °C produces three times less by-production of HCN compared to DIC. This, along with its excellent performance in SPPS, makes TBEC the best candidate to replace DIC (**Figure 3.8**).

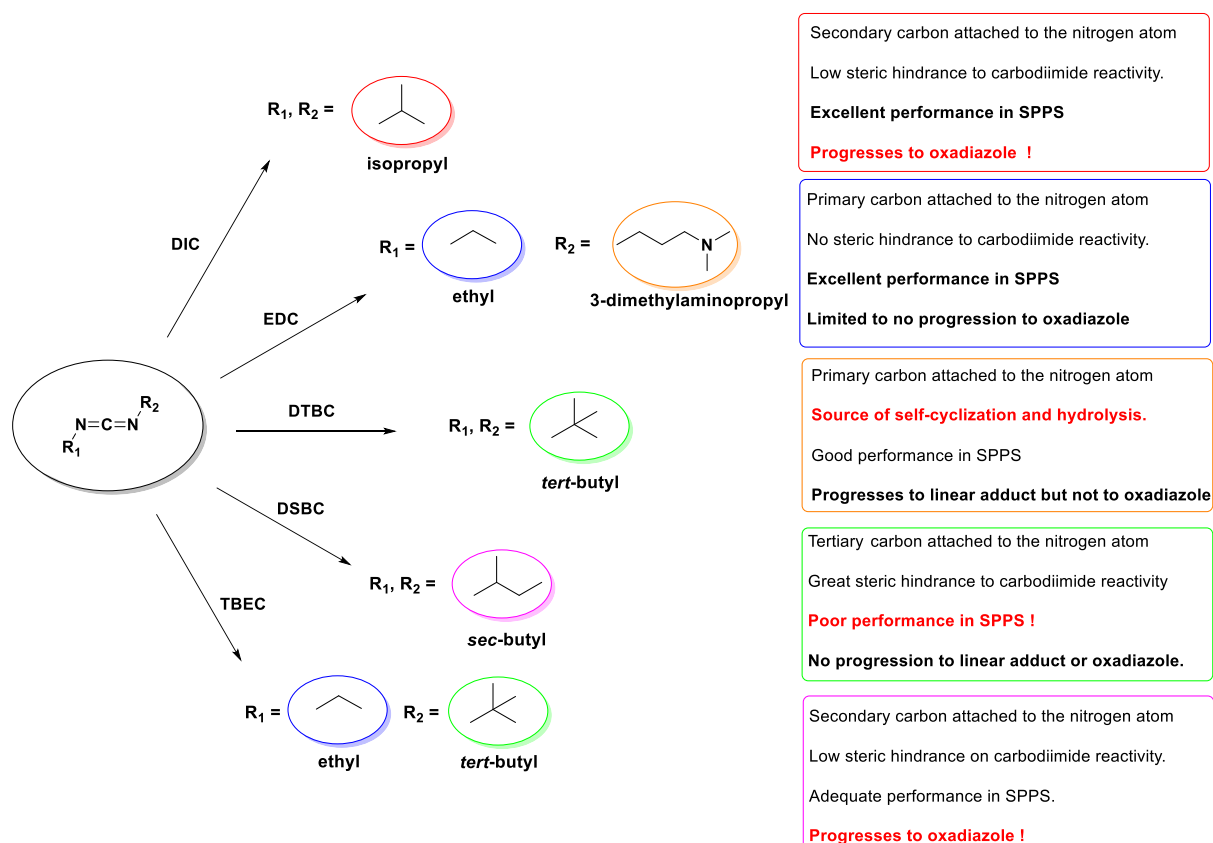
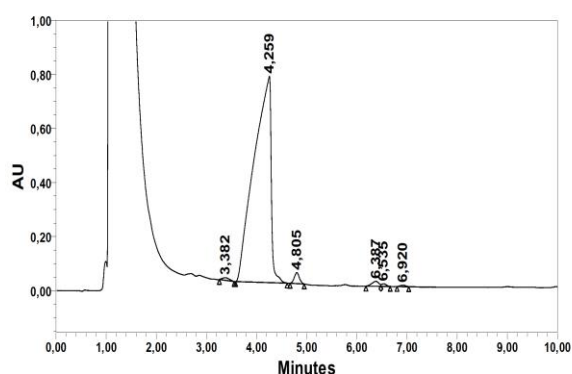


Figure 3.8 Schematic summary of the influence of the substituents on carbodiimide reactivity and its effects on synthetic performance of the model peptides and its ability to generate oxadiazole as a marker of HCN release.

3.2.3 Synthesis of a MSLN peptide using TBEC

In order to assess the viability of TBEC as a coupling reagent in a biologically relevant peptide, we selected the MSLN2 **P6** peptide sequence and synthesized it using a microwave-assisted methodology using both TBEC and DIC as the carbodiimide for the coupling reaction. We chose this sequence as the first candidate to be tested outside of the model peptides used in this study because it is a short sequence with a high density of hydrophobic residues, β -branched residues and repetitive motifs. As such, it represents a modestly challenging synthesis. The HPLC and LC-MS characterization of the crude peptide product shows that TBEC is comparable to DIC as both crudes have purities above 95% (**Figure 3.9**)

A P6 MSLN2 peptide synthesized with DIC



B P6 MSLN2 peptide synthesized with TBEC

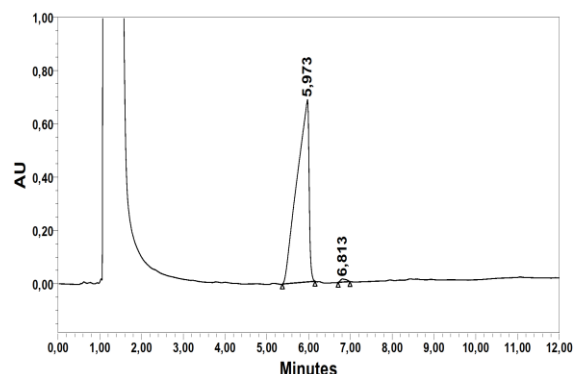


Figure 3.9 RP-HPLC characterization of **A:** P6 peptide synthesized with DIC, **B:** P6 synthesized with TBEC, in a C_8 column using gradients of **A:** 90-100%, **B:** 80-100% (A: H_2O + TFA 0.045%, B: CH_3CN + TFA 0.036%).

3.2.4 TBEC urea solubility evaluation

After selecting TBEC as the carbodiimide to replace DIC, the solubility of TBEC-derived urea in highly concentrated solutions was studied. For SPPS, this is an important property to study because the quality of the synthesis depends in no small part on the solubility not only of the reagents used, but also of the major reaction products that remain in solution, the most important of which is the substituted urea derived from the carbodiimide. Poorly soluble urea by-products are difficult to wash out in the cleaning steps between coupling cycles. It should be noted that *N,N'*-dicyclohexylcarbodiimide (DCC), long a staple for generating amide bonds in solution, has been discarded in favor of DIC for SPPS due to the insolubility of the corresponding urea. In this context, 1M solutions of TBEC or DIC were prepared with Oxyma and Fmoc-L-Ala-OH and the urea precipitation was observed. By visual inspection, after 5 minutes of reaction, it was found that 1,3-diisopropyl urea (derived from DIC) precipitated quantitatively (**Figure 3.10**, left), while 1-ethyl-3-(*tert*-butyl) urea did not (**Figure 3.10**, right). This makes it easier to remove TBEC-mediated activation and coupling by-products by filtration than with standard DIC. This simple data further enhances its applicability in scaled-up peptide syntheses by facilitating by-product (urea) removal with less solvent consumption for washing the solid support.

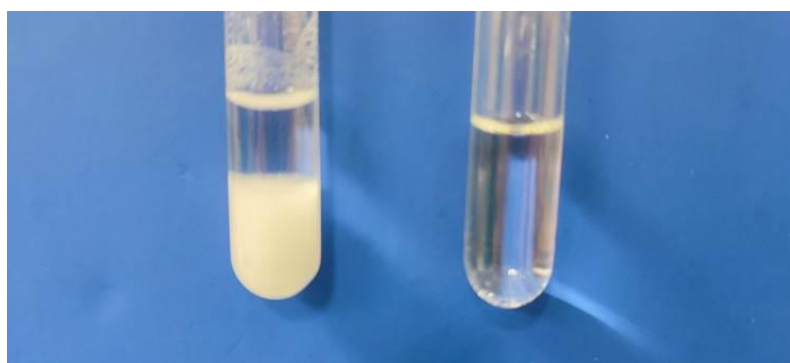


Figure 3.10 Solubility of ureas derived from the reaction of DIC (left) and TBEC (right) with Fmoc-L-Ala-OH at 1M.

Experimental Section

4.1 Materials

4.1.1 Reagents

Reagent	Provider
1-ethyl-3-(3-dimethylaminopropyl)carbodiimide hydrochloride	Iris Biotech GmbH
1- <i>tert</i> -butyl-3-ethylcarbodiimide	Kemilab Organics
1,2-ethanedithiol	Merck KGaA
2-chlorotriyl chloride resin (1.6 mmol/g, 100-200 mesh)	Iris Biotech GmbH
2,2,2-trifluoroacetic acid	Fluorochem
3-(tritylthio)propanoic acid	Fluorochem
3 β -[<i>N</i> -(<i>N</i> ', <i>N</i> '-dimethylaminoethyl)-carbamoyl]cholesterol	Sigma Aldrich [®]
4-aminobenzylamine	Sigma Aldrich [®]
4-dimethylamino pyridine	Sigma Aldrich [®]
4-(4-Hydroxymethyl-3-methoxyphenoxy)butyric acid Chemmatrix [®] resin (0.4 mmol/g, 35-100 mesh)	Sigma Aldrich [®]
5(6)-carboxyfluorescein	Sigma Aldrich [®]
Acetic anhydride	Sigma Aldrich [®]
Amino acids: Fmoc-L-Ala-OH*H ₂ O, Fmoc-L-Arg(Pbf)-OH, Fmoc-L-Asn(Trt)-OH, Fmoc-L-Asp(tBu)-OH, Fmoc-L-Cys(Trt)-OH, Fmoc-L-Gln(Trt)-OH, Fmoc-L-Glu(tBu)-OH*H ₂ O, Fmoc-Gly-OH, Fmoc-L-His(Trt)-OH, Fmoc-L-Ile-OH, Fmoc-L-Leu-OH, Fmoc-L-Lys(Alloc)-OH, Fmoc-L- Lys(Boc)-OH, Fmoc-L-Lys(Fmoc)-OH, Fmoc-L-Lys(Mmt)-OH, Fmoc- L-Met-OH, Fmoc-L-Phe-OH, Fmoc-L-Pro-OH*H ₂ O, Fmoc-L- Ser(tBu)-OH, Fmoc-L-Thr(tBu)-OH, Fmoc-L-Trp(Boc)-OH, and Fmoc-L-Tyr(tBu)-OH, Fmoc-L-Val-OH, H-L-Lys(Fmoc)-OH	Iris Biotech GmbH
Benzotriazol-1-yl-oxy-tris-pyrrolidino-phosphonium hexafluorophosphate (PyBOP)	Fluorochem
Chloranil	Sigma Aldrich [®]
Cholesterol-PEG ₂₀₀₀ -maleimide	BroadPharm
Ethyl 2-hydroximino-2-cyanoacetate (OxymaPure [®])	Iris Biotech GmbH
Fluorescein-5-maleimide	Sigma Aldrich [®]
Fmoc-amino-PEG-propionic acid (n=23)	Polypure AS
Formic acid	Merck KGaA
Myristalkonium chloride	TCI
Hydroxybenzotriazole monohydrate	Iris Biotech GmbH
<i>N,N</i> -DiBoc-1H-pyrazole-1-carboxamidine	Fluorochem
<i>N,N</i> -diisopropylcarbodiimide	Kemilab Organics
<i>N,N</i> -diisopropylethylamine	Sigma Aldrich [®]
<i>N,N</i> -di- <i>sec</i> -butylcarbodiimide	Kemilab Organics
<i>N,N</i> -di- <i>tert</i> -butylcarbodiimide	Kemilab Organics
Ninhydrin	Merck KGaA
Palmitic acid	Merck KGaA

Phenol	Merck KGaA
Phenylsilane	Sigma Aldrich®
Piperidine	Merck KGaA
Potassium cyanide	Merck KGaA
Rink Amide AM resin (0.71 mmol/g, 100-200 mesh)	Iris Biotech GmbH
Rink Amide ProTide™ resin LL (0.18 mmol/g, 100-200 mesh)	CEM Corp
Sephadex G-25	Cytiva
Sephadex G-50	Cytiva
Triisopropylsilane	Merck KGaA
Tris(2-carboxyethyl)phosphine hydrochloride	Merck KGaA

4.1.2 Solvents

Solvent	Provider
Acetone $\text{CO}(\text{CH}_3)_2$	Merck KGaA
Acetonitrile CH_3CN	Carlo Elba
Dichloromethane CH_2Cl_2	Carlo Elba
Diethylether Et_2O	Carlo Elba
Dimethylsulfoxide	Carlo Elba
Ethanol EtOH	Carlo Elba
Methanol MeOH	Carlo Elba
H_2O milliQ	-
pyridine	Merck KGaA
toluene	Merck KGaA
<i>N,N</i> -dimethylformamide	Carlo Elba

4.1.3 Instrumentation

Instrument	Provider	Software
Liberty Blue™ automated peptide synthesizer with a Discovery® microwave synthesizer.	CEM Corp.	Liberty Blue Application software v2.26929.26168
Arc™ HPLC system with Sample Manager FTN-R, 2998 PDA detector and Quaternary Solvent Manager R	Waters	Empower 3 Pro build 3471
Alliance™ HT LC-MS system with 2975 Separations module, 2996 PDA detector and micromass ZQ mass spectrometer.	Waters	MassLynx v4.1
PrepLC semi-preparative HPLC system	Waters	Empower 3 Pro build 3471
Hei-VAP Advantage rotary evaporator	Heidolph	
CombiFlash® Rf flash chromatography system	Teledyne ISCO	
Digicen 21 R centrifuge	Orto Alresa	

VirTis SP Scientific liophilizer

Benchtop Pro

4.2 General synthetic methods

4.2.1 Microwave-assisted synthesis

Peptide synthesis was conducted using low-loading resin Rink Amide ProTide LL (0.18 mmol/g, 100-200 mesh) in a Liberty Blue™ automated peptide synthesizer. For each peptide, 0.556 g of resin were employed (0.1 mmol scale). The resin was placed in a polypropylene syringe and swelled using DCM (three washes of one minute each, with the solvent aspirated into a manifold after each wash). Thereafter, the resin was transferred to the reaction vessel of the Liberty Blue™ automated peptide synthesizer.

The reagents were prepared as follows: All amino acids were prepared at a concentration of 0.2 M in DMF, the activator at 0.5 M in DMF, oxyma at 1 M in DMF, and piperidine at 20% v/v in DMF. The volumes of each solution were calculated using the Liberty Blue™ software, with the calculations dependent on the specific sequence in question. A synthesis method was then constructed for each peptide sequence using the Liberty Blue™ software, based on a standard method (see **Table 4.1**). The solvents and reagents were loaded into their respective recipients in the equipment, and the synthesis was initiated and monitored at designated intervals until completion to identify and address any potential issues.

The standard coupling and deprotection methods employed in the Liberty Blue™ synthesizer are outlined in **Table 4.1**. Typically, these microwave methods remained unaltered and were utilized as the default setting for each single coupling and double coupling cycle. These cycles operated with fixed quantities of the reagent solutions to perform the deprotection and coupling cycles, and these are summarized in **Table 4.2**.

Table 4.1 Microwave settings for Standard Deprotection and Coupling

Step	T (°C)	Power (W)	Hold Time (s) ^a
Deprotection	75	155	15
	90	30	50
Coupling	75	170	15
	90	30	110

^a Increased by 30% for the long peptide cycles

Table 4.2 Reagent Mix for deprotection and coupling steps

Step	Reagent	Stock Conc.	Vol. (mL) ^a	Final Conc.
Deprotection	Piperidine	20% v/v	4	20% v/v
	DIC	0.5 M	1	
Coupling	OxymaPure®	1.0 M	0.5	0.125 M
	Fmoc-amino acid-OH	0.2 M	2.5	

^a Increased by 30% for the long peptide cycles

The method was modified depending on the sequence, with the introduction of cycles of double coupling that involved a 30% increase in both reaction times and reagent volumes when the peptide sequence consisted of more than 20 residues. A summary of the synthetic profile for each sequence is presented in **Table 4.3**.

Table 4.3 General coupling Scheme for peptides synthesized in the Liberty Blue equipment

Peptide	ID	Single Coupling	Double Coupling	Long Peptide Double Coupling	Long Peptide Triple Coupling
MSLN1	P1-P3	Val15 to Glu6	Val5 to Pro1		
MSLN2	P4-P6	Leu10 to Asp5	Leu4 to Ala1		
MSLN3	P7-P9	Leu9 to Phe7	Leu6 to Ser 1		
MSLN4	P10-P12	Leu38 to Phe36	Leu35 to Leu19	Ala18 to Pro1	
TT	P13, P14	Leu15 to Ile10, Tyr 2	Phe9 to Ile3, Gln1		
OCV1	P15	Leu10 to Pro8, Tyr3 to Lys1	Arg7 to Leu4		
OCV2	P16	Ile9 to Leu6, Tyr2, Ser1	Leu5 to Gly3		
OCV3	P17	Ile9, Asn7 to Val3	Arg8, Phe2, Arg1		
OCV4	P18	Gly28 to Val26, Trp19, Tyr14	Arg30, Phe25, Glu20, Leu18 to Gly15, Ser13	Lys12 to Lys1	
K-Ras1	P19, P23	Gln25 to Leu19	Ala 18 to Leu6	Lys5 to Met1	
K-Ras2	P20, P24	Gln25 to Leu19	Ala 18 to Leu6	Lys5 to Met1	
K-Ras3	P21, P25	Leu42 to Ile37	Phe36 to Leu23	Gln22 to Tyr, Thr2, Met 1	Glu3
K-Ras4	P22, P26	Leu42 to Ile37	Phe36 to Leu23	Gln22 to Tyr, Thr2, Met 1	Glu3

4.2.2 Manual synthesis protocol

This protocol was used for the synthesis of neuroblastoma targeting peptides, the peptide fragments for the K-Ras convergent synthesis, the core of several MAP constructs, and the CF-LUC1-Cys, Ac-Leu-enkephalin, Ac-endomorphin, and Ac-adrenomorphin peptides. The final use of the peptides determined the choice of solid support, depending on whether they were ultimately used as peptide fragments in a convergent synthesis (C-terminal: carboxylic acid) or as final peptides (C-terminal: amide). **Table 4.4** shows the type of resin used for each peptide.

Table 4.4 Resin type used for each peptide synthesized through a manual protocol.

Peptide	ID	Resin
K-Ras fragment 1	P27	HMPB
K-Ras fragment 2	P28	HMPB
K-Ras fragment 3	P29	Sieber
K-Ras fragment 4	P30	2-CTC
K-Ras fragment 5	P31	Sieber
CF-LUC1-Cys	P32	Rink Amide AM
Ac-adrenomorphin	P33	2-CTC
Ac-leu enkephalin	P34	2-CTC

Ac-endomorphin	P35	2-CTC
NB1-5	P36-P40	Rink Amide AM

The synthesis was performed using a polypropylene syringe as reaction vessel fitted with a Teflon® rod and a Teflon® stopcock, which was assembled to a manifold connected to a vacuum pump (**Figure 4.1**). In general, the working scale was 0.1 mmol and the different solid supports or resin were weighed to achieve this scale, following the formula:

$$g \text{ resin} = \text{scale (mmol)} / \text{loading (mmol/g resin)}.$$

Then, the resin was placed in the syringe and swelled it using DMF (3 washes \times 1 min), DCM (3 washes \times 1 min), and DMF (3 \times 1 min) aspirating the solvent into the manifold each time.



Figure 4.1 Manifold vacuum ensemble for peptide synthesis in a syringe.

After swelling, the introduction of the first residue varied depending on the type of resin used for each peptide. While those synthesized in a 2-chlorotrytil resin followed the procedure described in section **4.2.2.1**, peptides synthesized in a HMPB resin followed the protocol described in section **4.2.2.2**, peptides synthesized in a high loading Rink Amide AM resin followed the protocol **4.2.2.4** and, finally, those synthesized in a Sieber resin followed the protocol described in section **4.2.2.5** to load the first amino acid.

4.2.2.1 Introduction of the first residue in a 2-CTC resin

A 2-CTC resin (1.6 mmol/g, 100-200 mesh) was used and placed in the synthesis reactor. 1 eq of amino acid was weighed and dissolved in 1-2 mL of DCM. If not completely soluble in DCM, DMF was added dropwise until the amino acid was completely dissolved. The protected amino acid was added to the synthesis reactor containing the 2-CTC resin, and 2 eq DIPEA was immediately added to the mixture, which was stirred intermittently for 10 minutes, after which another 3 eq of DIPEA was added, and the reaction was allowed to continue for 4 hours. After this time, 0.8 mL of methanol per gram of resin was added directly to the mixture and stirred for 15 minutes. The synthesis was continued from section **4.2.2.6**.

4.2.2.2 Introduction of the first residue in a HPMB resin

The HMPB resin (0.4 mmol/g, 35-100 mesh) was used and placed in the synthesis reactor. In this case, the introduction of the residue was carried out by the symmetrical anhydride method. This consisted of dissolving 2 eq of the amino acid in 1-2 mL of DCM and then adding 1 eq of DIC. The mixture was stirred thoroughly for 5 min and then the mixture was added to the resin placed in the synthesis reactor and 0.1 eq 4-dimethylaminopyridine (DMAP) dissolved in 100 μ L DMF was also quickly added, and the mixture was allowed to react overnight. This process was repeated a second time the following day, discarding the previous solution and adding a fresh one prepared as described. This time the reaction was carried out for 4 hours. The synthesis was continued from section **4.2.2.6**.

4.2.2.3 Fmoc removal

To remove the Fmoc protecting group, 1-2 mL of 20% piperidine/DMF were added to the resin in two treatments (2 \times 5 min) followed by washing three times with 1-2 mL DMF. In each treatment/wash solutions or solvents were aspirated into the manifold.

4.2.2.4 Introduction of the first residue in a Rink Amide AM resin

A Fmoc-Rink Amide AM (0.71 mmol/g, 100-200 mesh) was used and placed in a synthesis reactor. The Fmoc protecting group was removed following the method described in section **4.2.2.3**. The first residue and the oxyma were weighed (1.5 eq each) and dissolved in 1-2 mL DMF, and 1.5 eq DIC was added to the mixture, which was then added to the synthesis reactor containing the resin. The reaction was allowed to proceed for 4 hours at room temperature with gentle stirring. The solutions were discarded, then the resin was washed 2 \times 1 min with DMF and 2 \times 1 min with DCM and the washes were discarded. Finally, the remaining free sites were capped by acetylation. A solution of 135 μ L acetic anhydride (10 equiv. with respect to the full loading of the resin) and 247 μ L DIPEA (10 equiv. with respect to the full loading of the resin) was prepared in 3 mL of DCM. Two treatments of 15 min were performed, discarding the solution each time. The resin was washed five times with DCM for 1 min each, discarding each wash. The synthesis was continued from section **4.2.2.6**.

4.2.2.5 Introduction of the first residue in a Sieber resin

A NovaSyn[®]TG Sieber resin (0.25 mmol/g, 130 μ m) was used and placed in a synthesis reactor. The Fmoc protecting group was removed following the method described in section **4.2.2.3**. The first residue and the oxyma were weighed (3 eq each) and dissolved in 2-3 mL DMF, and 3 eq DIC was added to the mixture, which was then added to the synthesis reactor containing the resin. The reaction was allowed to proceed for 4 hours at room temperature with gentle stirring. The solutions were discarded, then the resin was washed 2 \times 1 min with DMF and 2 \times 1 min with DCM and the washes were discarded. The synthesis was continued from section **4.2.2.6**.

4.2.2.6 Peptide elongation

Peptides were obtained after the introduction of the first residue in the solid support by adding the subsequent residues through two-step cycles consisting of first removing the Fmoc protecting group and then coupling the amino acid, as summarized in **Table 4.5**. The completion of the reaction was checked using the Kaiser tests for primary amine couplings (section **4.2.2.8**) or the chloranil test when the residue is coupled onto a proline (section **4.2.2.9**).

Table 4.5 General elongation protocol for a manual peptide synthesis.

Process	Reagents	Iterations	Time
---------	----------	------------	------

Deprotection	Piperidine in DMF 20% v/v	2	5 min
Wash	DMF	3	1 min
	DCM	2	1 min
Coupling	Fmoc-amino acid-OH and coupling reagents in DMF	1	1 h
Wash	DMF	3	1 min
	DCM	3	1 min
Monitoring	Kaiser or chloranil test	1	3 min

4.2.2.7 Single Coupling

Every new residue was added to the elongating peptide by activating 3 eq of the Fmoc-amino acid-OH with 3 eq of DIC and 3 eq of oxyma dissolving in 1-2 mL of DMF. The mix was added to the resin and reaction was carried out for 1 h under mild stirring. Reagents were discarded and resin was washed, after which the Kaiser or chloranil tests were performed.

4.2.2.8 Kaiser test

A small amount of dried resin was removed with a spatula and placed in a small 0.6 mL glass tube. To these resin beads, 11 drops of Solution A and 3 drops of Solution B (see below for the preparation of these two solutions) were added, and the mixture was incubated at 100°C for 3 minutes. If the solution and/or resin turns blue, the test is positive, confirming the presence of free amines, and the coupling reaction/capping is not complete. If the solution and resin remain unchanged, the test is negative, confirming the absence of free amines and the coupling reaction is complete.

Solution A:

a: 200 mM KCN in water, dilute 2 mL in 100 mL total of pyridine.

B: 40 g phenol in 10 mL EtOH

Mix a and b entirely or in proportions of a to b of 9:1

Solution B:

5% p/v ninhydrin in EtOH

4.2.2.9 Chloranil Test

The chloranil test is used to detect free secondary amines, more frequently the one from L-proline. A saturated chloranil solution was prepared in toluene. A very small amount of dried resin was removed with a spatula and placed in a small 0.6 mL glass tube. Then 10 drops of the saturated chloranil solution and 20 drops of acetone were added and incubated for 3 minutes at room temperature. A positive test (presence of free secondary amines) is seen when the resin beads turn green, and the coupling reaction is incomplete. A negative test is seen when the resin remains unchanged, and the coupling reaction is complete.

4.2.2.10 Double couplings

For positive Kaiser or chloranil tests, indicating incomplete reaction, the residue was recoupled preparing a mix in 1-2 mL DMF with 1.5/1.5/1.5/3 eq of Fmoc-amino acid-OH/PyBOP/oxyma/DIPEA for 30 min at room temperature. **It is crucial not to let this reaction ongoing for more than 45 min**

due to the increased probability of amino acid racemization at its α -carbon chiral center under the basic conditions provided by DIPEA. After 30 min, the reagent mix was discarded and the resin washed and then the Kaiser or chloranil tests were performed. If negative synthesis was continued with the incorporation of the next amino acid.

4.2.3 Final deprotection and N-terminal modification

Either through automated or manual synthesis, once the peptide was finished, the Fmoc group of the final amino acid was removed following step 4.2.2.3. If the peptide was not further modified, it was cleaved. If not, the modifying group palmitoyl, PEG23-yl or 5(6)-carboxyfluoresceinyl were incorporated at the N-terminal peptide position with the same coupling reagents system (X-COOH/DIC/Oxyma, 3:3:3) used in the elongation process, and the incorporation was monitored by the Kaiser test or the chloranil test.

4.2.4 Cleavage

The peptidyl resin was swollen with DCM. A system was assembled with a 250 mL round-bottomed flask containing a stirring magnet, a reduction adapter, a vertical aspiration adapter, and a straight septum inlet flow control adapter with a polytetrafluoroethylene (PTFE) stopcock and the syringe containing the resin, with a magnetic stirrer attached to the top (Figure 4.2).



Figure 4.2 Glassware ensemble for peptide cleavage.

4.2.4.1 High TFA cleavage and global deprotection

To obtain the MSLN, TT, OCV, K-Ras, CF-LUC1-Cys and NB targeting peptides from the Rink Amide-type resins, the peptidyl resins were treated with a solution of TFA/H₂O/TIS (95:2.5:2.5; v/v/v) for 30 min, with occasional stirring during this time. The mixture was then filtered and collected in the round-bottomed flask of the system. The process was repeated once with fresh cleavage solution to ensure that all product was cleaved from the resin. The final acid solution was stirred for 1 hour to remove all side chain protecting groups from the peptide. The solution was then divided into 50 mL vials containing 20 mL of cold diethyl ether to promote peptide precipitation and centrifuged at 5000 rpm for 5 minutes. Alternatively, if the final peptides were highly hydrophobic, most of the TFA solution was removed under vacuum and the cleaved peptide precipitated onto 20 mL cold Et₂O. The

supernatant was discarded, and the pellet was washed three times with 10 mL Et₂O by centrifugation at 3500 rpm for 5 minutes each time. The pellet was dried under hood flow, dissolved in 10 mL H₂O/CH₃CN, frozen and lyophilized. If the peptide sequences contain cysteine or methionine, instead of using the previous acid mixture, the peptidyl resin was treated with a solution of TFA/H₂O/TIS/EDT (92.5:2.5:2.5:2.5, v/v/v/v).

4.2.4.2 Low TFA cleavage with no side chain deprotection

To obtain fragments for MAP constructs or for a convergent synthesis from the 2-CTC, HMPB or Sieber resins, the peptidyl resins were treated ten times with 3 mL of a solution consisting of 1% TFA in DCM. This allowed to obtain the fragments from the resin carrying all side chain protecting groups. Each treatment was performed for 5 min and collected onto a round-bottomed flask with 100 mL of milliQ H₂O. After collecting all treatments, DCM was eliminated by nitrogen flow to precipitate the peptides in the H₂O. After all the DCM was eliminated, the sample was divided into 50 mL vials and lyophilized.

4.2.5 Characterization by analytical RP-HPLC and HPLC-MS

Characterization of the crude and purified products was carried out by RP-HPLC and HPLC-MS. The elution system for RP-HPLC was A: H₂O (+0.045% CF₃COOH) and B: CH₃CN (+0.036% CF₃COOH) and for HPLC-MS was A: H₂O (+0.1% HCOOH) and B: CH₃CN (+0.07% HCOOH). Columns used were either a Kinetex® C8 (4.6 x 100 mm, 5 μm, 100 Å) for palmitoylated products in RP-HPLC and a X-Select 50x3.5some protected fragments or a XBridge® BEH C18 (4.6 x 100 mm, 3.5 μm, 100 Å) for the rest of the products with a 1 mL/min flow. Peptides were detected at 220 nm.

4.2.6 Purification of peptides by semi-preparative HPLC

Crude products were dissolved in either H₂O/CH₃CN (1:1), DMSO or TFA and purified in semi-preparative HPLC by injecting 30-50 mg into either an XBridge® Prep C18 OBD™ column (19 x 100 mm, 5 μm) or a Kinetex® C8 AXIA™ column (21.2 x 100 mm, 5 μm). The elution system was A: H₂O (+0.1% CF₃COOH) and B: CH₃CN (+0.1% CF₃COOH) at 16 mL/min and peptides were eluted at different gradients depending on the best resolution for each specific sequence. peptide detection was performed at 220 nm. Fractions containing the end product were manually collected immediately after detection. After collection and analysis of the fractions by analytical HPLC, the solvent was partially removed under vacuum and reduced to 20 mL, which was then lyophilized.

4.3 Antigenic peptides for nanovaccines

4.3.1 Synthesis of the antigenic peptides

Peptides were synthesized by the protocol described in section 4.2.1. These peptides were cleaved from the peptidyl resin following the protocols described in section 4.2.4. All peptides that carry a palmitoyl N-terminal modification, as well as the PEGylated MSLN2 peptide required the evaporation of TFA in vacuum before precipitation in cold Et₂O due to their highly hydrophobic nature.

4.3.2 Characterization of antigenic peptides for nanovaccines

Table 4.6 Characterization of anticancer nanovaccine candidate peptides

Peptide	N-terminal	ID	mg of pure peptide	% Purity at 220 nm	MS
MSLN1	H-NH-	P1	40	>99	Calc. [M+H] ⁺ = 1600.0, [M+2H] ²⁺ = 800.5 Found [M+H] ⁺ = 1600.6, [M+2H] ²⁺ = 800.9
	H-PEG23-NH	P2	44	>99	Calc. [M+2H] ²⁺ = 1364.3, [M+3H] ³⁺ = 909.9 Found [M+2H] ²⁺ = 1364.7, [M+3H] ³⁺ = 910.4

	Palm-NH-	P3	16	95	Calc. $[M+H]^+ = 1839.4$, $[M+2H]^{2+} = 920.2$ Calc. $[M+H]^+ = 1839.1$, $[M+2H]^{2+} = 920.1$
	H-NH-	P4	54	99	Calc. $[M+H]^+ = 1127.5$, $[M+2H]^{2+} = 564.3$ Found $[M+H]^+ = 1126.5$, $[M+2H]^{2+} = 564.2$
MSLN2	H-PEG23-NH	P5	104	96	Calc. $[M+H]^{2+} = 1128.4$, $[M+3H]^{3+} = 752.7$ Found $[M+H]^{2+} = 1136.6$, $[M+3H]^{3+} = 758.2^a$
	Palm-NH-	P6	17	99	Calc $[M+H]^+ = 1365.9$ Found $[M+Na]^+ = 1386.8$, $[M+K]^+ = 1402.8$
	H-NH-	P7	4	95	Calc. $[M+H]^+ = 1052.4$, $[M+2H]^{2+} = 526.7$ Found $[M+H]^+ = 1051.5$, $[M+2H]^{2+} = 526.7$
MSLN3	H-PEG23-NH	P8	30	95	Calc. $[M+H]^{2+} = 1090.9$, $[M+3H]^{3+} = 727.6$ Found $[M+H]^{2+} = 1099.0$, $[M+3H]^{3+} = 733.2^a$
	Palm-NH-	P9	17	98	Calc. $[M+H]^+ = 1289.8$ Found $[M+H]^+ = 1290.8$
MSLN4	H-PEG23-NH	P11	107	>99	Calc. $[M+3H]^{3+} = 1794.8$, $[M+4H]^{4+} = 1346.3$ Found $[M+3H]^{3+} = 1795.7$, $[M+4H]^{4+} = 1347.0$
	Palm-NH-	P12	68	97	Calc. $[M+3H]^{3+} = 1499.3$, $[M+4H]^{4+} = 1124.7$ Found $[M+3H]^{3+} = 1498.8$, $[M+4H]^{4+} = 1124.4$
TT	H-NH-	P13	15	97	Calc. $[M+H]^+ = 1724.0$, $[M+2H]^{2+} = 862.5$ Found $[M+H]^+ = 1725.0$, $[M+2H]^{2+} = 862.8$
	H-PEG23-NH	P14	101	>99	Calc. $[M+2H]^{2+} = 1426.3$, $[M+3H]^{3+} = 951.7$ Found $[M+2H]^{2+} = 1427.2$, $[M+3H]^{3+} = 951.7$
OCV1	H-NH-	P15	41	>99	Calc. $[M+H]^+ = 1255.8$, $[M+2H]^{2+} = 628.4$ Found $[M+H]^+ = 1255.6$, $[M+2H]^{2+} = 628.8$
OCV2	H-NH-	P16	20	98	Calc. $[M+H]^+ = 1078.6$, $[M+2H]^{2+} = 539.8$ Found $[M+H]^+ = 1078.5$, $[M+2H]^{2+} = 540.3$
OCV3	H-NH-	P17	28	>99	Calc. $[M+H]^+ = 1072.6$, $[M+2H]^{2+} = 536.8$ Found $[M+H]^+ = 1072.7$, $[M+2H]^{2+} = 537.2$
OCV4	H-NH-	P18	13	>99	Calc. $[M+3H]^{3+} = 1295.9$, $[M+4H]^{4+} = 972.2$ Found $[M+3H]^{3+} = 1295.5$, $[M+4H]^{4+} = 972.0$
K-Ras4	Palm-NH-	P22	3	91	Calc. $[M+3H]^{3+} = 1612.6$, $[M+4H]^{4+} = 1209.7$ Found $[M+3H]^{3+} = 1498.8$, $[M+4H]^{4+} = 1209.7$

a The predominant signals correspond to a mono-hydration due to the PEG moiety. Weak signals can be detected with the correct peptide mass.

4.3.3 PLGA nanoparticle synthesis for nanovaccine production

PLGA NPs with encapsulating adjuvants were prepared using an oil-in-water emulsion and solvent evaporation-extraction method. Briefly, 50 mg PLGA was dissolved in 3 mL DCM along with 5 μ L pIC and 2 mg R848 with or without the different antigenic peptides. The solution above was added dropwise to 20 mL of aqueous 2% (w/v) PVA and emulsified for 60 s with 5-sec rest each cycle using a sonicator (Sonifier 250, Branson, Danbury, USA). Following overnight evaporation of the solvents at 4 °C, the NPs were collected by centrifugation (14800 rpm for 30 min) at 4 °C and redissolved in water. After, the nanoparticle solution was added dropwise to 20 mL of 1% homogenized chitosan oligosaccharide lactate solution and stirred at 4°C for 2 hrs. The coated NPs were finally collected by lyophilization.

4.3.4 Biological assays

4.3.4.1 Animals and immunization

A total of 15 C57BL6 male mice (12 weeks old) were used in the experiment. Mice were obtained and kept at the animal facility of Max-Planck-Institute for Multidisciplinary Sciences under 12 h dark: light cycle with ad libitum access to food and water. All animal experimental procedures were performed

in compliance with the European (2010/63/EU) and German regulations on Animal Welfare and were approved by the administration of Lower Saxony (LAVES) (Nr. 33.19-42502-04-20/3527). Mice were immunized subcutaneously in the right flank once per week, for three weeks with nanoparticle containing the adjuvants polyinosinic:polycytidylic acid (polyI:C) and R848. The NPs were diluted in water and injected in a volume of 100 μ L, in a concentration of 2.5 μ g of polyI:C, and 3.75 μ g of R848. The mice were sacrificed 2 days after the last vaccination and the spleen was excised.

4.3.4.2 Stimulation of splenocytes and lymph node cells

Single-cell suspensions from spleen were prepared in sterile condition by mincing the cells through 40 and 100 μ L cell strainers (BD Falcon), respectively. Erythrocytes in spleen samples were lysed with 1 mL ACK buffer (150 mM NH_4Cl , 10 mM KHCO_3 , 0,1 mM EDTA, pH = 7.2–7.4) per spleen for 5 min. The reaction was stopped with PBS and spun down. Cells were resuspended in RPMI 1640 medium supplemented with 10% Fetal Bovine Serum, 100 μ g/mL penicillin, 100 μ g/mL streptomycin. Cells were seeded in 96-well plates with a density of 500.000 cells per well respectively in duplicates or triplicates. Splenocytes were stimulated with different peptides in a concentration of 10 μ g/mL. The supernatant was collected after 48 h of stimulation and kept frozen at -20 $^\circ\text{C}$ until cytokine analysis. After 48 h of stimulation, the cells were analyzed for viability.

4.3.4.3 ELISA

Cells were centrifuged and supernatants were collected and kept at -20 $^\circ\text{C}$ for further cytokine quantification. IFN- γ was quantified by ELISA (Thermoscientific, #88-7314-88). Briefly, the 96-well plates were incubated overnight at 4 $^\circ\text{C}$ with capture antibody. After washing and blocking, the plate was incubated at room temperature with samples for 2 h and then with detection antibody for 1 h. After that, the plate was incubated with avidin horseradish peroxidase (HRP) conjugate for 30 min. The color reaction was developed by adding TMB solution and the enzymatic reaction was stopped by adding 2 N H_2SO_4 . Optical density (OD) was determined at 450 nm.

4.3.4.5 Cell viability assay

For cell proliferation and cytotoxicity assay CellTiter 96[®] Aqueous One Solution Reagent (Promega) was used. The reagent contains a tetrazolium compound [3-(4,5-dimethylthiazol-2-yl)-5-(3-carboxymethoxyphenyl)-2-(4-sulfophenyl)-2H-tetrazolium, inner salt; MTS] and phenazine ethosulfate; PES. After 48 h of stimulation with the peptides, 20 μ L of the reagent was added to each well and the plate was incubated for 4 h. The absorbance at the wavelength of 490 nm was measured by a microplate reader.

4.3.4.6 Statistical Analysis

Results are expressed as the mean \pm SEM (standard error of the mean). Data were analyzed and statistical analyses were performed using GraphPad Prism v9.2.0 software. Each experiment was performed three times with triplicates per assay. Data are presented as mean \pm SEM. One-way analysis of variance (ANOVA) with Tukey's test for multiple comparisons was performed. A p-value of <0.05 was considered statistically significant.

4.4 Targeting moieties for neuroblastoma

4.4.1 Synthesis of peptides for neuroblastoma

Peptides were synthesized by manual solid phase following the protocol described in section 4.2.2 and cleaved from the resin following the protocol in section 4.2.4.

4.4.2 Characterization of neuroblastoma-targeting peptides

Table 4.7 Characterization of neuroblastoma-targeting peptides

Peptide	Cys thiol	ID	mg of pure peptide	% Purity at 220 nm	MS
NB1	-SH	P36	95	>99	Calc. $[M+2H]^{+2} = 848.9$, $[M+3H]^{+3} = 566.2$
					Found $[M+2H]^{+2} = 848.7$, $[M+3H]^{+3} = 566.3$
NB2	-SH	P38	102	>99	Calc. $[M+2H]^{+2} = 655.2$, $[M+3H]^{+3} = 437.2$
					Found $[M+2H]^{+2} = 655.8$, $[M+3H]^{+3} = 437.2$
NB3	-SH	P40	106	95	Calc. $[M+2H]^{+2} = 628.2$, $[M+3H]^{+3} = 419.2$
					Found $[M+2H]^{+2} = 628.6$, $[M+3H]^{+3} = 419.3$
NB4	-SH	P42	84	99	Calc. $[M+2H]^{+2} = 591.7$, $[M+3H]^{+3} = 394.8$
					Found $[M+2H]^{+2} = 591.9$, $[M+3H]^{+3} = 395.0$
NB5	-SH	P44	71	96	Calc. $[M+H]^+ = 1081.7$ $[M+2H]^{+2} = 541.6$
					Found $[M+H]^+ = 1081.7$ $[M+2H]^{+2} = 541.7$

4.4.3 Synthesis of fluoresceinated derivatives of the targeting peptides for neuroblastoma

0.01 mmol of the purified peptides **P36** to **P40** (10 to 17 mg) were dissolved in 1 mL NH_4HCO_3 pH = 8.0 and mixed quickly with 1.1 eq of Fluorescein-5-maleimide (0.011 mmol, 4.7 mg) in 1 mL DMF. Reaction was stirred for 2h under a nitrogen atmosphere. Solvent was eliminated and sample was lyophilized. Then peptides were purified by semi-preparative RP-HPLC as described above, after confirming the reaction was finished by RP-HPLC and ESI-MS.

Table 4.8 Characterization of fluorescein-labeled neuroblastoma-targeting peptides

Peptide	Cys thiol	ID	mg of pure peptide	% Purity at 220 nm	MS
NB1	-S-mal-Fl	P37	4.4	>99	Calc. $[M+2H]^{+2} = 1062.6$, $[M+3H]^{+3} = 708.7$
					Found $[M+2H]^{+2} = 1062.6$, $[M+3H]^{+3} = 708.8$
NB2	-S-mal-Fl	P39	2.4	>99	Calc. $[M+2H]^{+2} = 868.9$, $[M+3H]^{+3} = 579.6$
					Found $[M+2H]^{+2} = 868.9$, $[M+3H]^{+3} = 579.7$
NB3	-S-mal-Fl	P41	10.2	96	Calc. $[M+2H]^{+2} = 841.9$, $[M+3H]^{+3} = 561.6$
					Found $[M+2H]^{+2} = 841.6$, $[M+3H]^{+3} = 561.7$
NB4	-S-mal-Fl	P43	5.5	94	Calc. $[M+2H]^{+2} = 805.4$, $[M+3H]^{+3} = 537.2$
					Found $[M+2H]^{+2} = 805.3$, $[M+3H]^{+3} = 537.4$
NB5	-S-mal-Fl	P45	4.1	92	Calc $[M+2H]^{+2} = 755.8$ $[M+3H]^{+3} = 504.2$
					Found $[M+2H]^{+2} = 756.1$, $[M+3H]^{+3} = 504.4$

4.4.4 Synthesis of *p*-aminobenzylguanidine (PABG) derivatives4.4.4.1 Synthesis of DiBoc-*p*-aminobenzylguanidine (PABG)

4-aminobenzylamine (1.64 mmol, 0.186 mL) was guanidinylated by reacting with *N,N*-DiBoc-1H-pyrazole-1-carboxamide (1.64 mmol, 0.51 g) in the presence of DIPEA (1.64 mmol, 0.285 mL) in DCM for 4h at room temperature with mild stirring, after which solvent was eliminated obtaining PABG as a solid (224 mg, 95%). Purity by HPLC >99% (220 nm). HPLC-MS: calculated mass for $\text{C}_{18}\text{H}_{28}\text{N}_4\text{O}_4$ $[M + H]^+ = 364.5$ found by HPLC-MS (ESI): 365.8.

4.4.4.2 Synthesis of thiolated-PABG derivative

PABG was reacted with S-trityl-3-mercaptopropanoic acid via its aniline amine by a symmetric anhydride method. Thus, the S-trityl-3-mercaptopropanoic acid was turned into its anhydride by

mixing 2 eq (3.28 mmol, 1.12 g) with 1 eq of DIC (1.64 mmol, 0.254 mL) in DCM, stirring vigorously by vortex for 5 min and then adding to DiBoc-PABG (224 mg, 1.64 mmol) adding 1 eq of DIPEA (1.64 mmol, 0.285 mL) and stirred at room temperature overnight to generate the protected thiolated-PABG. After solvent elimination, this compound was then deprotected by treatment with 50% CF₃COOH in DCM with 5% TIS as scavenger to generate the thiolated-PABG (106 mg, 75%), which was then purified by automated flash chromatography (65 mg, 62%). Purity by HPLC >99% (220 nm). HPLC-MS: calculated mass for C₁₁H₁₆ON₄S [M + H]⁺ = 253.3 found by HPLC-MS (ESI): 253.4.

4.4.4.3 Synthesis of the fluoresceinyl-PABG derivative

A portion of the thiolated-PABG (0.1 mmol, 25.2 mg) is then conjugated with 1.1 eq of fluorescein-5-maleimide (0.11 mmol, 47 mg) by dissolving the fluorescent compound in 1 mL of DMF and mixing with the thiolated-PABG dissolved in 1 mL of NH₄HCO₃ 10 mM buffer pH =7.5. Reaction was carried out for 2h at room temperature with mild stirring under inert atmosphere. Reaction was checked by RP-HPLC and then the crude was purified by automated flash chromatography. HPLC-MS: calculated mass for C₃₅H₂₉N₅O₈S [M + H]⁺ = 680.7 found by HPLC-MS (ESI): 680.4.

4.4.5 Cell localization assays

Briefly, neuroblastoma cell lines were selected by overexpression of mainly the GD2 surface protein as assessed by labeled antibody recognition and other target receptors via qRT-PCR. Specifically CHLA-90, SK-N-BE(2) and SHSY-5Y were selected as positive cell lines for peptide localization assays while HEK293T was selected as negative control. For a positive binding control, labelled RGD peptide prepared in our group was used. The binding was tested at 5 μM for 1 and 24 h and visualized by confocal microscopy. The best performing peptides/organic molecules were selected to perform conjugation assays in nanoparticles based on their ability to accumulate in the cell membrane of neuroblastoma cell lines.

4.4.6 Formulation of QS nanoparticles by DELOS-susp

Quatsome (QS) nanovesicles were produced by DELOS-susp (Depressurization of an Expanded Liquid Organic Solution into aqueous solution). This process is schematized in **Figure 4.3**. Cholesterol-PEG2000-maleimide, and DC-cholesterol were weighed and dissolved in 3.2 mL ethanol by vigorous stirring and heating at 38°C, according to the quantities in **Table 4.9** for 2 μmol or 4 μmol of maleimide content. This was added onto the high-pressure plant and incubated at 55°C.

Table 4.9 Formulation of quatsome nanovesicles with a maleimide function

Reagent	2 μmol maleimide	4 μmol maleimide
DC-Chol	95.9 mg	95.9 mg
Chol-PEG ₂₀₀₀ -mal	13.0 mg	26.0 mg
MKC	13.0 mg	26.0 mg
EtOH	3.2 mL	3.2 mL
milliQ water	26.3 mL	26.3 mL

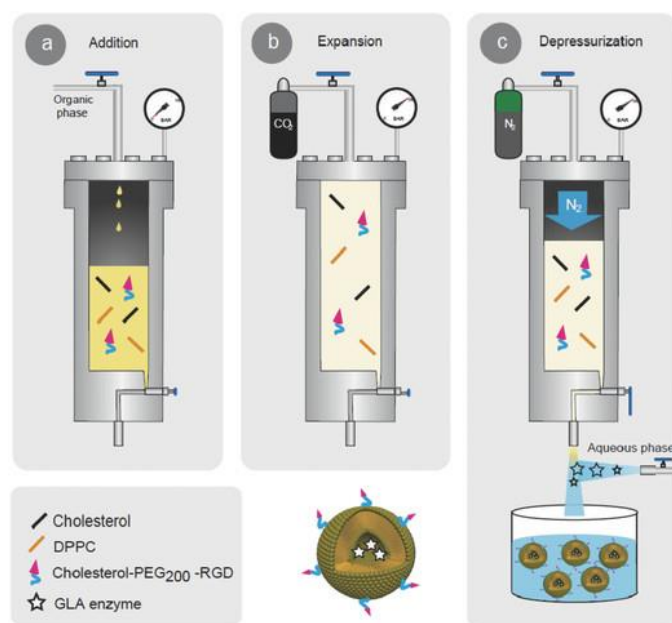


Figure 4.3 Schematic representation of the stages of the DELOS-susp methodology for the preparation of quatsomes. Components dissolved in organic solvent are added to the chamber (a), which is then expanded by gas (b) and then depressurizes into water with surfactant (c) to yield the nanoparticle

The solvent was expanded by the addition of CO₂ into the high-pressure plant. Expansion was carried out for 1h after which the contents of the plant were carefully bubbled by nitrogen flow into water with the surfactant MKC dissolved in it.

4.4.7 Characterization of QS nanovesicles by Dynamic Light Scattering (DLS) and Multi-Angle Dynamic Light Scattering (MADLS)

An aliquot of 1 mL of formulated sample was added into a spectrometer cuvette and analyzed in a ZetaSizer ZEN 3600 (Malvern Panalytical, United Kingdom) to characterize size distribution and then onto a Folded capillary Zeta cell (Malvern Panalytical, United Kingdom) to measure Z-potential.

4.4.8 Isolation of the free PABG in supernatant

Free PABG that was not conjugated was separated from the suspension of nanovesicles by three different methodologies.

4.4.8.1 Ultracentrifugation

1 mL of samples were loaded into an Open-Top Thickwall Polycarbonate Tube (Beckman-Coulter, Germany) and centrifuged in a Sorvall™ WX+ 2500 centrifuge (ThermoFischer Scientific, US). At 600000 for 6 h at 4°C. Supernatant was quickly and carefully recovered for analysis.

4.4.8.2 Filtration by AMICON® filter units

4 mL of samples were loaded into 4 mL AMICON® centrifugal filter units (Merck Millipore, 30 kDa MWCO) and centrifuged at 4000 x G for 40 min. Flow-through was recovered.

4.4.8.3 Size-Exclusion Chromatography in Sephadex G-25

Pre-packed PD Midi Trap G-25 columns (Cytiva Life Sciences, United Kingdom) were equilibrated with 20 mL water and 0.5 mL of sample was then loaded and eluted with 20 mL water, 20 mL water + 10

mL 10% v/v acetic acid or 30 mL water + 10 mL of an acetic acid gradient of pH = 5.5 and pH = 4.5. Depending on the expected eluate 5 or 10mL fractions were collected and analyzed.

4.4.9 Optimized method for targeting units conjugation to QS nanovesicles

QS nanovesicles were prepared with 4 μmol maleimide content as previously described and after characterization, pH was adjusted to 7.5 with bis-tris buffer 25 mM. The following day, **P40** peptide, the best candidate in cell localization assays, was conjugated to the nanovesicle (4.8 μmol , 7.66 mg) using 12 mL of QS suspension (10.8% ethanol, 89.2% miliQ water). The peptide was dissolved in 100 μL of water and added dropwise. Conjugation was carried out in 3 h at room temperature with mild stirring, adding a spatula tip of TCEP to prevent disulfide bonds between cysteine of neighboring peptide macromolecules. The same protocol was used to conjugate PABG (4.8 μmol , 1.43 mg) and compare to previous conjugation assays.

4.4.10 Isolation of non-conjugated targeting units by Sephadex G-50 size-exclusion chromatography

Immediately after conjugation 0.5 mL of the mix were loaded onto a Sephadex G50 with 8.3 mL of packed slurry (Cytiva Life Sciences, United Kingdom) and then an elution gradient was carried out first with 30 mL water, collecting 10 mL fractions, and then with 10 mL acetic acid solution at pH = 5.5 and 4.5, collecting 5 mL each time. Control of recovery was performed by loading on to a clean column purified **P40** peptide (4.8 μmol , 7.66 mg) in 0.5 mL of water and eluting as previously described. This control will be used to determine the amount peptide that is recovered from the column after it is loaded. The same protocol was carried out for PABG (4.8 μmol , 1.43 mg).

4.4.11 Estimation of the conjugation efficiency by analytical RP-HPLC

To estimate the amount of PABG or peptide conjugated to the nanovesicle, all elution fractions from the Sephadex G-50 were analyzed by RP-HPLC, injecting 25 μL and 50 μL for each sample, which were recovered as 5- and 10-mL fractions, respectively, to account for dilution. 2.5 μL of PABG or **P40** prepared in the same concentrations as they were loaded into the column, were injected, representing the fully unconjugated initial amount. Gradient used was of 5-70%B in the same elution system as described previously and the integrated area below the curve of the peak was used to estimate the amount of PABG or peptide. Peptide was monitored at 220 nm while PABG was monitored at 254 nm.

4.5 Selection of carbodiimides to replace DIC as a coupling reagent

4.5.1 Manual synthesis of Ile^{2,3}-Leu-Enkephalin (H-YIIFL-NH₂) and Leu-Enkephalin (H-YGGFL-NH₂), model peptides with five different carbodiimides

The peptides were manually synthesized in 141 mg of Rink Amide AM resin (0.71 mmol/g) for a 0.1 mmol scale, weighed into a 2 mL syringe acting as a synthesis reactor, coupled to a manifold collection system and vacuum pump, allowing easy disposal of reagents and solvents into the manifold. Each peptide was synthesized five times, one for each different carbodiimide. The resin was swollen by washing six times for 1 min each, alternating DMF and DCM, discarding the solvents after each wash. Fmoc was removed from the Fmoc-Rink amide resin by treatment with 1 mL piperidine/DMF (20:80, v/v) twice for 5 min before introducing the first residues and for 1 and 7 min for each subsequent deprotection step. The resin was then washed 4 times with 1 mL DMF for 1 min each time. Fmoc-amino acid/oxyma/carbodiimide coupling (5eq/5eq/5eq) was performed by first dissolving amino acid and oxyma in 0.8 mL DMF, mixing thoroughly by sonication and vortexing, adding to the resin and activating after 3 min with the corresponding carbodiimide, allowing to stand for 30 min at room temperature with gentle stirring. Then the coupling mixture was discarded, and the resin was washed

4 times with 1 mL DMF for 1 min each time. Deprotection and coupling were performed cyclically as described from C-terminal Leu to N-terminal Tyr until the sequence was complete and the last Fmoc was removed, after which the resin was washed as described and then swelled three times with 1 mL DCM. Acidolytic cleavage was then performed as described in section 4.2.10 and final peptides were characterized as described in section 4.2.11.

4.5.2 Determination of the the oxadiazole formation in carbodiimide/oxyma mixture as indicator of HCN release

The five carbodiimides (0.5 mmol) were dissolved in 2.5 mL DMF together with oxyma (0.5 mmol) to yield a 0.2 M solution. One set of solutions was stirred at 25 °C and another at 60 °C. The course of the reaction was analyzed by LC-HRMS performed on an Ultimate3000 with a Phenomenex C18 (dimensions 4.6 mm x 150 mm) column. The elution system was comprised of **A**: H₂O (+0.1% HCOOH), **B**: CH₃CN (0.1% HCOOH), flow 1.0 mL/min, UV detection 220 nm). Aliquots of 2 µL were taken, diluted with 498 µL of CH₃CN and analyzed. The solutions kept at 25°C were analyzed after 24 h and 4 days. Solutions kept at 60 °C were analyzed after 18 h. This study was performed in the University of KwaZuluNatal (Durban, South Africa) by the group led by Dr. Fernando Albericio.

4.5.3 Solubility of urea in DMF

To assess the solubility of concentrated urea resulting from the reaction first of carbodiimides and carboxylic acids (and amino acids by extension) to form a *O*-acylurea and then of oxyma with this *O*-acylurea, solutions of 1M Fmoc-L-Ala-OH, 1M oxyma and 1M carbodiimide were prepared and let react for 5 min at room temperature. Precipitation was then assessed visually.

Conclusions

Conclusions associated to chapter 1

- Eighteen synthetic epitopes extracted from PDAC overexpressed proteins with high antigenic potential, such as mesothelin (MSLN), K-Ras, tetanus toxoid (TT), were designed and synthesized. The different epitopes were synthesized as single epitopes (MSLN1-3, TT) and linear multiepitopes (MSLN4, K-Ras1-4) with different modifications at the N-terminal position (palmitoyl, PEG or unmodified).
- Four synthetic epitopes based on the OCV-C01 cancer vaccine were also synthesized. Three of them are single epitopes (OCV1-3) and the fourth is a novel construct based on a linear multiepitope combining the three single epitopes (OCV4).

From the synthesis point of view:

The MSLN- and TT-based epitopes were successfully obtained despite the difficulties associated with some sequences. The difficulty in these syntheses was related to the length of the peptides, as the linear multiepitope peptide (MSLN4) has 38 residues, and the intrinsic hydrophobicity of the MSLN sequences, which was increased when the peptide carried a palmitoyl moiety.

- K-Ras-based epitopes have been extremely difficult to obtain, mainly due to the aggregation tendency of their sequences, which complicates their purification. From the 4 epitopes designed, only the linear multiepitope K-Ras4 peptide was obtained, but small amounts with a purity of 90%.
- OCV-based epitopes were successfully obtained without major complications
- A multimodal and multivalent MAP has been explored as an alternative platform for multiepitope presentation. By combining different amino-protecting groups, a MAP core carrying up to three different peptides has been synthesized. Optimization is needed to improve the synthetic performance and to allow the introduction of a fourth moiety into the MAP core.

From the point of view of biological evaluation:

- The single epitope peptides synthesized in this study are not immunogenic, regardless of whether they carry self-adjuvant motifs. The combination of these peptides into a single multiepitope peptide confers greater immunogenicity.
- Palmitoylation increases the immunogenicity of the peptide sequence. However, the mode of presentation of the epitopes that make up the nanovaccine has a greater impact on the final immunogenicity.
- MSLN multiepitope linear peptides (MSLN4, palmitoylated and PEGylated) are the best presentation alternative for in vitro induction of CD8+ specific antitumor immune activity.
- Among them, the mesothelin nanovaccine formulated with MSLN4, a multiepitope peptide containing three epitopes and a palmitoyl moiety at the N-terminal position, showed a good immunogenic response in an in vitro model and in killing assays, initially suggesting a promising approach for PDAC treatment. However, in vivo experiments showed little effect on tumor size and immune response with the chosen schedule. Extended prophylactic and

therapeutic vaccination protocols will be performed by the Translational Molecular Imaging Group of the Max Planck Institute to confirm the efficacy of the MSLN4 nanovaccine in the in vivo models of PDAC.

- MSLN and OCV single epitopes (MSLN 1-3 and OCV 1-3) have been shown to activate an antitumor immune response when formulated as a mixture in a nanovaccine, but when the nanovaccine formulation is performed with a linear multiepitope composed of these single epitopes (MSLN4 and OCV4), the activation of the antitumor immune response is higher.
- Therefore, the linear multiepitope peptide composed by three epitopes of an antigenic protein is the best mode of presentation to elicit strong immune responses based in antitumoral specific CD8+ cytotoxic T cells.

Conclusions associated to chapter 2

- Six targeting units and the corresponding fluoresceinyl conjugated were synthesized. Five of them were peptide ligands of surface receptors overexpressed in neuroblastoma phenotypes (TkrB, h-NET and GD2) and one was a derivative of PABG, a ligand of the hNET protein.
 - Thiolated-PABG derivative (h-NET ligand) and **P40** peptide (GD2 receptor ligand) were selected as potential targeting/homing unit candidates for their ability to internalize in neuroblastoma cells. These targeting units were used to be conjugated to QS derivatized with a maleimide function.
 - A procedure to conjugate these targeting/homing ligands to quatsomes functionalized with maleimide was set up, exploring different parameters, of which the most crucial for higher conjugation efficiency are the quantity of maleimide function incorporated to the QSs (Chol-PEG-mal), the presence of a reducing agent during conjugation, the final pH of the nanovesicles suspension and the separation method used to isolate the final targeting ligand-QS conjugates.
 - Both targeting/homing ligands can be incorporated into a quatsome nanovesicle via maleimide-thiol chemistry following the process developed with preliminary loadings ranging from 40 to 65% of the available material.
 - Size-exclusion chromatography on Sephadex G-50 using an elution system based on H₂O and followed by a solution of CH₃COOH at pH = 5.5 has been established as the best separation method to purify the quatsome formulation from unreacted targeting unit. The method allows the indirect estimation of the targeting unit conjugated to the quatsomes and the conservation of the final targeted quatsomes, which have a regular size below 100 nm with low dispersion (PDI less than 0.2), that remains stable over a long period of time.
 - This formulation has demonstrated the ability to complex miR-323a-5p therapeutic RNA and this nanoformulation has been shown to be taken up by the IMR-32 neuroblastoma cell line when the formulation carries 1 μmol of Chol-PEG₁₀₀₀-mal. Formulations carrying 4 μmol of PEGyl moiety and when this moiety is a PEG₂₀₀₀, RNA can be complexed to the QS but no transfection to a neuroblastoma cell line occurs. This work is being continued by the research group of Dr. Nora Ventosa and Dr. Mariana Köber at the Instituto de Ciencias de Materiales de Barcelona (ICMAB-CSIC) and their collaborating group of Dr. Miguel Segura at the Vall d'Hebron

Institut de Recerca.

Conclusions associated to chapter 3

-Two model peptides, Leu Enkephalin and Ile^{2,3}-Leu Enkephalin, were synthesized manually using five different carbodiimides as coupling reagent in combination with oxyma. The carbodiimides used were DIC and four alternatives: TBEC, DSBC, DTBC and EDC. These carbodiimides represent varying substituents, with primary, secondary and tertiary carbons attached to the nitrogen atom in the core moiety of these reagents. The carbodiimides were evaluated in terms of their synthetic performance, compared to DIC as well as their ability to generate the unwanted HCN by-product when reacted directly with oxyma in the absence of amino acids and in conditions that favor the reaction.

- The carbodiimide DIC can be replaced by TBEC in peptide synthesis. This carbodiimide shows comparable synthetic performance to DIC when used in model peptides as well as in the synthesis of a hydrophobic short peptide, the palmitoylated single epitope MSLN2 peptide.
- TBEC reduces the formation of HCN 6-fold compared to DIC. This is not the lowest value obtained, but it is the lowest of any carbodiimide with synthetic performance comparable to DIC.
- TBEC combines the good performance of the *tert*-butyl substituent - no HCN formation at all - the ethyl substituent - only linear adduct formation - and that of a carbodiimide with two different substituents in which the nitrogen atom is attached to primary carbons, such as EDC-HCl.
- The asymmetric carbodiimide TBEC is therefore an effective replacement for DIC, as it ensures minimal formation of HCN and also performs fully comparable to standard DIC in SPPS for the model sequences studied and the MSLN2 palmitoylated peptide.

References

- 1.- Reeves B, Bernard SA. Systemic Effects of Cancer. In: *Pathobiology of Human Disease: A Dynamic Encyclopedia of Disease Mechanisms* Elsevier Inc., 2014; pp. 456–466.
- 2.- Kumai T, Kobayashi H, Harabuchi Y, Celis E. Peptide vaccines in cancer — old concept revisited. *Current Opinion in Immunology* **2017**. 45, 1–7.
- 3.- Song H, Su Q, Huang P, Zhang C, Wang W. Self-assembling, self-adjuvanting and fully synthetic peptide nanovaccine for cancer immunotherapy. *Smart Materials in Medicine* **2021**. 2, 237–249.
- 4.- Arbelaez CA, Estrada J, Gessner MA, Glaus C, Morales AB, Mohn D, et al. A nanoparticle vaccine that targets neoantigen peptides to lymphoid tissues elicits robust antitumor T cell responses. *npj Vaccines* **2020**. 5.
- 5.- Siegel RL, Miller KD, Wagle NS, Jemal A. Cancer statistics, 2023. *CA: A Cancer Journal for Clinicians* **2023**. 73, 17–48.
- 6.- American Cancer Society. Cancer Facts & Figures 2022. **2022**.
- 7.- *EU Country Cancer Profile: Austria 2023*. OECD. **2023**.
- 8.- *EU Country Cancer Profile: Belgium 2023*. OECD. **2023**.
- 9.- *EU Country Cancer Profile: France 2023*. OECD. **2023**.
- 10.- *EU Country Cancer Profile: Greece 2023*. OECD. **2023**.
- 11.- *EU Country Cancer Profile: Hungary 2023*. OECD. **2023**.
- 12.- *EU Country Cancer Profile: Italy 2023*. OECD. **2023**.
- 13.- *EU Country Cancer Profile: Netherlands 2023*. OECD. **2023**.
- 14.- *EU Country Cancer Profile: Spain 2023*. OECD. **2023**.
- 15.- Wood LD, Canto MI, Jaffee EM, Simeone DM. Pancreatic Cancer: Pathogenesis, Screening, Diagnosis, and Treatment. *Gastroenterology* **2022**. 163, 386-402.e1.
- 16.- Kleeff J, Korc M, Apte M, La Vecchia C, Johnson CD, Biankin A V., et al. Pancreatic cancer. *Nature Reviews Disease Primers* **2016**. 2.
- 17.- O’Kane GM, Ladak F, Gallinger S. Advances in the management of pancreatic ductal adenocarcinoma. *CMAJ* **2021**. 193, E844–E851.
- 18.- Tempero M, Oh DY, Tabernero J, Reni M, Van Cutsem E, Hendifar A, et al. Ibrutinib in combination with nab-paclitaxel and gemcitabine for first-line treatment of patients with metastatic pancreatic adenocarcinoma: phase III RESOLVE study. *Annals of Oncology* **2021**. 32, 600–608.
- 19.- Hewitt DB, Nissen N, Hatoum H, Musher B, Seng J, Coveler AL, et al. A Phase 3 Randomized Clinical Trial of Chemotherapy with or without Algenpantucel-L (HyperAcute-Pancreas) Immunotherapy in Subjects With Borderline Resectable or Locally Advanced Unresectable Pancreatic Cancer. *Annals of Surgery* **2022**. 275, 45–53.
- 20.- Hecht JR, Lonardi S, Bendell J, Sim ; Hao-Wen, Macarulla T, Charles ;, et al. Randomized Phase III Study of FOLFOX Alone or With Pegilodocakine as Second-Line Therapy in Patients With Metastatic Pancreatic Cancer That Progressed After Gemcitabine (SEQUOIA). *J Clin Oncol* **2021**. 39, 1108–1118.

- 21.- Ho WJ, Jaffee EM, Zheng L. The tumour microenvironment in pancreatic cancer — clinical challenges and opportunities. *Nature Reviews Clinical Oncology* **2020**. *17*, 527–540.
- 22.- Truong LH, Pauklin S. Pancreatic cancer microenvironment and cellular composition: Current understandings and therapeutic approaches. *Cancers* **2021**. *13*, 5028.
- 23.- Maris JM. Recent advances in neuroblastoma. *N Engl J Med*. **2010**. *362*, 2202–2211.
- 24.- Zeineldin M, Patel AG, Dyer MA. Neuroblastoma: When differentiation goes awry. *Neuron* **2022**. *110*, 2916–2928.
- 25.- Cañete A, Peris-Bonet R, Capocaccia R, Pardo-Romaguera E, Segura V, Muñoz-López A, et al. Neuroblastoma in Spain: Linking the national clinical database and epidemiological registries – A study by the Joint Action on Rare Cancers. *Cancer Epidemiology* **2022**. *78*, 102145.
- 26.- Cheung NK V., Dyer MA. Neuroblastoma: Developmental biology, cancer genomics and immunotherapy. *Nature Reviews Cancer* **2013**. *13*, 397–411.
- 27.- Matthay KK, Maris JM, Schleiermacher G, Nakagawara A, Mackall CL, Diller L, et al. Neuroblastoma. *Nature Reviews Disease Primers* **2016**. *2*, 16078.
- 28.- Baker DL, Schmidt ML, Cohn SL, Maris JM, London WB, Buxton A, et al. Outcome after Reduced Chemotherapy for Intermediate-Risk Neuroblastoma. *New England Journal of Medicine* **2010**. *363*, 1313–1323.
- 29.- Park JR, Bagatell R, London WB, Maris JM, Cohn SL, Mattay KM, et al. Children’s Oncology Group’s 2013 blueprint for research: Neuroblastoma. *Pediatric Blood and Cancer* **2013**. *60*, 985–993.
- 30.- Davidoff AM. Neuroblastoma. *Seminars in Pediatric Surgery* **2012**. *21*, 2–14.
- 31.- Valter K, Zhivotovsky B, Gogvadze V. Cell death-based treatment of neuroblastoma. *Cell Death and Disease* **2018**. *9*, 113.
- 32.- Smith V, Foster J. High-risk neuroblastoma treatment review. *Children* **2018**. *5*, 114.
- 33.- Valind A, Verhoeven BM, Enoksson J, Karlsson J, Christensson G, Mañas A, et al. Macrophage infiltration promotes regrowth in MYCN-amplified neuroblastoma after chemotherapy. *Oncolmmunology* **2023**. *12*, 2184130.
- 34.- Fosgerau K, Hoffmann T. Peptide therapeutics: current status and future directions. *Drug Discovery Today* **2015**. *20*, 122–28.
- 35.- Bin T, Junfeng L, Peigen R. *Peptide drugs application in metabolic diseases and discovery strategies*.
- 36.- Mun SJ, Cho E, Kim JS, Yang CS. Pathogen-derived peptides in drug targeting and its therapeutic approach. *Journal of Controlled Release* **2022**. *350*, 716–733.
- 37.- Liao Y, Wang M, Jiang X. Sulfur-containing peptides: Synthesis and application in the discovery of potential drug candidates. *Current Opinion in Chemical Biology* **2023**. *75*, 102336.
- 38.- Montalbetti CAGN, Falque V. Amide bond formation and peptide coupling. *Tetrahedron* **2005**. *61*, 10827–10852.

- 39.- Dalabehera NR, Meher S, Bhusana Palai B, Sharma NK. Instability of Amide Bond with Trifluoroacetic Acid (20%): Synthesis, Conformational Analysis, and Mechanistic Insights into Cleavable Amide Bond Comprising β -Troponylhydrazino Acid. *ACS Omega* **2020**. *5*, 26141–26152.
- 40.- Manne SR, Sharma A, Sazonovas A, El-Faham A, de la Torre BG, Albericio F. Understanding OxymaPure as a Peptide Coupling Additive: A Guide to New Oxyma Derivatives. *ACS Omega* **2022**. *7*, 6007–6023.
- 41.- Lau JL, Dunn MK. Therapeutic peptides: Historical perspectives, current development trends, and future directions. *Bioorganic and Medicinal Chemistry* **2018**. *26*, 2700–2707.
- 42.- Lovejoy DA, Hogg DW, Dodsworth TL, Jurado FR, Read CC, D'Aquila AL, et al. Synthetic Peptides as Therapeutic Agents: Lessons Learned From Evolutionary Ancient Peptides and Their Transit Across Blood-Brain Barriers. *Frontiers in Endocrinology* **2019**. *10*.
- 43.- de la Torre BG, Albericio F. The Pharmaceutical Industry in 2023: An Analysis of FDA Drug Approvals from the Perspective of Molecules. *Molecules* **2024**. *29*.
- 44.- Liu H, Shen W, Liu W, Yang Z, Yin D, Xiao C. From oncolytic peptides to oncolytic polymers: A new paradigm for oncotherapy. *Bioactive Materials* **2024**. *31*, 206–230.
- 45.- Barman P, Joshi S, Sharma S, Preet S, Sharma S, Saini A. Strategic Approaches to Improve Peptide Drugs as Next Generation Therapeutics. *International Journal of Peptide Research and Therapeutics* **2023**. *29*.
- 46.- Bendicho-Lavilla C, Seoane-Viaño I, Otero-Espinar FJ, Luzardo-Álvarez A. Fighting type 2 diabetes: Formulation strategies for peptide-based therapeutics. *Acta Pharmaceutica Sinica B* **2022**. *12*, 621–636.
- 47.- Recio C, Maione F, Iqbal AJ, Mascolo N, De Feo V. The potential therapeutic application of peptides and peptidomimetics in cardiovascular disease. *Frontiers in Pharmacology* **2017**. *7*.
- 48.- Sadeghian I, Heidari R, Sadeghian S, Raei MJ, Negahdaripour M. Potential of cell-penetrating peptides (CPPs) in delivery of antiviral therapeutics and vaccines. *European Journal of Pharmaceutical Sciences* **2022**. *169*.
- 49.- Giordano C, Marchiò M, Timofeeva E, Biagini G. Neuroactive peptides as putative mediators of antiepileptic ketogenic diets. *Frontiers in Neurology* **2014**. *5 APR*.
- 50.- Mukherjee AG, Wanjari UR, Gopalakrishnan AV, Bradu P, Biswas A, Ganesan R, et al. Evolving strategies and application of proteins and peptide therapeutics in cancer treatment. *Biomedicine and Pharmacotherapy* **2023**. *163*.
- 51.- Chinnadurai RK, Khan N, Meghwanshi GK, Ponne S, Althobiti M, Kumar R. Current research status of anti-cancer peptides: Mechanism of action, production, and clinical applications. *Biomedicine and Pharmacotherapy* **2023**. *164*.
- 52.- Shinde SD, Atpadkar P, Swain P, Apparao CV, Sandhya V, Sahu B. Peptide and protein in therapeutics. In: *Peptide and Protein Drug Delivery Using Polysaccharides* Elsevier, 2024; pp. 1–24.
- 53.- Zhao X, Zhang X, Liu D. Collagen peptides and the related synthetic peptides: A review on improving skin health. *Journal of Functional Foods* **2021**. *86*.

- 54.- Koerselman M, Morshuis LCM, Karperien M. The use of peptides, aptamers, and variable domains of heavy chain only antibodies in tissue engineering and regenerative medicine. *Acta Biomaterialia* **2023**.
- 55.- Shwaiki LN, Lynch KM, Arendt EK. Future of antimicrobial peptides derived from plants in food application – A focus on synthetic peptides. *Trends in Food Science and Technology* **2021**. 112, 312–324.
- 56.- Ho TNT, Turner A, Pham SH, Nguyen HT, Nguyen LTT, Nguyen LT, et al. Cysteine-rich peptides: From bioactivity to bioinsecticide applications. *Toxicon* **2023**. 230.
- 57.- Chen H, Cai X, Cheng J, Wang S. Self-assembling peptides: Molecule-nanostructure-function and application on food industry. *Trends in Food Science and Technology* **2022**. 120, 212–222.
- 58.- Silva JLL, de Miranda MRA, Souza PFN. The multiverse of action: how mechanisms of synthetic antifungal peptides could be employed in the food industry. *Current Opinion in Food Science* **2023**, 101089.
- 59.- Padhi A, Sengupta M, Sengupta S, Roehm KH, Sonawane A. Antimicrobial peptides and proteins in mycobacterial therapy: Current status and future prospects. *Tuberculosis* **2014**. 94, 363–373.
- 60.- Abbas M, Ovais M, Atiq A, Ansari TM, Xing R, Spruijt E, et al. Tailoring supramolecular short peptide nanomaterials for antibacterial applications. *Coordination Chemistry Reviews* **2022**. 460.
- 61.- Sharma S, Barman P, Joshi S, Preet S, Saini A. Multidrug resistance crisis during COVID-19 pandemic: Role of anti-microbial peptides as next-generation therapeutics. *Colloids and Surfaces B: Biointerfaces* **2022**. 211.
- 62.- Luong HX, Thanh TT, Tran TH. Antimicrobial peptides – Advances in development of therapeutic applications. *Life Sciences* **2020**. 260.
- 63.- Xu J, Wang F, Ye L, Wang R, Zhao L, Yang X, et al. Penetrating peptides: Applications in drug delivery. *Journal of Drug Delivery Science and Technology* **2023**. 84.
- 64.- Yang S, Wang M, Wang T, Sun M, Huang H, Shi X, et al. Self-assembled short peptides: Recent advances and strategies for potential pharmaceutical applications. *Materials Today Bio* **2023**. 20.
- 65.- Zhu D, Kong H, Sun Z, Xu Y, Han P, Xi Y, et al. Recent advance in tailoring the structure and functions of self-assembled peptide nanomaterials for biomedical applications. *Coordination Chemistry Reviews* **2023**. 494.
- 66.- Jia W, Peng J, Zhang Y, Zhu J, Qiang X, Zhang R, et al. Exploring novel ANGICon-EIPs through ameliorated peptidomics techniques: Can deep learning strategies as a core breakthrough in peptide structure and function prediction? *Food Research International* **2023**. 174.
- 67.- Aróstica M, Rojas R, Aguilar LF, Carvajal-Rondanelli P, Albericio F, Guzmán F, et al. Arginine Homopeptide of 11 Residues as a Model of Cell-Penetrating Peptides in the Interaction with Bacterial Membranes. *Membranes* **2022**. 12.
- 68.- Kumai T, Fan A, Harabuchi Y, Celis E. Cancer immunotherapy: moving forward with peptide T cell vaccines. *Current Opinion in Immunology* **2017**. 47, 57–63.

- 69.- Calvo Tardón M, Allard M, Dutoit V, Dietrich PY, Walker PR. Peptides as cancer vaccines. *Current Opinion in Pharmacology* **2019**. 47, 20–26.
- 70.- Zahedipour F, Jamialahmadi K, Zamani P, Reza Jaafari M. Improving the efficacy of peptide vaccines in cancer immunotherapy. *International Immunopharmacology* **2023**. 123.
- 71.- Xu F, Yuan Y, Wang Y, Yin Q. Emerging peptide-based nanovaccines: From design synthesis to defense against cancer and infection. *Biomedicine and Pharmacotherapy* **2023**. 158.
- 72.- Lim HX, Lim J, Jazayeri SD, Poppema S, Poh CL. Development of multi-epitope peptide-based vaccines against SARS-CoV-2. *Biomedical Journal* **2021**. 44, 18–30.
- 73.- Mustafa AS. Recombinant and synthetic peptides to identify Mycobacterium tuberculosis antigens and epitopes of diagnostic and vaccine relevance. In: *Tuberculosis* Vol 85., 2005; pp. 367–376.
- 74.- Xu S, Tan P, Tang Q, Wang T, Ding Y, Fu H, et al. Enhancing the stability of antimicrobial peptides: From design strategies to biomedical applications. *Chemical Engineering Journal* **2023**, 145923.
- 75.- Sharma K, Sharma KK, Sharma A, Jain R. Peptide-based drug discovery: Current status and recent advances. *Drug Discovery Today* **2023**. 28.
- 76.- Gattringer J, Gruber CW, Hellinger R. Peptide modulators of cell migration: Overview, applications and future development. *Drug Discovery Today* **2023**. 28, 103554.
- 77.- Brooks NA, Pouniotis DS, Tang CK, Apostolopoulos V, Pietersz GA. Cell-penetrating peptides: Application in vaccine delivery. *Biochimica et Biophysica Acta - Reviews on Cancer* **2010**. 1805, 25–34.
- 78.- Robles-Oteiza C, Wu CJ. Editorial overview: Vaccines: Reinvigorating therapeutic cancer vaccines. *Current Opinion in Immunology* **2022**. 76.
- 79.- Puleo J, Polyak K. A Darwinian perspective on tumor immune evasion. *Biochimica et Biophysica Acta - Reviews on Cancer* **2022**. 1877.
- 80.- Sari G, Rock KL. Tumor immune evasion through loss of MHC class-I antigen presentation. *Current Opinion in Immunology* **2023**. 83.
- 81.- Tsai CH, Chuang YM, Li X, Yu YR, Tzeng SF, Teoh ST, et al. Immunoediting instructs tumor metabolic reprogramming to support immune evasion. *Cell Metabolism* **2023**. 35, 118-133.e7.
- 82.- Waldman AD, Fritz JM, Lenardo MJ. A guide to cancer immunotherapy: from T cell basic science to clinical practice. *Nature Reviews Immunology* **2020**. 20, 651–668.
- 83.- Sarantis P, Koustas E, Papadimitropoulou A, Papavassiliou AG, Karamouzis M V. Pancreatic ductal adenocarcinoma: Treatment hurdles, tumor microenvironment and immunotherapy. *World Journal of Gastrointestinal Oncology* **2020**. 12, 173–181.
- 84.- Foley K, Kim V, Jaffee E, Zheng L. Current progress in immunotherapy for pancreatic cancer. *Cancer Letters* **2016**. 381, 244–251.
- 85.- Schizas D, Charalampakis N, Kole C, Economopoulou P, Koustas E, Gkotsis E, et al. Immunotherapy for pancreatic cancer: A 2020 update. *Cancer Treatment Reviews* **2020**. 86.

- 86.- Saxena M, van der Burg SH, Melief CJM, Bhardwaj N. Therapeutic cancer vaccines. *Nature Reviews Cancer* **2021**. *21*, 360–378.
- 87.- Martins F, Sofiya L, Sykiotis GP, Lamine F, Maillard M, Fraga M, et al. Adverse effects of immune-checkpoint inhibitors: epidemiology, management and surveillance. *Nature Reviews Clinical Oncology* **2019**. *16*, 563–580.
- 88.- Jo SJ, Chae SU, Lee C Bin, Bae SK. Clinical Pharmacokinetics of Approved RNA Therapeutics. *International Journal of Molecular Sciences* **2023**. *24*.
- 89.- Buonaguro L, Tagliamonte M. Selecting target antigens for cancer vaccine development. *Vaccines* **2020**. *8*, 1–14.
- 90.- Xie N, Shen G, Gao W, Huang Z, Huang C, Fu L. Neoantigens: promising targets for cancer therapy. *Signal Transduction and Targeted Therapy* **2023**. *8*.
- 91.- Blass E, Ott PA. Advances in the development of personalized neoantigen-based therapeutic cancer vaccines. *Nature Reviews Clinical Oncology* **2021**. *18*, 215–229.
- 92.- Arens R, van Hall T, van der Burg SH, Ossendorp F, Melief CJM. Prospects of combinatorial synthetic peptide vaccine-based immunotherapy against cancer. *Seminars in Immunology* **2013**. *25*, 182–190.
- 93.- Kowalczyk W, Monsó M, de la Torre BG, Andreu D. Synthesis of multiple antigenic peptides (MAPs)-strategies and limitations. *Journal of Peptide Science* **2011**. *17*, 247–251.
- 94.- Joshi VG, Dighe VD, Thakuria D, Malik YS, Kumar S. Multiple antigenic peptide (MAP): A synthetic peptide dendrimer for diagnostic, antiviral and vaccine strategies for emerging and re-emerging viral diseases. *Indian Journal of Virology* **2013**. *24*, 312–320.
- 95.- Shreewastav RK, Ali R, Uppada JB, Rao DN. Cell-mediated immune response to epitopic MAP (multiple antigen peptide) construct of LcrV antigen of *Yersinia pestis* in murine model. *Cellular Immunology* **2012**. *278*, 55–62.
- 96.- Chowdhury S, Toth I, Stephenson RJ. Dendrimers in vaccine delivery: Recent progress and advances. *Biomaterials* **2022**. *280*.
- 97.- Xu DH, Zhou CH, Xia YP, Qiu ZY, Wu YZ, Jia ZC, et al. Cytotoxic T lymphocyte response induced by an improved synthetic lipopeptide vaccine against cervical cancer. *Acta Pharmacologica Sinica* **2007**. *28*, 695–702.
- 98.- Thakur A, Sharma A, Alajangi HK, Jaiswal PK, Lim Y beom, Singh G, et al. In pursuit of next-generation therapeutics: Antimicrobial peptides against superbugs, their sources, mechanism of action, nanotechnology-based delivery, and clinical applications. *International Journal of Biological Macromolecules* **2022**. *218*, 135–156.
- 99.- Ansari A, Hussain A, Wadekar R, Altamimi MA, Malik A, Mujtaba MA, et al. Nanovesicles based drug targeting to control tumor growth and metastasis. *Advances in Cancer Biology - Metastasis* **2023**. *7*, 100083.
- 100.- Mirakabad FST, Nejati-Koshki K, Akbarzadeh A, Yamchi MR, Milani M, Zarghami N, et al. PLGA-based nanoparticles as cancer drug delivery systems. *Asian Pacific Journal of Cancer Prevention* **2014**. *15*, 517–535.

- 101.- Mahmudi H, Adili-Aghdam MA, Shahpouri M, Jaymand M, Amoozgar Z, Jahanban-Esfahlan R. Tumor microenvironment penetrating chitosan nanoparticles for elimination of cancer relapse and minimal residual disease. *Frontiers in Oncology* **2022**. 12.
- 102.- Vargas Nadal G. Novel Quatsome nanovesicles, prepared using compressed CO₂, for the development of advanced nanomedicines. **2020**.
- 103.- Ferrer-Tasies L, Moreno-Calvo E, Cano-Sarabia M, Aguilera-Arzo M, Angelova A, Lesieur S, et al. Quatsomes: Vesicles Formed by Self-Assembly of Sterols and Quaternary Ammonium Surfactants. *Langmuir* **2013**. 29, 6519–6528.
- 104.- Palomo JM. Solid-phase peptide synthesis: An overview focused on the preparation of biologically relevant peptides. *RSC Advances* **2014**. 4, 32658–32672.
- 105.- Weidmann J, Dimitrijević E, Hoheisel JD, Dawson PE. Boc-SPPS: Compatible Linker for the Synthesis of Peptide o-Aminoanilides. *Organic Letters* **2016**. 18, 164–167.
- 106.- Stewart JM. Cleavage methods following Boc-based solid-phase peptide synthesis. In: *Methods in Enzymology* Vol 289. Academic Press, 1997; pp. 29–44.
- 107.- Carpino LA, Han GY. 9-Fluorenylmethoxycarbonyl amino-protecting group. *The Journal of Organic Chemistry* **1972**. 37, 3404–3409.
- 108.- Fields GB. Methods for Removing the Finoc Group. In: *Peptide Synthesis Protocols* Humana Press, 2003; pp. 17–28.
- 109.- Zinieris N, Leondiadis L, Ferderigos N. N α -Fmoc removal from resin-bound amino acids by 5% piperidine solution. *Journal of Combinatorial Chemistry* **2005**. 7, 4–6.
- 110.- Luna OF, Gomez J, Cárdenas C, Albericio F, Marshall SH, Guzmán F. Deprotection reagents in Fmoc solid phase peptide synthesis: Moving away from piperidine? *Molecules* **2016**. 21.
- 111.- Guy CA, Fields GB. *Trifluoroacetic Acid Cleavage and Deprotection of Resin-Bound Peptides Following Synthesis by Fmoc Chemistry*. **1997**.
- 112.- López SE, Salazar J. Trifluoroacetic acid: Uses and recent applications in organic synthesis. *Journal of Fluorine Chemistry* **2013**. 156, 73–100.
- 113.- El-Faham A, Albericio F. Peptide coupling reagents, more than a letter soup. *Chemical Reviews* **2011**. 111, 6557–6602.
- 114.- Rich DH, Singh J. Chapter 5 - The Carbodiimide Method. In: *Major Methods of Peptide Bond Formation*. Editors: Gross E, Meienhofer J: Vol 1. Academic Press, 1979; pp. 241–261.
- 115.- König W, Geiger R. Eine neue Methode zur Synthese von Peptiden: Aktivierung der Carboxylgruppe mit Dicyclohexylcarbodiimid unter Zusatz von 1-Hydroxy-benzotriazolen. *Chemische Berichte* **1970**. 103, 788–798.
- 116.- Subirós-Funosas R, Prohens R, Barbas R, El-Faham A, Albericio F. Oxyma: An Efficient Additive for Peptide Synthesis to Replace the Benzotriazole-Based HOBt and HOAt with a Lower Risk of Explosion. *Chemistry – A European Journal* **2009**. 15, 9394–9403.
- 117.- Wehrstedt KD, Wandrey PA, Heitkamp D. Explosive properties of 1-hydroxybenzotriazoles. *Journal of Hazardous Materials* **2005**. 126, 1–7.

- 118.- Albericio F. Developments in peptide and amide synthesis. *Current Opinion in Chemical Biology* **2004**. *8*, 211–221.
- 119.- Lima PG, Oliveira JTA, Amaral JL, Freitas CDT, Souza PFN. Synthetic antimicrobial peptides: Characteristics, design, and potential as alternative molecules to overcome microbial resistance. *Life Sciences* **2021**. *278*.
- 120.- McFarland AD, Buser JY, Embry MC, Held CB, Kolis SP. Generation of Hydrogen Cyanide from the reaction from DIC and Oxyma. *Organic Process Research & Development* **2019**. *23*, 2099–2105.
- 121.- Erny M, Lundqvist M, Rasmussen JH, Ludemann-Hombourger O, Bihel F, Pawlas J. Minimizing HCN in DIC/Oxyma-Mediated Amide Bond-Forming Reactions. *Organic Process Research & Development* **2020**. *24*, 1341–1349.
- 122.- National Research Council (U.S.). Subcommittee on Acute Exposure Guideline Levels. *Acute exposure guideline levels for selected airborne chemicals. Volume 2*. National Academy Press. **2002**.
- 123.- Sarantis P, Koustas E, Papadimitropoulou A, Papavassiliou AG, Karamouzis M V. Pancreatic ductal adenocarcinoma: Treatment hurdles, tumor microenvironment and immunotherapy. *World Journal of Gastrointestinal Oncology* **2020**. *12*, 173–181.
- 124.- Castro F, Cardoso AP, Gonçalves RM, Serre K, Oliveira MJ. Interferon-gamma at the crossroads of tumor immune surveillance or evasion. *Frontiers in Immunology* **2018**. *9*.
- 125.- Thundimadathil J. Cancer Treatment Using Peptides: Current Therapies and Future Prospects. *Journal of Amino Acids* **2012**. *2012*, 1–13.
- 126.- Principe DR, Underwood PW, Korc M, Trevino JG, Munshi HG, Rana A. The Current Treatment Paradigm for Pancreatic Ductal Adenocarcinoma and Barriers to Therapeutic Efficacy. *Frontiers in Oncology* **2021**. *11*.
- 127.- Akce M, Zaidi MY, Waller EK, El-Rayes BF, Lesinski GB. The potential of CAR T cell therapy in pancreatic cancer. *Frontiers in Immunology* **2018**. *9*.
- 128.- Nguyen MN, Than VT. Chapter Eleven - RNA therapeutics in cancer treatment. In: *Progress in Molecular Biology and Translational Science*. Editors: Chu D-T, Than VT:Vol 203. Academic Press, 2024; pp. 197–223.
- 129.- Stephens AJ, Burgess-Brown NA, Jiang S. Beyond Just Peptide Antigens: The Complex World of Peptide-Based Cancer Vaccines. *Frontiers in Immunology* **2021**. *12*.
- 130.- Tang D, Kang R. Glimmers of hope for targeting oncogenic KRAS-G12D. *Cancer Gene Therapy* **2023**. *30*, 391–393.
- 131.- Pereira F, Ferreira A, Reis CA, Sousa MJ, Oliveira MJ, Preto A. KRAS as a Modulator of the Inflammatory Tumor Microenvironment: Therapeutic Implications. *Cells* **2022**. *11*.
- 132.- Bannoura SF, Khan HY, Azmi AS. KRAS G12D targeted therapies for pancreatic cancer: Has the fortress been conquered? *Frontiers in Oncology* **2022**. *12*.
- 133.- Beatty GL, O'Hara MH, Lacey SF, Torigian DA, Nazimuddin F, Chen F, et al. Activity of Mesothelin-Specific Chimeric Antigen Receptor T Cells Against Pancreatic Carcinoma Metastases in a Phase 1 Trial. *Gastroenterology* **2018**. *155*, 29–32.

- 134.- Hassan R, Thomas A, Alewine C, Le DT, Jaffee EM, Pastan I. Mesothelin immunotherapy for cancer: Ready for prime time? *Journal of Clinical Oncology* **2016**. *34*, 4171–4179.
- 135.- Faust JR, Hamill D, Kolb EA, Gopalakrishnapillai A, Barwe SP. Mesothelin: An Immunotherapeutic Target beyond Solid Tumors. *Cancers* **2022**. *14*.
- 136.- Watanabe K, Luo Y, Da T, Guedan S, Ruella M, Scholler J, et al. Pancreatic cancer therapy with combined mesothelin-redirected chimeric antigen receptor T cells and cytokine-armed oncolytic adenoviruses. *JCI insight* **2018**. *3*.
- 137.- Morello A, Sadelain M, Adusumilli PS. Mesothelin-targeted CARs: Driving T cells to solid Tumors. *Cancer Discovery* **2016**. *6*, 133–146.
- 138.- Miyazawa M, Katsuda M, Maguchi H, Katanuma A, Ishii H, Ozaka M, et al. Phase II clinical trial using novel peptide cocktail vaccine as a postoperative adjuvant treatment for surgically resected pancreatic cancer patients. *International Journal of Cancer* **2017**. *140*, 973–982.
- 139.- Tandel N, Patel D, Thakkar M, Shah J, Tyagi RK, Dalai SK. Poly(I:C) and R848 ligands show better adjuvanticity to induce B and T cell responses against the antigen(s). *Heliyon* **2024**. *10*.
- 140.- Schultz HS, Ostergaard S, Sidney J, Lamberth K, Sette A. The effect of acylation with fatty acids and other modifications on HLA class II: Peptide binding and T cell stimulation for three model peptides. *PLoS ONE* **2018**. *13*.
- 141.- Alharbi N, Skwarczynski M, Toth I. The influence of component structural arrangement on peptide vaccine immunogenicity. *Biotechnology Advances* **2022**. *60*.
- 142.- Ikeda Y, Nagasaki Y. PEGylation technology in nanomedicine. *Advances in Polymer Science* **2012**. *247*.
- 143.- Al-Naseri A, Al-Absi S, Mahana N, Tallima H, El Ridi R. Protective immune potential of multiple antigenic peptide (MAP) constructs comprising peptides that are shared by several cysteine peptidases against *Schistosoma mansoni* infection in mice. *Molecular and Biochemical Parasitology* **2022**. *248*, 111459.
- 144.- Cruz LJ, Iglesias E, Aguilar JC, González LJ, Reyes O, Albericio F, et al. A Comparative Study of Different Presentation Strategies for an HIV Peptide Immunogen. *Bioconjugate Chemistry* **2004**. *15*, 112–120.
- 145.- Esparza I, Kissel T. Parameters affecting the immunogenicity of microencapsulated tetanus toxoid. *Vaccine* **1992**. *10*, 714–720.
- 146.- Men Y, Thomasin C, Merkle HP, Gander B, Corradin G. A single administration of tetanus toxoid in biodegradable microspheres elicits T cell and antibody responses similar or superior to those obtained with aluminum hydroxide. *Vaccine* **1995**. *13*, 683–689.
- 147.- Arens R, van Hall T, van der Burg SH, Ossendorp F, Melief CJM. Prospects of combinatorial synthetic peptide vaccine-based immunotherapy against cancer. *Seminars in Immunology* **2013**. *25*, 182–190.
- 148.- Calvo Tardón M, Allard M, Dutoit V, Dietrich PY, Walker PR. Peptides as cancer vaccines. *Current Opinion in Pharmacology* **2019**. *47*, 20–26.

- 149.- Ferrazzano L, Corbisiero D, Tolomelli A, Cabri W. From green innovations in oligopeptide to oligonucleotide sustainable synthesis: differences and synergies in TIDES chemistry. *Green Chemistry* **2023**. *25*, 1217–1236.
- 150.- Mueller LK, Baumruck AC, Zhdanova H, Tietze AA. Challenges and Perspectives in Chemical Synthesis of Highly Hydrophobic Peptides. *Frontiers in Bioengineering and Biotechnology* **2020**. *8*.
- 151.- Krchňák V, Flegelová Z, Vágner J. Aggregation of resin-bound peptides during solid-phase peptide synthesis Prediction of difficult sequences. *International Journal of Peptide & Protein Research* **1993**. *42*, 450–454.
- 152.- Rezvantalab S, Drude NI, Moraveji MK, Güvener N, Koons EK, Shi Y, et al. PLGA-based nanoparticles in cancer treatment. *Frontiers in Pharmacology* **2018**. *9*.
- 153.- Chen Y, Ayaru L, Mathew S, Morris E, Pereira SP, Behboudi S. Expansion of anti-mesothelin specific CD4+and CD8+ T cell responses in patients with pancreatic carcinoma. *PLoS ONE* **2014**. *9*.
- 154.- Laheru D, Lutz E, Burke J, Biedrzycki B, Solt S, Onners B, et al. Allogeneic granulocyte macrophage colony-stimulating factor-secreting tumor immunotherapy alone or in sequence with cyclophosphamide for metastatic pancreatic cancer: A pilot study of safety, feasibility, and immune activation. *Clinical Cancer Research* **2008**. *14*, 1455–1463.
- 155.- Rammensee H-G, Bachmann J, Emmerich NPN, Bachor OA, Stevanović S. SYFPEITHI: database for MHC ligands and peptide motifs. *Immunogenetics* **1999**. *50*, 213–219.
- 156.- Parker KC, Bednarek MA, Coligan JE. Scheme for ranking potential HLA-A2 binding peptides based on independent binding of individual peptide side-chains. *The Journal of Immunology* **1994**. *152*, 163–175.
- 157.- Chen J, Zhang B, Xie C, Lu Y, Wu W. Synthesis of a highly hydrophobic cyclic decapeptide by solid-phase synthesis of linear peptide and cyclization in solution. *Chinese Chemical Letters* **2010**. *21*, 391–394.
- 158.- Subirós-Funosas R, El-Faham A, Albericio F. Aspartimide formation in peptide chemistry: Occurrence, prevention strategies and the role of N-hydroxylamines. *Tetrahedron* **2011**. *67*, 8595–8606.
- 159.- Samson D, Rentsch D, Minuth M, Meier T, Loidl G. The aspartimide problem persists: Fluorenylmethoxycarbonyl-solid-phase peptide synthesis (Fmoc-SPPS) chain termination due to formation of N-terminal piperazine-2,5-diones. *Journal of Peptide Science* **2019**. *25*.
- 160.- Abdel-Aal ABM, Papageorgiou G, Raz R, Quibell M, Burlina F, Offer J. A backbone amide protecting group for overcoming difficult sequences and suppressing aspartimide formation. *Journal of Peptide Science* **2016**. *22*, 360–367.
- 161.- Conchillo-Solé O, de Groot NS, Avilés FX, Vendrell J, Daura X, Ventura S. AGGRESKAN: A server for the prediction and evaluation of “hot spots” of aggregation in polypeptides. *BMC Bioinformatics* **2007**. *8*.
- 162.- Wang D, Farhana A. RNA Structure. In: *Biochemistry* StatPearls Publishing, 2023.
- 163.- O’Brien J, Hayder H, Zayed Y, Peng C. Overview of microRNA biogenesis, mechanisms of actions, and circulation. *Frontiers in Endocrinology* **2018**. *9*.

- 164.- Raina M, Ibba M. TRNAs as regulators of biological processes. *Frontiers in Genetics* **2014**. 5.
- 165.- Valadkhan S, Gunawardane LS. Role of small nuclear RNAs in eukaryotic gene expression. *Essays in Biochemistry* **2013**. 54, 79–90.
- 166.- Charbe NB, Amnerkar ND, Ramesh B, Tambuwala MM, Bakshi HA, Aljabali AAA, et al. Small interfering RNA for cancer treatment: overcoming hurdles in delivery. *Acta Pharmaceutica Sinica B* **2020**. 10, 2075–2109.
- 167.- Van Lint S, Heirman C, Thielemans K, Breckpot K. From a chemical blueprint for protein production to an off-the-shelf therapeutic. *Human Vaccines and Immunotherapeutics* **2013**. 9, 265–274.
- 168.- Gavrillov K, Saltzman WM. *Therapeutic siRNA: Principles, challenges, and strategies*. **2012**.
- 169.- Villaverde G, Alfranca A, González-Murillo Á, Melen GJ, Castillo RR, Ramírez M, et al. Molecular scaffolds as double-targeting agents for the diagnosis and treatment of neuroblastoma. *Angew. Chem. Int. Ed.* **2019**. 58, 3067–3072.
- 170.- Loi M, Di Paolo D, Soster M, Brignole C, Bartolini A, Emionite L, et al. Novel phage display-derived neuroblastoma-targeting peptides potentiate the effect of drug nanocarriers in preclinical settings. *Journal of Controlled Release* **2013**. 170, 233–241.
- 171.- Müller J, Reichel R, Vogt S, Müller SP, Sauerwein W, Brandau W, et al. Identification and tumour-binding properties of a peptide with high affinity to the Disialoganglioside GD2. *PLoS ONE* **2016**. 11.
- 172.- Ranjan S, Sood R, Dudas J, Glueckert R, Schrott-Fischer A, Roy S, et al. Peptide-mediated targeting of liposomes to TrkB receptor-expressing cells. *International Journal of Nanomedicine* **2012**. 7, 3475–3485.
- 173.- Zhongcai M, Xiaolan W, Mingmei C, Wei P, Fenlu Z, Jingshan C, et al. Selection of trkB-binding peptides from a phage-displayed random peptide library. *Science in China (Series C)* **2003**. 46, 77–86.
- 174.- Haddad Y, Charousova M, Zivotska H, Splichal Z, Merlos Rodrigo MA, Michalkova H, et al. Norepinephrine transporter-derived homing peptides enable rapid endocytosis of drug delivery nanovehicles into neuroblastoma cells. *Journal of Nanobiotechnology* **2020**. 18.
- 175.- Martínez-Jothar L, Doukeridou S, Schiffelers RM, Sastre Torano J, Oliveira S, van Nostrum CF, et al. Insights into maleimide-thiol conjugation chemistry: Conditions for efficient surface functionalization of nanoparticles for receptor targeting. *Journal of Controlled Release* **2018**. 282, 101–109.
- 176.- Ravasco JM, Faustino H, Trindade A, Gois PMP. Bioconjugation with Maleimides: A Useful Tool for Chemical Biology. *Chemistry - A European Journal* **2019**. 25, 43–59.
- 177.- Fontaine SD, Reid R, Robinson L, Ashley GW, Santi D V. Long-term stabilization of maleimide-thiol conjugates. *Bioconjugate Chemistry* **2015**. 26, 145–152.
- 178.- Wang J, Yang S, Zhang K. Multi-arm PEG-maleimide conjugation intermediate characterization and hydrolysis study by a selective HPLC method. *Journal of Pharmaceutical and Biomedical Analysis* **2019**. 164, 452–459.

- 179.- Lahnsteiner M, Kastner A, Mayr J, Roller A, Keppler BK, Kowol CR. Improving the Stability of Maleimide–Thiol Conjugation for Drug Targeting. *Chemistry - A European Journal* **2020**. *26*, 15867–15870.
- 180.- Szijj PA, Bahou C, Chudasama V. Minireview: Addressing the retro-Michael instability of maleimide bioconjugates. *Drug Discovery Today: Technologies* **2018**. *30*, 27–34.
- 181.- Sheehan JC, Hess GP. A new method of forming peptide bonds. *Proc. Soc. Exp. Biol. Med* **1955**. *77*, 1067–1068.
- 182.- Han SY, Kim YA. Recent development of peptide coupling reagents in organic synthesis. *Tetrahedron* **2004**. *60*, 2447–2467.
- 183.- Carpino LA, El-Faham A. *The Diisopropylcarbodiimide/ 1-Hydroxy-7-azabenzotriazole System: Segment Coupling and Stepwise Peptide Assembly**. **1999**.
- 184.- Hogue Angeletti R, Bibbs L, Bonewald LF, Fields GB, Kelly JW, McMurray JS, et al. Analysis of Racemization During “Standard” Solid Phase Peptide Synthesis: A Multicenter Study. *Techniques in Protein Chemistry* **1997**. *8*, 875–890.
- 185.- Kaiser T, Nicholson GJ, Kohlbau HJ, Voelter W. Racemization studies of Fmoc-Cys(Trt)-OH during stepwise Fmoc-Solid phase peptide synthesis. *Tetrahedron Letters* **1996**. *37*, 1187–1190.
- 186.- Han Y, Albericio F, Barany G. Occurrence and Minimization of Cysteine Racemization during Stepwise Solid-Phase Peptide Synthesis^{1,2}. *The Journal of Organic Chemistry* **1997**. *62*, 4307–4312.
- 187.- Cooper CE, Brown GC. The inhibition of mitochondrial cytochrome oxidase by the gases carbon monoxide, nitric oxide, hydrogen cyanide and hydrogen sulfide: Chemical mechanism and physiological significance. *Journal of Bioenergetics and Biomembranes* **2008**. *40*, 533–539.
- 188.- Niether D, Wiegand S. Thermodiffusion and hydrolysis of 1-Ethyl-3-(3-dimethylaminopropyl)carbodiimide (EDC). *European Physical Journal E* **2019**. *42*, 117.
- 189.- Williams A, Ibrahim T. A New Mechanism Involving Cyclic Tautomers for the Reaction with Nucleophiles of the Water-Soluble Peptide Coupling Reagent 1-Ethyl-3-(3-dimethylamino)propyl)carbodiimide (EDC). *J. Am. Chem. Soc* **1981**. *103*, 7090–7095.

Annex

This work has produced three indexed publications in ACS journals, listed below.

Publication 1:

The work performed in this publication involved the synthesis and purification of two model peptides using five different carbodiimides and characterize their synthetic performance, the design of the experiments and the writing and editing of the draft.



pubsacs.org/OrgLett

Letter

Amide Formation: Choosing the Safer Carbodiimide in Combination with OxymaPure to Avoid HCN Release

Srinivasa Rao Manne,[▽] Omar Luna,[▽] Gerardo A. Acosta, Miriam Royo, Ayman El-Faham, Gyorgy Orosz, Beatriz G. de la Torre,^{*} and Fernando Albericio^{*}

Cite This: *Org. Lett.* 2021, 23, 6900–6904

Read Online

ACCESS |

Metrics & More

Article Recommendations

Supporting Information

ABSTRACT: It has been reported that DIC can react with OxymaPure to render an *oxadiazole* compound with the concomitant formation of HCN. Here we demonstrate that this reaction is not a feature of all carbodiimides but rather depends on the alkyl structure that flanks the two N atoms of the carbodiimide. Furthermore, we have identified two carbodiimides, TBEC and EDC-HCl, whose reaction with OxymaPure is exempt from HCN formation.

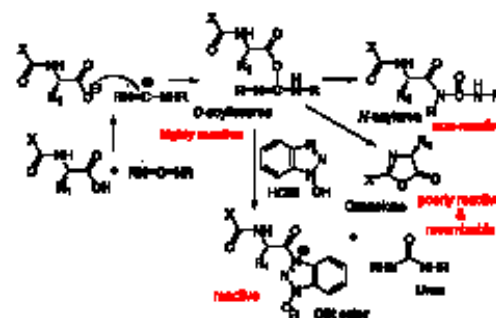
Carbodiimides	Cyclic Side-Product	Amide Bond Formation
TBEC	NO	✓
EDC-HCl	NO	✓
DIC	YES	✓
DCC	YES	✓
UABIC	YES	✓
NMC	NO	✗

The amide bond is the most common bond not only in nature but also in synthetic organic chemistry, as reflected by independent studies carried out by both academia and industry.^{1,2} The ACS Green Chemistry Institute (GCI) Pharmaceutical Roundtable (PR) has even included the amide bond as one of the 10 key green chemistry research areas,³ thus highlighting its relevance. As in the field of protecting groups,^{4,5} research on amide bond formation has been fueled by groups working in the peptide chemistry arena.⁶ In this regard, the seminal work of Sheehan and Hess on the use of dicyclohexylcarbodiimide (DCC) for *in situ* activation of the carboxylic group opened up new avenues for peptide chemistry,⁷ which crystallized a few years later with the advent of solid-phase peptide synthesis (SPPS) methodology proposed by Merrifield.⁸ These discoveries laid the foundation of what is today peptide synthesis.⁹

The reaction of a carboxylic acid with a carbodiimide renders the *O*-acylisourea as the reactive species (Scheme 1). In the early 1970s, König and Geiger at Hoechst proposed adding 1-hydroxybenzotriazole (HOBt) to the carbodiimide-mediated coupling.¹⁰ In that case, the active species was the OBt active ester. Although this ester was initially thought to be more reactive than the *O*-acylisourea, it is less reactive. However, in many cases this loss of reactivity is translated into greater efficacy because the OBt ester is free of rearrangement and formation of the oxazolone, which is a secondary reaction that takes place from the *O*-acylisourea, making the *O*-acylisourea less efficient than the OBt ester.⁶

Thus, the *O*-acylisourea rearrangement is a side reaction that renders the fully inactive *N*-acylurea. This reaction is important in dipolar aprotic solvents, such as *N,N*-dimethylformamide (DMF), which are to date the solvents of choice for the coupling reaction in SPPS.⁵ The highly reactive *O*-acylisourea

Scheme 1. Mechanism by Which Carbodiimides Activate a Protected Amino Acid



can evolve to an oxazolone, which again is less reactive than the parent compound and, more importantly, highly prone to racemization.⁶

Because of the aforementioned considerations, almost all peptide couplings have been done in the presence of HOBt, which is shown in tautomeric forms,^{11,12} or its analogues, either as an additive to the carbodiimides or as part of stand-alone reagents, mainly iminium and phosphonium salts.⁶ With the

Received: July 25, 2021
Published: August 23, 2021



implementation of the 9-fluorenylmethoxycarbonyl (Fmoc) strategy instead of the *tert*-butoxycarbonyl (Boc) approach, DCC was substituted by *N,N'*-diisopropylcarbodiimide (DIC), whose urea is more soluble and therefore easier to wash out after the coupling.

After September 11, 2001, the potentially explosive nature of HOBt and its related triazole/triazine analogues was highlighted.¹³ These compounds were recategorized into a Class 1 explosive category, thus jeopardizing their transportation.¹³

At that time, our group started a broad project to find a safe replacement for HOBt that would keep or even improve on its efficiency. In this regard, a few years later we presented ethyl 2-hydroxyimino-2-cyanoacetate (OxymaPure)¹⁴ as a superior reagent to HOBt in terms of coupling yield, minimization of racemization, and safety.¹⁵ Furthermore, we also proposed (1-cyano-2-ethoxy-2-oxoethylideneaminoxy)(dimethylamino)-(morpholino)carbenium hexafluorophosphate (COMU)¹⁶ and (1-cyano-2-ethoxy-2-oxoethylideneaminoxy)tri-1-pyrrolidino-phosphonium hexafluorophosphate (PyOxim) as OxymaPure-based stand-alone derivatives (Figure 1).¹⁷

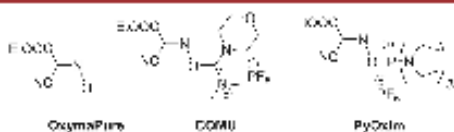


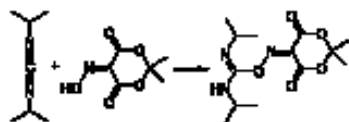
Figure 1. OxymaPure and OxymaPure-based stand-alone coupling reagents.

In spite of the excellent results given by OxymaPure derivatives as coupling additives/reagents, we continued our research to find more oxime derivatives to fulfill our motto "choosing the right peptide coupling reagent for each reaction".¹⁸ In this regard, we were very interested in preparing and testing the oxime derivative of Meldrum's acid¹⁹ because, although the pK_a of this derivative should be higher than that of OxymaPure, its rather rigid and planar structure with two carbonyl groups pointing out toward the potential oxime ester could favor an assisted basic catalysis similar to those described for 1-hydroxy-7-azabenzotriazole (HOAt), and *N*-ethoxycarbonyl-2-ethoxy-1,3-dihydroquinoline (EEDQ).⁶

Surprisingly, although the onium derivative of Meldrum's acid gave excellent results similar to those achieved by COMU, the simple additive 5-(hydroxyimino)-2,2-dimethyl-1,3-dioxane-4,6-dione (HONM) in conjunction with DIC was inefficient, as reflected by the lack of full conversion even for easy couplings.¹⁹ We demonstrated that the very poor performance of DIC and HONM was attributable to the efficient reaction of HONM with DIC to give the corresponding adduct, with the concurrent consumption of DIC and consequent inability to activate the carboxylic group (Scheme 2).¹⁹

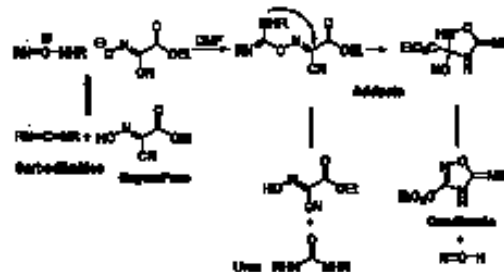
Kolis and co-workers at Eli Lilly recently observed that OxymaPure also reacts with DIC.²⁰ In this case, although the

Scheme 2. Reaction of HONM with DIC



formation of the adduct occurs to a much lesser extent than with HONM, it can cyclize to give an oxadiazole with the concomitant formation of HCN (Scheme 3).

Scheme 3. Reactions of Carbodiimides with OxymaPure²⁰



These results were corroborated by Pawlas and co-workers at Polypeptide.²¹ Those authors proposed a coupling reaction in the presence of dimethyl trisulfide (DMTS) as a HCN scavenger to further minimize its formation.

Herein we addressed the reaction of OxymaPure with various commercially available carbodiimides and their performance in SPPS. In addition to the most frequently used carbodiimides, we also studied DCC, DIC, and *N*-ethyl-*N'*-(3-(dimethylamino)propyl)carbodiimide hydrochloride (EDC or WSC), *N,N'*-di-*sec*-butylcarbodiimide (DSBC), *N,N'*-di-*tert*-butylcarbodiimide (DTBC), and *N-tert*-butyl-*N'*-ethylcarbodiimide (TBEC) (Figure 2).

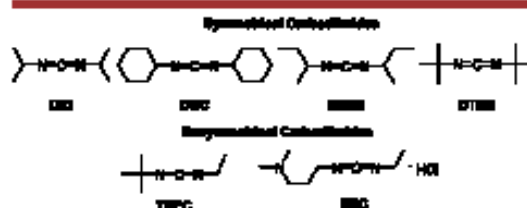


Figure 2. Structures of the carbodiimides used in this study.

All of the reactions were followed by liquid chromatography–mass spectrometry (LC–MS). It should be noted that the formation of the adduct does not involve the formation of HCN. This compound is formed only after the cyclization of the adduct to give the oxadiazole. Indeed, the formation of oxadiazole has been used as a marker for HCN release (Scheme 3).²¹

First, the six carbodiimides were dissolved in DMF together with OxymaPure at a ratio of 1:1. The absence of protected amino acid in the solution forces the side reaction to take place. One set of solutions were kept at 25 °C, and the course of the reaction was analyzed by LC–MS after 24 h and 4 days. A second set of solutions were kept at 60 °C and analyzed after 18 h.

The results are shown in Table 1. The results obtained with DIC are consistent with those reported in the literature by the groups at Eli Lilly and Polypeptide (entries 1, 8, and 15).^{20,21} Similar results were obtained when the experiment was repeated with DCC (entries 2 vs 1, 9 vs 8, and 16 vs 15). In both cases, the amount of adduct was low, and even almost nonexistent in the case of DCC (entry 2). It is important to

Table 1. LC–HRMS Analysis of the Reaction of OxymaPure with the Different Carbodiimides^a

entry	time/temp	carbodiimide	OxymaPure (%)	adduct (%)	oxadiazole (%)
1	24 h/25 °C	DIC	88.9	3.5	7.6
2		DCC	92.3	0.5	7.2
3		EDC-HCl ^b	25.9	14.7	–
4		EDC-HCl/ DIEA ^b	67.8	2.3	–
5		DTBC	100	–	–
6		DSBC	90.0	3.0	3.4
7		TBEC	71.8	28.2	–
8	4 days/ 25 °C	DIC	87.7	2.6	9.7
9		DCC	85.4	0.6	14.0
10		EDC-HCl ^b	38.0	15.4	–
11		EDC-HCl/ DIEA ^b	38.0	15.4	–
12		DTBC	100	–	–
13		DSBC	91.0	2.3	3.3
14		TBEC	75.8	23.7	0.6
15	18 h/ 60 °C	DIC	78.6	2.4	18.9
16		DCC	81.5	1.1	17.4
17		EDC-HCl ^b	45.9	13.2	–
18		EDC-HCl/ DIEA ^b	76.9	9.5	–
19		DTBC	100	–	–
20		DSBC	76.0	1.5	10.9
21		TBEC	83.5	10.4	6.1

^aReaction conditions: OxymaPure/carbodiimide (1:1) in DMF. ^bAn extra peak with $[M + H]^+ = 252.05$ is observed. See ref 22 for a tentative mechanism and structure. ^cOil bath.

highlight that from a structural perspective, DIC and DCC are similar in the sense that a secondary C atom is bound to each N atom of the carbodiimide.

When the reaction was repeated with DSBC, which is structurally similar to DIC and DCC, the reaction trend was the same as before in all cases (entries 6, 13, and 20). Interestingly, two peaks appeared with the same mass, which could be related to diastereomers.

The relevance of steric hindrance was confirmed when the reaction was studied with DTBC, in which the carbodiimide moiety is flanked by two *tert*-butyl groups. In this case, the carbodiimide was unaltered even after 4 days at 25 °C (entry 12) or 18 h at 60 °C (entry 19).

When the reaction was studied with the much less hindered EDC-HCl, an asymmetrical carbodiimide with primary carbons flanking the carbodiimide moiety, no formation of the oxadiazole was detected. However, this reaction yielded the greatest amount of the adduct of all the series (entries 3, 10, and 17). Because of the asymmetry of EDC-HCl, the chromatogram showed two peaks for the adduct (see the Supporting Information for structures). The reduced formation of the adduct after 4 days compared with 24 h (entry 10 vs 3) could be interpreted in terms of hydrolysis of the adduct, rendering again OxymaPure and the corresponding urea (in all

cases, urea was observed by LC–MS) (Scheme 3). Same trend was observed when the reaction was studied with EDC-HCl in the presence of *N,N*-diisopropylethylamine (DIEA), which resulted in no formation of the oxadiazole. Interestingly, in this case, in the absence and presence of DIEA, a new peak with $[M + H]^+ = 252.05$ is clearly observed. This could correspond to the six-membered-ring cyclic compound formed by the attack of the N atom to the carbonyl of the ethyl ester (see ref 22 for the mechanism and structure). This peak also was observed with EDC-HCl in the absence of DIEA, but in a very little extension. It is very important to note that this six-membered-ring compound contains the CN moiety. Therefore, its formation does not provoke the release of HCN and thus poses no risk.

Finally, TBEC, which could be considered a hybrid of DTBC (the *tert*-butyl part is rather unreactive) and EDC-HCl (the ethyl part renders only the adduct, with no progress to the cyclic structure) performed as expected on the basis of the results for DTBC and EDC-HCl separately, with no formation of the oxadiazole after 1 day and, importantly, no formation of HCN. Under the most energetic conditions (18 h at 60 °C), some oxadiazole formed.

The performance of five carbodiimides in SPPS was studied using two model peptides. DCC was not included because the insolubility of the dicyclohexylurea in DMF precludes its use in Fmoc chemistry. Leu-enkephalin (H-Tyr-Gly-Gly-Phe-Leu-NH₂) and Ile^{2,3}-Leu-enkephalin (H-Tyr-Ile-Ile-Phe-Leu-NH₂), with two β -branched amino acids in a row (Ile-Ile), which is a demanding coupling, were synthesized manually on Rink-amide resin. The results, which are summarized in Table 2, are in full agreement with the previous ones presented in

Table 2. Purities of the Peptides Synthesized Using Carbodiimide/OxymaPure^a as determined by HPLC

entry	carbodiimide	Leu-enkephalin (%)	Ile ^{2,3} -Leu-enkephalin (%)
1	DIC	>99.9	96.7
2	EDC-HCl	90.0	79.7
3	DTBC	72.5	39.8
4	DSBC	91.4	82.8
5	TBEC	98.4	96.6

^aCouplings were performed using 5 equiv of reagents without preactivation (in situ activation) in DMF at 25 °C for 30 min.

Table 1, which shows the reactivity of the carbodiimides with OxymaPure. Thus, both DIC (entry 1) and TBEC (entry 5) gave excellent results, showing no major differences in performance. On the other hand, the structurally similar DSBC gave a slightly poorer but acceptable performance, as did EDC-HCl. Finally, the performance of sterically hindered DTBC was much poorer, to the extent that it cannot be used in SPPS.

Finally, given that EDC-HCl is a reagent commonly found in all chemistry laboratories and that its use is not accompanied by the formation of HCN, we addressed SPPS optimization using this carbodiimide. Although preactivation gave very good results for nonhindered protected amino acids (Leu-enkephalin; Table 3, entry 2), in situ activation rendered better results overall (Table 3, entry 1). Finally, the addition of an equimolar amount of DIEA to the in situ activation using EDC-HCl gave results similar to those found with DIC and TBEC (Table 3, entry 3, vs Table 2, entries 1 and 5).

Table 3. Purities of the Peptides Synthesized Using EDC·HCl/OxymaPure^a as Determined by HPLC

entry	conditions	Leu-enkephalin (%)	Tle ³⁵ -Leu-enkephalin (%)
1	in situ activation ^b	90.0	79.7
2	preactivation ^c	>99.9	52.9
3	in situ activation ^d	98.3	92.8

^aCouplings were performed for 30 min using 5 equiv of reagents in DMF at 25 °C for 30 min. ^bTable 2, entry 2. ^cPreactivation of the protected amino acid for 5 min. ^dPreactivation of the protected amino acid for 5 min in the presence of 5 equiv of DIEA.

In conclusion, we have demonstrated that not all carbodiimides have the same reactivity with OxymaPure. Their reactivity is modulated by the steric hindrance of the allyl moieties that flank the carbodiimide backbone. Thus, tertiary carbon groups such as the *tert*-butyl groups in DTBC prevent the formation of the adduct, which is the first step of the secondary reaction. In contrast, primary substituents, such as those in EDC·HCl, enhance the formation of the adduct, but this compound does not evolve to the oxadiazole, and therefore, HCN does not form. Finally, in this structural analysis, the use of carbodiimides flanked by secondary substituents, namely, DIC, DCC, and DSBC, led to the formation of the oxadiazole with the formation of HCN. From the perspective of coupling efficiency, all of the carbodiimides except DTBC were found to be suitable for SPPS.

To avoid the formation of HCN, the use of the hybrid TBEC, which combines the good performance of the tertiary substituents (no reaction at all) and primary substituents (only formation of the adduct), or a carbodiimide with two primary substituents such as EDC·HCl would ensure a HCN-free reaction. Preliminary results carried out in our laboratory have shown that in a standard coupling, formation of the oxadiazole is not observed at all when the activation is carried out either with TBEC or EDC·HCl in the presence of DIEA. Furthermore, racemization using TBEC for protected His, which is the most demanding amino acid, is comparable to that observed with DIC (a complete study will be published elsewhere). To reinforce the validity of TBEC, Izdebski and Kunce reported that this carbodiimide (it was called BEC) showed performance similar to that of DIC in a model study.²³

■ ASSOCIATED CONTENT

Supporting Information

The Supporting Information is available free of charge at <https://pubs.acs.org/doi/10.1021/acs.orglett.1c02466>.

Materials and methods, reactivity of carbodiimides with OxymaPure, solid-phase peptide synthesis, and LC–MS of the products of all reactions carried out and peptides synthesized (PDF)

■ AUTHOR INFORMATION

Corresponding Authors

Fernando Albericio – Peptide Science Laboratory, School of Chemistry and Physics, University of KwaZulu-Natal, Durban 4001, South Africa; Institute for Advanced Chemistry of Catalonia (IQAC–CSIC), 08034 Barcelona, Spain; CIBER-BBN, Networking Centre on Bioengineering, Biomaterials and Nanomedicine, and Department of Organic Chemistry, University of Barcelona, 08028 Barcelona, Spain

orcid.org/0000-0002-8946-0462; Email: albericio@ulzn.ac.za

Beatriz G. de la Torre – KwaZulu-Natal Research Innovation and Sequencing Platform (KRISP), School of Laboratory Medicine and Medical Sciences, College of Health Sciences, University of KwaZulu-Natal, Durban 4001, South Africa; orcid.org/0000-0001-8521-9172; Email: garciadelatorre@ulzn.ac.za

Authors

Srinivasa Rao Manne – Peptide Science Laboratory, School of Chemistry and Physics, University of KwaZulu-Natal, Durban 4001, South Africa

Omar Luna – Institute for Advanced Chemistry of Catalonia (IQAC–CSIC), 08034 Barcelona, Spain; CIBER-BBN, Networking Centre on Bioengineering, Biomaterials and Nanomedicine, and Department of Organic Chemistry, University of Barcelona, 08028 Barcelona, Spain

Gerardo A. Acosta – Institute for Advanced Chemistry of Catalonia (IQAC–CSIC), 08034 Barcelona, Spain; CIBER-BBN, Networking Centre on Bioengineering, Biomaterials and Nanomedicine, and Department of Organic Chemistry, University of Barcelona, 08028 Barcelona, Spain

Miriam Royo – Institute for Advanced Chemistry of Catalonia (IQAC–CSIC), 08034 Barcelona, Spain; CIBER-BBN, Networking Centre on Bioengineering, Biomaterials and Nanomedicine, and Department of Organic Chemistry, University of Barcelona, 08028 Barcelona, Spain; orcid.org/0000-0001-5292-0819

Ayman El-Faham – Department of Chemistry, Faculty of Science, Alexandria University, Alexandria 21321, Egypt; orcid.org/0000-0002-3951-2754

Gyorgy Oroz – Luxembourg Bio Technologies, Ness Ziona 7403631, Israel

Complete contact information is available at: <https://pubs.acs.org/10.1021/acs.orglett.1c02466>

Author Contributions

[†]S.R.M. and O.L. contributed equally. The strategy was designed by all of the authors. The experiments were mainly carried out by S.R.M. and O.L. All of the authors discussed the results and prepared the manuscript.

Notes

The authors declare no competing financial interest.

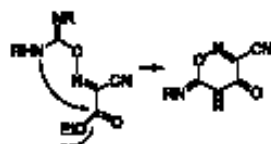
■ ACKNOWLEDGMENTS

We thank Yoav Luxembourg (Luxembourg Bio Technologies) for encouraging this work. This project received funding from the European Union's Horizon 2020 Research and Innovation Programme under Marie Skłodowska-Curie Grant Agreement 861190 (PAVE). O.L.'s work was funded by PAVE. The authors acknowledge an American Chemical Society (ACS) Green Chemistry Institute (GCI) Pharmaceutical Roundtable Ignition Grant awarded to S.R.M. The work carried out in South Africa was partially funded by the National Research Foundation (NRF) (Blue Sky's Research Programme 120386). Peptide preparation was performed at the NANBIOSIS–CIBER BBN Peptide Synthesis Unit (U3).

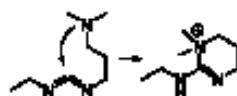
■ REFERENCES

(1) Roughley, S. D.; Jordan, A. M. *J. Med. Chem.* 2011, 54, 3451–3479.

- (2) Cooper, T. W. J.; Campbell, I. B.; Macdonald, S. J. *F. Angew. Chem., Int. Ed.* **2010**, *49*, 8082–8091.
- (3) Bryan, M. C.; Dunn, P. J.; Entwistle, D.; Gallou, F.; Koenig, S. G.; Hayler, J. D.; Hickey, M. R.; Hughes, S.; Kopach, M. E.; Moine, G.; Richardson, P.; Roschangar, F.; Steven, L. A.; Welberth, F. *J. Green Chem.* **2018**, *20*, 5082–5103.
- (4) Albericio, F. *Biopolymers* **2000**, *55*, 123–139.
- (5) Isidro-Llobet, A.; Alvarez, M.; Albericio, F. *Chem. Rev.* **2009**, *109*, 2455–2504.
- (6) El-Faham, A.; Albericio, F. *Chem. Rev.* **2011**, *111*, 6557–6602.
- (7) Sheehan, J. C.; Hess, G. P. A. *J. Am. Chem. Soc.* **1955**, *77*, 1067–1068.
- (8) Merrifield, R. B. *J. Am. Chem. Soc.* **1963**, *85*, 2149–2154.
- (9) Jad, Y. E.; El-Faham, A.; De la Torre, B. G.; Albericio, F. In *Peptide-Based Drug Discovery: Challenges and Opportunities*; Srivastava, V., Ed.; Discovery Series, No. 59; Royal Society of Chemistry: London, **2017**; pp 518–550.
- (10) König, W.; Geiger, R. *Chem. Ber.* **1970**, *103*, 788–798.
- (11) Barlos, K.; Papaloannou, D.; Theodoropoulos, D. *Int. J. Pept. Protein Res.* **1984**, *23*, 300–305.
- (12) Abdelmoty, I.; Albericio, F.; Carpino, L. A.; Foxman, B. F.; Kates, S. A. *Let. Pept. Sci.* **1994**, *1*, 57–67.
- (13) Wehrstedt, K. D.; Wandrey, P. A.; Heitkamp, D. *J. Hazard. Mater.* **2005**, *126*, 1–7.
- (14) Subirós-Funosas, R.; Prohens, R.; Barbas, R.; El-Faham, A.; Albericio, F. *Chem. - Eur. J.* **2009**, *15*, 9394–9403.
- (15) El-Faham, A.; Albericio, F. *J. Pept. Sci.* **2010**, *16*, 6–9.
- (16) El-Faham, A.; Subirós-Funosas, R.; Prohens, R.; Albericio, F. *Chem. - Eur. J.* **2009**, *15*, 9404–9416.
- (17) Subirós-Funosas, R.; El-Faham, A.; Albericio, F. *Org. Biomol. Chem.* **2010**, *8*, 3665–3673.
- (18) Albericio, F.; El-Faham, A. *Org. Process Res. Dev.* **2018**, *22*, 760–772.
- (19) El-Faham, A.; Subirós-Funosas, R.; Albericio, F. *Eur. J. Org. Chem.* **2010**, *2010*, 3641–3649.
- (20) McFarland, A. D.; Buser, J. Y.; Embry, M. C.; Held, C. B.; Kolis, S. P. *Org. Process Res. Dev.* **2019**, *23*, 2099–2105.
- (21) Erny, M.; Lundqvist, M.; Rasmussen, J. H.; Ludemann-Hombourger, O.; Bihel, F.; Pawlas, J. *Org. Process Res. Dev.* **2020**, *24*, 1341–1349.
- (22) A tentative mechanism for the formation of the six-membered ring cyclic compound from the initial adduct is shown below: For



unsymmetrical carbodiimides such as EDC-HCl, two isomers were observed. Interestingly, this product was not observed after reaction at 60 °C for 16 h, presumably because at this temperature the autoreaction of EDC to give its own adduct is favored:



- (23) Idebald, J.; Kuncze, D. *J. Pept. Sci.* **1997**, *3*, 141–144.

Publication 2:

The work performed in this publication involved the design of the experimental strategy and the writing and editing of the draft.



pubs.acs.org/OPRD

Article

tert-Butylethylcarbodiimide as an Efficient Substitute for Diisopropylcarbodiimide in Solid-Phase Peptide Synthesis: Understanding the Side Reaction of Carbodiimides with OxymaPure

Srinivasa Rao Manne, Damilola Caleb Akintayo, Omar Luna, Ayman El-Faham, Beatriz G. de la Torre,* and Fernando Albericio*

Cite This: *Org. Process Res. Dev.* 2022, 26, 2894–2899

Read Online

ACCESS |

Metrics & More

Article Recommendations

Supporting Information

ABSTRACT: The undesired reaction between carbodiimides (peptide coupling reagent) and OxymaPure (peptide coupling additive), which takes place in very low extension during peptide bond formation, is dependent on the steric hindrance around the carbodiimide backbone. Carbodiimides containing tertiary substituents on N such as di-*tert*-butylcarbodiimide do not activate the carboxylic group properly; the presence of secondary substituents such as in the case of diisopropylcarbodiimide (DIC) leads to the formation of oxadiazole and HCN; finally, primary substituents render an adduct of oxadiazine and no formation of HCN. *tert*-Butylethylcarbodiimide (TBEC), which is a hybrid of primary and tertiary substituents, leads to the formation of oxadiazine with no concomitant formation of HCN. Furthermore, TBEC outperforms DIC in terms of yield and minimization of racemization as it is demonstrated herein.

KEYWORDS: carbodiimides, OxymaPure, oxadiazine, oxadiazole, racemization

■ INTRODUCTION

The amide bond is probably the most common bond found in nature and synthetic chemistry.^{1,2} Its almost exclusive presence in peptides, together with the significant development of peptide synthesis in recent decades, has allowed methods originally developed for peptides to enter general organic synthetic chemistry.^{3–6} Since the application of *N,N*-dicyclohexylcarbodiimide (DCC) by Sheehan and Hess in 1955,^{7,8} carbodiimides have been the reagent of choice for peptide bond formation. However, over time, *N,N*-diisopropyl carbodiimide (DIC) has replaced DCC, whose urea formed as a side product showed solubility issues. DIC and other carbodiimides react with the carboxylic group to render the highly reactive *O*-acylisourea (Scheme 1), which undergoes rearrangement to the total inactive *N*-acylurea or, in the case of α -amino acids, evolves to oxazolone (Scheme 1), which shows poor reactivity and provokes the loss of chiral integrity.⁹ To keep the efficiency of carbodiimide-mediated coupling, König and Geiger proposed adding 1-hydroxybenzotriazole (HOBt) to the coupling cocktail¹⁰ because the OBt ester (Scheme 1) formed shows good acylation ability, although less than that of the *O*-acylisourea species, and therefore minimized the side reactions associated with the over-reactivity of *O*-acylisourea as shown in Scheme 1.

However, the explosive nature of HOBt-based additives led them to be grouped in the Class 1 category, thus restricting their use.¹¹ In this context, ethyl 2-hydroxyimino-2-cyanoacetate (OxymaPure),^{12–14} which has been classified as a green reagent by the ACS Green Chemistry Institute (GCI) Pharmaceutical Roundtable,¹⁵ has replaced HOBt.

Recently, Kolis and co-workers reported that OxymaPure reacts with an excess of DIC, forming a linear adduct. Furthermore, it can lead to the formation of oxadiazole and HCN as byproducts (Scheme 2).¹⁶ Later, Pawlas and co-workers demonstrated that the formation of HCN can be minimized by using the green solvent mixture *N*-butylpyrrolidone–ethyl acetate (EtOAc) (1:4) instead of *N,N*-dimethylformamide (DMF) in the presence of dimethyl trisulfide as an in situ scavenger.¹⁷

In this context, our group recently described that the formation of oxadiazole and HCN can be minimized and even suppressed with an appropriate protocol for the sequence of reagent addition.¹⁸ Thus, the best conditions were found to be the preactivation of the Fmoc-amino acid with only DIC for 2–5 min, followed by the addition of the resulting mixture to the peptide resin. OxymaPure can be added to the resin before or after the preactivation mixture.

Furthermore, we addressed the reactions between OxymaPure and several carbodiimides, such as DIC, DCC, *N,N*-disecbutylcarbodiimide (DSBC), *N,N*-di-*tert*-butyl carbodiimide (DTBC), *N-tert*-butyl-*N*-ethyl carbodiimide (TBEC), and *N*-ethyl-*N*-(3-(dimethylamino)propyl) carbodiimide hydrochloride (EDC-HCl or WSC), to study the extension of that side reaction (oxadiazole and HCN formation) with other

Received: July 12, 2022

Published: September 9, 2022



Table 1. LC–HRMS Analysis of the Reaction of OxymaPure with DIC and TBEC

#	DIC	time	linear adduct (2) (%), RT 6.3	oxadiazine (3) (%), RT 13.9	oxadiazole (4) (%), RT 5.9	OxymaPure (%), RT 6.4
1		20 min	1.69	-	-	98.31
2		1 h	0.94	-	0.25	98.81
3		4 h	1.64	-	1.08	97.28
4		5 h	1.66	0.35	1.56	96.42
5		4 d	-	0.53	4.46	95.01
#	TBEC	time	double adduct (1) (%), RT 13.9	oxadiazine (3) (%), RT 14.0	oxadiazole (4) (%), RT 5.8	OxymaPure (%), RT 6.4
6		20 min	0.37	3.85	-	95.78
7		1 h	0.38	3.73	-	95.89
8		4 h	1.00	3.15	-	95.83
9		5 h	0.22	4.02	-	95.68
10		4 d	-	5.74	0.70	93.56
#	DTBC	time	adducts (%)	oxadiazine (%)	oxadiazole (%)	OxymaPure (%), RT 6.4
11		20 min	-	-	-	100
12		1 h	-	-	-	100
13		4 h	-	-	-	100
14		5 h	-	-	-	100
15		4 d	-	-	-	100

the hydrophilic linear adduct (2) was observed at retention time (RT) 6.3 min (Figure S1). After 4 h, oxadiazole (4) with the concomitant formation of HCN appeared as shown in Scheme 2 (route A) (RT 5.9 min, Figure S1). After 4 days, the linear adduct (2) was completely converted to oxadiazole (4) and to a new compound, named the cyclic adduct (3) (oxadiazine, route B, Scheme 2), which was more hydrophobic (RT 13.9 min, Figure S1) than the linear adduct (2) but had the same mass (Scheme 2). Results are summarized in Table 1 (# 1–5). Neither we nor the groups of Kolis and Pawlas observed this compound in previous works.^{10–13}

Next, the reaction between TBEC and OxymaPure was studied under the same conditions as before. Interestingly, OxymaPure reacted with two molecules of TBEC to form tiny amounts of a double adduct (1), as shown in Scheme 2 (route C) (RT 13.9 min, Figure S4), and with one molecule of TBEC to render only the cyclic adduct (3) (oxadiazine with RT 14.0 min, Figure S4). In this case, the hydrophilic linear adduct (2) was not identified. This could be explained by its high reactivity, which probably allowed it to fully convert to the cyclic adduct (3), which is a stable molecule. Table 1 (# 6–10) summarizes the experimental results found.

Furthermore, we studied the reaction between DTBC and OxymaPure under similar conditions. However, no adducts and side products were identified (Table 1, # 11–15) (Figure S8). In the case of the reaction of EDC.HCl with OxymaPure, two adducts appeared at RT 4.27 and RT 5.73, respectively (Scheme S1 and Figures S10–S12). The crude reaction was injected into a preparative high-performance liquid chromatography (prep-HPLC) system for purification and analysis. The liquid chromatography–mass spectrometry (LC–MS) spectrum of purified peaks showed that the adducts are unstable and react with water and form corresponding hydrolyzed products (Scheme S2 and Figures S13 and S14).

The cyclic adduct (3) (oxadiazine) from the TBEC reaction was purified by silica-gel column chromatography and analyzed by NMR spectroscopy and LC–high-resolution MS (HRMS). The nitrile peak of OxymaPure, which appeared at 107.48 ppm in ¹³C NMR (Figure S18), completely disappeared after the reaction with TBEC. Similarly, a characteristic C=NH peak was observed at 9.24 ppm in the ¹H NMR spectrum corresponding to oxadiazine (3) (Figure S19). These results

are in consonance with the mechanism proposed in Scheme 2, where intramolecular cyclization involving the NH and nitrile groups in the linear adduct (2) leads to the formation of a corresponding six-membered cyclic oxadiazine (3). This oxadiazine (3) could also be formed from the double adduct (1); however, it was not possible to isolate it due to the tiny amount formed. Oxadiazine (3) was finally confirmed by electrospray ionization (ESI)-HRMS (Figure S21). This oxadiazine (3) was stable even after 4 days, and it prevented the formation of oxadiazole and HCN, unlike DIC-OxymaPure which forms oxadiazole and HCN (Figure S1).

Under these stress conditions (the reaction of just carbodiimide with OxymaPure in the absence of the carboxylic group), the only reaction possible was the formation of adducts with the concomitant formation of oxadiazine (3) in the case of TBEC and of oxadiazole (4) and HCN in DIC. Therefore, we studied a more real coupling case of Fmoc-Ala-OH onto H-Ala-Phe-Leu-O-chlorotrityl (CT) resin with carbodiimides and OxymaPure as a model reaction.¹⁸

The experiment (Table 2) was done under preactivation conditions using 3 equiv of reagents. Thus, Fmoc-Ala-OH and OxymaPure were mixed for 15 s, and carbodiimides were then added. After an additional 15 s, the mixture was added to the peptide resin. With DIC, the presence of the linear adduct (2) and oxadiazole (4) was observed in a short time (# 6–8, Table 2). However, in the case of TBEC and EDC.HCl/DIEA, no side product formation was observed [linear adduct (2), oxadiazine (3), or oxadiazole (4)] (# 1–5, 9–11, Table 2; Figures S15 and S16).

In our previous work with Leu-enkephalin peptides,¹³ a preliminary report demonstrated the efficiency of TBEC as a coupling reagent in terms of yield. However, to confirm its full suitability for a solid-phase synthesis protocol (SPPS), racemization during the coupling and its use for more complicated peptides require confirmation.

Among the 20 amino acids, His, Cys, and Ser are highly prone to racemization during coupling.^{20–22} Therefore, here, we used three sequences H-Gly-Xxx-Phe-NH₂, where Xxx denotes His(Trt), Cys(Trt), or Ser(tBu), as a model peptide to determine the degree of racemization.^{23–26} The tripeptides were assembled by stepwise solid-phase synthesis either with 2 min of preactivation or in situ activation using Fmoc-AA-OH-

Table 2. LC–HRMS Analysis of the Coupling of Fmoc-Ala-OH onto H-Ala-Phe-Leu-O-CT Resin Using Carbodiimides and OxymaPure at 25 °C

#	TBEC	time	oxadiazine (3) (%)	oxadiazole (4) (%)	OxymaPure (%)
1		1 min	-	-	100
2		40 min	-	-	100
3		80 min	-	-	100
4		1 d	-	-	100
5		4 d	-	-	100
#	DIC ^a	time	linear adduct (2) (%)	oxadiazole (4) (%)	OxymaPure (%)
6		1 min	1.5	-	98.5
7		40 min	0.7	0.1	99.2
8		80 min	0.3	0.3	99.4
#	EDC-HCl/DIEA	time	oxadiazine (3) (%)	oxadiazole (4) (%)	OxymaPure (%)
9		1 min	-	-	100
10		40 min	-	-	100
11		80 min	-	-	100

^aThese results were obtained from a previously published article.¹⁸

OxymaPure-carbodiimide (3 equiv, 1:1:1 ratio) for 1 h in DMF. To ensure the identification of the DL peptides, the diastereomers were previously synthesized, and the best elution method for each DL/LL pair was adjusted. The results are summarized in Table 3 (Figures S22–S48). In all three tripeptide sequences, TBEC showed a greater capacity to suppress racemization than DIC, EDC-HCl, and EDC-HCl/DIEA in both in situ and preactivation methods. This superior performance may be linked to the synergistic role of hybrid substituents in TBEC. In this regard, the primary moiety of carbodiimide should be more reactive than when secondary or tertiary substituents are present. It is important to highlight that unacceptable results were obtained with EDC-HCl/DIEA (# 4, 8, 12, Table 3).

Finally, the efficacy of TBEC as a coupling agent was demonstrated and compared with that of DIC for the synthesis of the following model peptides: ⁶⁵⁻⁷⁴ACP (H-VQAAIDYING-NH₂), ABRF 1992 (H-GVRGDKGNPGWPGAPY-NH₂), and modified decaalanine (H-AAAAAAAAAKKK-NH₂), a difficult and repetitive sequence prone to several deletions. The synthesis was conducted with Fmoc-Rink Amide AM-resin (0.52 mmol/g) in DMF as a solvent using a CEM microwave

peptide synthesizer (nonoptimized standard coupling of 125 s and deprotection of 95 s). The peptides were cleaved from the peptidyl resins, and the crude products were analyzed by HPLC (Table 4 and Figures S49–S54).

Table 4. Percentage Purity of Long-Chain Peptide

#	coupling reagent	⁶⁵⁻⁷⁴ ACP (%) ^a	ABRF92 (%) ^a	H-A ₁₀ K ₃ -NH ₂ (%) ^a
1	TBEC/OxymaPure	96.12	74.53	87.93
2	DIC/OxymaPure	89.49	73.78	85.30

^a% Purity determined by HPLC.

The acyl carrier protein (⁶⁵⁻⁷⁴ACP) is a unique and challenging molecule that has become a peptide of choice to validate the suitability of any given resin, coupling agent, or synthetic protocol for SPPS.^{27,28} ACP is appropriate because of its characteristic low yield, which results from internal reactions such as aspartimide formation and other modifications. HPLC revealed that the purity of the synthesis of ⁶⁵⁻⁷⁴ACP obtained with TBEC (Figure S50) was better than that obtained with DIC (Figure S49). Similarly, a higher purity was recorded for the analysis of ABRF92 with TBEC (Figure S52) than for the synthesis performed with DIC (Figure S51). Finally, the purity of the 13-mer peptide (modified decaalanine) obtained using TBEC (Figure S54) was again found to be better than when DIC was used (Figure S53).

In conclusion, carbodiimides could react with OxymaPure, although in very low extension (less than 1% during a normal coupling reaction using equimolar amounts of both reagents and protected amino acid). This reaction was found to be dependent on the steric hindrance around the carbodiimide backbone. Although carbodiimides containing tertiary carbon groups (DTBC) do not give this side reaction, they are also not very efficient as coupling additives.¹³ Those containing primary substituents such as EDC led to the formation of a cyclic adduct [oxadiazine (3)], which only represents non-productive consumption of carbodiimide. On the other hand, carbodiimide containing secondary substituents led to the formation of an oxadiazole (4) with a concomitant formation of HCN. Following this behavioral pattern, TBEC, which combines the good performance of the tertiary substituents (no reaction at all) and primary substituents [only formation of oxadiazine (3)], ensures an HCN-free reaction with less racemization (preactivation and in situ activation methods)

Table 3. Racemization Studies on the Solid-Phase Assembly of H-Gly-Xxx-Phe-NH₂ (Xxx = His, Cys, or Ser)^a

entry	coupling model	carbodiimide/OxymaPure	DL/LL (%) preactivation	DL/LL (%) in situ activation
1	H-Gly-His-Phe-NH ₂	TBEC	1.05	1.18
2		DIC	1.58	1.30
3		EDC-HCl	4.59	4.22
4		EDC-HCl/DIEA	7.54	6.82
5	H-Gly-Cys-Phe-NH ₂	TBEC	n.d.	n.d.
6		DIC	n.d.	0.71
7		EDC-HCl	0.20	0.59
8		EDC-HCl/DIEA	2.52	2.75
9	H-Gly-Ser-Phe-NH ₂	TBEC	0.27	0.18
10		DIC	0.29	0.35
11		EDC-HCl	n.d.	0.22
12		EDC-HCl/DIEA	5.35	4.95

^an.d. = not detected.

and shows similar or better reactivity than that of DIC as it has been demonstrated in the synthesis of complex model peptides.

This work also evidences that EDC-HCl in the presence of DIEA provokes an unacceptable level of racemization in the case of the coupling of protected His, Ser, and Cys residues in SPPS. Although EDC-HCl is broadly used in solution peptide chemistry, there is little information in the literature about the loss of chirality that it causes.

As a final conclusion, the results outlined in this work confirm that TBEC could be an efficient replacement for DIC. To the best of our knowledge, the chemical, physical, and toxicological properties of TBEC have not been thoroughly investigated, but TBEC as DIC does belong to the carbodiimide family, and therefore, it could also present allergenicity. However, the use of TBEC is not associated to the formation of HCN as the DIC does. Furthermore, in terms of keeping the chirality of the activated protected amino acid, the TBEC performs slightly better than DIC. On the other hand, the price of DIC is currently much more favorable based on many years of ton-scale usage of the reagent by many users in industry and academia alike. Although the price of TBEC could go down after the implementation in large-scale peptide synthesis, its price will probably be superior to the one of DIC due to the requirement of using ethyl isocyanate, which is an expensive starting material.

EXPERIMENTAL SECTION

General Information. All solvents and reagents used in the experiments were bought from commercial suppliers and were used further without any purification unless otherwise indicated. Fmoc amino acids, Fmoc-Rink Amide AM resin (0.74 mmol/g), and chlorotriethylchloride (CTC) resin (1.6 mmol/g) were purchased from Iris Biotech GmbH (Marktredwitz, Germany). Carbodiimides were gifts from Luxembourg Bio-Technologies, Ness Zion, and piperidine was supplied by Sigma-Aldrich (St. Louis, Missouri, USA). DMF and HPLC-quality CH₃CN were purchased from SRL (CRD-SRL, India). Milli-Q water was used for reverse-phase (RP)-HPLC analyses. Analytical HPLC was performed on an Agilent 1100 system using a Phenomenex AerisTMC18 (3.6 μm, 4.6 × 150 mm) column, with a flow rate of 1.0 mL/min and UV detection at 220 nm. Chemstation software was used for data processing. Buffer A: 0.1% trifluoroacetic acid (TFA) in H₂O; buffer B: 0.1% TFA in CH₃CN. LC-MS was performed on an Ultimate 3000, an AerisTM 3.6 μm wide pore column, and a Phenomenex C₁₈ (4.6 mm x150) column (system 2). Buffer A: 0.1% formic acid in H₂O; buffer B: 0.1% formic acid in CH₃CN, flow 1.0 mL/min, UV detection 220 nm. NMR spectra were recorded on a Bruker AVANCE III 400 MHz spectrometer using CDCl₃ as the solvent and tetramethylsilane as an internal standard. Chemical shifts (δ) were reported in parts per million, and spin-spin coupling constants (J) were given in hertz. Abbreviations to denote the multiplicity of a particular signal are s (singlet), d (doublet), t (triplet), q (quartet), and m (multiplet). The reaction products were purified by column chromatography using a silica gel (60–120 mesh) and EtOAc/hexane as an eluent. Solvents were removed under reduced pressure using a Buchi rotary evaporator.

Solid-Phase Peptide Synthesis for Racemization Studies. All peptides were synthesized following the standard Fmoc/tBu-based SPPS. Fmoc-Rink Amide AM resin (0.74 mmol/g) was used as a solid support for the peptides. Initially,

the resin was washed using DMF (3 × 1 min), DCM (3 × 1 min), and DMF (3 × 1 min). The Fmoc group was deprotected by treatment of the resin with 20% piperidine/DMF (1 × 1 min and 1 × 7 min), followed by washing with DMF. The protected Fmoc-amino acids (3 equiv) were incorporated using carbodiimide (3 equiv) and OxymaPure (3 equiv) in DMF, as coupling reagents, for 1 h at room temperature (rt). This was repeated until the final peptide was achieved. Fmoc from the last coupled amino acid was removed as explained above. After drying the peptidyl resin, cleavage was performed by treating with TFA/TIS/H₂O (95:2.5:2.5) for 1 h at rt. The cleavage mixture was then precipitated with Et₂O and centrifuged, and the pellet was redissolved in H₂O/MeCN (1:1) for analysis by HPLC and LC-MS.

Solid-Phase Peptide Synthesis of ⁶⁵⁻⁷⁴ACP, ABRF92, and Modified Decalanine. The syntheses were carried out on Fmoc-Rink Amide AM resin (loading 0.74 mmol/g) under microwave conditions using a CEM Liberty Blue system. The synthesis was carried out using a fivefold excess of protected amino acids and reagents. Peptides were synthesized using the nonoptimized standard coupling of 125 s. The peptidyl resins were cleaved by treatment with TFA-TIS-H₂O (95:2.5:2.5) (10 mL/g of resin) for 1 h at rt. Precipitation was then achieved by the addition of chilled diethyl ether (5 mL/mL cleavage cocktail). After centrifugation, the peptides were taken up in water. They were then analyzed by HPLC and LC-MS.

Characterization Data. (Z)-Ethyl 6-(tert-butylimino)-5-ethyl-4-imino-5,6-dihydro-4H-1,2,5-oxadiazine-3-carboxylate (Oxadiazine 3). Brown liquid; ¹H NMR (400 MHz, CDCl₃): δ 9.24 (br s, 1H), 4.43–4.38 (q, J = 6.8 Hz, 2H), 4.03–3.98 (q, J = 6.8 Hz, 2H), 1.41–1.37 (t, J = 7.2 Hz, 3H), 1.29 (s, 9H), 1.18–1.15 (t, J = 6.8 Hz, 3H); ¹³C NMR (150 MHz, CDCl₃): δ 160.8, 143.7, 140.1, 135.8, 63.4, 53.2, 37.8, 30.7, 14.1, 10.7; FT-IR (KBr): 3323, 2973, 2157, 1698, 1614 cm⁻¹; HRMS (ESI) m/z: [M + H]⁺ calcd for C₁₂H₂₁N₄O₃, 269.1614; found, 269.1619.

ASSOCIATED CONTENT

Supporting Information

The Supporting Information is available free of charge at <https://pubs.acs.org/doi/10.1021/acs.oprd.2c00220>.

HPLC, LCMS, and NMR characterization data of compounds (PDF)

AUTHOR INFORMATION

Corresponding Authors

Beatriz G. de la Torre – Peptide Science Laboratory, School of Chemistry and Physics, University of KwaZulu-Natal, Durban 4000, South Africa; KwaZulu-Natal Research Innovation and Sequencing Platform (KRISP), School of Laboratory Medicine and Medical Sciences, College of Health Sciences, University of KwaZulu-Natal, Durban 4041, South Africa; orcid.org/0000-0001-8521-9172; Email: albericio@ukzn.ac.za

Fernando Albericio – Peptide Science Laboratory, School of Chemistry and Physics, University of KwaZulu-Natal, Durban 4000, South Africa; CIBER-BBN, Networking Centre on Bioengineering, Biomaterials and Nanomedicine, and Department of Organic Chemistry, University of Barcelona, 08028 Barcelona, Spain; Institute for Advanced Chemistry of Catalonia (IQAC-CSIC), 08034 Barcelona,

Spain; orcid.org/0000-0002-8946-0462;
Email: garciadelatorreb@ukzn.ac.za

Authors

Srinivasa Rao Manne – Peptide Science Laboratory, School of Chemistry and Physics, University of KwaZulu-Natal, Durban 4000, South Africa

Damilola Caleb Akintayo – Peptide Science Laboratory, School of Chemistry and Physics, University of KwaZulu-Natal, Durban 4000, South Africa

Omar Luna – CIBER-BBN, Networking Centre on Bioengineering, Biomaterials and Nanomedicine, and Department of Organic Chemistry, University of Barcelona, 08028 Barcelona, Spain; Institute for Advanced Chemistry of Catalonia (IQAC-CSIC), 08034 Barcelona, Spain

Ayman El-Faham – Department of Chemistry, Faculty of Science, Alexandria University, Alexandria 21321, Egypt

Complete contact information is available at:
<https://pubs.acs.org/10.1021/acs.oprd.2c00220>

Author Contributions

The strategy was designed by all of the authors. Experimental work was performed by S.R.M. and D.C.A. All of the authors discussed the results and prepared the manuscript. All authors approved the final version of the manuscript.

Notes

The authors declare no competing financial interest.

ACKNOWLEDGMENTS

Thanks go to Yoav Luxembourg and Gyorgy Orosz (Luxembourg Bio Technologies) for encouraging this work and for the generous gift of TBEC, DIC, and OxymaPure. This work was partially funded by the National Research Foundation (NRF) (Blue Sky's Research Programme # 120386).

REFERENCES

- Hazza, S.; Gallou, F.; Handa, S. Water: An Underestimated Solvent for Amide Bond-Forming Reactions. *ACS Sustainable Chem. Eng.* 2022, 10, 5299–5306.
- MacMillan, D. S.; Murray, J.; Sneddon, H. F.; Jamieson, C.; Watson, A. J. B. Evaluation of alternative solvents in common amide coupling reactions: replacement of dichloromethane and N,N-dimethylformamide. *Green Chem.* 2013, 15, 596–600.
- Montalbetti, C. A. G. N.; Falque, V. Amide bond formation and peptide coupling. *Tetrahedron* 2005, 61, 10827–10852.
- Han, S.-Y.; Kim, Y.-A. Recent development of peptide coupling reagents in organic synthesis. *Tetrahedron* 2004, 60, 2447–2467.
- Valeur, E.; Bradley, M. Amide bond formation: beyond the myth of coupling reagents. *Chem. Soc. Rev.* 2009, 38, 606–631.
- Al-Warhi, T. I.; Al-Hazimi, H. M. A.; El-Faham, A. Recent development in peptide coupling reagents. *J. Saudi Chem. Soc.* 2012, 16, 97–116.
- Sheehan, J. C.; Hess, G. P. A New Method of Forming Peptide Bonds. *J. Am. Chem. Soc.* 1955, 77, 1067–1068.
- Sheehan, J. C. *The Enchanted Ring: The Untold Story of Penicillin*; MIT Press, 1982.
- El-Faham, A.; Albericio, F. Peptide Coupling Reagents, More than a Letter Soup. *Chem. Rev.* 2011, 111, 6557–6602.
- König, W.; Geiger, R. Eine neue Methode zur Synthese von Peptiden: Aktivierung der Carboxylgruppe mit Dicyclohexylcarbodiimid unter Zusatz von 1-Hydroxy-benzotriazolinen. *Chem. Ber.* 1970, 103, 788–798.
- Wehrstedt, K. D.; Wandrey, P. A.; Heitkamp, D. Explosive properties of 1-hydroxybenzotriazolines. *J. Hazard. Mater.* 2005, 126, 1–7.
- Manne, S. R.; de la Torre, B. G.; El-Faham, A.; Albericio, F. OxymaPure Coupling Reagents: Beyond Solid-Phase Peptide Synthesis. *Synthesis* 2020, 52, 3189–3210.
- Subirós-Fumosas, R.; Khattab, S. N.; Nieto-Rodríguez, L.; El-Faham, A.; Albericio, F. Advances in acylation methodologies enabled by oxyma-based reagents. *Aldrichim Acta* 2014, 45, 21–40.
- Subirós-Fumosas, R.; Prohens, R.; Barbas, R.; El-Faham, A.; Albericio, F. Oxyma: An Efficient Additive for Peptide Synthesis to Replace the Benzotriazole-Based HOBt and HOAt with a Lower Risk of Explosion[1]. *Chem.—Eur. J.* 2009, 15, 9394–9403.
- Bryan, M. C.; Dunn, P. J.; Entwistle, D.; Gallou, F.; Koenig, S. G.; Hayler, J. D.; Hickey, M. R.; Hughes, S.; Kopach, M. E.; Moine, G.; Richardson, P.; Roschangar, F.; Steven, A.; Weiberth, F. J. Key Green Chemistry research areas from a pharmaceutical manufacturers' perspective revisited. *Green Chem.* 2018, 20, 5082–5103.
- McFarland, A. D.; Buser, J. Y.; Embry, M. C.; Held, C. B.; Kolis, S. P. Generation of Hydrogen Cyanide from the Reaction of Oxyma (Ethyl Cyano(hydroxyimino)acetate) and DIC (Diisopropylcarbodiimide). *Org. Process Res. Dev.* 2019, 23, 2099–2105.
- Emy, M.; Lundqvist, M.; Rasmussen, J. H.; Ludemann-Hombourger, O.; Bihel, F.; Pawlas, J. Minimizing HCN in DIC/Oxyma-Mediated Amide Bond-Forming Reactions. *Org. Process Res. Dev.* 2020, 24, 1341–1349.
- Manne, S. R.; El-Faham, A.; de la Torre, B. G.; Albericio, F. Minimizing side reactions during amide formation using DIC and oxymaPure in solid-phase peptide synthesis. *Tetrahedron Lett.* 2021, 85, 153462.
- Manne, S. R.; Luna, O.; Acosta, G. A.; Royo, M.; El-Faham, A.; Orosz, G.; de la Torre, B. G.; Albericio, F. Amide Formation: Choosing the Safer Carbodiimide in Combination with OxymaPure to Avoid HCN Release. *Org. Lett.* 2021, 23, 6900–6904.
- Di Fenza, A.; Tancredi, M.; Galoppini, C.; Rovero, P. Racemization studies of Fmoc-Ser(tBu)-OH during stepwise continuous-flow solid-phase peptide synthesis. *Tetrahedron Lett.* 1998, 39, 8529–8532.
- Kaiser, T.; Nicholson, G.; Köhlbau, H.; Voelter, W. Racemization studies of Fmoc-Cys(Trt)-OH during stepwise Fmoc-Solid phase peptide synthesis. *Tetrahedron Lett.* 1996, 37, 1187–1190.
- Ishiguro, T.; Eguchi, C. Unexpected chain-terminating side reaction caused by histidine and acetic anhydride in solid-phase peptide synthesis. *Chem. Pharm. Bull.* 1989, 37, 506–508.
- Jad, Y. E.; Khattab, S. N.; de la Torre, B. G.; Gwender, T.; Kruger, H. G.; El-Faham, A.; Albericio, F. Oxyma-B, an excellent racemization suppressor for peptide synthesis. *Org. Biomol. Chem.* 2014, 12, 8379–8385.
- Han, Y.; Albericio, F.; Barany, G. Occurrence and Minimization of Cysteine Racemization during Stepwise Solid-Phase Peptide Synthesis 1,2. *J. Org. Chem.* 1997, 62, 4307–4312.
- Kumar, A.; Alhassan, M.; Lopez, J.; Albericio, F.; Torre, B. G. N-Butylpyrrolidinone for Solid-Phase Peptide Synthesis is Environmentally Friendlier and Synthetically Better than DMF. *ChemSusChem* 2020, 13, 5288–5294.
- Carpino, L. A.; El-Faham, A. The diisopropylcarbodiimide/1-hydroxy-7-azabenzotriazole system: Segment coupling and stepwise peptide assembly. *Tetrahedron* 1999, 55, 6813–6830.
- Hudson, D. Methodological implications of simultaneous solid-phase peptide synthesis. 1. Comparison of different coupling procedures. *J. Org. Chem.* 1988, 53, 617–624.
- Atherton, E.; Logan, C. J.; Sheppard, R. C. Peptide synthesis. Part 2. Procedures for solid-phase synthesis using N α -fluorenylmethoxycarbonylamino-acids on polyamide supports. Synthesis of substance P and of acyl carrier protein 65-74 decapeptide. *J. Chem. Soc., Perkin Trans. 1* 1981, 538–546.

Publication 3:

The work performed in this publication involved the synthesis, purification and characterization of all peptides, the writing and editing of this draft and the validation and curation of data.



Open Access

This article is licensed under [CC-BY-NC-ND 4.0](https://creativecommons.org/licenses/by-nc-nd/4.0/)<http://pubs.acs.org/journal/acsodf>

Article

Impact of N-Terminal PEGylation on Synthesis and Purification of Peptide-Based Cancer Epitopes for Pancreatic Ductal Adenocarcinoma (PDAC)

Omar F. Luna,[○] Yomkippur V. Perez,[○] Daniele P. Ferrari, Sana S. Sayedipour, Miriam Royo, Gerardo A. Acosta, Luis J. Cruz, Frauke Alves, Erik Agner, Magne O. Sydnes,* and Fernando Albericio*

Cite This: *ACS Omega* 2024, 9, 34544–34554

Read Online

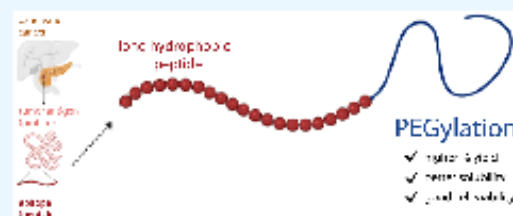
ACCESS |

Metrics & More

Article Recommendations

Supporting Information

ABSTRACT: Peptide-based cancer vaccines have shown promising results in preclinical trials focusing on tumor immunotherapy. However, the presence of hydrophobic amino acid segments within these peptide sequences poses challenges in their synthesis, purification, and solubility, thereby hindering their potential use as cancer vaccines. In this study, we successfully synthesized peptide sequences derived from mesothelin (MSLN), a tumor-associated antigen overexpressed in pancreatic ductal adenocarcinoma (PDAC) by conjugating them with monodisperse polyethylene glycol (PEG). By PEGylating mesothelin epitopes of varying lengths (ranging from 9 to 38 amino acids) and hydrophobicity (60–90%), we achieved an effective method to improve the peptide yield and facilitate the processes of synthesis and purification. PEGylation significantly enhanced the solubility, facilitating the single-step purification of lengthy hydrophobic peptides. Most importantly, PEGylation did not compromise cell viability and had little to no effect on the immunogenicity of the peptides. In contrast, the addition of a palmitoyl group to increase immunogenicity led to reduced yield and solubility. Overall, PEGylation proves to be an effective technique for enhancing the solubility and broadening the range of utility of diverse long hydrophobic peptides.



INTRODUCTION

Pancreatic ductal adenocarcinoma (PDAC) is one of the most aggressive forms of cancer, killing about nine in ten patients within 5 years after diagnosis.^{1,2} PDAC is extremely difficult to diagnose at its early stage,³ and most patients are diagnosed only after the cancer is metastasized.⁴ Currently, the only curative therapy for PDAC is surgical resection, but fewer than 20% of patients have resectable tumors at the time of diagnosis.¹ More than 80% of patients are diagnosed with advanced-stage tumors, for which median survival with chemotherapy is less than 1 year.^{4,5} In stark contrast to other tumor types, targeted therapies in multiple large-scale trials have been unsuccessful for PDAC.^{6–8} Nonetheless, a broader understanding of the resistant PDAC tumor and its intricate interactions with the immune system has opened new avenues of treatment.

Recently, the incorporation of immunotherapy in the treatment of various solid tumors has marked a paradigm shift in oncology.^{9,10} Immune-based therapies aim to recruit and activate immune cells to eliminate tumor cells. Among these therapies are peptide-based cancer vaccines.¹¹ Cancer vaccines work by the same principles as vaccines for other diseases, where the active ingredient triggers an immune response that generates a long-term immunity to a foreign antigen. Cancer vaccines train the immune system to identify

tumor antigens as “foreign,” targeting and eliminating cancer cells.^{12,13} Peptide-based cancer vaccines are made up of a sequence of amino acids derived from tumor antigens that are either present in both normal and cancer cells but overexpressed in the latter (tumor-associated antigen) or solely found in cancer cells (tumor-specific antigen).¹⁴ From these tumor antigens, the selected sequence can be in the form of a single epitope, a long peptide chain containing multiple epitopes or a cocktail containing multiple separate epitopes.¹⁵ Long multi-epitope peptide vaccines are ideal since they elicit a strong immune response and are less prone to enzymatic digestion and elimination from the body (Figure 1).¹⁶ However, the synthesis of combined long peptides comes with challenges in handling and solubility.¹⁷

Since its introduction in 1963 by Merrifield,¹⁸ solid-phase peptide synthesis (SPPS) has become the strategy of choice for the synthesis of peptides used in research and for the vast

Received: March 17, 2024

Revised: May 30, 2024

Accepted: June 10, 2024

Published: August 1, 2024



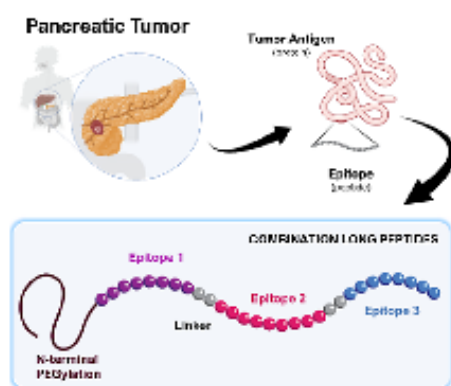


Figure 1. PEGylated peptide-based cancer vaccines for PDAC immunotherapy.

majority of peptide-based pharmaceutical ingredients.^{19,20} Synthesis of long peptides (>25 amino acid (aa) residues) implies a greater likelihood of being accompanied by many impurities derived from incomplete amino acid couplings²¹ and secondary reactions in the deprotection,²² coupling,²³ or cleavage steps.²⁴ There are also small and medium-sized peptides (up to 10 and 25 aa residues, respectively), which are very difficult to synthesize with a decent quality by SPPS.²⁵ The impurities, mostly truncated peptides, are often difficult to chromatographically resolve from one another, especially as the sequence grows longer. This makes the mandatory purification step much more difficult.²⁶ Furthermore, the recovery of pure products declines with increasing hydrophobicity of the sequence.²⁷ Finally, the hydrophobicity of certain sequences greatly limits their downstream application, as they are often restricted to dimethyl sulfoxide (DMSO) for solubilization, which then needs to be diluted with aqueous buffers for compatibility in bioassays due to the toxicity of most organic solvents.²⁸

We hypothesized that these synthesis, purification, and solubility problems can be overcome by conjugating polyethylene glycol (PEG) to the hydrophobic peptide sequences. Herein, we delineate our efforts toward this end using combined peptide sequences covering epitopes from well-described tumor-associated antigens overexpressed in PDAC.

RESULTS AND DISCUSSION

In this study, we selected peptide sequences that cover mesothelin epitopes that are known or predicted to elicit an immune response against PDAC. These selected mesothelin epitopes were synthesized either as a single epitope (short) or

as a multiple epitope (long) peptide sequence. A palmitoyl group was also added to increase the immunogenicity of the sequences. We investigated the impact of PEGylation on the synthesis, purification, and solubility of the peptides. Furthermore, we conducted bioassays to evaluate the effect of PEGylation on the cell viability and immunogenicity of the peptides.

Design of Peptide Sequences. Mesothelin (MSLN) is a 40 kDa cell surface glycoprotein demonstrated previously by gene expression analysis to be a tumor marker for PDAC.^{29,30} It has limited expression in normal tissues and has significant overexpression in almost 90% of PDAC cases,³¹ making it an attractive candidate for cancer immunotherapy. MSLN overexpression has been demonstrated to promote proliferation, advancement of the cell cycle, and survival of cancer cells.^{32,33} In many PDAC cases, it is also associated with shorter overall survival and resistance to chemotherapy, which underscores the importance of targeting MSLN.³⁴

As such, we selected three hydrophobic MSLN epitopes, MSLN 1–3 that have been predicted to trigger an immune response using publicly available epitope prediction servers,^{35,36} namely SYFPEITHI³⁷ and BIMAS.³⁸ The sequences were joined together using a cathepsin-like cleavage site (KK or Lys-Lys)³⁹ to obtain the long-combined peptide MSLN 4 (Table 1). The peptide sequences MSLN 1–4 include a range of lengths, covering amino acid residues from 9 to 38, and exhibit diversity in relative hydrophobicity levels, extending from 60% to 90%. The peptides were PEGylated to enhance their solubility and palmitoylated to increase their immunogenicity.^{40,41} Although the specific mechanisms for how fatty acid increases immunogenicity are still being discussed, the positive effect has been reported.⁴⁰ Modifications such as those in peptide sequences derived from self-antigens are necessary given their low immunogenicity, potential for inducing immune tolerance, and the generally poor immune response against tumor antigens.⁴²

Peptide PEGylation. Synthesis of Fmoc-PEG 23 Propionic Acid 4. For peptide PEGylation, we first synthesized a monodisperse heterobifunctional PEG with Fmoc and a carboxylic acid functional group. It was crucial to start with high-purity polyethylene glycol for the PEGylation of peptides to reduce the necessary purification work later and to ensure a single molecular identity. We chose a >1000 Da PEG since it is one of the very few long PEG oligomers that are available in monodisperse form in multigram quantity.

Monodisperse Fmoc-PEG 23 propionic acid was synthesized from monodisperse amino PEG acid 1 obtained from Polypure (see Scheme S1). Amino-PEG acid was first converted to amino-PEG methyl ester 2 by a repeated cycle of heating in methanol with HCl and evaporation under reduced pressure. Amino-PEG methyl ester 2 was protected with a Fmoc group

Table 1. Mesothelin Epitopes for PDAC Cancer Vaccines

epitope	coverage in MSLN	sequence	length	% hydrophobic residues ^a	hydrophilicity score ^b
MSLN 1	541–555	PLTVAEVQKLLGPHV	15	60	−0.34
MSLN 2	117–126	ALPLDLLLFL	10	90	−1.08
MSLN 3	20–28	SLLFLLFSL	9	78	−1.49
MSLN 4	541–555,117–126,20–28	PLTVAEVQKLLGPHVKKALPLDLLLFLKKSLLFLLFSL	38	66	−0.46

^aPeptide relative hydrophobicity (% hydrophobic residues) was calculated using the peptide2.com hydrophobicity calculator. ^bHydrophilicity scores were calculated via the BACHEM peptide calculator tool (<https://www.bachem.com/knowledge-center/peptide-calculator/>).

giving compound 3, and the ester functionality was cleaved upon treatment with HCl (aq) to give acid 4. Fmoc-PEG 23 propionic acid 4 (yellowish oil) was recovered by extraction with dichloromethane (DCM) in a yield of 94% (30 g) with a purity of >98% based on LC–MS analysis. The ^1H and ^{13}C NMR analyses further confirmed the purity of the compound. The total ion chromatogram (retention time: 7.5 min) and mass spectrum of the final product (ESI-MS: $[\text{M} + \text{H}]^+ = 1368.7$) are shown in Figure 2. The ^1H and ^{13}C NMR spectra are shown in Figures S1 and S2.

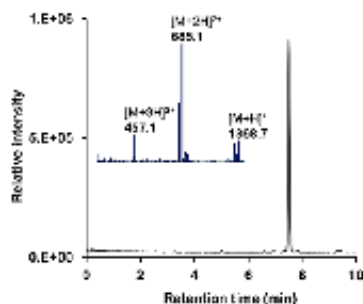


Figure 2. HPLC chromatogram and MS spectrum (inset) of Fmoc-PEG 23 propionic acid 4. Retention time at 7.5 min in a 5 to 75% B gradient (A: 0.1% TFA in H_2O and B: CH_3CN) for 10 min. ESI-MS: $[\text{M} + \text{H}]^+ = 1368.7$, $[\text{M} + 2\text{H}]^{2+} = 685.1$, $[\text{M} + 3\text{H}]^{3+} = 457.1$.

Ensuring a high PEG oligomer purity is of utmost importance, as even a one-unit deviation in PEG length (either $n - 1$ or $n + 1$) can persist throughout the subsequent peptide synthesis. This variance in the oligomer length significantly increases the potential impurities during peptide purification. Purifying peptides with PEG impurities presents a greater challenge since a PEG unit weighs 44 Da, whereas the smallest amino acid residue, glycine, weighs 57 Da.

The successful synthesis of monodisperse Fmoc-PEG 23 propionic acid 4 was reported by Wang et al.,⁴¹ where they used a macrocyclic sulfate-based approach starting from PEG 4 diol on a 5 g scale. However, an assessment of the purity of the resulting product was not discussed. Herein, we have synthesized a monodisperse Fmoc-PEG 23 and evaluated the oligomer purity of the amino-PEG acid using LC–MS in selected ion mode (SIM) looking for $n - 2$, $n - 1$, and $n + 1$ impurities. A linear range in which the injection volume is proportional to the concentrations (area under the curve) of the different PEG oligomers was identified (Figure 3). Our results showed an average purity of 99.5% across varying injection volumes (Table 2).

Synthesis of PEGylated and Palmitoylated Peptides. The peptides were synthesized manually or automatically using a Liberty Blue automated microwave peptide synthesizer following a standard Fmoc/*t*-Bu-based solid-phase synthesis protocol (SPPS).⁴³ The bulk of these sequences was synthesized by microwave-assisted automated synthesis, as it provides quick, reliable, and reproducible production of crude peptides. Furthermore, our previous experiences with manual synthesis of these types of peptides have pointed to the need for automated synthesis for MSLN 3 and MSLN 4 as these are the most synthetically challenging of the four peptides. The exception here is MSLN 2 as P13 and P14 are not quite as

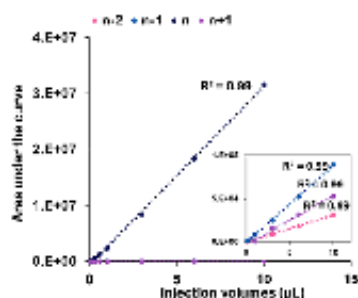


Figure 3. Analysis of amino-PEG 23 propionic acid oligomer purity. Linearity of different injection volumes (0.1, 0.3, 0.6, 1.0, 3.0, 6.0, and 10.0 μL) and PEG oligomer concentrations (area under the curve of chromatogram).

Table 2. Percent Purity of the PEG Oligomers^a

injection volume (μL)	oligomer percent %			
	$n - 2$	$n - 1$	n	$n + 1$
0.1	0.00	0.35	99.65	0.00
0.3	0.13	0.29	99.57	0.00
0.6	0.12	0.26	99.62	0.00
1	0.09	0.35	99.56	0.00
3	0.11	0.30	99.42	0.18
6	0.10	0.28	99.45	0.17
10	0.10	0.28	99.46	0.17

^aThe selected ion monitoring (SIM) method in HPLC–MS was used to quantitate the oligomer purity of different injection volumes for 0.4 μM concentration of amino-PEG acid.

challenging and could be produced by manual synthesis. Fmoc Rink Amide AM resin was used as solid support, and the first amino acid was coupled to obtain a 0.5 mmol/g loading. The remaining free sites were capped by acetylation, followed by deprotection using 20% piperidine/dimethylformamide (DMF). Further residues were incorporated using standard protected Fmoc amino acids, *N,N'*-diisopropylcarbodiimide (DIC), and OxymaPure in DMF as coupling reagents. PEGylation and palmitoylation were prepared manually using monodisperse Fmoc-PEG 23 propionic acid 4 and palmitic acid (Scheme S2). Subsequent cleavage was performed by treatment with TFA/TIS/ H_2O (95/2.5/2.5). The cleavage mixture was precipitated with cold diethyl ether and centrifuged, and the resulting pellet was redissolved in $\text{H}_2\text{O}/\text{ACN}$ (1:1) for lyophilization, followed by characterization by HPLC and LC–MS.

The crude yield and recovery of the synthesized peptides are summarized in Table 3. The quantity (milligrams) of crude peptides nearly doubled upon PEGylation, as expected. The incorporation of the high molecular weight PEG moiety (1367 Da) naturally increases the amount of crude oil while maintaining the integrity of the peptide sequence. This offers a distinct advantage as it provides a larger amount of material available for subsequent purification and use in bioassays.

Crude Peptides. Crude amounts (mmol) of PEGylated products P2, P8, and P11 for MSLN 1, 3, and 4 epitopes are higher than the unmodified peptides P1, P7, and P10 and significantly higher than their palmitoylated versions (P3, P9, and P12), respectively. This trend is not seen for MSLN 2, where the highest recovery is observed for the unmodified

Table 3. Summary of Yield, Purity, and Solubility of Synthesized Peptides

epitope	ID	N-terminal	MW (Da)	mmol obtained ^a	% purity	% yield ^b	mmol purified	% purity	% recovery ^c	solubility (1 mg/mL)
MSLN 1	P1	NH ₂ -	1599.9	0.080	84	67	0.025	>99	37	water
	P2	PEG23-NH-	2728.3	0.084	81	68	0.016	>99	24	water
	P3	Palm-NH-	1838.4	0.046	83	38	0.009	95	22	ACN/water (1:1)
MSLN 2	P4	NH ₂ -	1126.5	0.095	82	78	0.048	99	61	ACN/water (1:1)
	P5	PEG23-NH-	2254.8	0.074	86	63	0.046	96	70	water
	P6	Palm-NH-	1364.9	0.072	76	55	0.012	99	23	DMSO
MSLN 3	P7	NH ₂ -	1051.3	0.059	56	33	0.004	95	11	ACN/water (1:1)
	P8	PEG23-NH-	2179.7	0.072	55	40	0.014	95	33	water
	P9	Palm-NH-	1289.8	0.036	75	27	0.013	98	47	DMSO
MSLN 4	P10	NH ₂ -	4256.4	0.058	71	41	0.011	73 ^d	19	ACN/water (1:1) ^d
	P11	PEG23-NH-	5384.7	0.069	81	56	0.020	>99	36	ACN/water (1:1)
	P12	Palm-NH-	4494.8	0.049	57	28	0.015	97	53	ACN/water (1:1)

^aThe peptides were synthesized in a 0.1 mmol scale. ^b% Yield = (crude mmol × crude purity)/(theoretical mmol). ^c% Recovery = (purified mmol × purity)/(crude mmol × crude purity) × 100. ^dCannot be purified to more than 90% due to a des-Leu impurity. Gels in water/acetonitrile at high concentrations.

peptide P4 while the palmitoylated P6 and PEGylated P5 modified peptides display similar levels of recovery. Since the automated peptide synthesis process for the same base sequence is the same up to the final modification of the N-terminus, the variation in yield of the peptide must be related to the efficiency of the cleavage from the solid support and the following workup. This can be attributed to better precipitation in the cold diethyl ether. Palmitoylated peptides do not readily precipitate unless TFA is removed by evaporation first, a requirement not common for most cleaved synthetic peptides. The palmitoyl moiety increased the hydrophobicity of the sequence and made it more difficult for these peptides to adequately precipitate in diethyl ether when TFA is present. Moreover, it is worth noting that the sequences exhibit a tendency toward greater hydrophobicity, as indicated by their negative hydrophilicity scores. Specifically, the base sequences of MSLN 2, MSLN 3, and MSLN 4 are predominantly composed of hydrophobic amino acid residues (Table 1). This makes precipitation challenging even in the absence of fatty acids, as we observed *in situ*. This is a hallmark of hydrophobic peptides, whereas most peptides carry enough polar and charged residues to not be solvated by diethyl ether and thus precipitate. Unlike these two cases, the PEGylated peptides that we studied precipitated easily and without the need to fully remove TFA first.

When calculating yields, which consider the purity of the crude product, the following trends appear: first, all palmitoylated peptides P3, P6, P9, and P12 have very low yields compared with their counterparts. Second, yields for PEGylated peptides are either higher (P8 and P11) or similar (P2) compared to the unmodified peptides. The exception is, again, MSLN 2, which is the only case where the unmodified peptide P4 shows a better yield than the PEGylated peptide P5. The low mmol values obtained inherently affect the yield, this is especially noticeable for the palmitoylated peptides. Individually, for example, MSLN 1 variants all have similar purities, and so the low absolute amount of mmol of crude obtained peptide P3 makes it the product with the lowest yield. With a trend very clear for palmitoyl peptides, we compared the situation between the unmodified peptide and the PEGylated peptide. The driving force involved between all these pairs of peptides is similar. MSLN 2 seems to be a particular case. It can be proposed that the single positive charge provided by TFA in the N-terminal free amine is overall

more effective in the smaller unmodified peptide P4 than in the larger PEGylated peptide P5 and thus precipitates better in diethyl ether, which explains the excellent absolute recovery. This in turn drives the high yield of the unmodified peptide compared to that of the PEGylated peptide P5 and certainly with respect to that of the palmitoylated peptide P6.

Two other versions of MSLN 2 were synthesized in which we attached both PEG and palmitoyl to the base sequence. These versions are P13 (Palm-PEG11-MSLN 2) with a shorter PEG 11 moiety and P14 (Palm-PEG23-MSLN 2) with a longer PEG 23. Here, our findings revealed that both the length of the PEG chain and the hydrophobicity of the underlying amino acid sequence affect the precipitation of the peptides. Contrary to P14, which had a longer PEG chain and rapidly precipitated, P13 with the shorter PEG chain did not undergo precipitation in a single step. This suggests that throughout the precipitation and subsequent washing stages after cleavage a certain amount of peptide is inadvertently lost due to incomplete precipitation. PEGylation using a longer PEG chain mitigates this problem, leading to higher yields.

Purified Products. The final mmol obtained of purified products (as shown in Table 3, column 8) was higher for the PEGylated peptides P8 and P11 in comparison to their unmodified counterparts P7 and P10, respectively, although it should be noted that MSLN 2 escapes this trend. The other exception is MSLN 1, in which the unmodified peptide P1 was obtained in a larger amount than that of the PEGylated peptide P2. The absolute recovery in mmol of pure PEGylated peptides increased in all cases when compared to their palmitoylated versions and even the least hydrophobic sequence, namely MSLN 1, saw a substantial increase in recovered material. For MSLN 3, however, this recovery is not significantly greater. Palmitoylated MSLN4 peptide P12 shows better rates of recovery compared to their counterparts P10 and P11. This is due to the distribution of impurities (see the Supporting Information) further away from the main peptide peak. While the overall purity is lower than that for P10 and P11, this distribution facilitates the purification. This is not the case for P10 and P11, in which we observe most of the impurities overlapping the main peak. This leads to sacrificing more of the desired product as perfect resolution of impurities close to the product peak is not possible. Obtaining a larger quantity of pure product from a single synthetic and purification process is the most important advantage that

PEGylation can bring to peptide production, in addition to the well-established benefits it offers for enhancing bioavailability.

In terms of percent recovery, which considers the recovery of a product with an acceptable purity of 95% or greater from the initially available peptide from the crude mass (refer to Table 3, column 10), the most noticeable effect can be seen with MSLN 2, in which recovery improves substantially for PEGylated peptide P5, particularly when compared to that of the palmitoylated sequence P6. While the initial specific yield was highest for P6 (mainly due to a +96 Da impurity, likely trifluoroacetylation, appearing sometimes but mostly in sequences that do not carry a palmitoyl moiety and thus capped N-terminal amine), recovery of this peptide was extremely low, unlike the case for P5. Recovery of palmitoylated peptides is, however, higher for MSLN 3 and 4. In the case of MSLN 3, this is mainly due to the higher purity of the P9 crude, while for MSLN 4, the impurities of P12 are spread widely across the gradient and are thus more easily resolved.

For MSLN 3, the trend seen for MSLN 2 is also true with respect to the base sequence in peptide P7, if not for the palmitoylated version P9, as recovery in the relative percentage is better. Nevertheless, both P8 and P9 have better absolute recoveries than base sequence P7 (0.004 mmol P7, 0.014 mmol P8, and 0.013 mmol P9). The latter pattern is seen also in MSLN 4, and it is more noticeable compared to the base sequence in peptide P10. In fact, in this case, a *des*-Leu impurity (among others), present in the long MSLN 4 sequence, could not even be resolved, and we were unable to obtain a purified peptide P10 (at best, we improved the purity from 71 to 73%; see the Supporting Information). This is likely due to three issues: first, PEGylated peptides generate sharper chromatographic peaks, whereas both the palmitoylated and unmodified versions have more triangular and wider dragging peaks (see the Supporting Information for chromatograms). This affects resolution, especially in semipreparative scales, which means that collecting less of the peak is necessary to maintain adequate purities, which causes the loss of more product in exchange for greater purity. For MSLN 4, the increased retention in the column of the unmodified sequence P10 giving these "dragging" peaks is less affected by PEG23, yet PEGylation proves adequate for obtaining pure product P11.

The second variable is the hydrophobicity. The PEG moiety has a greater effect on the solubility of MSLN 2 peptide P4 than for the more hydrophilic sequence MSLN 1 P1, in which the effect is even reversed (P2 has a marginally higher retention time in a C18 stationary phase). Hydrophobic sequences are more retained in the column due to stronger interactions with the hydrocarbon chain of the stationary phase, whereas the hydrophilic PEG moiety favors solvation in the mobile phase. This is also seen in MSLN 3 comparing unmodified peptide P7 and PEGylated version P8.

The third variable is the size. The shorter MSLN 2 peptide P4 is more affected by PEGylation as seen for peptide P5, and the effect on its recovery is greatly increased compared to a longer sequence like MSLN 4 (P10 and P12), in which the effect is lessened.

In a few cases, however, we observed a better recovery rate in palmitoylated peptides. Although due to the way this parameter was calculated, this was mainly an effect of the crude simply being purer to begin with or containing impurities that were easier to resolve chromatographically. This is something

to be noted, as besides the usual synthetic issues, especially with deletions in longer sequences, the potential modification by secondary reactions in downstream processing, namely, during cleavage, is yet another source of problems. Mass spectrometry analyses of the studied sequences showed an unwanted +96 Da modification due to trifluoroacetylation of (likely) serine and threonine residues which was more prevalent when the N-terminal amine was not capped. It must also be noted that palmitoylation is not a random modification that we chose to test. It was included in the sequence to improve its immunogenic potential. As such, we must focus mainly on what happens between PEGylation and palmitoylation and the possibility of combining the two. The potential arises from the fact that PEGylation offers a suitable modification strategy for enhancing the solubility of a hydrophobic peptide as well as other benefits upon application in biological systems such as increasing its half-life. PEGylation can be implemented prior to introducing a palmitoyl moiety with the aim of enhancing solubility. In turn, this should lead to improvements in precipitation in diethyl ether, chromatographic resolution, and the reduction of interactions with the stationary phase of semipreparative chromatographic columns. These collective enhancements would contribute to obtaining a greater yield of a pure product. It is anticipated that introducing a PEG 23 moiety prior to palmitoylation would combine the initial high purity observed in some palmitoylated products with the improved crude yields seen in the PEGylated variants as well as their generally higher absolute recoveries. This approach would effectively counteract the significant hydrophobic nature of palmitoylated products and address the tendency toward cleavage-specific secondary reactions similar to the likely *O*-trifluoroacetylation of serine/threonine that we observed in peptides with an unmodified N-terminal amine.⁴⁴

Solubility. Visual assessment of the solubility at 1 mg/mL in some common solvents for peptides was carried out. PEGylation increased the solubility of the hydrophobic base sequences in water and facilitated biological testing. Palmitoylation, however, decreased the solubility in water, as expected for a fatty acid chain attachment.

PEGylation increased the solubility of base sequences P4 and P7 from ACN/water (1:1) to 100% water (Table 3). Palmitoylation made peptides P6 and P9 insoluble in ACN/water (1:1) and soluble only in DMSO. No significant changes in solubility were observed for PEGylation of P1 to P2, while a decrease of solubility in water is observed with palmitoylation, P3.

To test the increase in the solubility of palmitoylated peptides, we performed a preliminary study in which we synthesized one batch of the base sequence of MSLN 2 and split it to make three modifications (Figure 4): (A) palmitoylation P6 and PEGylation with either, (B) PEG 11 P13, or (C) PEG 23 P14, followed by palmitoylation. We observed decreasing retention times (Figure 4A–C): 9.2 min for P6 (falling outside of the gradient range), 6.4 min for P13, and 5.4 min for P14. We also observed much sharper peaks for the two PEGylated peptides P13 and P14. These results point in the direction we proposed, although it should be noted that to confirm this, careful individual analysis of yields and recoveries must also be performed.

The significance of these PEGylated epitopes being more soluble in aqueous medium than the originally designed epitopes while still retaining the properties for downstream applications cannot be overstated. PEGylation proves to be an

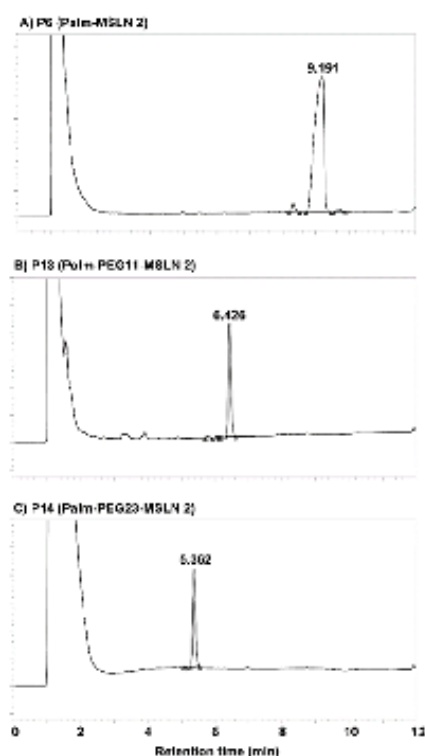


Figure 4. Chromatograms of (A) P6 (Palm-MSLN 2), (B) P13 (Palm-PEG11-MSLN 2), and (C) P14 (Palm-PEG23-MSLN 2) in 60–100% A: 0.045% TFA in H₂O and B: 0.036% TFA in CH₃CN for 8 min.

effective modification technique for enhancing solubility and broadening the range of utility of bioactive substances like peptides.

Effect of PEGylation of Peptides in Cell Stimulation.

To verify whether the PEGylation of the peptides would influence the proliferation and activation of immune cells, we

tested splenocytes from 15 C57BL/6 male mice immunized with PLGA nanoparticles containing the well-known adjuvants, poly I:C and R848.^{45,46} The cells were restimulated *in vitro* with positive control (Concanavalin A) or the unmodified peptides P1, P4, and P7, PEGylated peptides P2, P5, P8, and P11, and palmitoylated long peptide P12 soluble in ACN/water (1:1) at 10 μg/mL for 48 h.

After the stimulation, a viability assay was performed, and we found no difference in the proliferation of the cells when stimulated with the PEGylated peptides, in comparison with the unmodified version (Figure 5A). For P12, the cells were more proliferative. This suggests that palmitoylation of MSLN 4 is not toxic and induces cell growth.

The activation of the stimulated cells was assessed using ELISA by measuring interferon-gamma (IFN-γ) levels. IFN-γ is a marker for the activation of cytotoxic T CD8⁺ cells mediated by Th1 cells and is related to antiproliferative, proapoptotic, and antitumoral activity as well as tumor immune surveillance. As such, its secretion is expected to increase in antiviral and antitumoral immune responses. This cytokine is positively associated with cancer survival. It is thus a useful marker to study whether the peptides are activating antitumoral T CD8⁺ cells.⁴⁷

We did not find a significant difference in the levels of IFN-γ secreted in the supernatant of the cells when stimulated with PEGylated peptides compared to cells stimulated with unmodified peptides except for MSLN 2 P5 (Figure 5B). This difference can be attributed to the possibility that the long PEG chain might have hindered the interaction of the active site of the short MSLN 2.

The increased levels of IFN-γ for both the palmitoylated P12 and PEGylated long peptide P11 (modified MSLN 4) demonstrate that indeed, multiple-epitope long peptide sequences can elicit a stronger immune response than single-epitope short peptide sequences. The unmodified long peptide P10 was not tested since the peptide could not be purified to more than 95% purity.

In this case, PEGylation proves to be an effective technique for enhancing the solubility and broadening the range of utility of diverse long hydrophobic peptides. This result also further enhances our proposed strategy of combining both modifications in the MSLN 4 sequence.

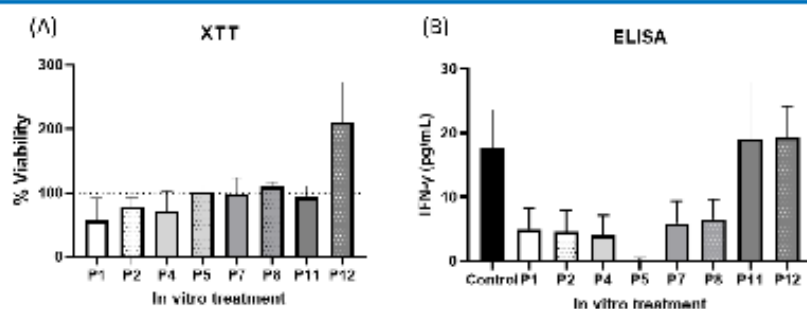


Figure 5. Effect of cell stimulation with PEGylated peptides. Splenocytes from vaccinated mice (adjuvants in PLGA nanoparticle vaccines) were stimulated with unmodified and PEGylated peptides for 48 h. (A) PEGylation of the peptides did not have influence on the viability of the cells. Data was normalized to the absorbance levels of nonstimulated cells. Cell proliferation was measured by the XTT assay. (B) PEGylation of the peptides did not change the levels of IFN-γ in the supernatant measured by ELISA except for MSLN 2.

■ CONCLUSIONS

In this study, we synthesized peptide sequences from mesothelin, a tumor antigen overexpressed in PDAC and conjugated them with monodisperse PEG. N-terminal PEGylation of peptides of varying lengths (<40 aa residues) and hydrophobicity (up to 90% of hydrophobic residue content) proved to be an excellent method to increase yield and recovery during synthesis and purification. PEGylation also improved solubility, making it possible for a long multipeptide hydrophobic peptide to be purified in one step and biologically tested. Cell viability and immunogenicity of peptides were not significantly affected by PEGylation. Peptides exceeding 40 amino acids with a hydrophobic residue content of more than 80% are promising candidates for PEGylation with extended PEG units such as PEG-45 or longer. In contrast, our results also underscore the influence of palmitoylation on peptide synthesis and purification. This is also in line with the trend of producing longer synthetic peptides as bioactive compounds. The addition of a palmitoyl group, aimed at increasing immunogenicity, led to lower yield and solubility, thereby complicating subsequent biological evaluation. The effects of palmitoylation on synthesis and purification are sequence dependent. However, we observed a general trend toward more difficult processing of the peptide. This is very clear in the cases of MSLN 2 and MSLN 3, where elution from a C18 stationary phase column was not quantitative (data not shown) and even a C8 stationary phase, required aggressive gradients of 80–100% to 90–100% of organic mobile phase, a drastic change from their unmodified or PEGylated variants (see the [Supporting Information](#)). Purifying by semipreparative chromatography, a similar trend can be observed for MSLN 4 although it is less pronounced. In addition, the MSLN 4 base sequence can not be purified in one step (Table 3), a problem that was solved by PEGylation. A combined strategy of palmitoylation and PEGylation, especially for longer sequences with inherent synthetic difficulties, such as MSLN 4, is therefore a sound approach to attempt in future assays, as it represents a compromise between improving the intended biological activity while decreasing difficulties in synthesis and purification and at the same time maintaining adequate solubility for biological evaluation.

■ EXPERIMENTAL PROCEDURES

General Experimental. Reagents and Solvents. The monodisperse PEG products (amino-PEG 23 acid and Fmoc-PEG 11 propionic acid) were provided by Polypure AS (Oslo, Norway). Solvents, dichloromethane (DCM), tetrahydrofuran (THF), and acetonitrile (ACN) used for the synthesis of the monodisperse PEG were obtained from Chiron AS (Trondheim, Norway). Potassium *tert*-butoxide (KO^t-Bu), *tert*-butyl acrylate (*t*-Bu acrylate), mesyl chloride (MsCl), triethylamine (TEA), ammonia (NH₃), trifluoroacetic acid (TFA), and *N*-(9H-fluoren-9-ylmethoxycarbonyloxy) succinimide (Fmoc-ONSu) were purchased from Merck KGaA (Darmstadt, Germany).

The 20 standard Fmoc amino acids, Fmoc Rink Amide AM resin (loading 0.71 mmol/g, 100–200 mesh), and 2-cyano-enzotriazolino)acetate (OxymaPure) were purchased from Iris Biotech GmbH (Marktredwitz, Germany). Piperidine, DCM, *N,N*-dimethylformamide (DMF), ACN, diethyl ether (Et₂O), and dimethyl sulfoxide (DMSO) were supplied by Carlo Erba

Reagents (Val-de-Reuil, France). Palmitic acid, triisopropylsilane (TIS), acetic anhydride, and *N,N*-diisopropylethylamine (DIPEA) were purchased from Sigma-Aldrich Chemie GmbH (Steinheim, Germany). Benzotriazol-1-yloxytripyrrolidino-phosphonium hexafluorophosphate (PyBOP) and TFA were obtained from Fluorochem Ltd. (Hadfield, UK). *N,N*-diisopropylcarbodiimide (DIC) was purchased from KEMILAB Organics Ltd. (Veszprém, Hungary). Formic acid was purchased from Merck KGaA (Darmstadt, Germany). Rink Amide ProTide LL resin (0.18 mmol/g loading, 100–200 mesh) was obtained from CEM Corp (Charlotte, US). Poly(vinyl alcohol) (PVA, *M_n* 9000–10,000 80% hydrolyzed), polyinosinic-polycytidylic acid sodium salt (Poly(I:C) or pIC), resiquimod (R848), and chitosan oligosaccharide lactate (ave. *M_n* = 5000) were purchased from Sigma-Aldrich (Merck KGaA, Darmstadt, Germany). PLGA (*M_n*: 17,000, PURASORB PDLG 5002A) was obtained from Corbion PURAC (Amsterdam, NL).

Characterization. Characterization of Monodisperse Fmoc-PEG-23 Propionic Acid. High-performance liquid chromatography–tandem mass spectrometry (HPLC-MS) was carried out by using an Agilent 1269 Infinity II LC/MSD System. The HPLC system was operated using Solutions A (MilliQ water, 0.1% TFA) and B (ACN) running through a 30 mm × 2.1 mm analytical C18 column (Avantor). Single quadrupole MS was operated with an electrospray ionization source (ESI) using the following settings: ionization mode: positive, drying gas temperature = 350 °C, capillary voltage = 3000 V, drying gas flow = 12.0 L/min, nebulizer gas pressure = 35 psig and acquisition range = 100–1000 or 3000 *m/z*. ¹H and ¹³C NMR spectra were recorded at 25 °C on a Bruker Ascend 600 MHz Avance NEO spectrometer.

Characterization of Peptides. Crude products obtained from the cleavage step were characterized by HPLC to assess purity, using Alliance chromatographic equipment (Waters Corp., US) with a XBridge BEH C18 column (dimensions 4.6 mm × 100 mm, particle size 3.5 μm). A gradient of 5–100% of B in min was used where A: MilliQ water with 0.045% TFA and B: ACN with 0.036% TFA. For more hydrophobic peptides, a Kinetex C8 column (dimensions 4.6 × 100 mm, particle size: 5 μm) was used with 50–100% and 80–100% B gradients, depending on the peptide. Data was acquired at 220 nm and analyzed with the Empower 3 Pro software (build 3471, Waters Corp., US). Crude peptides were also characterized by LCMS to confirm their identity. Low-resolution mass spectrometry analyses were carried out in an AllianceHT chromatograph with a micromass ZQ mass spectrometer (Waters Corp., US). Data was acquired and analyzed with the MassLynx software (v4.1, Waters Corp., US).

Experimental Section. Synthesis of Monodisperse Fmoc-PEG 23 Propionic Acid 4. Amino-PEG acid 1 was converted to amino-PEG methyl ester 2 by a repeated cycle of heating in methanol with HCl and evaporation under reduced pressure. The following solutions were then prepared: (A) amino-PEG methyl ester (29 g, 0.025 mol) in 150 mL of DCM and (B) *N*-(9-fluorenylmethoxycarbonyloxy) succinimide or Fmoc-ONSu (8.43 g, 0.025 mol) in 50 mL of DCM. Solutions A and B were mixed and allowed to react for 1 h at rt. This was followed by 1.0 mL additions of triethylamine (TEA) until the reaction was complete (a total of 5 mL of TEA was added). The reaction solution was washed with 0.1 M KHSO₄ (60 mL) and then with water (60 mL). Both aqueous phases were extracted with DCM (60 mL × 2). The combined organic

fractions were evaporated under reduced pressure. The resulting crude product **3** was redissolved in HCl (1.5 M) and stirred for 48 h. The solution was then filtered and extracted with DCM (4 × 60 mL). The organic extracts were combined, and the solvent was evaporated (yellow oil), treated with a small aliquot of diethyl ether, and dried giving compound **4** (30 g, 94%, > 98% purity) as a white powder. ¹H NMR (600 MHz, CDCl₃) δ 7.76 (d, *J* = 7.5 Hz, 1H), 7.61 (d, *J* = 7.5 Hz, 1H), 7.40 (t, *J* = 7.5 Hz, 1H), 7.31 (td, *J* = 7.5, 1.1 Hz, 1H), 4.40 (d, *J* = 7.0 Hz, 1H), 4.22 (t, *J* = 7.0 Hz, 0H), 3.70–3.59 (m, 49H), 2.60 (t, *J* = 6.1 Hz, 1H); ¹³C NMR (151 MHz, CDCl₃) δ 172.9, 156.6, 144.0, 141.3, 127.7, 127.1, 125.1, 120.0, 66.7, 47.3, 41.0, 35.0.

Analysis of Oligomer Purity of Amino-PEG 23 Acid 1. The selected ion monitoring (SIM) method in an Agilent 1269 Infinity II LC/MSD System was used to look for the *n* – 2, *n* – 1, and *n* + 1 impurities. Different injection volumes (0.1, 0.3, 0.6, 1.0, 3.0, 6.0, and 10.0 μL) of a 0.4 μM concentration of amino-PEG acid were used for the analysis. PEG oligomer concentrations (area under the curve of the chromatogram) were plotted against the injection volumes, and a linear range was determined.

Synthesis of Peptides. Peptides were synthesized following a standard Fmoc/tBu-based solid-phase synthesis protocol (SPPS).

Manual Synthesis. Fmoc Rink Amide AM resin (0.71 mmol/g loading, 100–200 mesh) was used as a solid support for the peptides. Initially, the resin was swelled using DMF (3 × 1 min), DCM (3 × 1 min), and DMF (3 × 1 min). Deprotection of the Fmoc group was achieved by treatment of the resin with 20% piperidine/DMF (2 × 5 min) followed by washing with DMF. The first amino acid was coupled to reach a 0.5 mmol/g resin loading (1.5/1.5/1.5 equiv amino acid/DIC/oxyrma) for 4 h, then remaining free sites were capped via acetylation treating the resin with acetic anhydride (10 equiv) and DIPEA (10 equiv) in DCM for 15 min. Further residues were incorporated using standard protected Fmoc-amino acids (3 equiv), DIC (3 equiv), and OxyrmaPure (3 equiv) in DMF, as coupling reagents, for 60 min at rt. To monitor couplings, the Kaiser test was performed. When detecting incomplete reactions, a new coupling was carried out using PyBOP and DIPEA (1.5 and 3 equiv) for 30 min at rt. This was repeated until the final peptide was achieved. Fmoc from the last coupled amino acid was removed as explained above.

Automated Synthesis. Microwave-assisted synthesis was carried out in a Liberty Blue automated peptide synthesizer (CEM Corp., US). Fmoc-removal was carried out with 20% v/v piperidine in DMF at 90 °C for 1 min. Couplings were performed mixing 0.125 M of Fmoc amino acids, 0.125 M of OxyrmaPure, and 0.125 M of DIC at 90 °C for 2 min. Rink Amide ProTide LL resin (0.18 mmol/g loading, 100–200 mesh) was used as solid support. Manual PEGylation was followed using Fmoc-PEG 23 propionic acid and the same coupling agents listed above. For P13, Fmoc PEG-11 propionic acid was used. Some peptides were synthesized carrying N-terminal palmitoylation, added as a normal coupling. Cleavage was performed after drying the peptidyl resin by treating with TFA/TIS/H₂O (95/2.5/2.5) for 1 h at rt. The cleavage mixture was then precipitated with cold diethyl ether, centrifuged, and the pellet redissolved in H₂O/ACN (1:1) for lyophilization, after which it was characterized by HPLC and LC–MS.

Purification of Peptides. Crude products were dissolved in either water/acetonitrile (1:1) or DMSO and purified in a semipreparative HPLC Waters PrepLC System (Waters Corp., US) injecting 30–50 mg into either a XBridge Prep C18 OB column (dimensions 19 × 100 mm, particle size 5 μm) or a Kinetex C8 AXI column (dimensions 21.2 × 100 mm, particle size: 5 μm). The monitoring of peptides was done at 220 nm, and elutions were carried in varying gradients of water with 0.1% TFA and acetonitrile with 0.1% TFA, depending on the best resolution for each specific sequence. Data was acquired and analyzed with the Empower 3 software (build 3471, Waters Corp., US). Fractions containing the desired product were manually collected immediately after detection. After the collection and analysis of fractions by analytical HPLC and ESI-MS to confirm purity of 95% or above, the solvent was evaporated by rotavapor and reduced to 20 mL, which was then lyophilized.

Nanoparticle Synthesis. PLGA NPs with encapsulated adjuvants were prepared by using an oil-in-water emulsion and solvent evaporation–extraction method. Briefly, 50 mg of PLGA was dissolved in 3 mL of DCM along with 5 μL of pIC and 2 mg of R848. The solution above was added dropwise to 20 mL of aqueous 2% (w/v) PVA and emulsified for 60 s with 5 s rest each cycle using a sonicator (Sonifier 250, Branson, Danbury, USA). Following overnight evaporation of the solvents at 4 °C, the NPs were collected by centrifugation (14,800 rpm for 30 min) at 4 °C and redissolved in water. After, the nanoparticle solution was added dropwise to 20 mL of 1% homogenized chitosan oligosaccharide lactate solution and stirred at 4 °C for 2 h. The coated NPs were finally collected by lyophilization.

Animals and Immunization. A total of 15 C57BL6 male mice (12 weeks old) were used in the experiment. Mice were obtained and kept at the animal facility of Max-Planck-Institute for Multidisciplinary Sciences under a 12 h dark: light cycle with ad libitum access to food and water. All animal experimental procedures were performed in compliance with the European (2010/63/EU) and German regulations on Animal Welfare and were approved by the administration of Lower Saxony (LAVES) (Nr. 33.19-42502-04-20/3527). Mice were immunized subcutaneously in the right flank once per week, for 3 weeks with nanoparticle containing the adjuvants polyinosinic:polycytidylic acid (polyIC) and R848. The NPs were diluted in water and injected in a volume of 100 μL, in a concentration of 2.5 μg of polyIC, and 3.75 μg of R848. The mice were sacrificed 2 days after the last vaccination, and the spleen was excised.

Stimulation of Splenocytes. Single-cell suspensions from the spleen were prepared in sterile conditions by mincing the cells through 40 and 100 μm cell strainers (BD Falcon). Erythrocytes in spleen samples were lysed with 1 mL of ACK buffer (150 mM NH₄Cl, 10 mM KHCO₃, 0.1 mM EDTA, pH = 7.2–7.4) per spleen for 5 min. The reaction was stopped with PBS and spun down. Cells were resuspended in RPMI 1640 medium supplemented with 10% Fetal Bovine Serum, 100 μg/mL penicillin, and 100 μg/mL streptomycin. Cells were seeded in 96-well plates with a density of 500,000 cells per well in duplicates or triplicates. Splenocytes were stimulated with concanavalin A (2 μL/mL, 00-4978-03, ThermoFisher) or different peptides in a concentration of 10 μg/mL. The supernatant was collected after 48 h of stimulation and kept frozen at –20 °C until cytokine analysis.

After 48 h of stimulation, the cells were analyzed for their viability.

ELISA. Cells were centrifuged, and supernatants were collected and kept at $-20\text{ }^{\circ}\text{C}$ for further cytokine quantification. IFN- γ was quantified by ELISA (ThermoScientific, #88-7314-88). Briefly, the 96-well plates were incubated overnight at $4\text{ }^{\circ}\text{C}$ with the capture antibody. After being washed and blocked, the plate was incubated at room temperature with samples for 2 h and then with detection antibody for 1 h. After that, the plate was incubated with the avidin horseradish peroxidase (HRP) conjugate for 30 min. The color reaction was developed by adding TMB solution, and the enzymatic reaction was stopped by adding $2\text{ N H}_2\text{SO}_4$. Optical density (OD) was determined to be 450 nm.

Cell Viability Assay. For cell proliferation and cytotoxicity assay, CellTiter 96 AQueous One Solution Reagent (Promega) was used. The reagent contains a tetrazolium compound [3-(4,5-dimethylthiazol-2-yl)-5-(3-carboxymethoxyphenyl)-2-(4-sulfophenyl)-2H-tetrazolium, inner salt; MTS] and phenazine ethosulfate; PES. After 48 h of stimulation with the peptides, $20\text{ }\mu\text{L}$ of the reagent was added to each well, and the plate was incubated for 4 h. The absorbance at a wavelength of 490 nm was measured by a microplate reader.

Statistical Analysis. Results are expressed as mean \pm SEM (standard error of the mean). Data were analyzed, and statistical analyses were performed using the GraphPad Prism v9.2.0 software. Each experiment was performed three times with triplicates per assay. Data are presented as mean \pm SEM. One-way analysis of variance (ANOVA) with Tukey's test for multiple comparisons was performed. A p -value of <0.05 was considered statistically significant.

■ ASSOCIATED CONTENT

Supporting Information

The Supporting Information is available free of charge at <https://pubs.acs.org/doi/10.1021/acsomega.4c02604>.

Synthesis of Fmoc-PEG 23 propionic acid along with ^1H and ^{13}C NMR spectra; characterization of peptides; chromatogram (crude and purified) and MS spectrum of synthesized peptides (PDF)

■ AUTHOR INFORMATION

Corresponding Authors

Magne O. Sydnes – Department of Chemistry, Bioscience, and Environmental Engineering, University of Stavanger, Stavanger 4036, Norway; orcid.org/0000-0001-9413-6969; Email: magne.o.sydnes@uis.no

Fernando Albericio – Department of Organic Chemistry, University of Barcelona, and CIBER-BBN, Networking Centre on Bioengineering, Biomaterials, and Nanomedicine, Barcelona 08028, Spain; Peptide Science Laboratory, School of Chemistry and Physics, University of KwaZulu-Natal, Durban 4001, South Africa; orcid.org/0000-0002-8946-0462; Email: albericio@ub.edu

Authors

Omar F. Luna – Department of Organic Chemistry, University of Barcelona, and CIBER-BBN, Networking Centre on Bioengineering, Biomaterials, and Nanomedicine, Barcelona 08028, Spain

Yomkippur V. Perez – Polypure AS, Fornebu 1364, Norway; Department of Chemistry, Bioscience, and Environmental

Engineering, University of Stavanger, Stavanger 4036, Norway

Daniele P. Ferrari – Translational Molecular Imaging, Max Planck Institute of Multidisciplinary Sciences, Göttingen 37075, Germany

Sana S. Sayedipour – Department of Radiology, Leiden University Medical Center, Leiden 2333, Netherlands

Miriam Royo – Department of Organic Chemistry, University of Barcelona, and CIBER-BBN, Networking Centre on Bioengineering, Biomaterials, and Nanomedicine, Barcelona 08028, Spain; Institute for Advanced Chemistry of Catalonia (IQAC) of the Spanish Council for Scientific Research (CSIC), Barcelona 08028, Spain; orcid.org/0000-0001-5292-0819

Gerardo A. Acosta – Department of Organic Chemistry, University of Barcelona, and CIBER-BBN, Networking Centre on Bioengineering, Biomaterials, and Nanomedicine, Barcelona 08028, Spain; Institute for Advanced Chemistry of Catalonia (IQAC) of the Spanish Council for Scientific Research (CSIC), Barcelona 08028, Spain

Luis J. Cruz – Department of Radiology, Leiden University Medical Center, Leiden 2333, Netherlands

Frauke Alves – Translational Molecular Imaging, Max Planck Institute of Multidisciplinary Sciences, Göttingen 37075, Germany

Erik Agner – Polypure AS, Fornebu 1364, Norway

Complete contact information is available at: <https://pubs.acs.org/10.1021/acsomega.4c02604>

Author Contributions

O.L. and Y.P. contributed equally to the work. O.L. contributed to validation, formal analysis, investigation, data curation, writing—review and editing, and visualization. Y.P. contributed to validation, formal analysis, investigation, data curation, writing—original draft, writing—review and editing, and visualization. D.F. contributed to validation, formal analysis, investigation, writing—review and editing, and visualization. S.S.S. contributed to formal analysis and investigation. M.R. contributed to resources and supervision. G.A. contributed to methodology and supervision. L.J.C. contributed to conceptualization, resources, and supervision. F.A. contributed to conceptualization, methodology, validation, resources, writing—review and editing, and supervision. E.A. contributed to conceptualization, methodology, resources, writing—review and editing, and supervision. M.O.S. contributed to conceptualization, writing—review and editing, and supervision. F.A. contributed to conceptualization, methodology, resources, writing—review and editing, and supervision.

Funding

The project received funding from the European Union's Horizon 2020 research and innovation program under the Marie Skłodowska-Curie PAVE-ITN project (grant agreement no. 861190).

Notes

The authors declare no competing financial interest.

■ ACKNOWLEDGMENTS

We thank Aleksandra Stasiak (Polypure AS) for helping us with the PEG synthesis. We also thank Joseph Lumba and Dr. Solon Oikonomopoulos (NTNU, Norway) for the NMR analysis. The U3 (Synthesis of Peptide Unit) of the ICTS "NANBIOSIS" at the IQAC-CSIC is acknowledged for the

assistance and support related to the synthesis of the different peptides used in this work.

■ ABBREVIATIONS

PEG: polyethylene glycol; SPPS: solid-phase peptide synthesis; PDAC: pancreatic ductal adenocarcinoma; MSLN: mesothelin; ELISA: enzyme-linked immunosorbent assay concentration; HPLC: high-performance liquid chromatography; MS: mass spectroscopy; NMR: nuclear magnetic resonance

■ REFERENCES

- (1) Siegel, R. L.; Miller, K. D.; Fuchs, H. E.; Jemal, A. *Cancer Statistics, 2022*. *CA: Cancer J. Clin.* 2022, 72, 7–33.
- (2) American Cancer Society. *Cancer Facts & Figures 2022*; Cancer News: Atlanta, 2022.
- (3) Wood, L. D.; Canto, M. I.; Jaffee, E. M.; Simeone, D. M. Pancreatic Cancer: Pathogenesis, Screening, Diagnosis, and Treatment. *Gastroenterology* 2022, 163, 386–402.e1.
- (4) Kleeff, J.; Korc, M.; Apte, M.; La Vecchia, C.; Johnson, C. D.; Biankin, A. V.; Neale, R. E.; Tempero, M.; Tuveson, D. A.; Hruban, R. H.; et al. Pancreatic Cancer. *Nat. Rev. Dis. Primers* 2016, 2, 16022.
- (5) O’Kane, G. M.; Ladak, F.; Gallinger, S. Advances in the Management of Pancreatic Ductal Adenocarcinoma. *Can. Med. Assoc. J.* 2021, 193, No. E844–E851.
- (6) Tempero, M.; Oh, D.-Y.; Tabernero, J.; Reni, M.; Van Cutsem, E.; Hendifar, A.; Waldschmidt, D.-T.; Starling, N.; Bachet, J.-B.; Chang, H.-M.; et al. Ibrutinib in Combination with NAB-Paclitaxel and Gemcitabine for First-Line Treatment of Patients with Metastatic Pancreatic Adenocarcinoma: Phase III Resolve Study. *Ann. Oncol.* 2021, 32, 600–608.
- (7) Hewitt, D. B.; Nissen, N.; Hatoum, H.; Musher, B.; Seng, J.; Coveler, A. L.; Al-Rajabi, R.; Yeo, C. J.; Leiby, B.; Banks, J.; et al. A Phase 3 Randomized Clinical Trial of Chemotherapy with or without Algenpantucel-L (Hyperacute-Pancreas) Immunotherapy in Subjects with Borderline Resectable or Locally Advanced Unresectable Pancreatic Cancer. *Ann. Surg.* 2022, 275, 45–53.
- (8) Hecht, J. R.; Lonardi, S.; Bendell, J.; Sim, H.-W.; Macarulla, T.; Lopez, C. D.; Van Cutsem, E.; Muñoz Martin, A. J.; Park, J. O.; Greil, R.; et al. Randomized Phase III Study of Folfex Alone or with Peglotecakin as Second-Line Therapy in Patients with Metastatic Pancreatic Cancer That Progressed after Gemcitabine (Sequoia). *J. Clin. Oncol.* 2021, 39, 1108–1118.
- (9) Waldman, A. D.; Fritz, J. M.; Lenardo, M. J. A Guide to Cancer Immunotherapy: From T Cell Basic Science to Clinical Practice. *Nat. Rev. Immunol.* 2020, 20, 651–668.
- (10) Sarantis, P.; Koustas, E.; Papadimitropoulou, A.; Papavassiliou, A. G.; Karamouzis, M. V. Pancreatic Ductal Adenocarcinoma: Treatment Hurdles, Tumor Microenvironment and Immunotherapy. *World J. Gastrointest. Oncol.* 2020, 12, 173–181.
- (11) Foley, K.; Kim, V.; Jaffee, E.; Zheng, L. Current Progress in Immunotherapy for Pancreatic Cancer. *Cancer Lett.* 2016, 381, 244–251.
- (12) Schizas, D.; Charalampakis, N.; Kole, C.; Economopoulou, P.; Koustas, E.; Gkotsis, E.; Ziogas, D.; Psyrri, A.; Karamouzis, M. V. Immunotherapy for Pancreatic Cancer: A 2020 Update. *Cancer Treat Rev.* 2020, 86, 102016.
- (13) Saxena, M.; van der Burg, S. H.; Melief, C. J.; Bhardwaj, N. Therapeutic Cancer Vaccines. *Nat. Rev. Cancer.* 2021, 21, 360–378.
- (14) Buonaguro, L.; Tagliamonte, M. Selecting Target Antigens for Cancer Vaccine Development. *Vaccines* 2020, 8, 615.
- (15) Stephens, A. J.; Burgess-Brown, N. A.; Jiang, S. Beyond Just Peptide Antigens: The Complex World of Peptide-Based Cancer Vaccines. *Front. Immunol.* 2021, 12, 696791.
- (16) Slingluff, C. L. The Present and Future of Peptide Vaccines for Cancer. *Cancer J.* 2011, 17, 343–350.
- (17) Paradis-Bas, M.; Tulla-Puche, J.; Albericio, F. The Road to the Synthesis of “Difficult Peptides”. *Chem. Soc. Rev.* 2016, 45, 631–654.
- (18) Merrifield, R. B. Solid Phase Peptide Synthesis. I. The Synthesis of a Tetrapeptide. *J. Am. Chem. Soc.* 1963, 85, 2149–2154.
- (19) de la Torre, B. G.; Albericio, F. The Pharmaceutical Industry in 2018. An Analysis of FDA Drug Approvals from the Perspective of Molecules. *Molecules* 2019, 24, 809.
- (20) Craik, D. J.; Fairlie, D. P.; Liras, S.; Price, D. The Future of Peptide-Based Drugs. *Chem. Biol. Drug Des.* 2013, 81, 136–147.
- (21) Yang, Y. Chapter 1: Peptide Fragmentation/Deletion Side Reactions. In *Side reactions in peptide synthesis*; Academic Press, an imprint of Elsevier: London, UK, 2016; pp. 131.
- (22) Yang, Y. Chapter 6: Intramolecular Cyclization Side Reactions. In *Side reactions in peptide synthesis*; Academic Press, an imprint of Elsevier: London, UK, 2016; pp. 119161.
- (23) Yang, Y. Chapter 5: Side Reactions upon Amino Acid/Peptide Carboxyl Activation. In *Side reactions in peptide synthesis*; Academic Press, an imprint of Elsevier: London, UK, 2016; pp. 95118.
- (24) Yang, Y. Chapter 3: Peptide Global Deprotection/Scavenger-Induced Side Reactions. In *Side reactions in peptide synthesis*; Academic Press, an imprint of Elsevier: London, UK, 2016; pp. 4375.
- (25) Zheng, J.; Yu, M.; Qi, Y.; Tang, S.; Shen, F.; Wang, Z.; Xiao, L.; Zhang, L.; Tian, C.; Liu, L. Expedient Total Synthesis of Small to Medium-Sized Membrane Proteins via Fmoc Chemistry. *J. Am. Chem. Soc.* 2014, 136, 3695–3704.
- (26) Zou, H.; Zhang, Y.; Hong, M.; Lu, P. Some Retention Characteristics of Dipeptides in Reversed-Phase High-performance Liquid Chromatography. *J. Liq. Chromatogr.* 1992, 15, 1797–1806.
- (27) Condron, M.; Monien, B.; Bitan, G. Synthesis and Purification of Highly Hydrophobic Peptides Derived from the C-Terminus of Amyloid β -Protein. *Open Biotechnol. J.* 2008, 2, 87–93.
- (28) Joshi, D. R.; Adhikari, N. An Overview on Common Organic Solvents and Their Toxicity. *J. Pharm. Res. Int.* 2019, 28 (3), 1–18.
- (29) Chang, K.; Pastan, I.; Willingham, M. C. Isolation and Characterization of a Monoclonal Antibody, K1 Reactive with Ovarian Cancers and Normal Mesothelium. *Int. J. Cancer* 1992, 50, 373–381.
- (30) Thomas, A. M.; Santarsiero, L. M.; Lutz, E. R.; Armstrong, T. D.; Chen, Y.-C.; Huang, L.-Q.; Laheru, D. A.; Goggins, M.; Hruban, R. H.; Jaffee, E. M. Mesothelin-Specific CD8+ T Cell Responses Provide Evidence of in Vivo Cross-Priming by Antigen-Presenting Cells in Vaccinated Pancreatic Cancer Patients. *J. Exp. Med.* 2004, 200, 297–306.
- (31) Argani, P.; Iacobuzio-Donahue, C.; Ryu, B.; Rosty, C.; Goggins, M.; Wilentz, R. E.; Murugesan, S. R.; Leach, S. D.; Jaffee, E.; Yeo, C. J.; et al. Mesothelin is overexpressed in the vast majority of ductal adenocarcinomas of the pancreas: identification of a new pancreatic cancer marker by serial analysis of gene expression (SAGE). *Clin. Cancer Res.* 2001, 7, 3862–3868.
- (32) Montemagno, C.; Cassim, S.; Pouyssegur, J.; Broisat, A.; Pagès, G. From Malignant Progression to Therapeutic Targeting: Current Insights of Mesothelin in Pancreatic Ductal Adenocarcinoma. *Int. J. Mol. Sci.* 2020, 21, 4067.
- (33) Nichetti, F.; Marra, A.; Corti, F.; Guidi, A.; Raimondi, A.; Prinzi, N.; de Braud, F.; Pusceddu, S. The Role of Mesothelin as a Diagnostic and Therapeutic Target in Pancreatic Ductal Adenocarcinoma: A Comprehensive Review. *Target Oncol.* 2018, 13, 333–351.
- (34) Hassan, R.; Thomas, A.; Alewine, C.; Le, D. T.; Jaffee, E. M.; Pastan, I. Mesothelin Immunotherapy for Cancer: Ready for Prime Time? *J. Clin. Oncol.* 2016, 34, 4171–4179.
- (35) Chen, Y.; Ayaru, L.; Mathew, S.; Morris, E.; Pereira, S. P.; Behboudi, S.; Rakonczy, Z. Expansion of Anti-Mesothelin Specific CD4+ and CD8+ T Cell Responses in Patients with Pancreatic Carcinoma. *PLoS One* 2014, 9, No. e88133.
- (36) Laheru, D.; Lutz, E.; Burke, J.; Biedrzycki, B.; Solt, S.; Onners, B.; Tartakovsky, I.; Nemunaitis, J.; Le, D.; Sugar, E.; et al. Allogeneic Granulocyte Macrophage Colony-Stimulating Factor–Secreting Tumor Immunotherapy Alone or in Sequence with Cyclophosphamide for Metastatic Pancreatic Cancer: A Pilot Study of Safety, Feasibility, and Immune Activation. *Clin. Cancer Res.* 2008, 14, 1455–1463.

- (37) Rammensee, H.-G.; Bachmann, J.; Emmerich, N. P.; Bachor, O. A.; Stevanović, S. SYPPPEITHI: Database for MHC Ligands and Peptide Motifs. *Immunogenetics* 1999, 50, 213–219.
- (38) Parker, K. C.; Bednarek, M. A.; Coligan, J. E. Scheme for Ranking Potential HLA-A2 Binding Peptides Based on Independent Binding of Individual Peptide Side-Chains. *J. Immunol.* 1994, 152, 163–175.
- (39) Cruz, L. J.; Iglesias, E.; Aguilar, J. C.; González, L. J.; Reyes, O.; Albericio, F.; Andrea, D. A Comparative Study of Different Presentation Strategies for an HIV Peptide Immunogen. *Bioconjugate Chem.* 2004, 15, 112–120.
- (40) Stolk, D. A.; Horrevorts, S. K.; Schetters, S. T. T.; Kruijssen, L. J. W.; Duinkerken, S.; Keuning, E.; Ambrosini, M.; Kalay, H.; van de Ven, R.; Garcia-Vallejo, J. J.; et al. Palmitoylated Antigens for the Induction of Anti-Tumor CD8+ T Cells and Enhanced Tumor Recognition. *Mol. Ther. Oncolytics*. 2021, 21, 315–328.
- (41) Wang, J.; Deng, T.; Liu, Y.; Chen, K.; Yang, Z.; Jiang, Z.-X. Monodisperse and Polydisperse Pegylation of Peptides and Proteins: A Comparative Study. *Biomacromolecules* 2020, 21, 3134–3139.
- (42) Blankenstein, T.; Coulie, P. G.; Gilboa, E.; Jaffee, E. M. The determinants of tumour immunogenicity. *Nat. Rev. Cancer* 2012, 12, 307–313.
- (43) Carpino, L. A.; Han, G. Y. 9-Fluorenylmethoxycarbonyl Function, a New Base-Sensitive Amino-Protecting Group. *J. Am. Chem. Soc.* 1970, 92, 5748–5749.
- (44) Kocsis, L.; Ruff, F.; Orosz, G. The effect of peptide length on the cleavage kinetics of 2-chlorotrityl resin-bound ethers. *J. Pept. Sci.* 2006, 12, 428–436.
- (45) Hänel, G.; Angerer, C.; Petr, Y. K.; Lichtenegger, F. S.; Subklewe, M. Blood DCs activated with R848 and poly(I: C) induce antigen-specific immune responses against viral and tumor-associated antigens. *Cancer Immunol., Immunother.* 2022, 71, 1705–1718.
- (46) Tandel, N.; Patel, D.; Thakkar, M.; Shah, J.; Tyagi, R. K.; Dalai, S. K. Poly(I: C) and R848 ligands show better adjuvanticity to induce B and T cell responses against the antigen(s). *Heliyon* 2024, 10, No. e26887.
- (47) Castro, F.; Cardoso, A. P.; Gonçalves, R. M.; Serre, K.; Oliveira, M. J. Interferon-Gamma at the Crossroads of Tumor Immune Surveillance or Evasion. *Front. Immunol.* 2018, 9, 847.